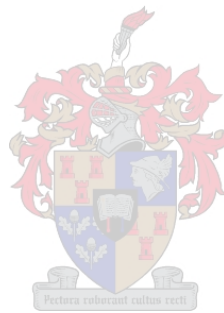


**CALCULATION OF THE FORCES ON A MOORED SHIP
DUE TO A PASSING CONTAINER SHIP**

Pierre Brink Swiegers



Thesis presented in fulfilment of the requirements for the
degree of Master in the Science of Engineering

Study Leader: G Toms

December 2011

By submitting this thesis electronically, I declare that the entirety of the work contained therein is my own, original work, that I am the authorship owner thereof (unless to the extent explicitly otherwise stated) and that I have not previously in its entirety or in part submitted it for obtaining any qualification.

Date:

Summary

When a sailing ship passes a moored ship the moored ship experiences forces and moments. These forces and moments cause the moored ship to move. The resulting ship motions due to the passing ship can sometimes be more severe than the ship motions due to ocean waves and can cause serious accidents at moorings such as the failing of mooring lines or even the total break away of the ship from the berth. Since bulk carriers and tankers were traditionally the largest seafaring ships, passing ship studies have focused mainly on these vessels, but recently container ships have grown to a comparable size. In this study an existing numerical model "Passcat" is validated with physical model measurements for a Post Panamax container ship passing a Panamax bulk carrier. Other existing mathematical formulae are also evaluated by comparison with these model tests.

In the physical model tests the passing speed (V), passing distance (G), depth draft ratio (d/D) and the presence of walls and channels were varied. It was found that the passing ship forces are proportional to the passing speed to the power of 2.32. This is slightly higher than the generally accepted quadratic relationship for passing ship induced forces. Similar relationships were found for the other variables.

The numerical model results were compared to the physical model measurements by determining agreement ratios. A perfect agreement between the numerical and physical models would result in an agreement ratio of 1. Agreement ratio boundaries, wherein agreement would be regarded as good, were drawn between 0.7 and 1.3. The numerical model, Passcat, was found to under predict the passing ship forces. It was found that Passcat is valid for a wide range of sensitivities and remains within the agreement ratio limits as long as passing speed is limited to 10 knots (kt), depth draft ratio to more than 1.164, passing distance to less than four times the moored ship beam (B_m) for surge and sway estimation and passing distance to less than three times the moored ship beam for yaw estimations. These limits are true for no structures in the water. For structures in the water only the passing speed limits are different. When quay walls are present, the surge and sway forces will only provide acceptable answers at passing speeds below 9kt. When $9B_m$ or $12B_m$ channels are present, the sway force will only provide acceptable answers at passing speeds below 7kt. When a $6B_m$ channel is present, the yaw moments will only provide acceptable answers at passing speeds below 6kt.

From the mathematical model evaluation study it was found that empirical or semi empirical methods can not provide answers with good agreement to the physical model when walls or channels are present. For the open water case, it is only the Flory method that can provide answers with good agreement to the physical model for surge, sway and yaw forces. The Flory method can provide answers with acceptable agreement within narrow boundaries of passing distance (1 to 2 times the beam of the moored ship), passing speed (4 kt to 14 kt) and depth draft ratio (less than 1.7). The numerical model, Passcat can be used with little effort to provide answers with better agreement to the physical model for a larger range of variables.

Opsomming

Wanneer 'n skip verby 'n vasgemeerde skip vaar, ondervind die vasgemeerde skip kragte en momente. Hierdie kragte induseer beweging van die vasgemeerde skip. Die beweging kan soms groter wees as die effek van wind of golwe. Indien die bewegings groot genoeg is kan dit van die vasmeer lyne van die skip laat breek, of al die lyne laat breek sodat die skip vry in die hawe ronddryf. Aangesien erts skepe en tenk skepe vir jare die grootste skepe in the wêreld was, het die meeste van die skip interaksie studies op daardie skepe gefokus. Die grootte van behouering skepe het egter in die onlangse tye gegroei om dimensies soortgelyk aan die van erts en tenk skepe te hê. In hierdie studie word 'n bestaande numeriese model "Passcat" gestaaf met fisiese model metings op 'n Post Panamax behoueringskip wat verby 'n Panamax erts skip vaar. Bestaande wiskundige formules is ook getoets deur dit met dieselfde fisiese model metings te vergelyk.

In die fisiese model studie is die spoed van die skip (V), tussenafstand (G), diepte diepgang verhouding (d/D) en die teenwoordigheid van kaai mure en kanale in die water getoets. Daar is gevind dat die kragte op die vasgemeerde skip direk eweredig is aan die spoed van die skip tot die mag 2.32. Dit is effens meer as die algemeen aanvaarde kwadratiese verhouding tussen vloeistof sleurkrag en vloeisnelheid asook tussen skip interaksie kragte en vaar snelheid. Soortgelyke verhoudings is vir al die veranderlikes bereken.

Numeriese model resultate is vergelyk met die fisiese model om die verhouding van ooreenstemming te bepaal. 'n Perfekte ooreenstemming word voorgestel deur 'n verhouding van ooreenstemming van 1. Grense waarbinne die verhouding van ooreenstemming as goed beskou word is getrek tussen 0.7 en 1.3. Daar is gevind dat die numeriese model, Passcat, kragte oor die algemeen onderskat. Passcat is geldig vir 'n breë reeks van veranderlikes en sal geldig bly solank die skip spoed tot 10 knope, diepte diepgang verhouding tot meer as 1.164, tussenafstand tot minder as vier skipwydtes (B_m) vir 'surge' en 'sway' kragte en tot minder as drie skipwydtes vir 'yaw' momente beperk word. Hierdie grense is opgestel vir geen strukture in die water. Vir strukture in die water word slegs die skip spoed aangepas. Wanneer daar mure in die water is sal 'surge' en 'sway' slegs geskikte antwoorde gee as die skip spoed tot 9 knope beperk word. Vir $9B_m$ of $12B_m$ kanale sal geskikte antwoorde vir 'sway' kragte slegs voorkom met 'n skip spoed minder as 7 knope. Vir $6B_m$ kanale sal geskikte antwoorde vir 'yaw' momente slegs voorkom met 'n skip spoed van minder as 6 knope.

Van die wiskundige model evaluasie studie is gevind dat empiriese of semi empiriese metodes nie resultate met goeie ooreenstemming tot the fisiese model metings kan gee, wanneer daar kaai of kanaal mure in die water is nie. Vir die oopwater geval is dit slegs die Flory metode wat antwoorde kan voorsien wat goed ooreenstem met die fisiese model vir 'surge', 'sway', en 'yaw' kragte. Die Flory metode voorsien hierdie resultate binne noue grense vir tussenafstand (1 tot 2 wydtes van die vasgemeerde skip), verbyvaar spoed (4 knope tot 14 knope) en diepte diepgang verhouding (minder as 1.7). Die numeriese model, Passcat, kan met min moeite antwoorde bereken wat beter ooreenstemming vir 'n groter reeks veranderlikes gee.

Acknowledgments

To have completed this thesis would not have been possible without the valuable contributions of others.

Geoff Toms, my study leader, provided the initial motivation and direction towards an interesting and suitable subject. Geoff has been very effective at keeping my focus on one goal, planning ahead and structuring the thesis report.

The CSIR, who has taken me in for one year, has provided access to the hydraulics laboratory in Stellenbosch and the free use of computers, software and building materials. The CSIR employees have been a very sociable group of people who have always shown interest in my project and were always ready for a beer at the local pub.

Special thanks to Doctor Wim van der Molen for providing technical knowledge and vast experience in the ship interaction study field. Wim pulled me back on track when I lost interest and has been a learned mentor and good friend throughout the process. Wim provided the initial reference list for the literature review and has been the main author of the conference paper, based on the calculations done for this thesis.

Hans Moes and Professor Marc Vantorre were co-authors of the paper presented at Trondheim. Hans has been cheering everyone up with his jovial attitude and has also been a great source of experience in the study field. Professor Vantorre has made available physical model tests of passing ships done at Ghent University.

WSP Africa Coastal Engineers, my employer, has given me the opportunity to be subcontracted to the CSIR to gain experience in physical and numerical modelling.

The Canadian visitors from W.F. Baird and Associates Coastal Engineers provided a passing ship literature list which extended the literature provided by Doctor van der Molen.

Special thanks to my wife, Leandri, for supporting me through the many late nights and weekends at work. Leandri provided emotional support, motivation, distraction and dedicated her own time in the editing of the thesis.

TABLE OF CONTENTS

LIST OF FIGURES	IX
LIST OF TABLES	XI
LIST OF EQUATIONS	XII
LIST OF SYMBOLS.....	XIII
1 INTRODUCTION	1
1.1 BACKGROUND	1
1.2 OBJECTIVES.....	2
1.3 OVERVIEW OF STUDY.....	2
2 LITERATURE REVIEW	4
2.1 INTRODUCTION	4
2.2 SHIP MOTIONS	4
2.3 PASSING SHIP INTERACTION CONCEPT	6
2.4 HISTORY OF PASSING SHIP ACCIDENTS	10
2.5 PASSING SHIP STUDIES	13
2.6 SHORTCOMINGS IN PASSING SHIP STUDIES.....	23
2.7 FLOW DYNAMICS.....	24
2.8 SUMMARY AND CONCLUSIONS.....	27
3 PHYSICAL MODEL STUDY	29
3.1 INTRODUCTION	29
3.2 TEST SETUP.....	29
3.3 CALIBRATIONS.....	34
3.4 TEST PROCEDURE.....	36
3.5 TEST CONDITIONS	37
3.6 OUTPUT AND PROCESSING.....	38
3.7 ANALYSES.....	41
3.8 SCALING EFFECTS.....	51
3.9 SUMMARY AND CONCLUSIONS.....	52
4 NUMERICAL MODEL VALIDATION.....	53
4.1 INTRODUCTION	53
4.2 NUMERICAL MODEL	53
4.3 COMPARISON OF NUMERICAL AND PHYSICAL MODELS	57
4.4 SUMMARY AND CONCLUSIONS.....	70
5 MATHEMATICAL FORMULAE EVALUATION	71
5.1 INTRODUCTION	71
5.2 MATHEMATICAL METHODS.....	71
5.3 COMPARISON OF MATHEMATICAL AND PHYSICAL MODELS.....	72
5.4 CONCLUSIONS.....	81
6 CONCLUSIONS	82
7 RECOMMENDATIONS.....	83

REFERENCES 84

APPENDICES

APPENDIX A: GENERAL

APPENDIX B: IMAGES

APPENDIX C: COMPARISON OF NUMERICAL AND PHYSICAL MODELS

APPENDIX D: TRENDS IN PHYSICAL AND NUMERICAL MODEL RESULTS

APPENDIX E: COMPARISON OF MATHEMATICAL AND PHYSICAL MODELS

APPENDIX F: CONFERENCE PAPER

LIST OF FIGURES

Figure 2-1: The six degrees of freedom of a ship i.e. surge (x), sway (y), heave (z), roll (Φ), pitch (θ) and yaw (ψ) (Journée and Massie 2001).....	4
Figure 2-2: Relation between cargo handling efficiency and ship motions (PIANC 1995).....	5
Figure 2-3: Definition of axes and symbols for a parallel passing ship incident.....	7
Figure 2-4: Pressure distribution around a moving ship due to the suction effect (after Spencer et al 2008).....	8
Figure 2-5: Interpretation of forces due to the suction effect during a passing ship interaction (after Flory 2002)	9
Figure 2-6: Wake wash waves (after USA Department of Defence 2005)	10
Figure 2-7: Above waterline damage to the Olympic (left) and damage to the HMS Hawke (right) due to a passing ship incident (Colledge and Warlow 2006).....	11
Figure 2-8: Photograph taken from the Titanic during its incident with the New York (Pinkster 2009)	11
Figure 2-9: A burnt out tanker Jupiter following a passing ship accident (Seelig 2001).....	12
Figure 2-10: Subsections of passing ship force predictions.....	13
Figure 2-11: Set up of a test conducted by Remery (Remery 1974).....	14
Figure 2-12: Normalized surge force (Flory 2002).....	16
Figure 2-13: Setup for passing ship computations using a panel model (Pinkster 2004)	18
Figure 2-14: A passing event being measured at Port Hedland (O' Brien and Hens 2007)..	22
Figure 2-15: Development of the boundary layer at an airfoil (Schlichting 2003)	26
Figure 2-16: Flow past an airfoil, (a) attached flow, (b) separated flow (Schlichting 2003)...	26
Figure 3-1: Layout of the passing ship setup in the 3D wave basin at the CSIR.....	30
Figure 3-2: Passing ship rail with the container ship.....	32
Figure 3-3: Fixed frame with the bulk carrier	33
Figure 3-4: The passing and moored ships in the rail and fixed frame.....	34
Figure 3-5: Calibration of forces for tension and compression in the force frame	35
Figure 3-6: Repeatability tests of test 01 to test 05.....	36
Figure 3-7: Test conditions.....	38
Figure 3-8: Test 10 physical model results raw and smoothed	39
Figure 3-9: Physical model results as a function of speed for ships passing in the same and opposite directions.....	42
Figure 3-10: Physical model results as a function of depth draft ratio for different speeds and channel walls	43
Figure 3-11: Physical model results as a function of passing distance for different speeds .	44
Figure 3-12: Physical model results as a function of walls and channels for different passing speeds and depth draft ratios.....	45
Figure 3-13: Histogram of empirical factors for surge forces to assess the accuracy of the combination of proportionalities.....	49
Figure 4-1: Meshes of the bulk carrier (left) and the container ship (right).....	54
Figure 4-2: Mesh setup of test 17	55
Figure 4-3: Passcat input file.....	55
Figure 4-4: Passcat output file (shortened).....	56
Figure 4-5: Test 10 physical and numerical model results.....	58

Figure 4-6: Agreement ratio for variation in speed for ships in both directions..... 60

Figure 4-7: Agreement ratio for variation in passing distance for the ship passing at 6kt and 8kt..... 61

Figure 4-8: Agreement ratio for variation in depth draft ratio for the ship passing at 6kt and 8kt..... 62

Figure 4-9: Agreement ratio for different obstructions in the water for the ship passing at 6kt and 8kt..... 63

Figure 4-10: Agreement ratio percentage by speed for combination runs..... 65

Figure 4-11: Agreement ratio by depth draft ratio for combination runs 66

Figure 4-12: Agreement ratio by walls and channels for combination runs 67

Figure 4-13: Agreement ratio for depth draft ratio of the Flanders data and CSIR data for 8kt 69

Figure 5-1: Mathematical methods evaluated..... 71

Figure 5-2: Comparison of empirical and semi-empirical calculations with numerical and physical model results for test 10 73

Figure 5-3: Agreement ratio by speed for mathematical and physical model results 77

Figure 5-4: Agreement ratio by passing distance for mathematical and physical model results 78

Figure 5-5: Agreement ratio by depth draft ratio for mathematical and physical model results 79

Figure 5-6: Agreement ratio by walls and channels for mathematical and physical model results 80

LIST OF TABLES

Table 2-1: Maximum allowable ship motion amplitudes (PIANC 1995).....	6
Table 2-2: Ship characteristics of Flanders model.....	17
Table 3-1: Ship characteristics	31
Table 3-2: Physical model maximum results of all tests for surge sway and yaw	40
Table 3-3: Relationships between forces and variables.....	47
Table 3-4: Coefficient of variation for combined surge, combined sway and combined yaw proportionalities.....	49
Table 4-1: Limits for good agreement between Passcat and the physical model.....	64
Table 5-1: Boundaries wherein the empirical or semi-empirical models give good agreement with physical model measurements.....	74
Table 5-2: Ranking of mathematical models	75
Table 5-3: Criteria for the selection of a calculation method for the open water case	76

LIST OF EQUATIONS

Equation 2-1: Deep water surge force (Wang 1975)	15
Equation 2-2: Deep water sway force (Wang 1975)	15
Equation 2-3: Deep water yaw moment (Wang 1975)	15
Equation 2-4: Surge force (Flory 2002)	16
Equation 2-5: Flory sway force (Flory 2002)	16
Equation 2-6: Yaw moment (Flory 2002)	16
Equation 2-7: Shallow water correction factor for Wang deepwater surge force (Seelig 2001)	17
Equation 2-8: Shallow water correction factor for Wang deepwater sway force and yaw moment (Seelig 2001).....	17
Equation 2-9: Shallow water correction factor for Wang deep water surge force (Kriebel 2005)	18
Equation 2-10: Shallow water correction factor for Wang deep water sway force (Kriebel 2005)	19
Equation 2-11: Shallow water correction factor for Wang deep water yaw moment (Kriebel 2005)	19
Equation 2-12: Kriebel surge force empirical equation (Kriebel 2005)	19
Equation 2-13: Kriebel sway force empirical equation (Kriebel 2005)	19
Equation 2-14: Kriebel yaw moment empirical equation (Kriebel 2005).....	19
Equation 2-15: Formulae for the determination of surge force using the Varyani method (Varyani and Vantorre 2006).....	20
Equation 2-16: Formula for the determination of sway force using the Varyani Vantorre method (Varyani and Vantorre 2006)	21
Equation 2-17: Formula for the determination of yaw moments using the Varyani Vantorre method (Varyani and Vantorre 2006)	21
Equation 2-18: Velocity potential function (Chadwick et al 2006).....	24
Equation 2-19: Reynolds number	24
Equation 2-20: Blasius laminar boundary layer (Schlichting 2003)	25
Equation 2-21: Schlichting turbulent boundary layer (Schlichting 2003)	25
Equation 3-1: Derivation of empirical factors for each test.....	48
Equation 3-2: New empirical relationship for passing ship surge forces	50
Equation 3-3: New empirical relationship for passing ship sway forces	50
Equation 3-4: New empirical relationship for passing ship yaw moments	50
Equation 4-1: Potential flow equations	53
Equation 4-2: Agreement ratio	59

LIST OF SYMBOLS

$A(\xi')$	Filter function	[-]
B_m	Beam of the moored ship	[m]
B_p	Beam of the passing ship	[m]
CF_x	Correction factor for Wang surge force	[-]
CF_y	Correction factor for Wang sway force	[-]
CM_z	Correction factor for Wang yaw moment	[-]
d	Water depth	[m]
dh	Depth of the ship hull (deck to keel)	[m]
D	Ship draft	[m]
D_m	Moored ship draft	[m]
dwt	Deadweight tons	[t]
F	Depth related Froude number	[-]
F_x	Surge force	[N]
F_y	Sway force	[N]
F_1	Empirical relationship for surge force	[-]
F_2	Empirical relationship for sway force	[-]
F_3	Empirical relationship for yaw moment	[-]
G	Board to board lateral distance between the ships	[m]
i	Test number	[-]
K	Empirical factor	[N]
L	Length (dimension)	[m]
L_c	Characteristic ship length $(L_m + L_p) / 2$	[m]
L_m	Length of the moored ship	[m]
L_p	Length of the passing ship	[m]
LOA	Ship length over all	[m]
LBP	Ship length between perpendiculars	[m]
LCG	Distance from aft perpendicular to centre of gravity	[m]
M_z	Yaw moment	[Nm]
n	Unit normal vector	
n_x	Partial derivative of unit normal vector	
Re	Reynolds number	[-]
$S_1(x_1)$	Moored ship parabolic sectional area distribution	
$S_2(x_2)$	Passing ship parabolic sectional area distribution	
V	Passing speed	[m/s]
V	Speed	[m/s]
WF_1	Wall factor for surge force	[-]
WF_2	Wall factor for sway force	[-]

WF_3	Wall factor for yaw moment	[-]
x_b	Distance downstream from the start of the boundary layer	[m]
\mathcal{B}	Sea bed surface	
\mathcal{H}_M	Body surface of the moored ship	
\mathcal{W}	Surface of structures	
Δ	Displacement volume of the ship	[t]
Δ_D	Displacement ratio	[-]
Δ_S	Separation ratio	[-]
δ	Boundary layer thickness	[m]
η	Centre to centre lateral distance between the ships	[m]
μ	Absolute viscosity	[kg/m s]
ν	Kinematic viscosity	[m ² /s]
ξ	Centre to centre stagger distance between the ships	[m]
ξ'	Non dimensional stagger distance	[-]
ρ	Water density	[kg/m ³]
ϕ	Velocity potential	
ϕ_n	Velocity potential in the direction of a unit vector	
ϕ_{xx}, ϕ_z	Partial derivatives of velocity potential	

1 INTRODUCTION

1.1 BACKGROUND

When a moving ship passes a moored ship, the moored ship will experience forces and moments. These forces and moments cause the moored ship to move. In some situations the resulting ship motions due to the passing ship can be more severe than the ship motions due to ocean waves and can cause serious accidents at moorings such as the failing of mooring lines or even the total break away of the ship from the berth. An example of such an event happened when tanker Jupiter was moored at Saginaw River at Bay City, Michigan, USA. A ship passing at 20m passing distance at 4.2 knots (kt) caused the fuel lines of tanker Jupiter to break (1990). The leaking fuel found an ignition source and the tanker was totally destroyed (Seelig 2001).

Since bulk carriers and tankers were traditionally the largest seafaring ships, passing ship studies have focused mainly on these vessels, but recently container ships have grown to a comparable size. Container ships are lighter than bulk carriers of the same length or draft and are built more streamlined. For this reason they will have a lesser effect on a moored ship under the same passing conditions, but container ships are equipped with strong engines and thrusters, allowing them to accelerate and decelerate quicker than bulk carriers. Often very large bulk carriers and tankers have dedicated berths on the outskirts of ports due to draft restrictions. Container ships on the other hand, have to frequent congested waterways together with smaller bulk carriers and tankers. The size of container ships coupled with their high speed and their movement in congested waterways has caused container ships to become a risk for modern port accidents.

Ships often berth at dedicated terminals and in most cases ships of the same type will interact. At the terminal, ships are usually brought to a halt to berth, or take off from standstill. For this reason higher sailing speeds are usually present further away from the berths. A typical scenario found in channels is where a large container ship passes a moored bulk carrier or tanker at high speed.

Passing ship studies ruled that parameters such as passing distance, passing speed, passing angle, ship sizes and depth draft ratio all had a significant effect on the forces experienced by the moored ship.

Empirical formulae were all derived from a limited number of tests which were done on similar sized bulk carriers in open water. For this reason, concerns exist about the validity of the empirical formulae for conditions other than those for which they have been derived.

Numerical methods were derived to provide a more general way of estimating passing ship forces. A drawback of numerical methods is that they are based on a set of assumptions which can over simplify and underestimate complex processes. Numerical models need to be calibrated. Ideally calibration should be done with prototype measurements but since these are very expensive and difficult to achieve in practice, numerical models are mostly calibrated with physical model data under controlled situations (Bertram 2000). The numerical model, Passcat, which was developed at the CSIR, is a 3D panel model that calculates passing ship forces. Passcat determines the forces in the surge and sway directions as well as yaw moments and needs to be validated against model test results when it is to be used under a new set of assumptions.

Chapter 1: Introduction

A limited number of passing ship studies involving container ships has been done (van Wijhe and Pinkster 2008). Conclusions drawn from the observation of bulk carriers and tankers are currently used to predict behaviour for all ships, including container ships. It would be valuable if similar studies for container ships could be done. From the results of these studies an existing numerical model, like Passcat, can be validated. It would also be valuable to evaluate if conclusions drawn from previous studies, on bulk carrier and tankers, also applies to container ships.

1.2 OBJECTIVES

The first objective is to extend knowledge of the interaction between a passing container ship and a moored bulk carrier by doing and interpreting physical modelling tests of a range of scenarios.

The second objective is to validate the numerical model Passcat with a wide set of parameters to reach confidence in its results. During the validation process limits will be determined where the Passcat result can be applied with confidence.

The third objective is to evaluate existing mathematical formulae against the physical model results to determine whether they apply for the case where a container ship passes a moored bulk carrier, even though they were derived from model tests on bulk carriers and tankers.

1.3 OVERVIEW OF STUDY

The literature study (Chapter 2) commences by addressing what the causes of ship motions are and why they are important. Factors affecting ship motions are discussed and those that have the most significant effect on ship motions are highlighted. For the passing ship effect, the mechanisms causing ship motions are discussed. This is done to give a better understanding of why they cause ship motions and which of the mechanisms are the most relevant for this study. The history of passing ship accidents is studied to explore the conditions where accidents occurred. Hereafter the development of passing ship studies is discussed to trace the development of human thought and to give more details on this subject. Following the section on passing ship studies, a section is dedicated to the shortcomings of passing ship studies in general. Flow dynamics are investigated to understand the processes involved during a passing ship interaction. A section is dedicated to the numerical model, Passcat, to highlight the working thereof. A summary and conclusions highlights the key aspects, the character of passing ship interactions and the need for further studies on passing ship interactions. In the summary and conclusions, physical model studies, calculation methods and field measurements are handled separately.

The physical modelling chapter (Chapter 3) gives a description of the model testing facilities at the CSIR as used in this study. All calibrations are discussed after which a procedure is discussed how each individual test is done to ensure similar conditions throughout the study. After the discussion of the test procedure, a motivation of the chosen test cases follows. The output and preliminary data processing is given before a more thorough analysis of the output is done. The analysis interprets plots to find relationships in the data. Finally scaling effects in the physical model are discussed.

The chapter on the validation of the numerical model (Chapter 4) covers a description of how Passcat is used and what input needs to be generated. The numerical and the physical

Chapter 1: Introduction

models are compared by plotting force series' on the same axes. A ratio of agreement is calculated to determine rough boundaries wherein the numerical model results can be regarded as acceptable. A comparison between the numerical model and existing data for bulk carriers was done to assess the effect of different ships.

The chapter on the evaluation of the mathematical methods (Chapter 5) starts with a description of the mathematical methods that were applied. The mathematical methods are compared by force series graphs and agreement ratio plots. From this, acceptable boundaries are drawn. To assess the mathematical methods against each other and against Passcat, they are ranked by their performance.

The Conclusions (Chapter 6) gives a brief outline of the outcomes and conclusions of the study for the physical model tests, the numerical model study and the mathematical model assessment. At the end of the report (Chapter 7) recommendations are given to assist future studies.

2 LITERATURE REVIEW

2.1 INTRODUCTION

In the first section of this chapter, a background of ship motions is given. The six degrees of freedom and the causes of the motions are discussed. It is explained why ship motions need to be limited. After giving background on ship motions, it is explained how a passing ship causes moored ship motions. Some recorded accidents are given and discussed and passing ship studies are investigated through a chronological discussion thereof. A section discusses the shortcomings in passing ship studies regarding physical modeling and mathematical methods. A brief outline of basic flow dynamics and the numerical model Passcat is given. A summary and conclusions lifts out the relevant conclusions from the investigation of past studies and outlines the need for more information.

2.2 SHIP MOTIONS

Ship motions are caused by external influences such as winds, currents, waves, seiches, tides, passing ships and cargo handling operations (PIANC 1995). Ships move in six degrees of freedom (Journée and Massie 2001). The first three degrees of freedom move in translation and the last three move in rotation. The first three degrees of freedom are surge, sway and heave and they correspond to movement in the ship bound x , y and z directions. The last three degrees of freedom are roll, pitch and yaw and they correspond to rotation about the x , y and z axes. The six degrees of freedom of a ship are presented in Figure 2-1.

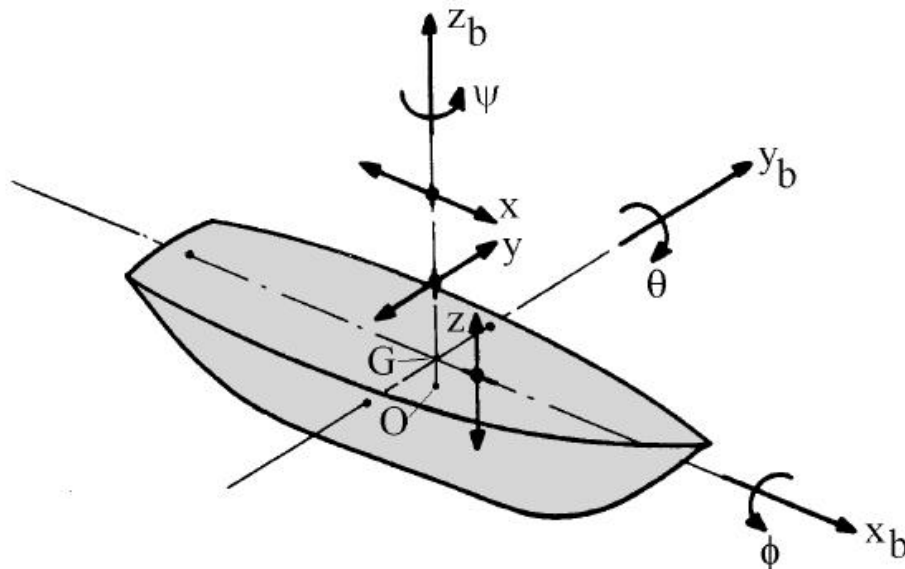


Figure 2-1: The six degrees of freedom of a ship i.e. surge (x), sway (y), heave (z), roll (Φ), pitch (θ) and yaw (ψ) (Journée and Massie 2001)

The magnitude of ship motions is of particular importance at moorings. A relation between cargo handling efficiency and ship motions is presented in Figure 2-2. When ship motions are small the productivity is virtually unaffected (A to B). Intermediate ship motions cause uncomfortable loading conditions and a subsequent lower loading efficiency (B to C). If the ship motions become large, ship loading is halted to prevent loading accidents (C to D). If there are very large ship motions, ships need to leave the port to prevent mooring lines from

Chapter 2: Literature Review

parting and subsequent collisions (beyond D). The logic in Figure 2-2 is easy to interpret for weather induced ship motions since step C and D can be triggered by wave and wind measurements. For passing ship induced ship motions it is more complicated since passing vessels come in various sizes, at different speeds and at different times. For wind and wave induced ship motions the ship is always prepared to take a step should the conditions worsen, but with passing ship accidents the event happens too sudden for the moored ship to be prepared.

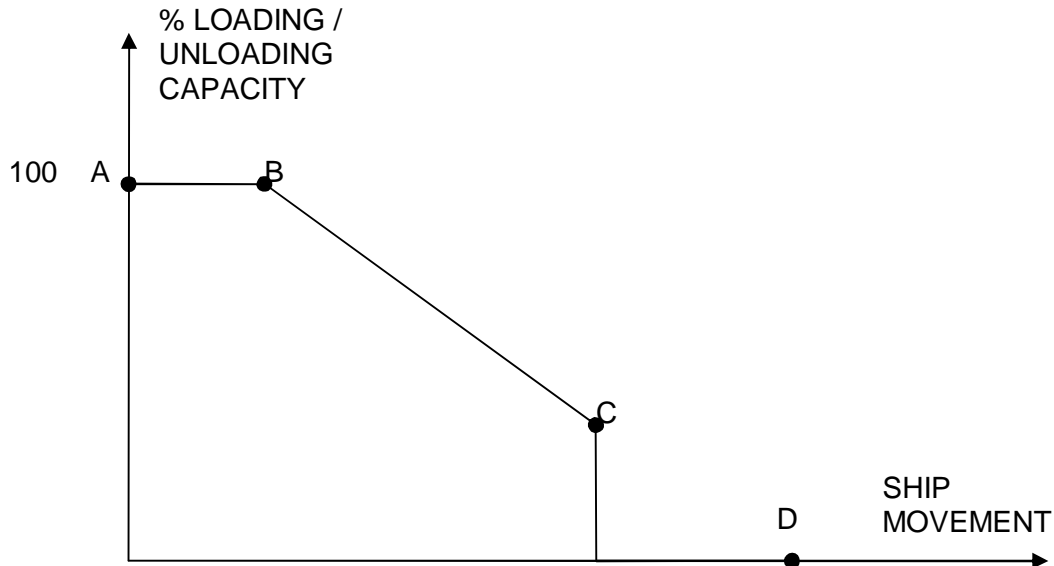


Figure 2-2: Relation between cargo handling efficiency and ship motions (PIANC 1995)

According to the summary of allowable ship motions in Table 2-1, different loading gear can handle different magnitudes of ship motions. Tankers can handle large ship motions due to flexible hoses while Roll-on-roll-off (Ro/Ro) ships need to be very stable while machinery are using on or off ramps. Passing ship events occur only a small fraction of the time and are therefore not a major concern for downtime considerations. Since moored ships are not prepared for the passing ship events, breakage of mooring lines is a larger concern since it can lead to injuries to personnel, fires, collision of the ship with port structures or collision of the ship with other ships.

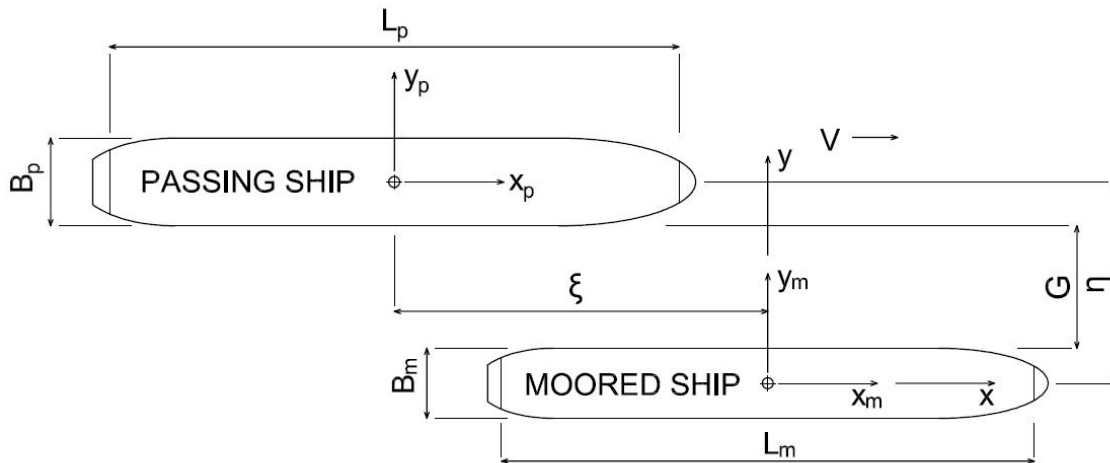
Table 2-1: Maximum allowable ship motion amplitudes (PIANC 1995)

Ship type	Cargo handling equipment	Surge (m)	Sway (m)	Heave (m)	Roll (°)	Pitch (°)	Yaw (°)
Fishing Vessels	Elevator Crane	0.2	0.2	-	-	-	-
	Lift-on-lift-off	1.0	1.0	0.4	3	3	3
	Suction pump	2.0	1.0	-	-	-	-
Freighters, coasters	Ships gear	1.0	1.2	0.6	1	1	2
	Quarry cranes	1.0	1.2	0.8	2	1	3
Ferries, Ro-Ro	Side Ramp	0.6	0.6	0.6	1	1	2
	Dew/Storm ramp	0.8	0.6	0.8	1	1	4
	Linkspan	0.4	0.6	0.8	3	2	4
	Rail ramp	0.1	0.1	0.4	-	1	1
General cargo		2.0	1.5	1.0	3	2	5
Container vessels	100% efficiency	1.0	0.6	0.8	1	1	3
	50% efficiency	2.0	1.2	1.2	1.5	2	6
Dry bulk carriers	Cranes	2.0	1.0	1.0	2	2	6
	Elevator / Bucket wheel	1.0	0.5	1.0	2	2	2
	Conveyor belt	5.0	2.5	-	3	-	-
Oil tankers	Loading arms	3.0	3.0	-	-	-	-
Gas tankers	Loading arms	2.0	2.0	-	2	2	2

2.3 PASSING SHIP INTERACTION CONCEPT

This section is dedicated to defining basic symbols and axes systems used in passing ship studies. This section is also used for investigating the basic process behind passing ship interaction forces.

Different passing ship studies have used similar coordinate systems. Although symbols often differ, the basic concept remains the same. Figure 2-3 is an example of such a coordinate system with general dimensions used in a parallel passing ship study. This coordinate system will be the definition sketch used in this study. When reporting on work by other authors, their work will be reported on using the symbols in Figure 2-3.

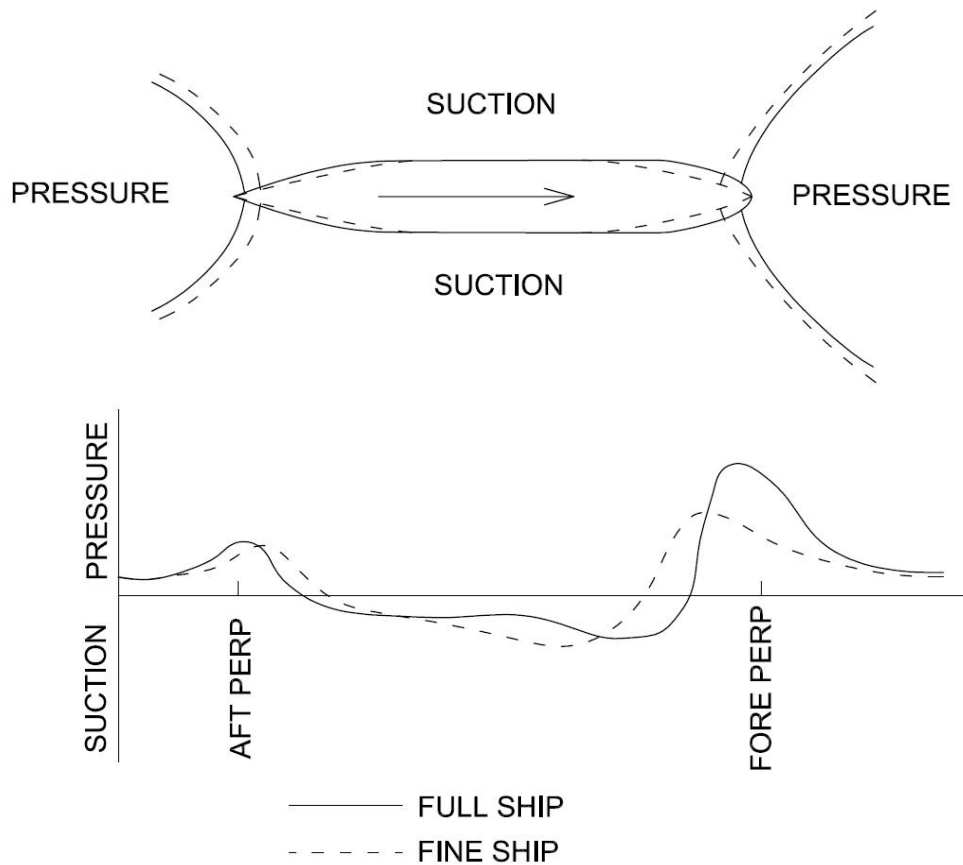


B_m	Beam of the moored ship	[m]
B_p	Beam of the passing ship	[m]
G	Board to board lateral distance between the ships	[m]
L_C	Characteristic ship length $(L_m + L_p) / 2$	[m]
L_m	Length of the moored ship	[m]
L_p	Length of the passing ship	[m]
V	Passing Speed	[m/s]
η	Centre to centre distance between the ships	[m]
ξ	Centre to centre stagger distance	[m]

Figure 2-3: Definition of axes and symbols for a parallel passing ship incident

The effect of a passing ship can be divided into three components, the suction effect, wake wash and, in the case of non-uniform geometry, harbour oscillations (Pinkster 2009).

A picture with the pressure distribution around a moving ship is presented in Figure 2-4. While the ship is moving, water needs to be displaced from the front of its bow to behind its stern. At the bow a local high pressure field, and higher water elevations, occurs where water is compressed by the ship. Water flows to either side of the ship towards the stern to converge and create another local high pressure field. Alongside the ship the higher water velocities cause a low pressure field and lower water elevations. The water surface will be sloping between the higher water level, lower water level and the still water level further away from the ship. When another ship is in the vicinity of the pressure fields and the sloping water surface, that ship will experience a force down the slope of the water surface. The force can also be described as a pressure force away from the higher water elevation and a suction force towards a lower water elevation.



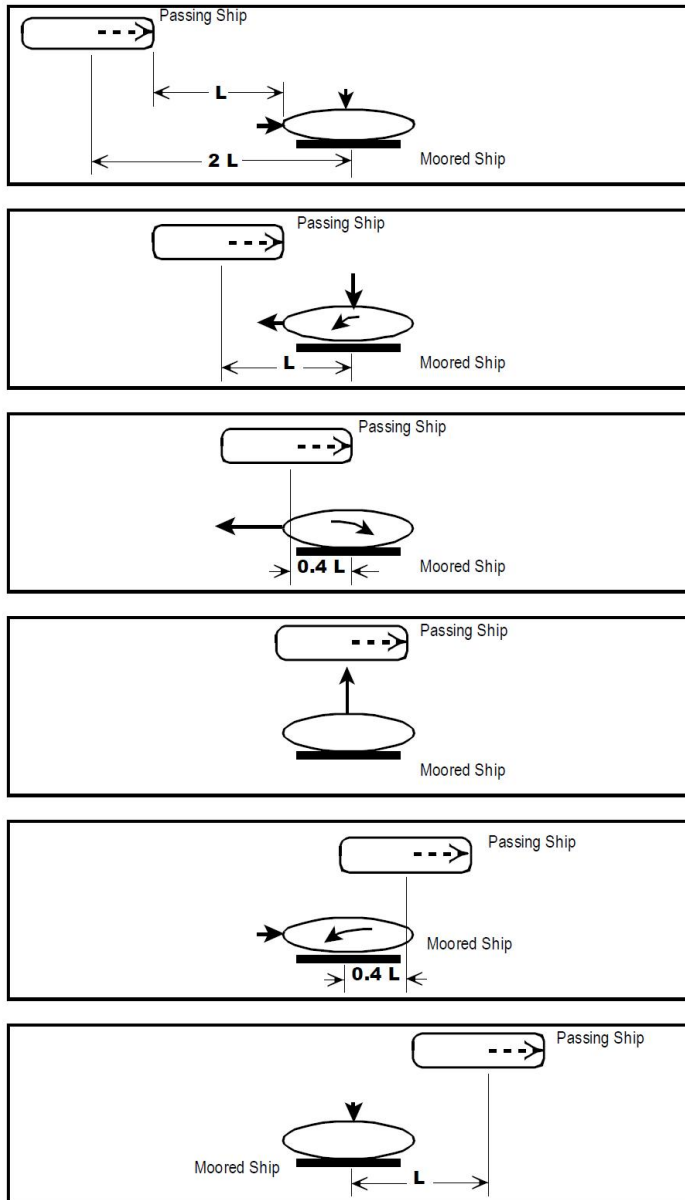
FULL SHIP: A bulky ship with a high block coefficient
 FINE SHIP: A slender ship with a low block coefficient

Figure 2-4: Pressure distribution around a moving ship due to the suction effect (after Spencer et al 2008)

The suction effect can occur in open water or in confined water such as at moorings. These forces are known to have pulled moored ships from the quay by causing mooring lines to part (Pinkster 2009).

In Figure 2-5 the forces, due to the suction effect, experienced by a moored ship during a passing ship event are described in six figures (Flory 2002). Using the logic outlined above in Figure 2-4 the forces given in Figure 2-5 can be derived. In image three, the stagger between the ships is $-0.4L_m$. Due to the suction zone of the passing ship being at the stern of the moored ship, and the pressure zone closer to the bow of the moored ship, the moored ship will experience a maximum negative surge force. In image four, the stagger between the ships is zero. The suction zone of the passing ship will be directly alongside the moored ship. The moored ship will thus experience a maximum positive sway force (Flory 2002).

Chapter 2: Literature Review



One ship length separation:

First Influence
 Small positive surge force
 Small negative sway force
 Essentially zero yaw moment

Bow to stern:

Small negative surge force
 Greatest negative sway force
 Small positive yaw moment

Almost bow to midship:

Greatest negative surge force
 Essentially zero sway force
 Greatest negative yaw moment

Side by side:

Essentially zero surge force
 Greatest positive sway force
 Essentially zero yaw moment

Almost stern to midship:

Greatest positive surge force
 Essentially zero sway force
 Greatest positive moment

Stern to bow:

Essentially zero surge force
 Small negative sway force
 Essentially zero yaw moment

Note:
 Passing and moored ship heading in the same direction

Figure 2-5: Interpretation of forces due to the suction effect during a passing ship interaction (after Flory 2002)

Wake wash was first described mathematically by William Thomson (Lord Kelvin) and is therefore also known as Kelvin ship waves. Wake wash waves are a combination of waves diverging off the sides of a passing ship and transverse waves that travel behind the ship (Figure 2-6). The diverging waves and transverse waves superimpose to form cusps on a locus line (UFC 2005). Wake wash cause very short waves in comparison with the suction wave and therefore has a lesser effect on large ships. Wake wash is usually more significant at higher speeds of the passing ship (Pinkster 2009).

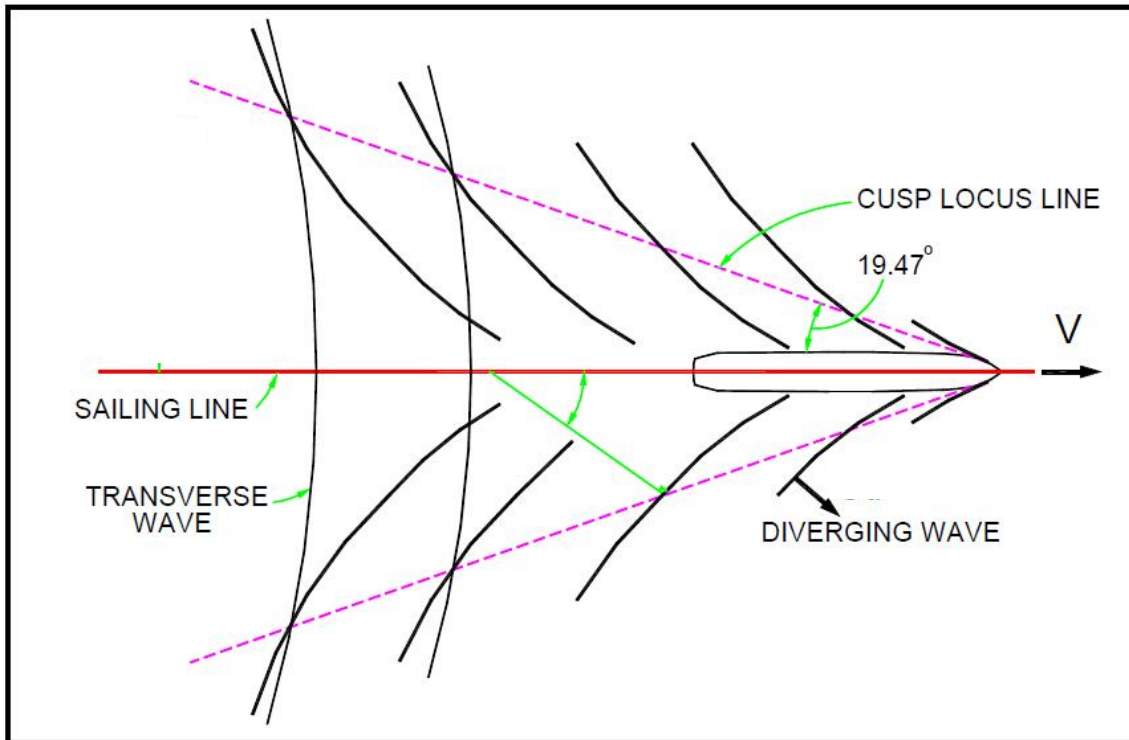


Figure 2-6: Wake wash waves (after USA Department of Defence 2005)

Large ships passing close to the entrances of docks can cause harbour oscillation and related ship motion problems due to either suction effects or wake wash waves (Pinkster 2009).

2.4 HISTORY OF PASSING SHIP ACCIDENTS

Ships in all ports experience the suction effect induced by passing ships. Where vessel size, passing distance and passing speed is combined in an unfavourable way, accidents can be expected to occur. Accidents can be defined as incidents where ship motions, due to a passing ship, cause the moored ship to break away from the quay or as events where ship motions, due to a passing ship, cause damage to ship loading equipment. A summary of a selection of documented passing ship accidents is given below.

On 20 September 1911 the Olympic, sister ship of the Titanic, collided with the HMS Hawke, a British Warship due to the passing ship effect (Colledge and Warlow 2006). The two ships were passing each other when the warship was pulled into the Olympic because of the suction effect of both vessels. Both vessels were seriously damaged. Figure 2-7 displays the damage to both ships after the accident.

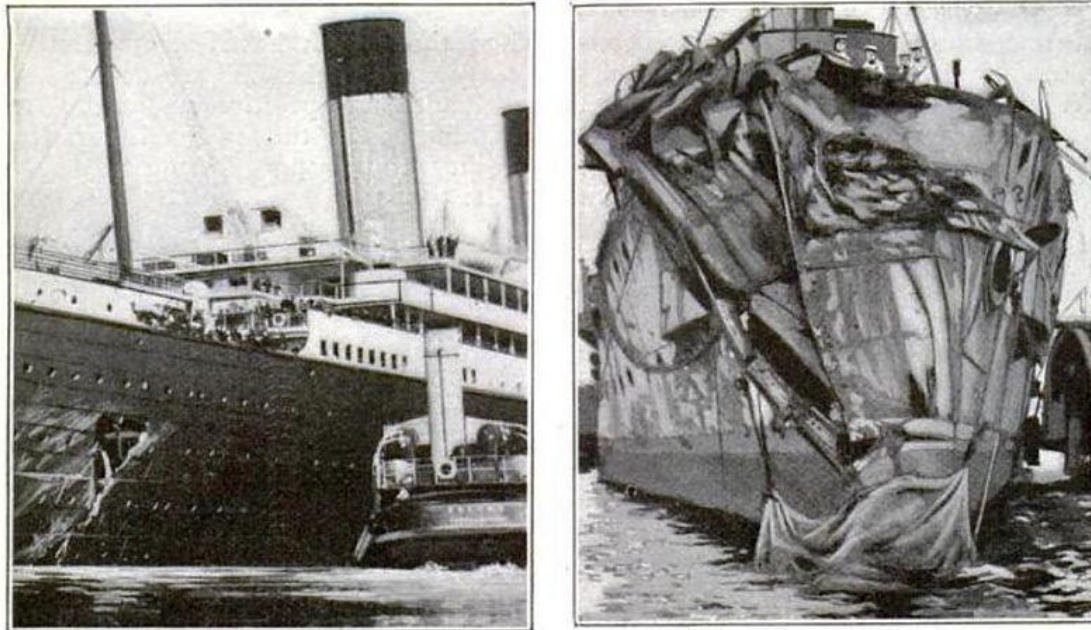


Figure 2-7: Above waterline damage to the Olympic (left) and damage to the HMS Hawke (right) due to a passing ship incident (Colledge and Warlow 2006)

On 2 April 1912 the passenger ship Titanic was leaving Southampton. As the Titanic passed a liner, New York, it was pulled from its mooring causing its mooring lines to part. Swift action by the captains of both ships and the assistance of a tug prevented a collision (Pinkster 2009). A photograph was taken from the Titanic during the incident and is presented in Figure 2-8.



Figure 2-8: Photograph taken from the Titanic during its incident with the New York (Pinkster 2009)

On 7 January 1976 the Queen Elizabeth caused various accidents in one incident (Seelig 2001). The Queen Elizabeth, which is 294m long, 32m wide and has a draft of 10m, passed about 500m from the Norfolk VA waterfront at a speed of 15 to 20 knots. It caused a floating dry dock to break three 3.5 inch mooring chains during which the ship in dock shifted on its

Chapter 2: Literature Review

blocks. Many mooring lines were snapped all along the quay and some pier piles were broken.

On 16 September 1990 tanker U.S. Jupiter was totally destroyed in a passing ship incident (Seelig 2001). A ship of 17,500 deadweight tonnes (dwt) (194m long) passed the 10,900 dwt tanker Jupiter (116m long) by about 20m. This caused breakage of the mooring lines and the discharge hose. Leaking fuel found an ignition source and resulted in the loss of a life and the total destruction of tanker Jupiter (Seelig 2001). A picture of the burnt out tanker Jupiter is presented in Figure 2-9.

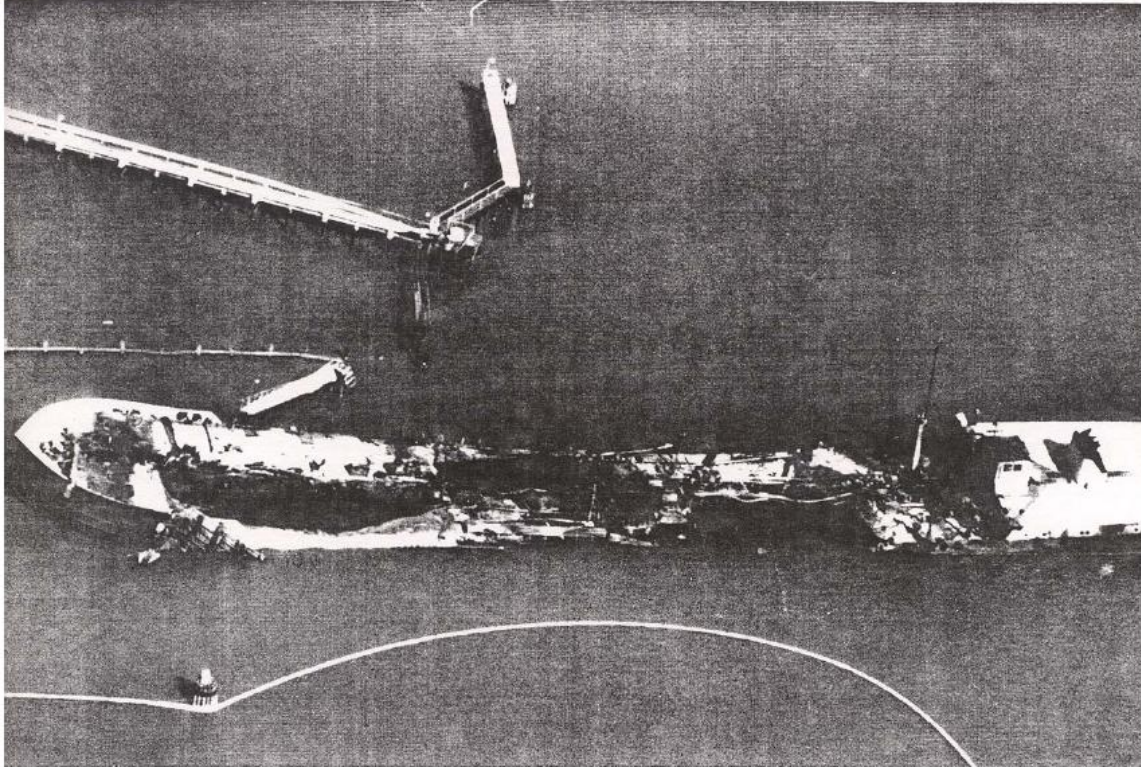


Figure 2-9: A burnt out tanker Jupiter following a passing ship accident (Seelig 2001)

In the 1990's two battleships moored at the Philadelphia Naval Shipyard experienced passing ship effects (Seelig 2001). The ships were moored side by side with more than twenty 2.5 inch chains. The ships experienced a surge of about 4m due to passing commercial ships. This accelerated the wear on mooring lines and bollards.

On 13 June 1998 passing ships in the Mississippi river caused the USNS Regulus and USNS Pollus, moored alongside each other, to surge severely (Seelig 2001). The surge caused a woman and a child to be severely hurt when they were run over by a 3000 pound gangway.

In 2006 the LNG carrier, Golar Freeze, was discharging at a new terminal on Elba Island Georgia. A passing tanker caused the LNG carrier to pull away from the jetty (Pinkster 2009). Due to the automatic disconnection of the cryogenic arms and the prompt reaction of tugs no LNG was spilled and damage to the ship and jetty was prevented.

Many ports experience this problem and increasing ship size and more congested waterways are expected to increase the risk of moored ship breakaways (Varyani and Vantorre 2006).

2.5 PASSING SHIP STUDIES

2.5.1 SUBSECTIONS OF PASSING SHIP STUDIES

Many passing ship studies have been done to assist the better prediction of passing ship forces. Passing ship force predictions can be based on prototype measurements, physical model measurements or mathematical methods as indicated in Figure 2-10. Mathematical methods can be empirical, semi-empirical or theoretical. Empirical methods are based purely on trends in observations of prototype or physical model measurements. Semi-empirical methods use some theoretical background to make a prediction, but are still corrected with empirically derived factors. Theoretical methods are based on mathematical solutions using assumptions about the characteristics of passing ship events. Theoretical methods can either be analytical, where an exact solution is calculated through the direct solution of the equations, or it can be solved numerically to find approximate, yet accurate solutions to the equations. Numerical methods are usually used where the equations are too intricate to be solved analytically.

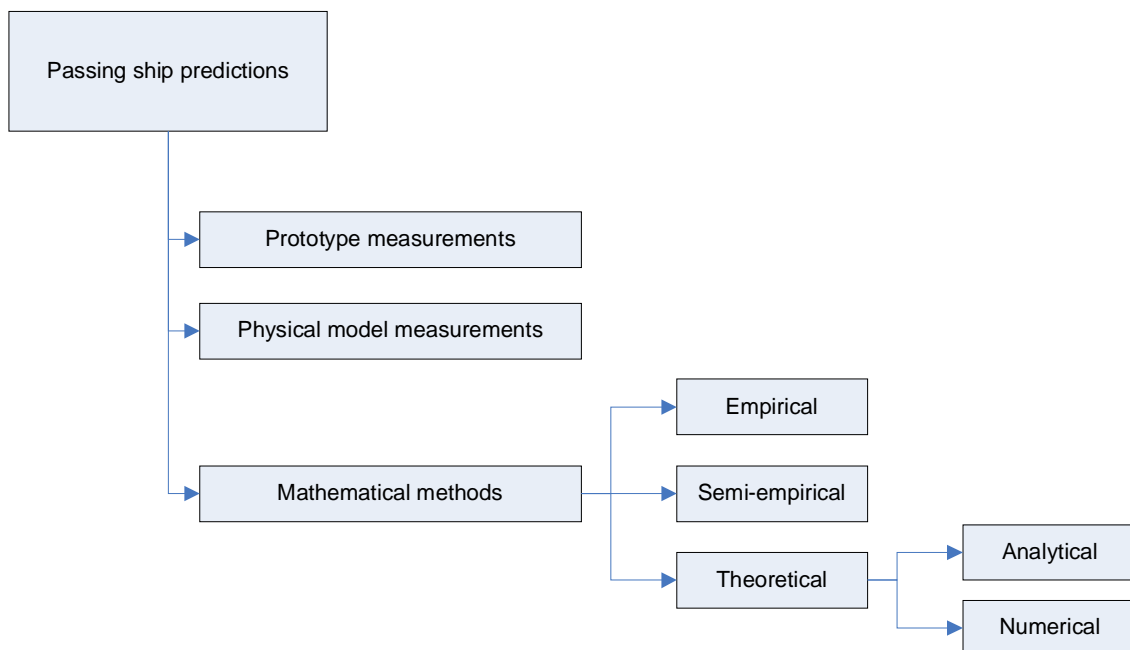


Figure 2-10: Subsections of passing ship force predictions

2.5.2 PASSING SHIP STUDIES PRE 2000

In the thirty years following World War 2, tanker size grew from 16,500 deadweight tonnes (dwt) to the heaviest ship to ever be built, the Knock Nevis of 564,736 dwt in 1979 (Woodman 1998). As the tankers grew in size, so did the interest in passing ship studies. Passing ships have been studied by field observations, prototype tests, scale tests and mathematical theories.

In 1974 Remery published the results of 1:60 scale model tests conducted to determine mooring forces induced by passing ships (Remery 1974). The passing ship size, passing speed and passing distance were varied and the depth draft ratio, heading and moored ship size were kept constant. The tests were done in unrestricted water with the ship moored alongside a jetty structure. His main findings were that the loads induced by the passing ship on the moored ship are proportional to the square of the speed of the passing ship. He also

found that the passing ship forces are related to the relative position between the vessels. Remery (1974) concluded that the stiffness of the mooring system has a considerable effect on the mooring forces. A stiffer system would result in smaller mooring forces. Refer to Figure 2-11 for a tanker passing a moored tanker in the physical model by Remery.

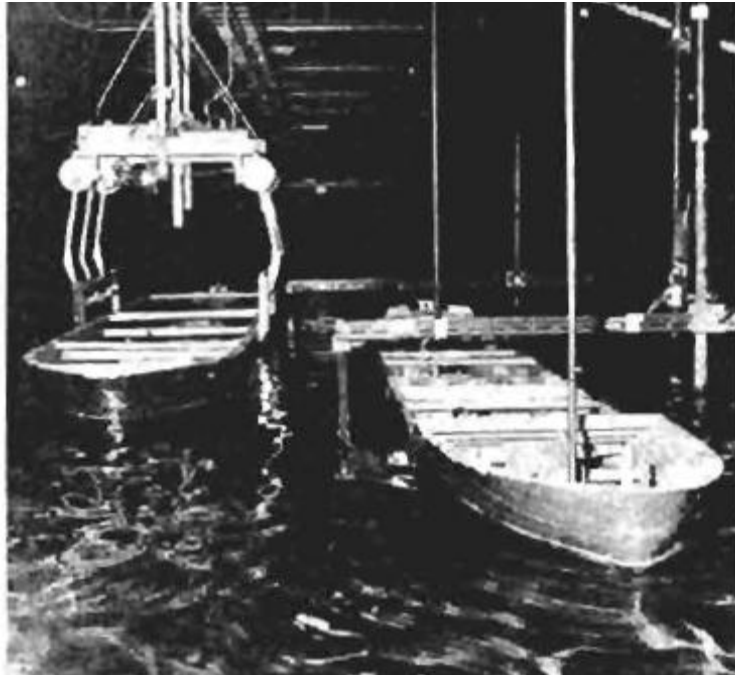


Figure 2-11: Set up of a test conducted by Remery (Remery 1974)

The results of similar tests of larger tankers were reported a year later by Muga et al (1975). The 1:68 scale model tests comprised one 250,000 dwt ship passing another at distances of 150 ft, 250 ft and 350 ft (45.7m, 76.2m and 106.7m). Speeds were varied between 4kt and 6kt. Underkeel clearance to draft ratios of 0.3, 0.1 and 0.06 were tested and tests were done for no current and a 2kt current. It was found that forces decrease with increase in separation distance, decrease with decreasing velocities, decrease with increasing underkeel clearance and increase with increasing vessel size

Muga et al (1975) developed a theoretical method for estimating forces and moments between two passing ships. This was done by simplifying the ship hulls with prismatic elliptic cylinders passing one another in an infinite ideal fluid. The theory did not take the under keel clearance of passing ships into account. The model testing results discussed above were used to find correction factors for under keel clearance. Their conclusions were that their theory provides an accurate prediction of the tested conditions. For accurate predictions the vessel's hull must be close to an elliptic cylinder, passing vessel speed must be sufficiently low to prevent the development of large wake waves and the ratio of absolute to relative velocities must be within certain limits (Muga et al 1975).

In 1975 Wang developed an accurate slender body numerical theory where the ship hulls are simplified by a slender body with a parabolic cross section. The method assumes the water is an infinite ideal fluid with the ship hulls seen as double bodies moving through the infinite space. If the infinite space would be cut on the water surface, two mirror images of the ships and their semi-infinite water depth would result. This means that a rigid water level is assumed. Wang derived equations that could be solved for many steps during a passing ship event for surge, sway and yaw. For shallow water, empirical correction factors were calculated to take the effect of underkeel clearance into account (Wang 1975). The deepwater equations are presented in Equation 2-1, Equation 2-2 and Equation 2-3. The

Chapter 2: Literature Review

equations of Wang can be solved numerically by applying double Simpson integration over a rectangle.

Equation 2-1: Deep water surge force (Wang 1975)

$$F_{X_WANG}(\xi, \eta) = \frac{\rho V^2}{2\pi} \int_{Lm} S_1'(x_1) \int_{Lp} \frac{S_2^1(x_2)(x_2 - x_1 + \xi) dx_2}{[(x_2 - x_1 + \xi)^2 + \eta^2]^{3/2}} dx_1$$

Equation 2-2: Deep water sway force (Wang 1975)

$$F_{Y_WANG}(\xi, \eta) = \frac{\rho V^2 \eta}{\pi} \int_{Lm} S_1'(x_1) \int_{Lp} \frac{S_2'(x_2) dx_2}{[(x_2 - x_1 + \xi)^2 + \eta^2]^{3/2}} dx_1$$

Equation 2-3: Deep water yaw moment (Wang 1975)

$$M_{Z_WANG}(\xi, \eta) = \frac{\rho U^2 \eta}{\pi} \int_{Lm} [S_1'(x_1)x_1 + S_1(x_1)] \int_{Lp} \frac{S_2'(x_2) dx_2}{[(x_2 - x_1 + \xi)^2 + \eta^2]^{3/2}} dx_1$$

Symbols used in Equation 2-1 to Equation 2-3:

F_{X_WANG}	Surge force	[N]
F_{Y_WANG}	Sway force	[N]
M_{Z_WANG}	Yaw moment	[Nm]
ξ	Centre to centre stagger between the ships	[m]
η	Centre to centre lateral distance between the ships	[m]
ρ	Water density	[kg/m ³]
V	Passing speed	[m/s]
Lm	Length of the moored ship	[m]
Lp	Length of the passing ship	[m]
$S_1(x_1)$	Moored ship parabolic sectional area distribution	
$S_2(x_2)$	Passing ship parabolic sectional area distribution	

After the preliminary work done by Remery (1974), Muga et al (1975) and Wang (1975), passing ship research did not receive much attention for many years.

2.5.3 PASSING SHIP STUDIES POST 2000

Since 2000 passing ship effects received renewed attention and knowledge in all subclasses of passing ship studies have been extended.

Using the model studies of Remery (1974), Muga et al (1975) and Lean et al (1977), John F Flory developed simple empirical formulae for passing ships. The empirical formulae calculated forces and moments by using the passing ship velocity, displacement ratio and separation ratio of the two ships. The forces and moments could then be subsequently scaled to the right ship length and corrected for the underkeel clearance. The formulae for calculating the forces by the Flory method are presented in Equation 2-4, Equation 2-5 and Equation 2-6. Flory produced typical normalized graphs, with peak maxima equal to one, which could be multiplied by the maximum forces to obtain force against ship stagger graphs. Figure 2-12 presents the normalized surge force graph with the ship stagger on the

Chapter 2: Literature Review

x-axis given in characteristic lengths. More information of Flory's method was published in his papers (Flory 2001 and Flory 2002).

Equation 2-4: Surge force (Flory 2002)

$$F_{X_MAX_FLORY} = 1.5 \times 10^{-5} L_m^2 e^{\left(0.0955 - \frac{0.6367d}{D}\right)} V_p^2 [0.171 + 0.134 \ln(\Delta_D) - \{0.71 + 0.28 \ln(\Delta_D)\} \ln(\Delta_S - 0.06)]$$

Equation 2-5: Flory sway force (Flory 2002)

$$F_{Y_MAX_FLORY} = 1.5 \times 10^{-5} L_m^2 e^{\left(0.5157 - \frac{3.348d}{D}\right)} V^2 [e^{(1.168\Delta_R - 2.25)} - \{4.41 + 1.93 \ln(\Delta_R)\} \ln(\Delta_S)]$$

Equation 2-6: Yaw moment (Flory 2002)

$$M_{Z_MAX_FLORY} = 59 \times 10^{-9} L_m^3 e^{\left(0.343 - \frac{2.288d}{D}\right)} V^2 [e^{(-0.47\Delta_D + 2.651)} - \{171.9 + 51.4 \ln(\Delta_D)\} \ln(\Delta_S - 0.06)]$$

Symbols used in Equation 2-4 to Equation 2-6:

$F_{X_MAX_FLORY}$	Surge force	[N]
$F_{Y_MAX_FLORY}$	Sway force	[N]
$M_{Z_MAX_FLORY}$	Yaw moment	[Nm]
L_m	Length of the moored ship	[m]
V	Passing speed	[m/s]
Δ_D	Displacement ratio	[-]
Δ_S	Separation ratio	[-]

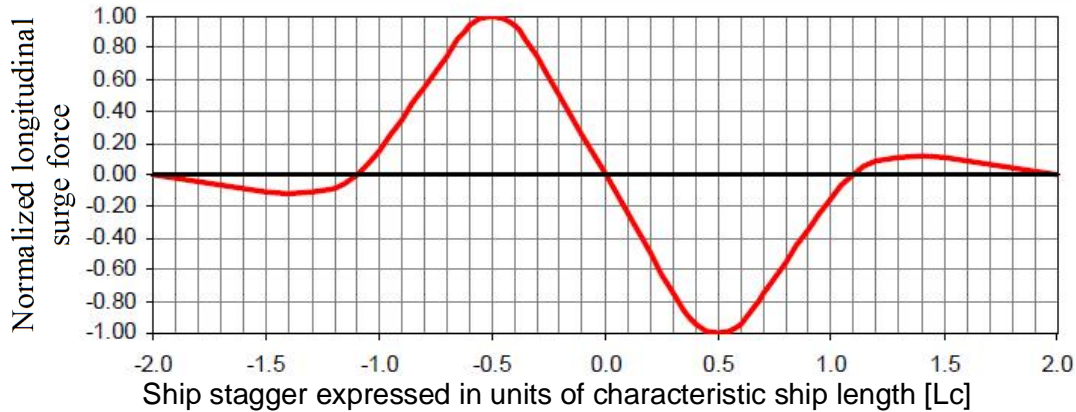


Figure 2-12: Normalized surge force (Flory 2002)

Seelig developed shallow water correction factors, Equation 2-7 and Equation 2-8, to be applied to the theory of Wang (Seelig 2001). The shallow water correction factors were calculated from physical model results of Remery (1974), Muga et al (1975) and Cohen et al (1983). This method will be referred to as the Wang Seelig method. Seelig created the commercial software, Passmoor, based on the Wang Seelig method. More information about the Wang Seelig method and Seelig's correction factors can be found in his paper (Seelig 2001).

Equation 2-7: Shallow water correction factor for Wang deepwater surge force (Seelig 2001)

$$CF_{X_SEELIG} = 1 + 16(D/d)e^{(-0.08((G/B_m)-3.5)^2)}$$

Equation 2-8: Shallow water correction factor for Wang deepwater sway force and yaw moment (Seelig 2001)

$$CF_{Y_SEELIG} = CM_Z = 1 + 25(D/B_m)^{-0.35} (D/d)^4 e^{(-0.08((G/B_m)-3.3)^2)}$$

Symbols used in Equation 2-7 to Equation 2-8:

CF_{X_SEELIG}	Correction factor for Wang surge force	[-]
CF_{Y_SEELIG}	Correction factor for Wang sway force	[-]
CM_Z	Correction factor for Wang yaw moment	[-]
D	Ships draft	[m]
d	Water depth	[m]
B_m	Beam of the moored ship	[m]
G	Board to board distance between the ships	[m]

In 2001 a paper was published about passing ship model studies done at Flanders hydraulics in Antwerp, Belgium. Numerous model tests have been carried out at Flanders Hydraulics on a 1:75 scale in a 7m wide channel for different types of ships. Speed, passing distance, ship sizes and depth draft ratios were varied (Vantorre et al 2001). Tests were done on a container ship, a bulk carrier and tankers. All combinations of these ships except for combinations of the same ship were tested. Data of a 214,000 dwt tanker passing a 145,000 dwt bulk carrier was obtained from Prof M. Vantorre of Flanders University. In the set of 10 tests the speed was kept constant at 8kt and the passing distance at 75.6m. The depth was varied between 18.63m, 23.04m and 17.08m. The draft of the tanker was varied between 15.53 and 19.2m and the draft of the bulk carrier was varied between 13.5m and 15m. All tests were one for ships in the same and opposite directions. Vantorre concluded that passing ship forces increased significantly with an increase in the moored ship draft, increase significantly with a decrease in passing ship draft and decrease with increase in passing distance. For passing distance wake wash can have an effect with large or very small passing distance (Vantorre et al 2001). Table 2-2 summarizes the ship characteristics of the Flanders data.

Table 2-2: Ship characteristics of Flanders model

Name			Passing Ship		Moored Ship	
			E (tanker)	E (tanker)	C (bulk carrier)	C (bulk carrier)
Displacement	Δ	t	128538	145193	170039	213639
Length between perpendiculars	LBP	m	298.8	298.8	286.8	286.8
Beam	B	m	37.8	37.8	46.8	46.8
Draft	D	m	13.5	15	15.53	19.2

Pinkster developed a double body flow model representing the ship hull with panels. He modified the model to take free surface effects into account (Pinkster 2004). Figure 2-13 presents the setup of a double body panel model. He concluded that a normal double body model is sufficient where ships are moored at open jetties and long straight quay walls.

However at complex harbour geometries free surface effects should be included into the calculations. He also concluded that for complex harbour geometries the numerical model should still be validated against physical model results. When a ship is moored at a vertical quay, the surge forces are about 80% larger and the sway force and yaw moment is about 60% smaller (Pinkster 2004). He advised that for quay walls, channels and complex harbour geometries, open water model data should not be used.

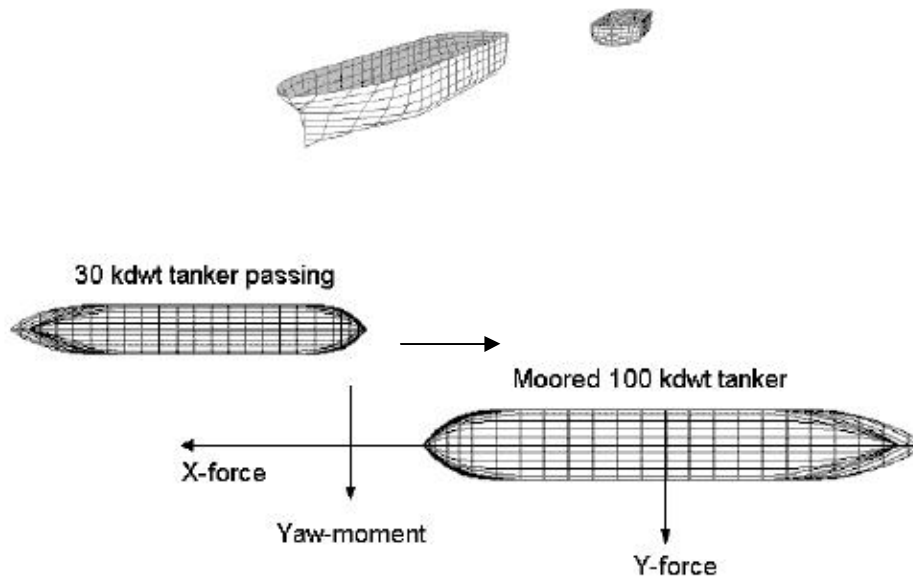


Figure 2-13: Setup for passing ship computations using a panel model (Pinkster 2004)

In 2005 results of 1:135 scale model tests were published by David Kriebel (Kriebel 2005). The speed, passing distance, passing ship size and depth draft ratios were varied. Tests were done mainly for parallel passing ships and a limited number of tests were done at 45° and 90°. Kriebel used generic series 60 hulls for all his tests and recommended that additional tests should be done to determine the effect of real hull shapes. Kriebel concluded that the correction factors derived by Seelig consistently under predicted the mooring forces if compared to his tests. Kriebel derived new shallow water correction factors from his model tests. The new shallow water correction factors could be applied to the Wang deep water forces. This method is from now on referred to as the Wang Kriebel method. The commercial software created by Seelig, Passmoor, was subsequently updated to use the Wang Kriebel method instead of the Wang Seelig method. The shallow water correction factors are presented in Equation 2-9, Equation 2-10 and Equation 2-11. Kriebel also derived empirical formulae from his data. The empirical formulae are presented in Equation 2-12, Equation 2-13 and Equation 2-14.

Equation 2-9: Shallow water correction factor for Wang deep water surge force (Kriebel 2005)

$$CF_{X_KRIEBEL} = 1 + 1.70e^{(2.94(d/D))} e^{(-0.08((G/B_m)-3)^2)}$$

Equation 2-10: Shallow water correction factor for Wang deep water sway force (Kriebel 2005)

$$CF_{Y_KRIEBEL} = 1 + 0.52e^{(4.33(d/D))} e^{(-0.08((G/B_m)-2)^2)}$$

Equation 2-11: Shallow water correction factor for Wang deep water yaw moment (Kriebel 2005)

$$CM_{Z_KRIEBEL} = 1 + 0.48e^{(3.87(d/D))} e^{(-0.08((G/B_m)-2)^2)}$$

Symbols used in Equation 2-9 to Equation 2-11:

$CF_{X_KRIEBEL}$	Correction factor for Wang surge force	[-]
$CF_{Y_KRIEBEL}$	Correction factor for Wang sway force	[-]
$CM_{Z_KRIEBEL}$	Correction factor for Wang yaw moment	[-]
D	Ships draft	[m]
d	Water depth	[m]
G	Board to board lateral distance between the ships	[m]
B_m	Beam of the moored ship	[m]

Equation 2-12: Kriebel surge force empirical equation (Kriebel 2005)

$$F_{X_KRIEBEL} = \frac{1}{2} \rho D L m V^2 0.0074 \Delta_D e^{2.6(D/d)} e^{-1.5(\Delta_S)}$$

Equation 2-13: Kriebel sway force empirical equation (Kriebel 2005)

$$F_{Y_KRIEBEL} = \frac{1}{2} \rho D L m V^2 0.0126 \Delta_D e^{3.6(D/d)} e^{-2.0(\Delta_S)}$$

Equation 2-14: Kriebel yaw moment empirical equation (Kriebel 2005)

$$M_{Z_KRIEBEL} = \frac{1}{2} \rho D L m^2 V^2 0.0044 \Delta_D e^{3.2(D/d)} e^{-3.4(\Delta_S)}$$

Chapter 2: Literature Review

Symbols used in Equation 2-9 to Equation 2-11:

$F_{X-_KRIEBEL}$	Surge force (negative peak)	[N]
$F_{Y+_KRIEBEL}$	Sway force (positive peak)	[N]
$M_{Z-_KRIEBEL}$	Yaw force (negative peak)	[Nm]
ρ	Water density	[kg/m ³]
D	Ships draft	[m]
d	Water depth	[m]
L_m	Length of the moored ship	[m]
V	Passing speed	[m/s]
Δ_D	Displacement ratio	[-]
Δ_S	Separation ratio	[-]

In the Port of Brisbane, Differential Global Positioning System (DGPS) measurements were taken at the bow and stern of a moored vessel while a ship was passing by 96m at 7kt. The tonnages of the moored and passing ships were 42,564 dwt and 34,777 dwt respectively. A peak to peak surge of 1.25m was measured. The start and end positions of the vessel were not the same due to fender friction. Physical model tests were done with similar conditions, but unfortunately measurements or a comparison between the two are not available (Savioli et al 2005).

Varyani and Vantorre developed a numerical calculation method for determining forces due to passing ships. It was based on an analytical slender body theory that calculates velocity potentials similar to the theory of Wang (1975). The results were validated with numerous physical model tests. Where calculated and measured results did not match, correction factors were applied to the calculated results. The validated and corrected numerical results were used to produce a database of conditions with a wide range of parameters. At last a set of semi-empirical formulae were developed by using the database (Varyani and Vantorre 2006). The method is presented in Equation 2-15 and Equation 2-17.

Equation 2-15: Formulae for the determination of surge force using the Varyani method (Varyani and Vantorre 2006)

$$F_{X_V\&V} = 0.072 \sin[0.85\pi(\xi'-0.05)]e^{-0.98\xi'^2} (1 - 0.25\xi') \times$$

$$A(\xi') \left[\frac{d/D}{1.5} \right]^{-1.0} \left[2 \frac{\eta}{L_m} \right]^{-1.3} \left[\frac{L_m}{L_p} \right]^{-4.1} \times \left(\frac{1}{2} \rho V^2 B_m D_m \right)^{-1}$$

$$A(\xi') = 1 - ae^{-b(\xi'-\xi_0+\Delta)^2}$$

$$\xi' = 2\xi / (L_m + L_p)$$

Equation 2-16: Formula for the determination of sway force using the Varyani Vantorre method (Varyani and Vantorre 2006)

$$F_{Y_V\&V} = 0.14 \cos(0.85\pi\xi') e^{-0.98\xi'^2} (1 - 0.25\xi') \times \left[\frac{d/D_m}{1.5} \right]^{-1.0} \left[2 \frac{\eta}{L_m} \right]^{-1.3} \left[\frac{L_m}{L_p} \right]^{-4.1} \times$$

$$\left(\frac{1}{2} \rho V^2 B_m D_m \right)^{-1}$$

$$A(\xi') = 1 - a e^{-b(\xi' - \xi'_0 + \Delta)^2}$$

$$\xi' = 2\xi / (L_m + L_p)$$

Equation 2-17: Formula for the determination of yaw moments using the Varyani Vantorre method (Varyani and Vantorre 2006)

$$M_{Z_V\&V} = 0.05 \sin[0.95\pi(\xi' - 0.05)] e^{-0.98\xi'^2} (1 - 0.25\xi') \times$$

$$A(\xi') \left[\frac{d/D_m}{1.5} \right]^{-1.0} \left[2 \frac{\eta}{L_m} \right]^{-1.3} \left[\frac{L_m}{L_p} \right]^{-4.1} \times \left(\frac{1}{2} \rho V^2 B_m D_m \right)^{-1}$$

$$A(\xi') = 1 - a e^{-b(\xi' - \xi'_0 + \Delta)^2}$$

$$\xi' = 2\xi / (L_m + L_p)$$

Symbols used in Equation 2-15 to Equation 2-17:

$F_{X_V\&V}$	Surge force	[N]
$F_{Y_V\&V}$	Sway force	[N]
$M_{Z_V\&V}$	Yaw force	[Nm]
ρ	Water density	[kg/m ³]
D_m	Ships draft	[m]
d	Water depth	[m]
L_m	Length of the moored ship	[m]
L_p	Length of the passing ship	[m]
V	Passing speed	[m/s]
B_m	Beam of the moored ship	[m]
ξ	Centre to centre stagger distance between the ships	[m]
ξ'	Non dimensional stagger	[-]
$A(\xi')$	Filter function	[-]

Measurements of water levels and current speeds were taken at two locations for the validation of a numerical model. The first were taken in the inner harbour waterway at the Port of Oakland, USA, for four high speed ferries. The second set of tests in the Mississippi river gulf outlet was taken for a passing general cargo carrier (Fenical et al 2006).

In 2007 high accuracy DGPS measurements were taken from a moored bulk carrier while being passed at a Port Hedland iron ore terminal in Australia. The results were compared with calculations with OMC's SPMS numerical modelling package. SPMS is based on potential flow theory (O' Brien and Hens 2007). Unfortunately the measurements are not

freely available. Figure 2-14 displays a passing event at Port Hedland (O' Brien and Hens 2007).



Figure 2-14: A passing event being measured at Port Hedland (O' Brien and Hens 2007)

Huang and Chen (2007) presented a Reynolds Averaged Navier Stokes (RANS) based Computational Fluid Dynamics (CFD) method for estimating passing ship forces. The model takes into account free surface effects, vorticity, viscous flow physics, exact basin boundaries as well as mooring conditions. The model requires complicated model input and uses a large amount of computing power, but it is currently the most detailed method for computing passing ship effects.

In 2008 van Wijhe and Pinkster carried out 1:38.2 scale model tests for a 12500 twenty foot equivalent unit (TEU) container ship passing a Panamax container ship in a 600m wide channel. Speed, passing distance, depth draft ratio and drift angle were varied throughout the tests (Van Wijhe and Pinkster 2008). Van Wijhe and Pinkster concluded that passing ship forces increase with increasing passing velocity, increase with decrease in passing distance and decrease with an increase in water depth. Decreasing the draft of the passing vessel reduces forces on the moored ship and drifting due to currents or wind significantly increases forces on the moored ship.

A paper describing the latest software developed at the CSIR was released in 2010 (van der Molen et al 2010). The computer program, Passcat, was described. Passcat calculates hydrodynamic forces on a moored ship due to a passing ship. Passcat is a double body potential flow model similar to the basic double body model by Pinkster (2004).

A joint industry project, Research on Passing Effects on Ships (ROPES), was started in November 2010 and was planned to span over three years (Marin 2010). The objectives of ROPES are to develop, validate and deliver a computer tool to predict the effects of passing ships. The project will also investigate the feasibility of passive and active concepts to restrict ship motions and mooring loads (Marin 2010).

2.6 SHORTCOMINGS IN PASSING SHIP STUDIES

There are limitations to knowledge from existing passing ship studies. Some of the limitations are discussed below.

The increase in container traffic has led to larger container ships. The Maersk E series of ships has a carrying capacity, based on the standard capacity definition, of 14,770 TEU. These ships have a length of 397m a beam of 56m and a draft of 15.5m. With a deadweight tonnage of 157,000, these ships are still much smaller than the 300,000 dwt tankers and bulk carriers. There are speed limits in ports, but with container ships having more powerful engines than bulk carriers, there is a higher risk of speeding container ships. Most of the past studies have focused on tankers and more information is needed to know whether the same theories apply to passing container ships.

Most of the previous model tests have been done for open pier structures. The amount of tests with quay walls or confined channels is very limited. Of the available tests one was done for a ship at a quay and in a channel. Since many ships are moored against quay walls and often in channels, physical model tests with quay walls and channels would be useful for determining the agreement of mathematical models with physical model measurements.

For deep water conditions theoretical time histories compare reasonably well with experimental time histories, but in calculations under shallow water conditions, there are often discrepancies. The discrepancies are caused by assumptions made to simplify the calculation methods. The assumptions neglect some of the influences when they become critical in shallow water conditions.

The empirical methods by Flory and Seelig were both derived from the model tests on tankers by Remery (1974) and Muga & Fang (1975). The two sets of tests were very similar. These two empirical models need to be compared with model tests of ships other than tankers to determine whether they still apply.

Kriebel used generic Series 60 hull forms, with high block coefficients at a scale of 1:135. The hulls do not represent any real ship hull and the scale was smaller than previous physical model studies. The empirical model and shallow water correction factors by Kriebel need to be tested against physical model tests of a passing container ship to verify whether it can be applied to passing container ships.

Potential flow models appear to give good estimations of passing ship forces for large bulky ships in simple harbour geometries (Pinkster 2004). It is unclear whether the same applies to slender container ships.

From the above considerations it is clear that more tests of container ships passing bulk carriers need to be done to extend the existing knowledge to more slender ships. From the results of such a study a potential flow model need to be validated for slender container ships. It will also be useful to assess whether empirical and semi empirical methods, derived from tests with bulky ships, can be applied to slender container ships. The objectives of this study, as given in Chapter 1.2, aim to reach the above.

2.7 FLOW DYNAMICS

Fluids can be subdivided into gases and liquids. Liquids are relatively incompressible while gases are relatively compressible. The behaviour of fluids is generally influenced by viscosity, surface tension and bulk modulus (a measure of compressibility).

To simplify flow dynamics calculations the concept of an ideal fluid has been developed. In an ideal fluid, the flow is inviscid, incompressible, homogeneous and has no surface tension. For an ideal fluid, flow patterns can be visualized by drawing streamlines that follow the direction of velocity vectors. Flows that can be represented by streamlines are known as potential flows or ideal flows and are described in Chadwick et al (2006). Potential flows are only applicable to ideal fluids and are irrotational. The flow can be described by means of a velocity potential ϕ (Equation 2-18), which is defined such that the gradient of the velocity potential is equal to the flow velocity V .

Equation 2-18: Velocity potential function (Chadwick et al 2006)

$$\frac{d\phi}{dL} = V$$

$$\phi = \int V dL$$

Symbols:

ϕ	Velocity potential	
L	Length (dimension)	[m]
V	Speed	[m/s]

The shape of very small waves is dominated by surface tension. Waves dominated by surface tension, or capillary waves described by the USA Department of the Interior (1980). Since very small waves do not have any significant effect on ship motions (Journ e et al 2001), it is safe to disregard surface tension effects in a model.

The compressibility of a fluid has an effect when there are very high differences in pressures and temperatures in the water. Ships create waves with a small wave height, and therefore do not produce very high pressure differences in the water. For this reason, the compressibility of the water has a negligible effect and can be assumed not to occur.

The Reynolds number is the ratio of inertia force to viscous force (Equation 2-19). A very high Reynolds number indicates that inertia forces dominate. If inertia forces dominate significantly, it is safe to assume that viscous forces will not have an effect and that flow is irrotational.

Equation 2-19: Reynolds number

$$Re = \frac{\rho VL}{\mu} = \frac{VL}{\nu}$$

Chapter 2: Literature Review

Symbols

Re	Reynolds number	[-]
ρ	Density of liquid	[kg/m ³]
V	Velocity	[m/s]
L	Length	[m]
μ	Absolute viscosity	[kg/m s]
ν	Kinematic viscosity	[m ² /s]

A boundary layer exists at all the boundaries of objects moving in real fluids and therefore the common assumption that the flow is irrotational and that viscosity of the water can be neglected can cause errors.

The boundary layer will start as a laminar flow under shear, but will eventually develop into a turbulent boundary layer (Chadwick et al 2006). For flat plates, the laminar boundary layer thickness can be calculated with the Blasius formula (Equation 2-20) and the turbulent boundary layer thickness with the Schlichting formula (Equation 2-21). The transition point (x_{crit}), where the laminar boundary layer will become turbulent, is where the Reynolds number becomes 3×10^5 (Schlichting 2003). Figure 2-15 illustrates the transition between the laminar and turbulent boundary layers.

Equation 2-20: Blasius laminar boundary layer (Schlichting 2003)

$$\delta_{BLASIUS} \approx 4.91x Re^{-0.5}$$

Symbols:

δ	Boundary layer thickness	[m]
x_b	Distance downstream from the start of the boundary layer	[m]
Re	Reynolds number	[-]
ρ	Density of fluid	[kg/m ³]
V	Velocity	[m/s]
μ	Absolute viscosity	[kg/m s]

Equation 2-21: Schlichting turbulent boundary layer (Schlichting 2003)

$$\delta_{SCHLICHTING} \approx 0.37x Re^{-0.2}$$

Symbols:

δ	Boundary layer thickness	[m]
x_b	Distance downstream from the start of the boundary layer	[m]
Re	Reynolds number	[-]

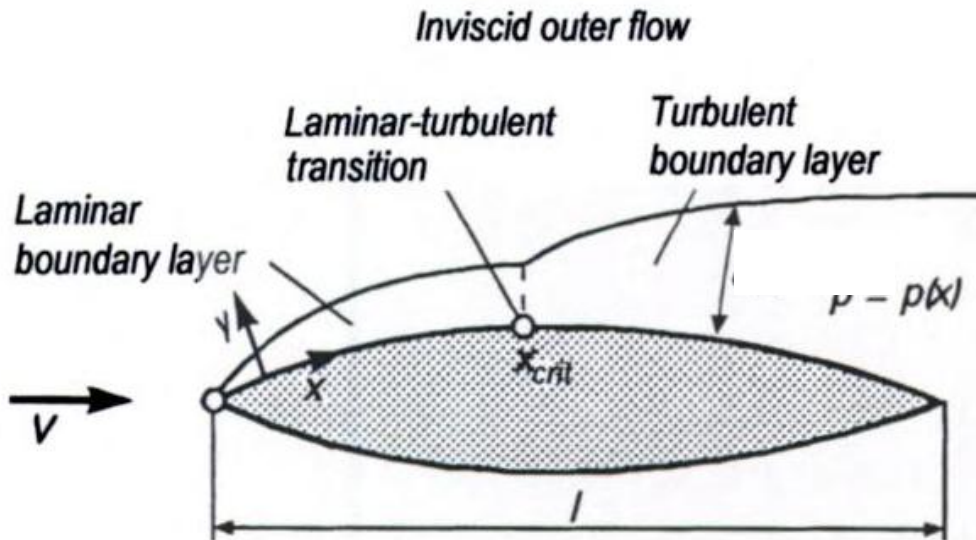


Figure 2-15: Development of the boundary layer at an airfoil (Schlichting 2003)

At some point, the flow might reverse to flow against the global pressure gradient. This occurrence is called flow separation. Flow separation is initiated by high local pressure gradients. Local pressure gradients remain low with streamlined objects, and the flow remains attached, but with non-streamlined objects, the flow will separate. Since laminar boundary layers are thinner than turbulent boundary layers, laminar boundary layers have a higher pressure gradient. Due to the higher pressure gradient in laminar boundary layers, they cause an earlier onset of flow separation (Webber 1974). Flow separation causes higher drag forces on objects in a fluid (Schlichting 2003). The larger drag forces cause more disturbance of the fluid, or larger waves and currents generated by a moving ship.

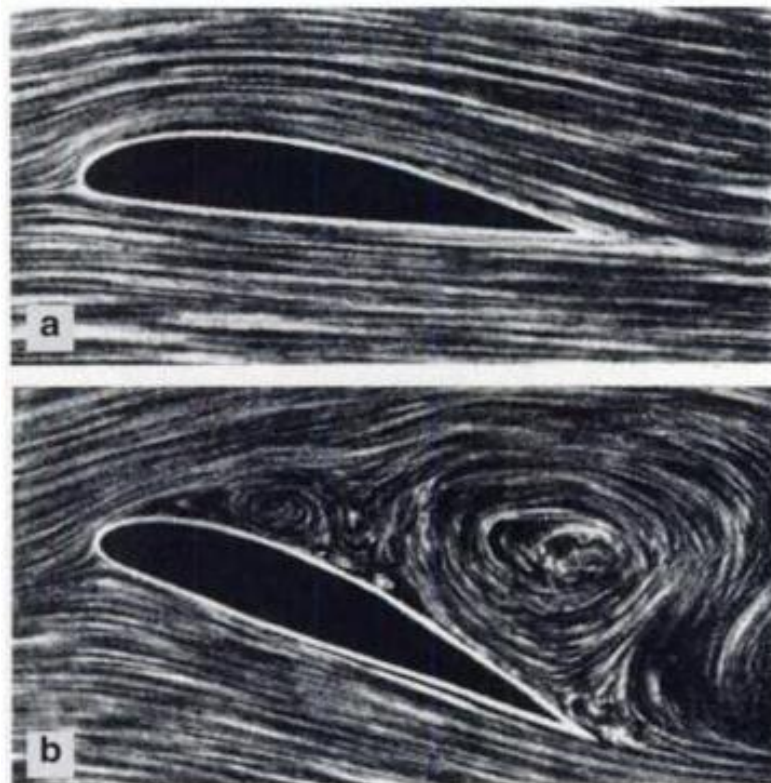


Figure 2-16: Flow past an airfoil, (a) attached flow, (b) separated flow (Schlichting 2003)

Numerical models make simplifying assumptions about the real fluid dynamics to enable faster computation time. These simplifying assumptions can cause that real fluid effects like boundary layers are not taken into account leading to subsequent inaccuracies in numerical model results.

2.8 SUMMARY AND CONCLUSIONS

2.8.1 PHYSICAL MODEL STUDIES

Physical model test data is available through conference papers. The data of Remery (1974), Muga et al (1975), Cohen and Beck (1983), Vantorre (2001), Kriebel (2005) and some data of van Wijhe & Pinkster (2008) is available. Unfortunately all the data is either for bulk carriers and tankers or does not apply to the case where a container ship passes a moored bulk carrier. The available physical model data includes tests for bulk carriers and tankers between 30,000 dwt and 250,000 dwt for passing and between 100,000 dwt and 250,000 dwt for moored ships.

The conclusions drawn from different physical model studies all point to the same characteristics of passing ship interactions. Various authors have found that passing ship forces are proportional to the square of the passing speed even though the conclusion was based on physical model results with a narrow band of passing speeds (Pinkster 2004). Some intuitive conclusions include that the use of larger ships, or the increase in the draft of either the passing or the moored ship, increases the passing ship forces. Another conclusion is that passing ship forces increase with a decrease in passing distance (Vantorre 2001). By confining the water around the ships by decreasing underkeel clearance or by using channels, the passing ship forces are increased (Muga 1975). Passing ship forces increase significantly if the passing ship sails at a drift angle due to side currents or winds (van Wijhe et al 2008).

The focus of many physical model studies was passing bulk carriers in open water or at piled jetties. Only a few physical model studies have been done on quay walls or channels. Many of the studies were done in narrow towing tanks. Where the tank boundary walls are close to either the passing ship or the moored ship, measurements will be influenced due to the water flow being affected. At small scales, scaling effects or modelling inaccuracies can have an effect on the results. It is unavoidable to select a small scale when a large number of tests need to be done without a large project cost. Most physical models reported above selected small scales. The authors named above did not raise major concerns about scaling effects; however, scaling effects can not be ignored when working with physical models. Due to the growth in container ship sizes, the need for physical model data with passing container ships is also growing. New physical model data needs to address container ships in especially confined water since this is where most accidents occur.

2.8.2 PROTOTYPE MEASUREMENTS

The results of three prototype measurements of passing ship events are available from three different sources. These tests were not done on resultant forces on ships, but on either water levels and currents or on ship motions. Of the prototype measurements of ship motions the mooring conditions are not known and resulting forces can therefore not be calculated. The existing prototype measurements are thus unsuitable for comparison with physical and mathematical models.

2.8.3 EMPIRICAL AND SEMI-EMPIRICAL MODELS

There are several empirical and semi-empirical methods available for estimating passing ship forces. Among empirical methods there are the method of Flory (2001) and Kriebel (2005) and among semi-empirical methods there are Wang (1975) and Seelig (2001), Wang (1975) and Kriebel (2005) and the method of Varyani and Vantorre (2006).

The method of Flory (2001) was developed on the model tests of Remery (1974) and Muga et al (1975). Seelig (2001) derived shallow water correction factors to be applied to the theoretical model of Wang (1975). The shallow water correction factors were derived from Remery (1974) and Muga et al (1975). Kriebel (2005) derived shallow water correction factors to be applied to the theoretical model of Wang (1975) and also created an empirical model from his physical model tests. Varyani and Vantorre calibrated a numerical model for a wide range of variables. The model was calibrated for different ship types and a large range of different variables. The calibrated model was then used to calculate a database of passing ship conditions. From this database Varyani and Vantorre created their semi-empirical model.

All the available empirical or semi-empirical models were either based on model test results of tankers or on a combination of the tanker test data and slender body theory. Only the method by Kriebel was not using the tanker data, but used tests with series 60 hulls. Furthermore all the methods were derived for open water conditions. Concerns exist about all the empirical or semi-empirical models on their applicability to confined water. Concerns also exist about their applicability to passing container vessels.

2.8.4 NUMERICAL MODELS

Theoretical models can be divided into slender body models, where the ship is represented by an approximation, and panel models where the ship hull is closely modelled with a fine 3D mesh. Due to the more accurate description of the ship hull, panel models provide more accurate solutions. Panel models use more computing effort and for this reason slender body models have been more popular in the past. With faster computers, panel models have become more popular since they are easy to set up, while providing acceptable answers for confined water. Wang (1975) developed a slender body model that approximates ship hulls with a parabolic cross section. It provides good answers for deep water conditions, but for shallow water, empirically derived correction factors have to be used. Passcat, similar to a model by Pinkster (2004) is a panel model based on potential flow theory. Potential flow does not take the free surface effects into account, but still provide good answers for many passing ship conditions including confined water (Pinkster 2004). Pinkster modified his potential flow model to also take free surface effects into account. This model proved to accurately predict more complicated harbour geometries and the effect of basin oscillation, but he also concluded that models should still be calibrated with physical model data. Huang and Chen (2003) used a RANS CFD model for passing ships that takes the effect of vorticity, viscosity and the free surface into account. This model is complicated to set up and requires long computing times, but produces very good answers in complex basins.

A study was done with Pinkster's improved model to determine the effect of quay walls. It concluded that the presence of a quay wall magnifies the surge force by 80% and reduces the sway force and yaw moment by 60% (Pinkster 2004). These findings can be useful for the application of empirical or semi-empirical models at quay walls.

3 PHYSICAL MODEL STUDY

3.1 INTRODUCTION

Information about the setup of the physical model is given after which calibrations for the study are described. The test procedure is outlined and the selection of test conditions is motivated. Information on the output and preliminary data processing is given before it is interpreted in the section on data analyses. Finally, the effect scaling is discussed.

3.2 TEST SETUP

The passing ship tests were conducted in 54 m long by 32 m wide by 1 m deep 3D basin at the CSIR Hydraulics Laboratory in Stellenbosch. Two ships were used, a Panamax bulk carrier as the moored ship and a 4500 TEU Post Panamax container ship as the passing ship. The container ship was the largest container ship available at the CSIR. There were larger bulk carriers available, but the bulk carrier was selected since it has a similar draft than the container ship and represents a large fraction of bulk carriers that are currently being used. The bulk carrier was moored to a fixed frame in open water and the passing container ship was attached to a rail passing on a parallel course past the bulk carrier. Forces on the bulk carrier could be measured at a sampling rate of 50Hz with force transducers attached to the fixed frame.

In hydraulic physical modeling two scaling laws are generally used, Reynolds and Froude scaling. Reynolds scaling applies when viscous effects dominate and Froude scaling applies when inertial forces dominate. For very low flow velocities and small objects, the viscous effects of the fluid are the most significant. For higher flow velocities and larger objects the inertial forces dominate. The Reynolds number gives the ratio of inertial to viscous forces and indicates which scaling law applies. In this study, the Reynolds numbers are very high ($Re_{\text{PROTOTYPE}} > 5.6 \times 10^8$), and the Froude scaling was used. The available ships were built to a scale of 1:100. All model entities were scaled by the Froude scaling law on a scale of 1:100. The following scaling factors were derived.

Length	L	1:100
Time	\sqrt{L}	1:10
Velocity	\sqrt{L}	1:10
Mass	L^3	1:1000000
Force	L^3	1:1000000

Figure 3-1 is a sketch of the layout of the 54 m long by 32 m wide by 1 m deep basin at the CSIR Hydraulics Laboratory. The basin was used for a previous model which required a constant depth bathymetry cut from a shallower bathymetry. The slope between the two basin levels was at all times a distance of at least 9 moored ship beams (Bm) from the passing ship and 11Bm from the moored ship. It was assumed that this distance was enough to not have a significant influence on the physical model. Wave absorption slopes were used on the boundaries of the basin to absorb any waves that would be generated by the moving ships and to limit basin oscillations. The absorption beaches were made with gravel with a D_{90} of 13mm placed at a slope of 1:25.

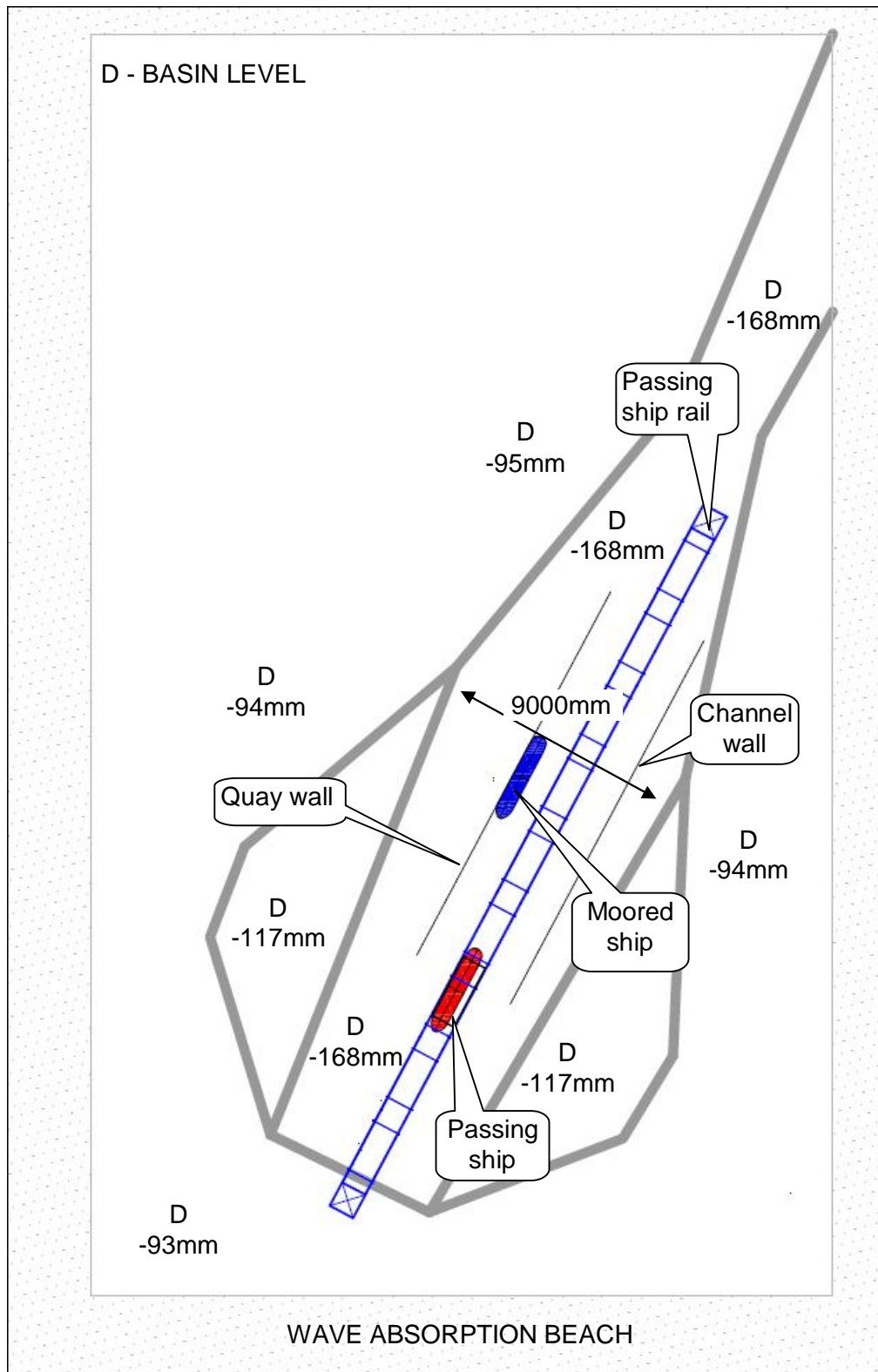


Figure 3-1: Layout of the passing ship setup in the 3D wave basin at the CSIR

A container ship passing a bulk carrier in open water (no quay wall) formed the basic model set up. Both ships were laden to the same draft of 14m. The ships were weighed after being loaded to their draft lines. The container ship weighed 83.370 kg and the bulk carrier 90.157 kg. Using the scaling ratio provided above the weight of the prototype ships could be determined. The displacement of the bulk carrier was determined to be 90,157 t, while the

Chapter 3: Physical Model Study

displacement of the container ship was determined to be 83,370 t. More characteristics are provided in Table 3-1.

Table 3-1: Ship characteristics

Name	Symbol	Unit	Bulk carrier (moored)	Container Ship (passing)
Displacement	Δ	t	90157	83370
Length over all	LOA	m	256	275.3
Length between perpendiculars	LBP	m	243.4	260
Beam	B	m	32	40
Depth of ship hull	dh	m	17.5	29
Draft	D	m	14	14
CoG forward of midship	LCG	m	5.5	-6.7

The 21m ship guiding rail consisted of a rectangular trolley with four wheels rolling on two rails suspended a small distance above the water surface (Figure 3-2). At both ends of the rail a stiff end structure braced the rail in the longitudinal direction. A pulley system and a drive motor were attached to the end structures to pull the rectangular trolley. The rectangular trolley was attached to the ship with two vertical sliding guides. These guides restrained the surge, sway and yaw of the ship with respect to the trolley. The sliding guide allowed the ship to heave, roll and pitch freely. The ship was driven with an alternating current (AC) induction motor and a line looped around two pulleys. The AC induction motor runs at the frequency of the alternating current that it receives. By using an inverter between the main power source and the AC induction motor, the frequency can be ramped up from 0Hz and be operated between 25 and 70 Hz without overheating the motor. A 20:1 reduction gearbox and small pulleys had to be used to reduce the ship speed to acceptable levels. The inverter was set to accelerate the ship from standstill within a specified time (5s), remain on a constant frequency and to decelerate to standstill within a specified time (2s).



Figure 3-2: Passing ship rail with the container ship

The bulk carrier was fixed in place with three 5mm aluminium rods, two lateral rods restraining the sway and yaw and one rod restraining the surge (Figure 3-3). The other ends of the rods were attached to force transducers which could measure with an accuracy of 0.01mN, or 10 kN in prototype, at a frequency of 50Hz. The rods were attached to the ships and force transducers with small plastic universal joints acting as a pinned connection. Force transducers was attached to a sturdy steel plate which was suspended on 8 short 10mm diameter steel rods which were kept in place by friction against the concrete floor.

Chapter 3: Physical Model Study

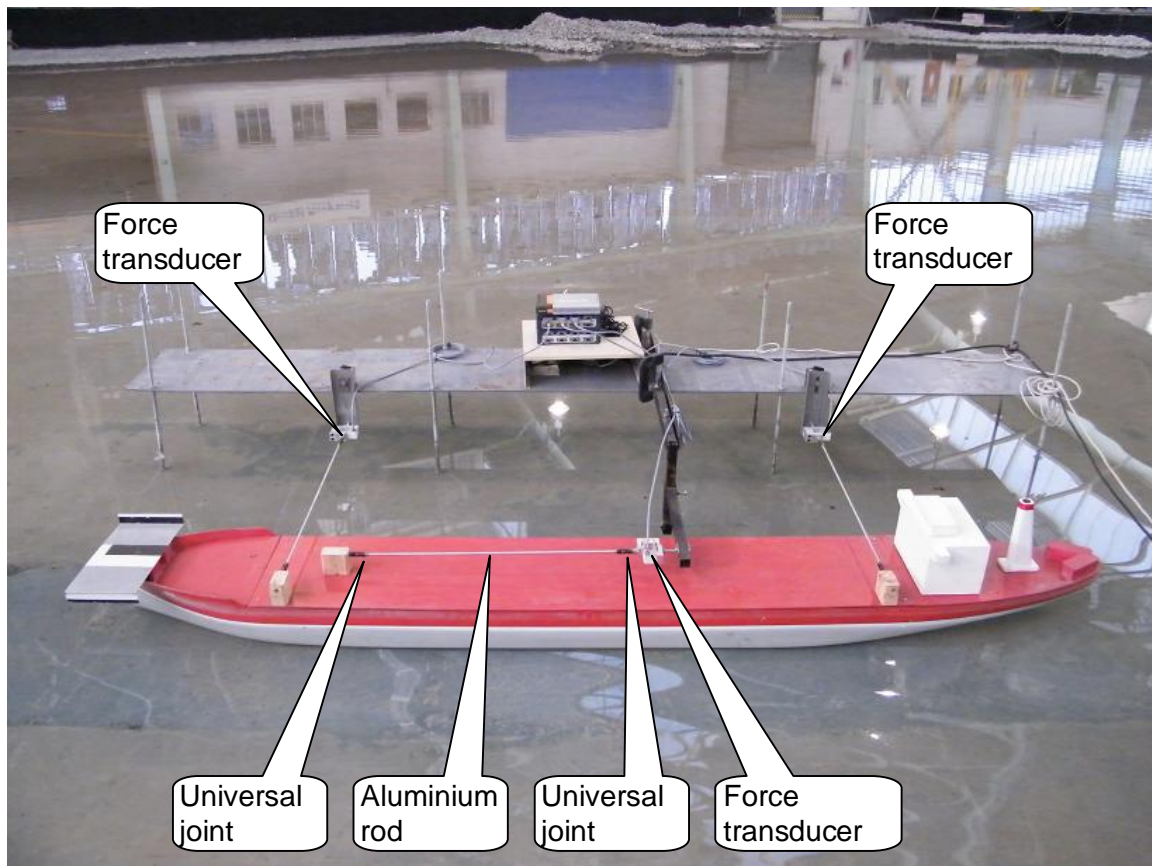


Figure 3-3: Fixed frame with the bulk carrier

Quay walls and channels were both constructed by placing marine ply wave guides vertically in the water to create an impenetrable barrier (Figure 3-4). Wave guides were placed firmly against each other and gaps sealed with duct tape to ensure that flow would not leak through the boundary. Where a quay wall needed to be placed between the force frame and the fixed bulk carrier, lower steel guides (red) were used since the wooden guides were too large to fit. To duplicate a channel or quay wall 5x 3m wave guides were used to create walls which stretched a distance of three times the moored ship length to either side of the centre of the moored ship. The first influence due to the passing ship is expected to only start once the centre to centre stagger between the two ships is about two ship lengths (Figure 2-5). The wall lengths were subsequently assumed to be long enough to represent a very long quay wall or channel.

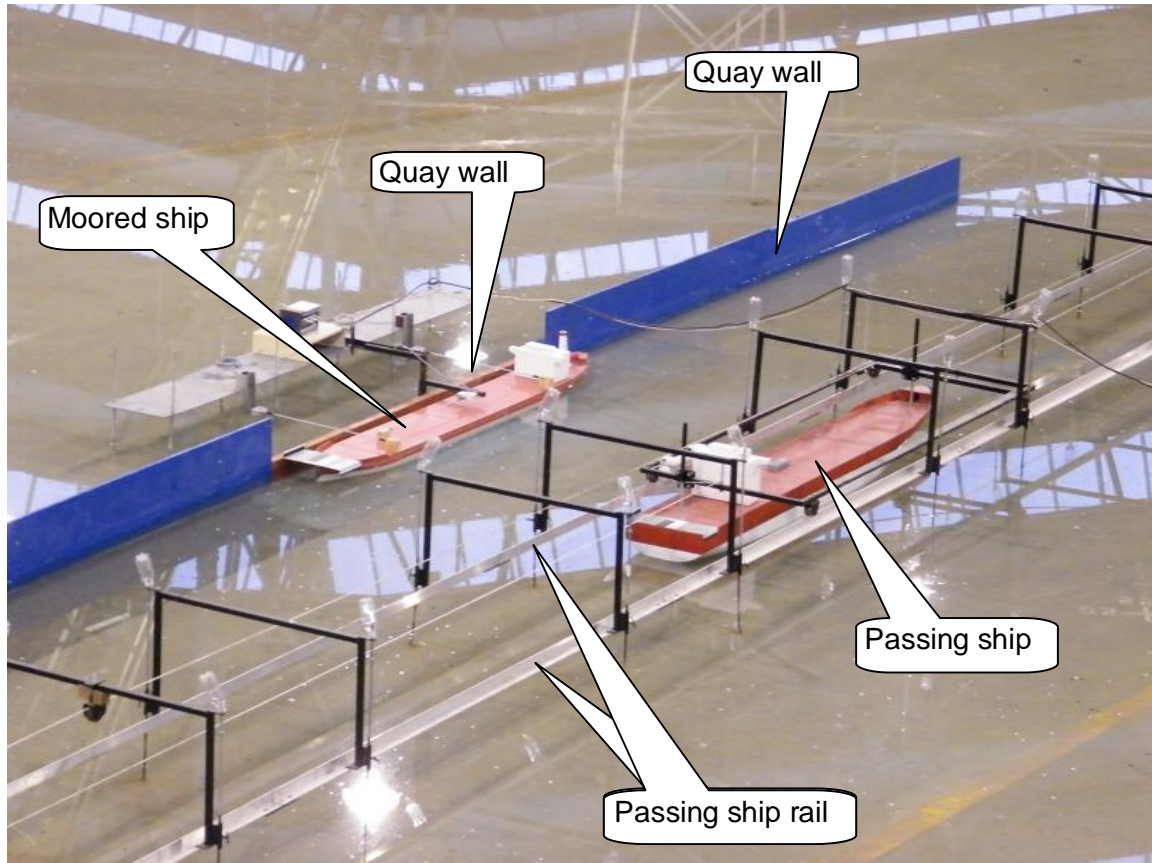


Figure 3-4: The passing and moored ships in the rail and fixed frame.

3.3 CALIBRATIONS

Both ships were laden to a 14m draft. This determined the total ship weight which could be measured afterwards. To get the ship to an even 14m draft a line was traced on the ship hulls and lead weights were placed and moved on the inside until both ships were up to the traced lines in the water.

The force transducers with the force rods had to be calibrated in the horizontal plane. This was done by creating a horizontal force with a weighted line and a pulley (Figure 3-5). The line was attached to the force transducer, guided over the pulley and the weight exerted a force through gravity. Tension and compression were calibrated this way by changing the angle between the line and the rod from 180 degrees to 0 degrees. When taking a measurement the value returned by the force transducer was set equal to the weight of the mass. This procedure was repeated several times to ensure that variation in the calibration could be eliminated. Once the force transducers were calibrated their readings were tested with a range of light and heavy weights ranging from 25g to 1000g. The force transducers produced a linear relationship between the applied and measured forces. This confirmed the low linearity deviation (0.0166%) which the supplier of the force transducers guaranteed.

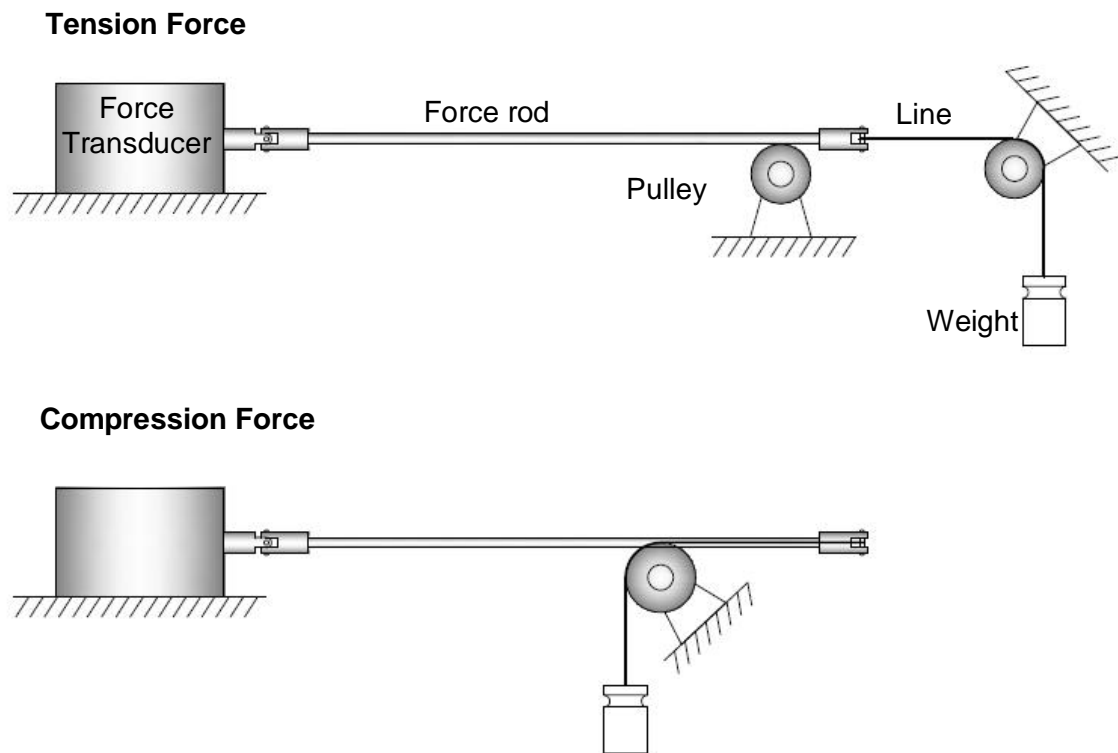


Figure 3-5: Calibration of forces for tension and compression in the force frame

The speed of the ship could be calibrated by taking time over distance measurements with a stopwatch for varying frequencies of the inverter. A linear trend line through the measured points was used to determine a formula which could be used to derive a frequency for any speed. Where a certain speed required a frequency beyond the safe limits for the motor, another pulley had to be calibrated. All speeds derived from the trend lines were double checked by taking additional measurements.

The measurement of similar tests can differ because of known or unknown reasons. Some known reasons include noise in the measuring system and random motions in heave, roll and pitch of the moving ship. To assess the extent of these effects a series of similar tests were done to compare the extent of the variation. In Figure 3-6 identical tests, test 1 to test 5, are compared and it proves that the extent of variation is very small.

Chapter 3: Physical Model Study

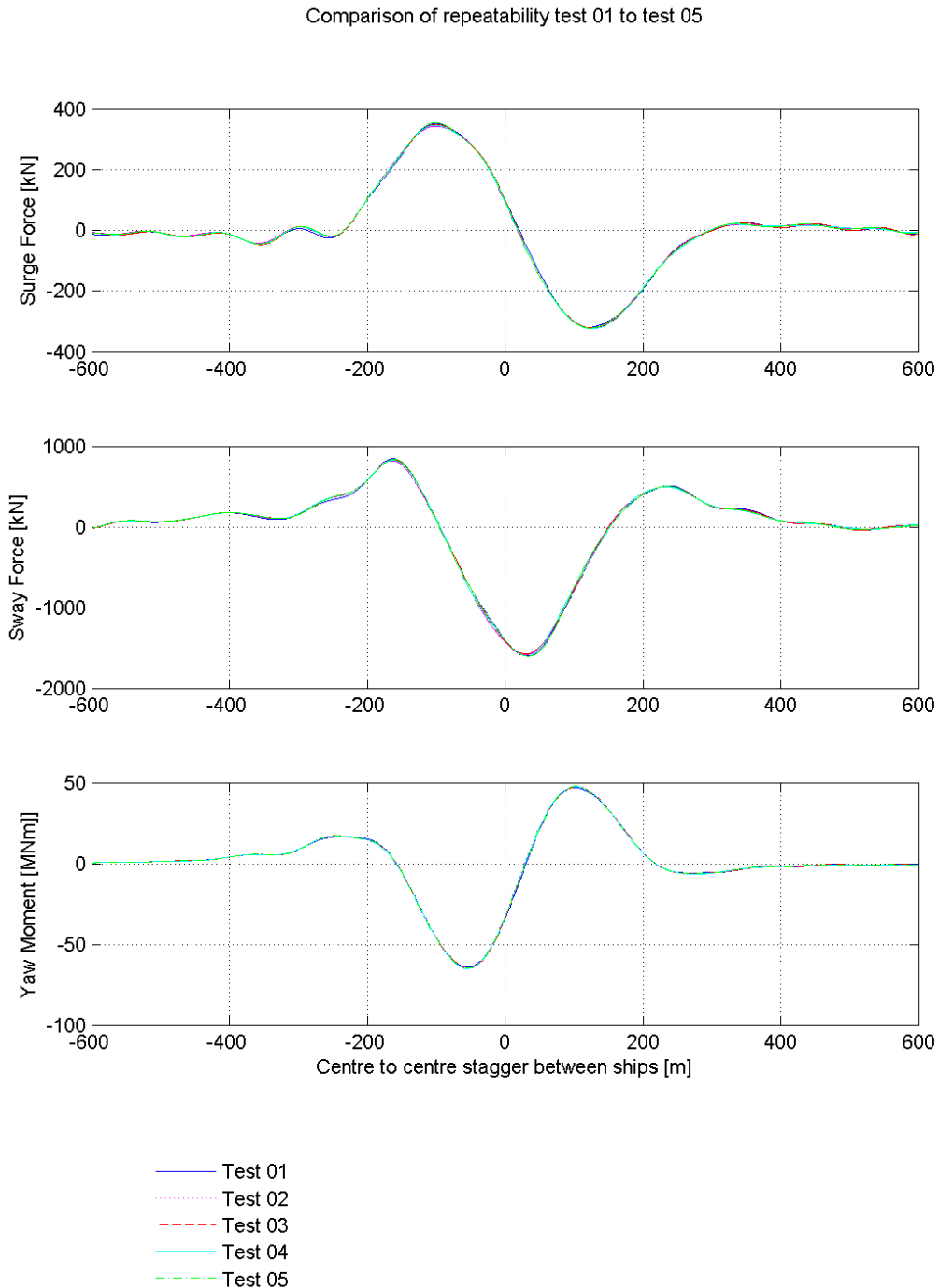


Figure 3-6: Repeatability tests of test 01 to test 05

3.4 TEST PROCEDURE

A testing procedure was used to ensure that tests were done in a similar way and to prevent unnecessary errors. During the procedure a record was kept to refer back to if unexpected results would occur.

The passing ship was towed to the starting position. After reaching standstill a period of seven minutes was timed to allow the basin to settle. During this time the test number was

Chapter 3: Physical Model Study

written down, the water level was set and the motor frequency was set to the corresponding frequency in the testing schedule. After the waiting period the measurement was started. To test for noise in the basin, measurement was done for two minutes at still water before the ship run was started. During the noise test the water level and motor frequency was double checked. The ship started accelerating exactly two minutes after the start of the measurement. The ship accelerated for 5 seconds to the preset speed, remained constant throughout the run and decelerated for 5 seconds after hitting the trip switch at the end of the run. During the run, the time, until the two ships were exactly alongside each other, was taken. After the completion of the run the ship was towed back to the starting position. Before starting a new test the maximum reading from the data acquisition system was written down and interpreted as a quick check for errors.

Each time when the model was changed to accommodate a new set of tests and the water was disturbed, the basin was left to settle for a time of 30 minutes.

3.5 TEST CONDITIONS

A list of tests was selected to not only cover, but also exceed conditions that can be expected in ports. With such a wider set of data it would be easier to spot trends.

In the literature review a large amount of variables is described that have an influence on passing ship forces (Chapter 2.5). The most significant of these variables were selected for the physical model tests. The selected variables included passing speed, passing distance, depth draft ratio and quay or channel walls. Some variables were selected to remain constant due to their lesser effect on the passing forces or due to model restraints. The maximum draft of the bulk carrier of 14m was used in the study since a deeper loaded ship would experience higher forces. The passing container ship was also loaded to 14m since the deeper loaded passing vessels induces larger forces on moored ships. Since ships rarely pass at angles other than 0 degrees (parallel) this variable was also fixed.

General variables were selected for the basic run. The basic run was the one run that was compared with all the tests. Sensitivity runs differed from the basic runs only in one variable so that the sensitivity of that variable could be tested. Combination runs differed from the basic run in up to four variables to test whether the conclusions drawn from the sensitivity runs were still true when more than one variable was changed at a time. The test schedule consisted of many sensitivity runs and a low amount of combination runs.

For the sensitivity runs, different passing speeds were selected between a slow 4kt and a fast 14kt at 2kt increments. Passing distance was varied in fractions of the passing ship width of 0.5Bm, 1Bm, 2Bm, 3Bm and 5Bm. Depth draft ratios were varied between 1.114, 1.164, 1.2, 1.4 and 1.75 corresponding to an underkeel clearance of 1.6m, 2.3m, 2.8m, 5.6m and 10.5m. Tests were done for no walls, a quay wall and channels with a width of 6Bm, 9Bm and 12Bm. The base case, that would be the one test that all sensitivity runs would have in common, was selected to be the test with the passing speed of 6kt, depth draft ratio of 1.2, passing distance of 2Bm (64m) and with no quay or channel walls. For the combination runs the speed would be varied between 6 and 8 knots, depth draft ratio between 1.114, 1.164 and 1.2. These combinations would be repeated for no walls, quay wall and the narrow 6Bm channel. In Figure 3-7 the different types of test conditions, described above, are outlined once again. For the complete test schedule refer to Appendix A.

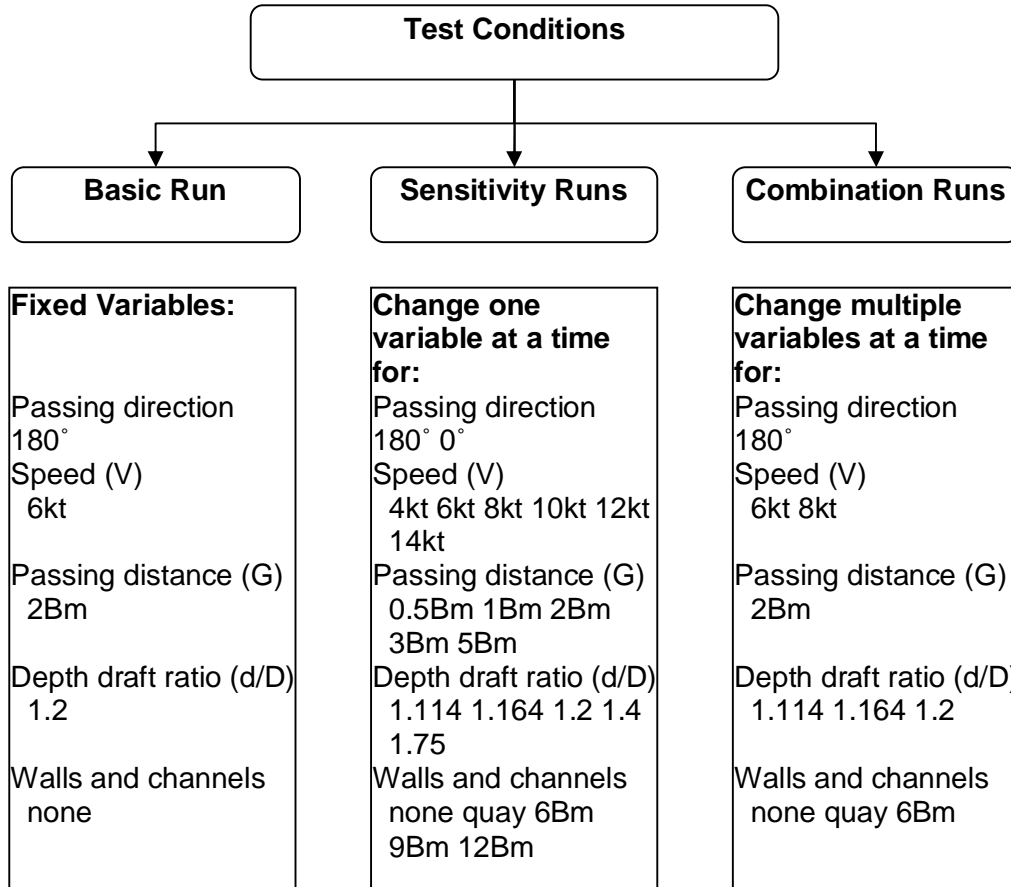


Figure 3-7: Test conditions

3.6 OUTPUT AND PROCESSING

The data acquisition software, CatmanEasy, saved data in ASCII format. The data had to be analysed with mathematical software, Matlab, to transform the readings to forces. The force data is scaled to prototype and the data series shortened to include only the measurements where the passing ship is close to the moored ship. Due to high frequency waves in the wake of the ship the force series of the forces appears rough. These high frequency waves have a small effect on the ships because of the ships high inertia. The high frequency waves were filtered out from the force series to create a smoothed graph of the lower frequency waves. Refer to Figure 3-8 for a graph with raw data and filtered data. Both the original and smooth data series' are saved, but only the smoothed data series was eventually used for comparisons and find the maximum forces. Outputs are given for the three measured forces, surge, sway and yaw, in the form of a data series, a max file and a plot of the data series.

The result of physical model measurements is given as a force series for surge, sway and yaw for each test. Figure 3-8 displays the raw and filtered versions of test 10. The rest of the smoothed force series is presented in Appendix C together with the numerical results. For all the tests the maximum and minimum loads were calculated and compared in Table 3-2.

Chapter 3: Physical Model Study

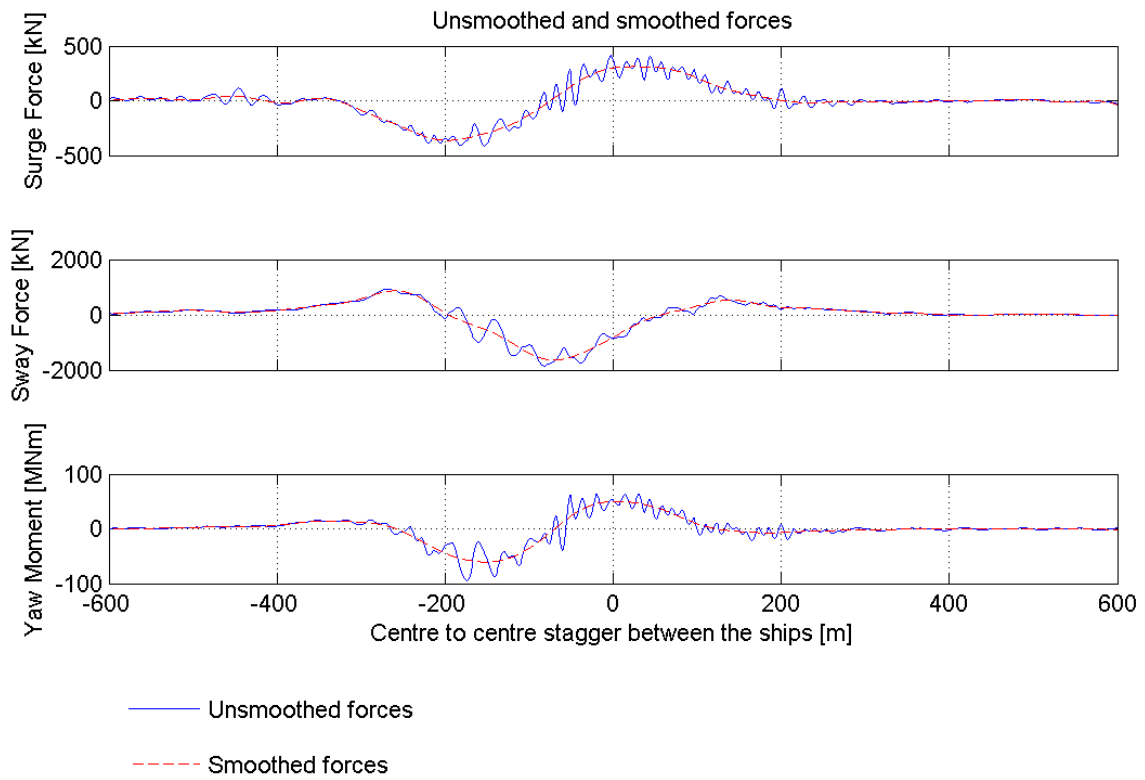


Figure 3-8: Test 10 physical model results raw and smoothed

Chapter 3: Physical Model Study

Table 3-2: Physical model maximum results of all tests for surge sway and yaw

Test No.	Surge (kN)		Sway (kN)		Yaw (MNm)	
	Min	Max	Min	Max	Min	Max
1	-319	351	-1601	846	-64.2	47
2	-321	342	-1574	819	-64.7	47.3
3	-321	349	-1567	831	-64.5	47.4
4	-324	345	-1587	822	-65	47.5
5	-322	354	-1604	838	-64.7	47.8
6	-622	704	-3269	1479	-119.7	89.4
7	-1046	1150	-5052	2307	-204.2	153.9
8	-1783	1727	-8146	3617	-323.7	268.8
9	-2772	2735	-12483	7466	-508.7	443.9
10	-362	312	-1640	868	-60.7	50.1
11	-704	638	-3162	1397	-115	97.7
12	-1178	1088	-5096	2331	-192.7	174.4
13	-1785	1788	-7922	3295	-314.1	300.8
14	-2681	2783	-12275	7004	-498.2	527.7
15	-697	579	-576	355	-17.9	24.6
16	-1341	1146	-1055	515	-32.4	46.4
17	-949	775	-742	258	-16.6	29.9
18	-1838	1441	-1259	723	-29.9	60.6
19	-715	614	-548	351	-17.3	26.3
20	-1453	1177	-1328	673	-31.1	47.5
21	-684	579	-485	323	-18.7	25.9
22	-1342	1150	-1225	729	-31.7	46.5
23	-667	634	-3281	1627	-150.4	124.5
24	-1284	1222	-6207	2862	-286.4	240
25	-518	510	-2417	1329	-108	89.9
26	-1012	950	-4758	2141	-205.8	170.5
27	-231	220	-1178	525	-38.6	32.1
28	-463	447	-2169	958	-71.5	64.4
29	-146	137	-573	233	-14.4	13.7
30	-246	211	-1165	493	-33.6	23.9
31	-397	349	-1895	915	-67.9	57.7
32	-762	676	-3595	1679	-130	111.6
33	-411	354	-2177	977	-79.2	62.3
34	-794	699	-4491	2046	-153.6	123.9
35	-287	257	-1009	465	-43.1	36.2
36	-541	521	-1840	873	-80	71.8
37	-208	186	-566	295	-28.5	24.8
38	-410	372	-1080	519	-52.6	47.7
39	-144	147	-652	309	-26.1	21.6
40	-669	601	-638	329	-18.7	28.6
41	-814	697	-817	405	-20.2	35.6
42	-969	791	-791	304	-16.6	32.2
43	-1091	822	-992	434	-14.4	42
44	-1382	1229	-1100	751	-32.9	58
45	-1553	1351	-1622	784	-31.4	70.1
46	-1876	1536	-1500	824	-32.3	70.6
47	-2122	1726	-1897	778	-32.8	91.7

Refer to Appendix A Table 01 for a summary of the test conditions

3.7 ANALYSES

The physical model study results were compared against each other to spot trends. These trends were compared with conclusions drawn from similar studies done on bulk carriers to check for similarities or new findings.

Maximum forces were compared for variations in passing speed (Figure 3-9), depth draft ratio (Figure 3-10) passing distance (Figure 3-11) and for the presence of quay or channel walls (Figure 3-12).

From Figure 3-9 it can be seen that passing ship forces are similar with the passing ship in any parallel passing direction relative to the moored ship. It can also be seen that the passing ship forces are proportional to a multiple of the passing speed. From Figure 3-10, it appears as if the passing ship forces are inversely proportional to the depth draft ratio. Passing ship forces are inversely proportional to passing distance, as can be seen in Figure 3-11. In Figure 3-12, the results are compared for conditions with walls and channels. The presence of a quay wall in the water has a significant effect, but a channel wall only has an effect when it creates a very narrow channel.

Chapter 3: Physical Model Study

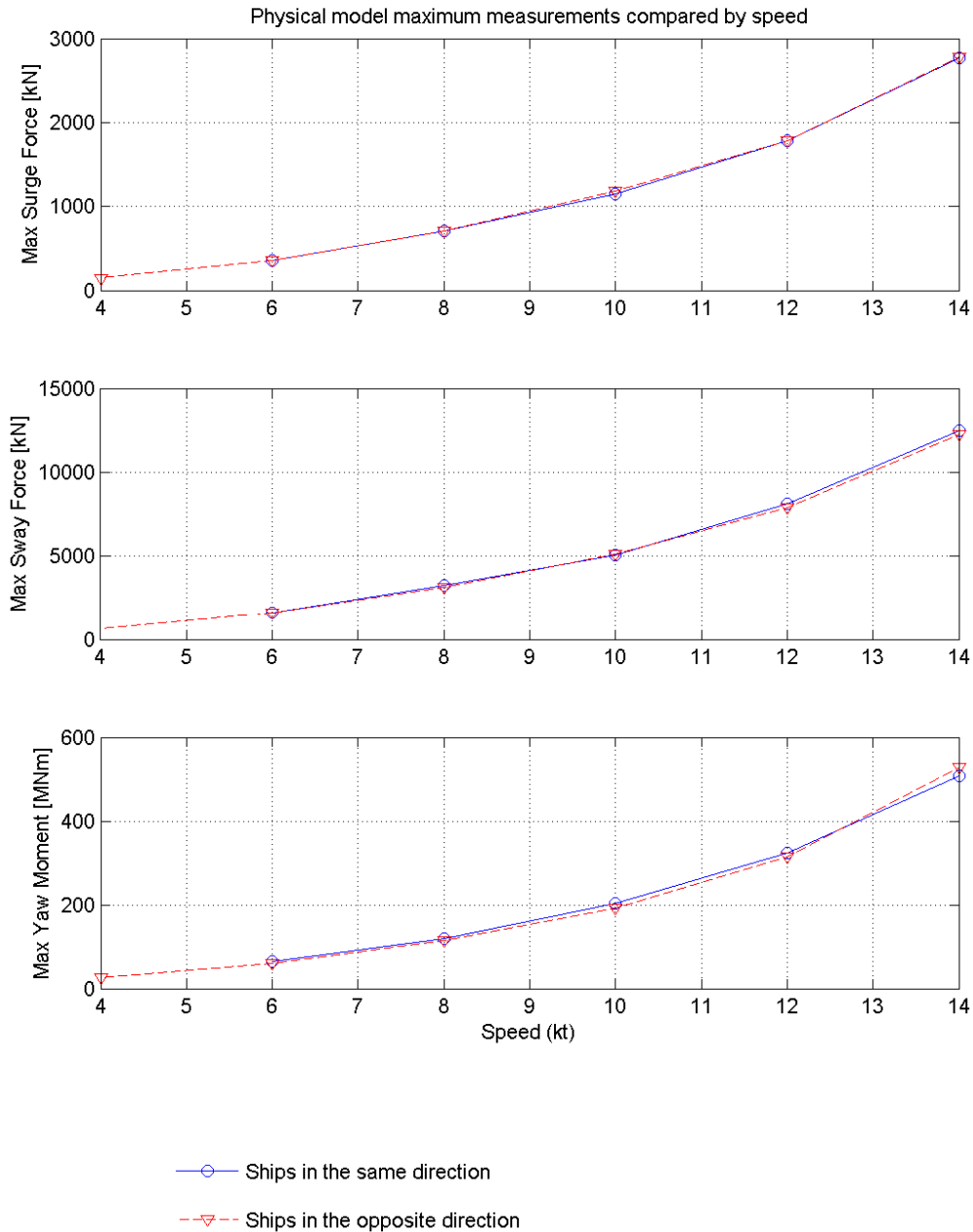


Figure 3-9: Physical model results as a function of speed for ships passing in the same and opposite directions

Chapter 3: Physical Model Study

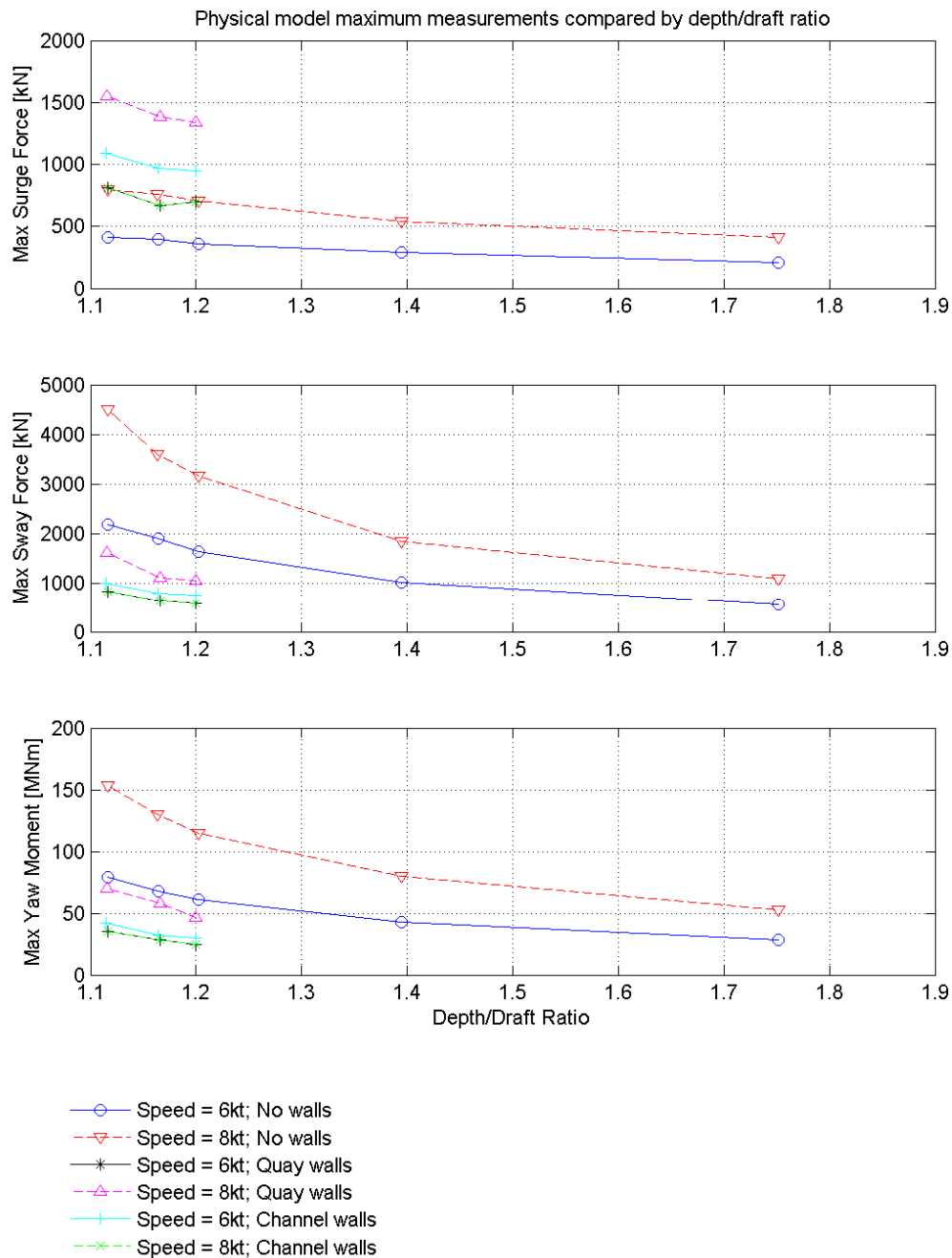


Figure 3-10: Physical model results as a function of depth draft ratio for different speeds and channel walls

Chapter 3: Physical Model Study

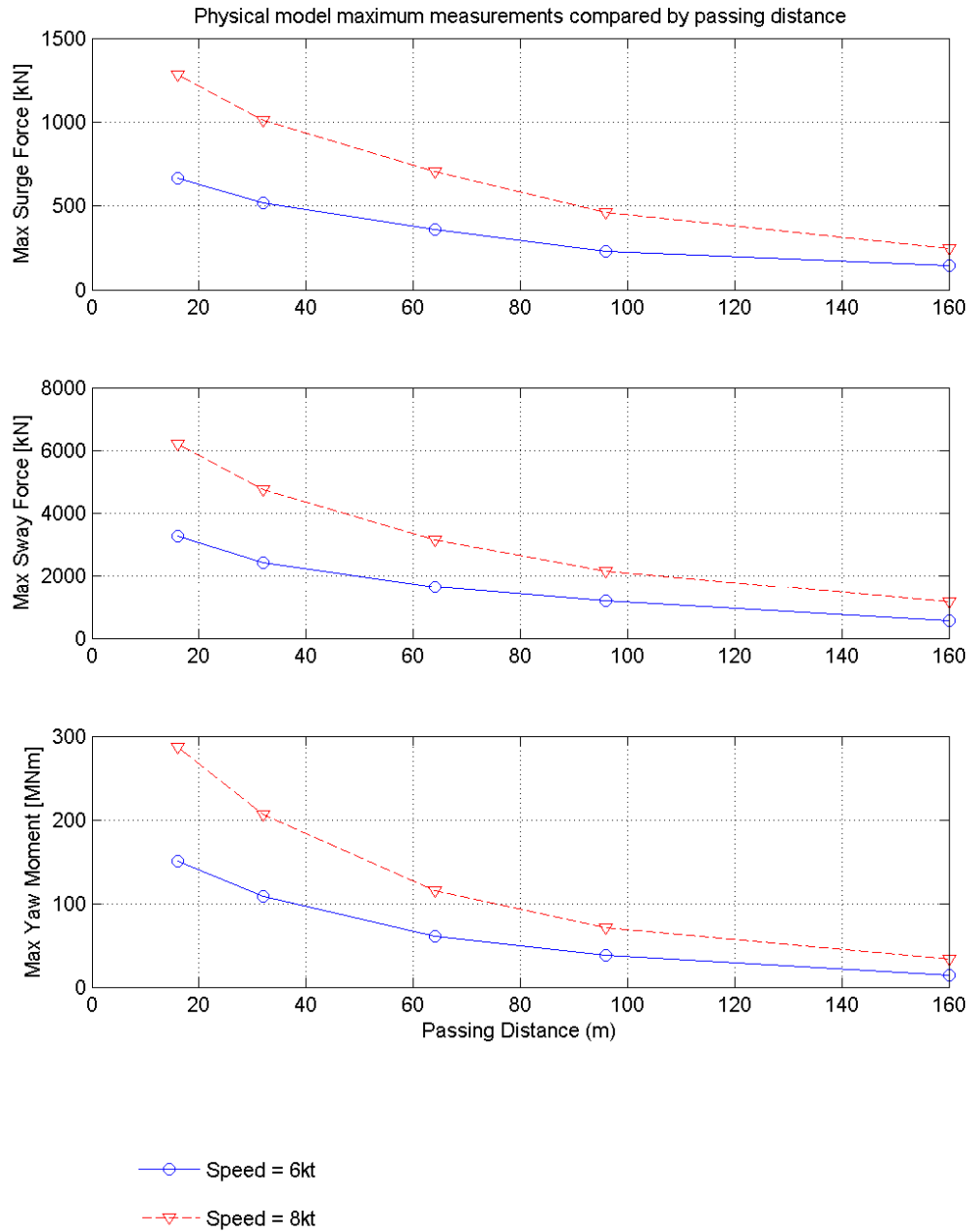


Figure 3-11: Physical model results as a function of passing distance for different speeds

Chapter 3: Physical Model Study

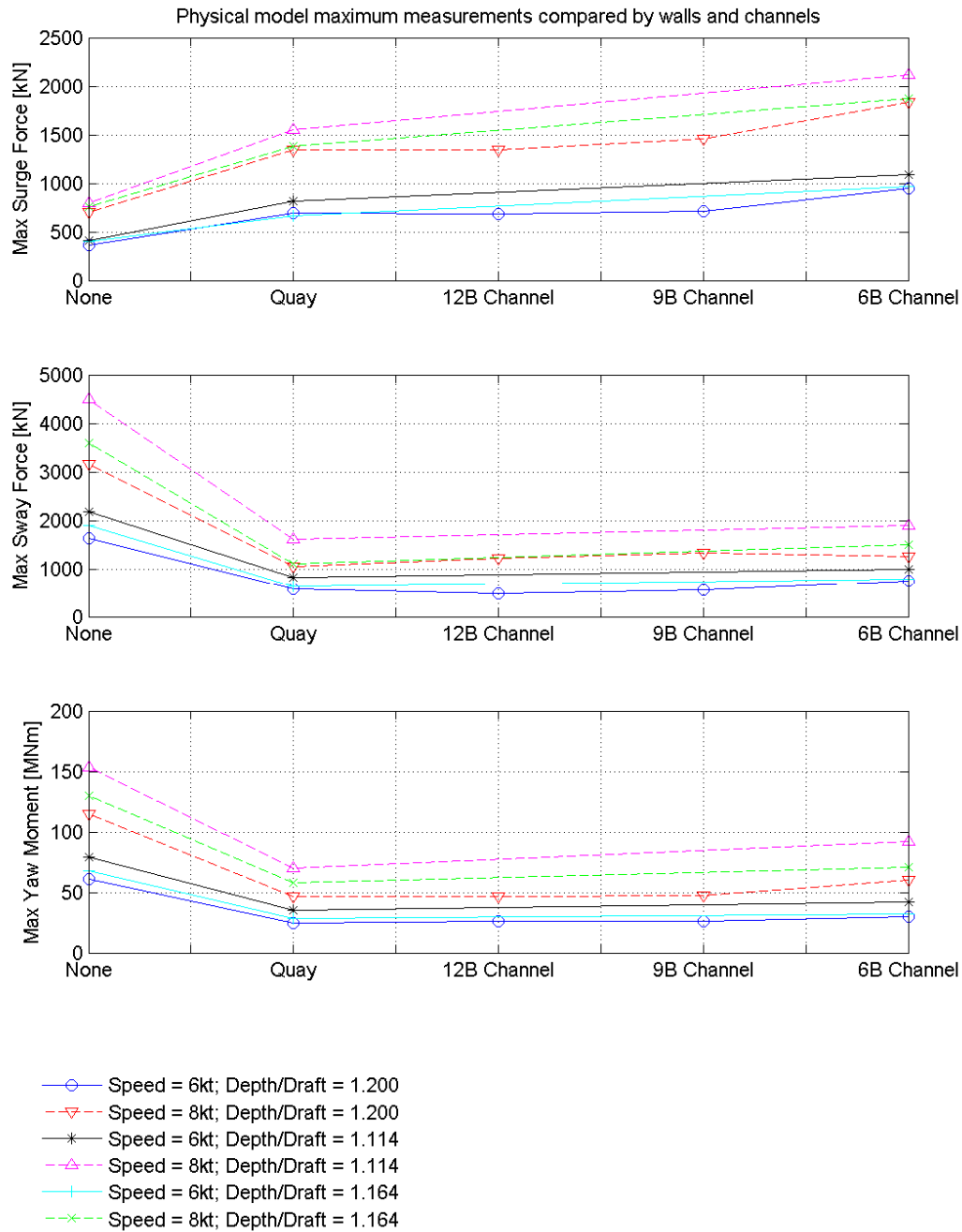


Figure 3-12: Physical model results as a function of walls and channels for different passing speeds and depth draft ratios

Chapter 3: Physical Model Study

By performing regression analysis, trends were found for the sensitivity runs. These relationships were compared to findings by previous authors. The results are summarized in Table 3-3.

Passing ship forces (surge, sway and yaw) are proportional to the passing speed to the power of 2.32. Pinkster (2004) made a similar conclusion, but only with passing speed to the power of 2.00. The coefficients of determination, R^2 , for proportionalities with factors of 2.32 and 2.00 were 0.993 and 0.978 respectively. This proves that both proportionalities are suitable, but that the power of 2.32 is slightly more accurate for the set of physical model results from this study.

The proportionality between passing ship force and speed stated by Pinkster (2004) corresponds with the well-known quadratic proportionality between fluid drag force and fluid velocity. The slightly higher value derived in this study can be attributed to ship squat, secondary wash waves, increased boundary layer effects at higher speeds and model scale effects.

For passing distance, proportionality exists by modifying the passing distance with an exponential function. The exponential function uses the multiplication of the passing distance with different factors for surge, sway and yaw. The multiplication factors for surge, sway and yaw are -0.0110, -0.0115 and -0.0154 respectively.

For depth draft ratio, proportionality exists between the forces and the depth draft ratio to the power of -1.5, -3.1 and -2.3 for surge sway and yaw respectively. However, the proportionality is not as distinct as the proportionality of passing speed with passing ship forces.

For quay and channel walls a multiplication factor was derived that would transform the forces to open water measurements. Multiplication factors for the transformation of measurements with quay walls, 9B channels and 12B channels; to open water were determined to be 1.92, 0.34 and 0.43 for surge, sway and yaw forces respectively. For narrow channels (6B), the multiplication factors are 2.63, 0.31 and 0.53. Pinkster (2004) concluded similar factors. Pinkster concluded that, when quay walls are present, the multiplication factor for surge force was 1.8. He concluded that for sway forces and yaw moment the multiplication factor was 0.4. There is only a slight difference between the multiplication factors suggested by Pinkster (2004) and those derived in this study.

Table 3-3: Relationships between forces and variables

Description		Surge force	Sway force	Yaw moment
Passing speed	Relationship	$y \propto x^{2.32}$	$y \propto x^{2.32}$	$y \propto x^{2.32}$
	R ²	0.999	0.999	0.994
Passing distance	Relationship	$y \propto e^{-0.011x}$	$y \propto e^{-0.0115x}$	$y \propto e^{-0.0154x}$
	R ²	0.989	0.992	0.994
Depth draft ratio	Relationship	$y \propto x^{-1.5}$	$y \propto x^{-3.1}$	$y \propto x^{-2.3}$
	R ²	0.990	0.981	0.982
Transform quay walls, 12B and 9B channels to open water	Relationship	x1.92	x0.34	x0.43
Transform 6B channels to open water	Relationship	x2.63	x0.31	x0.53
NOTE: " y " represents the force and " x " represents the variable				

By multiplying the proportionalities by constants, empirical formulae can be created. These formulae would be easy to apply for calculating passing ship forces, but the answers would only be valid for the specific ships that were used in the physical model. A relationship for relative ship sizes and relative depth draft ratios should still be added to the list of proportionalities before the empirical relationships can be transformed into generic empirical formulae. To derive these formulae additional model tests need to be done. Empirical factors were however derived to assess the accuracy of the combination of proportionalities from Table 3-3. In Equation 3-1 the derivation of empirical factors is described as the measured force divided by the proportionalities. In Figure 3-13 the empirical factors derived from each test result for surge are plotted in a histogram. The histogram indicates the variation in the empirical factors, and conversely the combined accuracy, of the derived proportionalities. The standard deviation and the coefficient of variance for surge, sway and yaw proportionalities are summarized in Table 3-4.

Chapter 3: Physical Model Study

Equation 3-1: Derivation of empirical factors for each test

$$F_x i = K_x i \times F_1 i \times WF_1 i$$

$$K_x i = \frac{F_x i}{F_1 i \times WF_1 i}$$

$$i = 1, 2, 3, \dots, 47$$

$$F_1 = V^{2.32} \times e^{-0.011G} \times (d/D)^{-1.5}$$

$$WF_1 = \begin{cases} 1.00 & \text{if open water} \\ 0.52 & \text{if quay, 12Bm or 9Bm channel} \\ 0.38 & \text{if 6Bm channel} \end{cases}$$

Symbols:

K	Empirical factor	[N]
F_x	Surge Force	[N]
F_1	Empirical relationship for surge force	[-]
WF_1	Wall factor for surge force	[-]
V	Passing Speed	[m/s]
d	Water depth	[m]
D	Ship draft	[m]
G	Board to board distance between the ships	[m]
Bm	Beam of the moored ship	[m]
i	Test number	[-]

Chapter 3: Physical Model Study

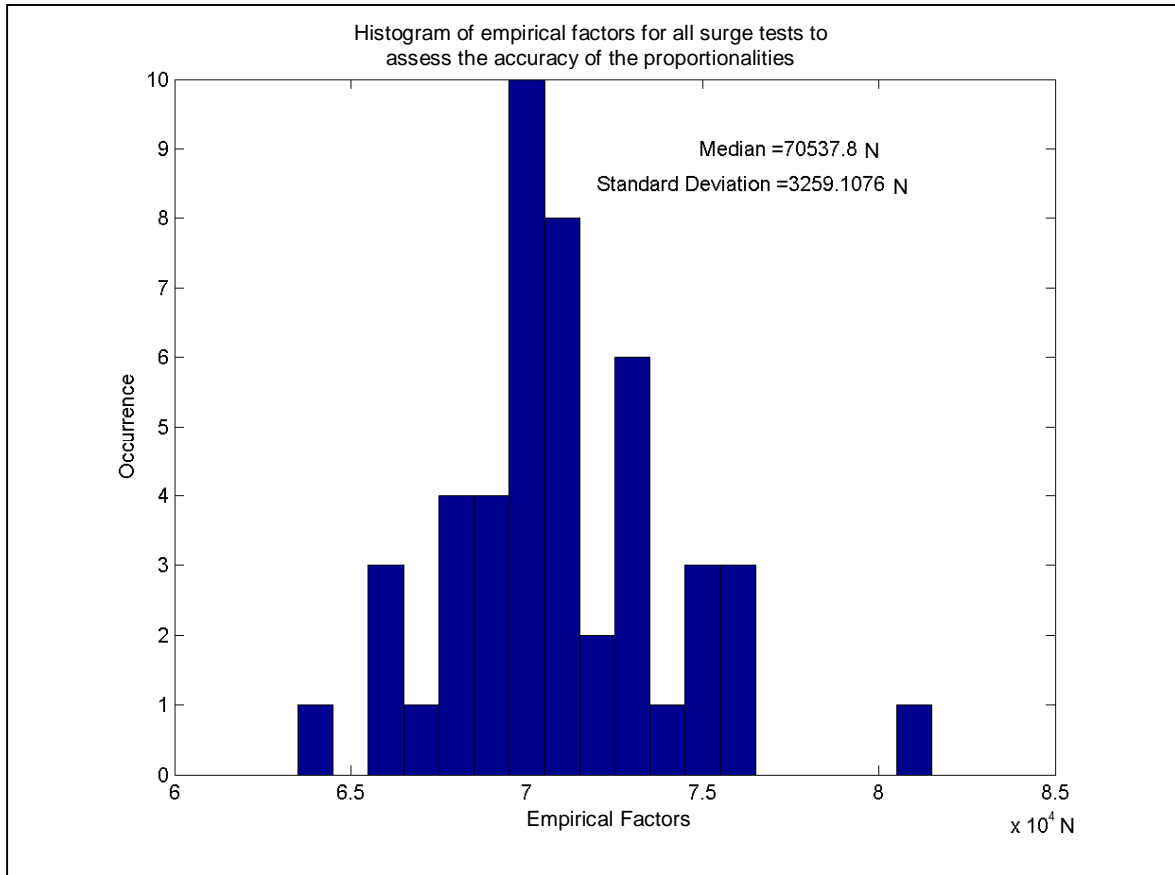


Figure 3-13: Histogram of empirical factors for surge forces to assess the accuracy of the combination of proportionalities

Table 3-4: Coefficient of variation for combined surge, combined sway and combined yaw proportionalities.

	Median of empirical factors	Standard deviation	Coefficient of variation x 100
Surge	70.5×10^3	3.26×10^3	4.6
Sway	450×10^3	33.9×10^3	7.5
Yaw	19.0×10^6	1.51×10^6	7.9

Although the current information is not useful for determining exact forces for other ship dimensions, the current relationships can be used to estimate proportional changes in forces due to changes in variables. The empirical relationships are given in Equation 3-2 to Equation 3-4.

Chapter 3: Physical Model Study

Equation 3-2: New empirical relationship for passing ship surge forces

$$F_{X_DERIVED} \propto F_1 \times WF_1$$

$$F_1 = V^{2.32} \times e^{-0.011G} \times (d/D)^{-1.5}$$

$$WF_1 = \begin{cases} 1.00 & \text{if open water} \\ 0.52 & \text{if quay, 12Bm or 9Bm channel} \\ 0.38 & \text{if 6Bm channel} \end{cases}$$

Equation 3-3: New empirical relationship for passing ship sway forces

$$F_{Y_DERIVED} \propto F_2 \times WF_2$$

$$F_2 = V^{2.32} \times e^{-0.0115G} \times (d/D)^{-3.1}$$

$$WF_2 = \begin{cases} 1.00 & \text{if open water} \\ 2.94 & \text{if quay, 12Bm or 9Bm channel} \\ 3.22 & \text{if 6Bm channel} \end{cases}$$

Equation 3-4: New empirical relationship for passing ship yaw moments

$$M_{Z_DERIVED} \propto F_3 \times WF_3$$

$$F_3 = V^{2.32} \times e^{-0.0154G} \times (d/D)^{-2.3}$$

$$WF_3 = \begin{cases} 1.00 & \text{if open water} \\ 2.33 & \text{if quay, 12Bm or 9Bm channel} \\ 1.89 & \text{if 6Bm channel} \end{cases}$$

Symbols used in Equation 3-2 to Equation 3-4:

$F_{X_DERIVED}$	Surge Force	[N]
$F_{Y_DERIVED}$	Sway Force	[N]
$M_{Z_DERIVED}$	Yaw Moment	[Nm]
F_1	Empirical relationship for surge force	[-]
F_2	Empirical relationship for sway force	[-]
F_3	Empirical relationship for yaw moment	[-]
WF_1	Wall factor for surge force	[-]
WF_2	Wall factor for sway force	[-]
WF_3	Wall factor for yaw moment	[-]
V	Passing Speed	[m/s]
d	Water depth	[m]
D	Ship draft	[m]
G	Board to board distance between the ships	[m]
Bm	Beam of the moored ship	[m]

3.8 SCALING EFFECTS

Physical model tests of ships where both Froude's and Reynolds' laws apply does not exist (Volker 2000). Since inertial forces dominate, Froude scaling was selected since Froude scaling scales inertial forces correctly. Due to the Reynolds similarity being neglected, some errors will occur due to viscous effects.

Viscous forces occur due to direct shearing of water and are magnified by boundary layers and flow separation (Balmer 2007). Flow separation occurs in the lee of objects moving in water and happens more readily when the boundary layer is laminar (Fielding 2005). The transition of a boundary layer from laminar to turbulent occurs earlier for a higher flow speed (0.7m for 14kt). In the model, the boundary layer will be turbulent once it reaches the lee of the ship. For lower speeds the transition zone of the boundary layer is close to the lee of the ship (2.44m for 4kt), but due to the ship being streamlined, and the speed low, flow separation does not occur (Fielding 2005).

The thickness of the boundary layer itself is an occurrence that may introduce inaccuracies. In Chapter 2.7 boundary layers have been described and equations were given for boundary layers at flat plates. The boundary layer equations for flat plates are used below to provide a better understanding of the difference between boundary layers in the prototype and the physical model. There are more complex and accurate methods for estimating boundary layers at ship hulls. For the scope of this study, the formulae for flat plates are regarded as suitable since the relative difference between the boundary layers in prototype and the model will be assessed. At flat plates the transition of the boundary layer from laminar to turbulent may occur when the $Re=3 \times 10^6$. The transition occurs at a distance of 1.46m from the upstream side of the plate. If this distance is applied to the ships, then the prototype ship will have a turbulent boundary layer over 99% of its length and the model ship will have a turbulent boundary layer over 47% of its length. For the prototype ship, the boundary layer thickness will be 4.5% of the ship beam (1.81m) and for the model ship, it will be 12.5% of the ship beam (0.050m). The boundary layer in the model is thus exaggerated by 2.7 times. For 14kt, the boundary layer in the model is exaggerated by 3.6 times. The boundary layer is thus exaggerated in the physical model and will cause a slight over prediction of forces. The exaggerated boundary layer may in part be a reason for the slightly higher proportionality, between passing speed and passing ship forces, which was derived from the physical model in comparison to the generally accepted quadratic proportionality.

Where the boundary layer is fully developed, i.e. the boundary layer thickness is more than the under keel clearance, the water between the ship and the seabed is experiencing a direct shear. Scaling errors might be significant due to the inappropriate scaling of viscosity. The fluid shear stress between the ship hull and the bathymetry is exaggerated 1000 times. This will cause more water to displace to the sides of the ship, the return flow to increase and higher forces (van der Molen et al 2010).

It is unavoidable to use small scales when doing physical modeling of ship interaction. Scaling effects will have an effect on the results. Due to a thicker boundary layer and higher shear force in the fluid, small scale models will over predict prototype passing ship forces. When using the model test results for designs the slight over prediction of forces adds safety to the final solution. The scaling effects have been regarded to be small in previous studies at similar scales (Chapter 2.5). For this study, a small scale has also been accepted and it should be kept in mind that forces might be slightly lower in prototype than in the physical model.

3.9 SUMMARY AND CONCLUSIONS

This chapter described the physical modeling setup in the passing ship basin at the CSIR. The model was conducted at a scale of 1:100 for an 83,370 t container ship passing a 90,157 t bulk carrier.

Tests were done using a passing ship rail and a force frame that allows free movement of heave, roll and pitch motions at the passing and moored ships. Speed of the motor and force measurements of the force transducers were calibrated by doing a number of tests. The effect of variability between similar tests was checked in a set of repeatability tests. It was found that tests can be repeated and that the newly measured data would closely resemble the data measured previously. The physical model tests were done to obtain a database of results for different sensitivities. The speed, passing distance, depth draft ratio and walls and channels were tested by testing the sensitivity of each. Combination runs, where more than one variable changes at a time, were also done. High frequencies were filtered from the measured data to obtain a smooth time history of passing ship forces. Smoothed force series was used to determine the minimum and maximum forces for the surge, sway and yaw of the moored ship. The data was analyzed by using graphs of the maximum forces compared to the different sensitivities. The analysis yielded trends in the forces due to changes in the variables.

For passing speed, it was found that the passing ship forces are proportional to the passing speed to the power of 2.32. This is slightly higher than the quadratic proportionality drawn from literature and is thought to be due to ship squat, increased boundary layer effects at high speed and secondary wash waves. Scaling effects of the physical model also magnifies this phenomenon. For passing distance it was found that the passing ship forces are proportional to an exponential function of the passing distance multiplied by a different constants for surge (-0.0110), sway (-0.0115) and yaw (-0.0154). For depth draft ratio it was found that the passing ship forces are proportional to the depth draft ratio to the power of -1.5 for surge, -3.1 for sway and -2.3 for yaw. When the channel is wider than 9 times the beam of the moored ship, the effect of the channel wall can be neglected. For wide channels, the effect is thus the same as for quay walls. When quay walls or wide channels (more than 9 times the beam of the moored ship) are present the surge forces increased by 1.92 times, sway forces by 0.34 times and yaw forces by 0.43 times. This is similar, with small differences, to what Pinkster (2004) found for bulk carriers. When there is a narrow channel, the surge forces decrease to 2.63 times the forces in open water. Also for narrow channels, the sway forces increase by 0.31 times and yaw forces by 0.53 times. By using the above trends, empirical relationships were derived. The empirical relationships can either be used together with the empirical factors to calculate forces for the 83,370 t container ship passing the 90,157t bulk carrier, or it can be used on its own to assess relative change in forces on similar ships due to a change in variables. Since only one combination of ships was used in the set of tests, the conclusions can not be regarded as generic for any container ship passing any bulk carrier. Conclusions from previous studies on tankers can be applied to passing container ships, but with average confidence. For ships with roughly similar dimensions than the ones used in this physical model study, the newly derived relationships should rather be used if possible. To achieve generic conclusions for container ships passing bulk carriers, a larger range of different ship dimensions need to be tested to find proportionalities for different ship dimensions and different depth draft ratios.

It would be useful to do additional physical model tests with differently sized and laden ships. From those tests, proportionalities can be found for ships with different dimensions and depth draft ratios so that the empirical relationships can be converted into empirical formulae for passing container ships.

4 NUMERICAL MODEL VALIDATION

4.1 INTRODUCTION

This chapter gives a description of how Passcat is used and what input needs to be generated. The numerical and the physical model are compared by comparing the maximum forces for the numerical and the physical results. Extreme forces are compared in table format and the ratio of agreement is calculated. In this way, rough boundaries are drawn wherein the model results can be regarded as good.

4.2 NUMERICAL MODEL

Passcat is a 3D potential flow model that calculates the flow around a passing ship and the corresponding forces on a moored ship (van der Molen et al 2010). Being a potential flow model implies that the fluid is inviscid, incompressible and homogeneous and that the flow is irrotational. Passcat makes a double body flow assumption similar to Korsmeyer et al (1993) and Pinkster (2004). The fluid flow around the bodies is described by a velocity potential ϕ . The velocity potential can be defined such that the gradient of ϕ is equal to the flow velocity. The velocity potential has to meet the conditions in Equation 4-1 (van der Molen et al 2011):

Equation 4-1: Potential flow equations

$$\nabla^2 \phi = F_h^2 \phi_{xx}, \quad (2-22-1)$$

$$\phi_n = Un_x \text{ on } \mathcal{H}_p, \quad (2-22-2)$$

$$\phi_n = 0 \text{ on } \mathcal{H}_M, \mathcal{B} \text{ and } \mathcal{W}, \quad (2-22-3)$$

$$\phi_z = 0 \text{ on } z = 0 \text{ and } z = -h, \quad (2-22-4)$$

$$\phi = 0 \text{ for } R \rightarrow \infty, \quad (2-22-5)$$

Symbols used in Equation 4-1:

ϕ	Velocity potential	
ϕ_{xx}, ϕ_z	Partial derivatives of velocity potential	
F	Depth related Froude number	[-]
ϕ_n	Velocity potential in the direction of a unit vector	
V	Speed	[m/s]
n	Unit normal vector	
n_x	Partial derivative of unit normal vector	
d	Water depth	[m]
\mathcal{H}_M	Body surface of the moored ship	
\mathcal{B}	Sea bed	
\mathcal{W}	Surface of structures	

Sources and sinks of velocity potentials are generated on all the boundaries taking the rigid still water level and a restricted water level into account. Water pressures are calculated at any point by taking the pressure of the primary return flow wave and reducing it by the pressure reduction due to the flow velocity. This step is similar to the Bernoulli equation

which uses hydrostatic and velocity terms. By integration of the pressures, Passcat computes interaction forces on all bodies in 6 degrees of freedom. The computation of forces on the bodies focuses on the flow of water from the front to the back of the passing ship. Water levels can be calculated from the water pressures, but does not have an effect on the flow or on the force calculations. To make the model more accurate at higher passing speeds a few depth related Froude number terms have been added to the basic potential flow model.

Due to the nature of potential flow models, Passcat neglects high frequency wash waves which become important at near critical or supercritical speeds, such as for high speed ferries (Van der Molen et al, 2005). In shallow and confined water the free surface has a significant effect on the ships. By neglecting the free surface, underestimation of forces and moments may result. Ships progressing through shallow or confined waterways are subject to viscous effects (van der Molen et al 2011) of the water due to the boundary layer on the hull surface and the channel floor. Flow separation adds considerable drag forces, but is neglected by Passcat due to the assumptions. It is clear that Passcat neglects some important characteristics of real fluid flow. Past studies have indicated that similar potential flow models gave good agreement between measured and calculated results.

Passcat requires a 3D panel mesh of the passing ship, the moored ship, the bathymetry and any other obstructions. Panels need to be small enough to allow stable numerical calculations, but should also be chosen large enough to allow faster calculation time. The meshes and a combined panel mesh are presented in Figure 4-1 and Figure 4-2. Passcat does not have an elaborate user interface, but relies on text files to serve as input files (Figure 4-3). In the input file the meshes are pinned in a global coordinate axes and are given a heading and a forward speed. A time step duration and amount is given based on the amount of data points required and the ship speed. An important parameter is the Froude number option. It is important that the option is set to 1 to switch on the Froude number related terms in the calculation. The numerical runs are done in a sequence by using batch files. Output is also given in text files (Figure 4-4). It provides characteristics of the ships and details of the specific run. For both ships it provides force series' due to the currents (F_{vel2}), the water pressures (F_{wave}) and the combined effect of the two (F_{total}). Since Passcat generates no visual output, the force series has to be modified and plotted with other software.

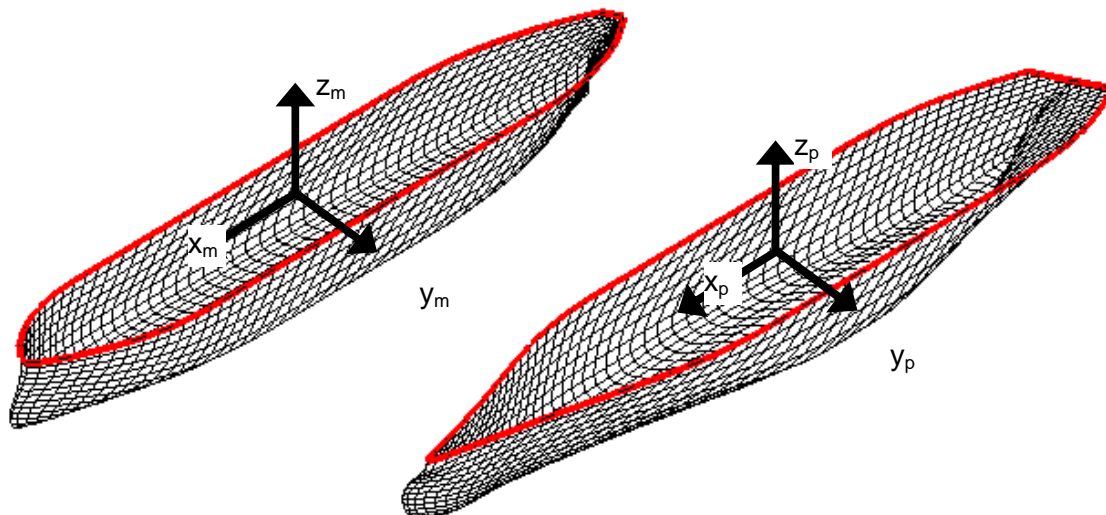


Figure 4-1: Meshes of the bulk carrier (left) and the container ship (right)

Chapter 4: Numerical Model Validation

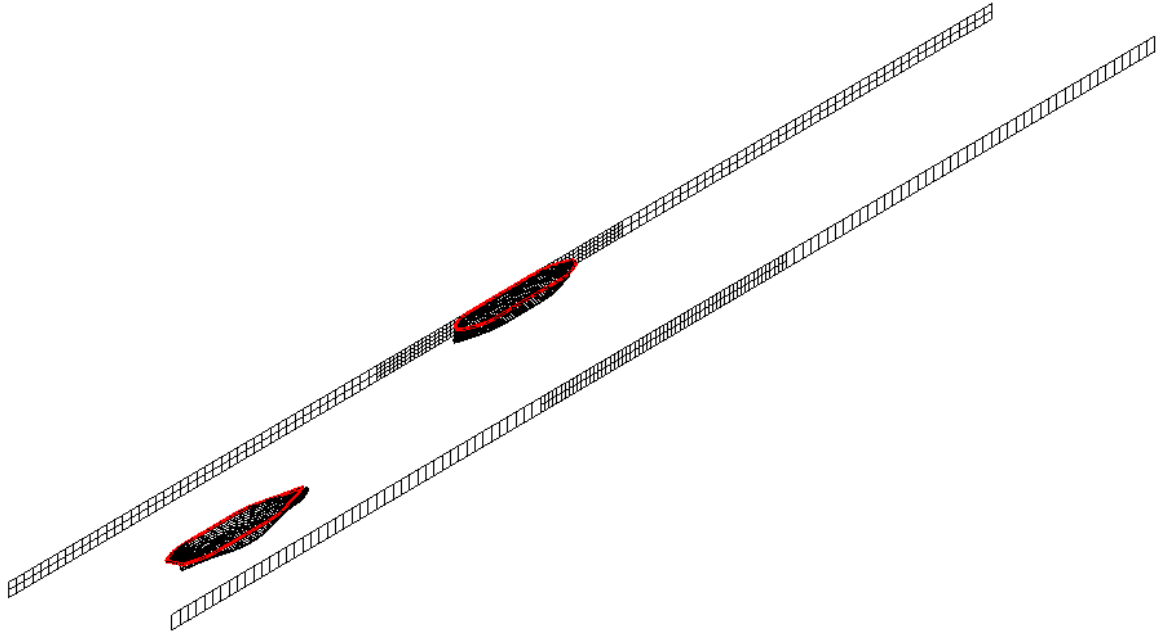


Figure 4-2: Mesh setup of test 17

```
# INPUTFILE FOR PASSCAT
#
# CONSTANTS
#
# Density of the fluid [kg/m3]
998
#
# Water depth [m]
16.830
#
# Froude number option
1
#
# RUN PARAMETERS
#
# Description of the run
'Run P10 Speed = 6.0 Waterdepth = 16.83 Passing dist = 64.0'
#
# Number of bodies
2
#
# Mesh files for each body (on separate lines)
'ContainerShip.msh'
'BulkCarrier.msh'
#
# Body number, x and y position [m], heading [deg] and forward speed [m/s]
# of the ship in the global coordinate system
1 730.197 100 180 3.08667 0
2 0 0 0 0.00000 0
#
# Number time steps, dt [s]
61 7.88550
#
# Wave force file (output)
10.wfo
```

Figure 4-3: Passcat input file

Chapter 4: Numerical Model Validation

```

Run P10 Speed = 6.0 Waterdepth = 16.83 Passing dist = 64.0 20110702

Dimensions of the passing ship: ContainerShip.msh
Length between perpendiculars 260.00 m
Breadth moulded 40.00 m
Draft 14.00 m
Block coefficient 0.626

Dimensions of the moored ship:
Length between perpendiculars 243.40 m
Breadth moulded 32.00 m
Draft 14.00 m

Water depth 16.83 m
Start position 730.20 m
Passing speed 3.09 m/s
Passing distance 64.00 m
Passing direction 180.00 deg
Passing side: Port side

3.087 U
61 Nt
7.885 dt

F_total
Body 1
TIME SURGE SWAY HEAVE ROLL PITCH YAW
s kN kN kN kNm kNm kNm
0.000 24.46 0.05 -8866.29 0.2 -16938.6 6.0
7.885 24.46 0.06 -8866.19 0.3 -16938.3 7.1
15.771 24.46 0.07 -8866.12 0.3 -16937.9 8.2
...Omitted Data
457.359 24.49 0.07 -8866.07 -0.5 -16923.4 -7.1
465.244 24.49 0.06 -8866.16 -0.4 -16926.4 -6.0
473.130 24.49 0.05 -8866.23 -0.4 -16929.1 -5.2

F_total
Body 2
TIME SURGE SWAY HEAVE ROLL PITCH YAW
s kN kN kN kNm kNm kNm
0.000 -4.35 -6.76 116.99 33.2 -595.5 -98.3
7.885 -4.82 -7.87 125.01 38.6 -682.5 -118.4
15.771 -5.30 -9.04 133.28 44.3 -773.4 -140.0
...Omitted Data
457.359 5.15 -9.12 127.55 47.7 2282.9 130.1
465.244 4.67 -7.93 119.04 41.5 2088.2 109.5
473.130 4.21 -6.80 110.81 35.5 1901.0 90.3

F_wave
Body 1
TIME SURGE SWAY HEAVE ROLL PITCH YAW
s kN kN kN kNm kNm kNm
0.000 -0.03 0.05 0.89 -0.1 3.0 0.8
7.885 -0.03 0.06 1.05 -0.1 2.9 0.8
15.771 -0.04 0.07 1.21 -0.1 3.0 0.8
...Omitted Data
457.359 0.04 0.07 1.24 -0.2 30.4 0.0
465.244 0.03 0.06 1.06 -0.2 25.2 0.0
473.130 0.02 0.05 0.92 -0.1 20.7 -0.1

F_wave
Body 2
TIME SURGE SWAY HEAVE ROLL PITCH YAW
s kN kN kN kNm kNm kNm
0.000 -4.36 -6.76 117.24 33.2 -599.7 -95.8
7.885 -4.83 -7.86 125.30 38.6 -687.7 -115.5
15.771 -5.32 -9.03 133.62 44.3 -779.8 -136.6
...Omitted Data
457.359 5.17 -9.11 127.87 47.7 2291.0 126.9
465.244 4.68 -7.92 119.31 41.4 2094.7 106.8
473.130 4.22 -6.80 111.04 35.5 1906.4 88.1

F_vel2
Body 1
TIME SURGE SWAY HEAVE ROLL PITCH YAW
s kN kN kN kNm kNm kNm
0.000 24.49 0.00 -8867.19 0.3 -16941.5 5.2
7.885 24.49 0.00 -8867.25 0.4 -16941.2 6.3
15.771 24.49 -0.01 -8867.33 0.4 -16940.9 7.4
...Omitted Data
457.359 24.46 0.00 -8867.31 -0.3 -16953.8 -7.1
465.244 24.46 0.00 -8867.22 -0.3 -16951.6 -5.9
473.130 24.46 0.00 -8867.15 -0.2 -16949.8 -5.1

F_vel2
Body 2
TIME SURGE SWAY HEAVE ROLL PITCH YAW
s kN kN kN kNm kNm kNm
0.000 0.01 0.00 -0.25 0.0 4.3 -2.4
7.885 0.01 -0.01 -0.29 0.0 5.2 -2.9
15.771 0.02 -0.01 -0.34 0.0 6.4 -3.4
...Omitted Data
457.359 -0.02 -0.01 -0.32 0.1 -8.0 3.2
465.244 -0.01 -0.01 -0.27 0.1 -6.5 2.6
473.130 -0.01 -0.01 -0.22 0.0 -5.3 2.2
    
```

Figure 4-4: Passcat output file (shortened)

4.3 COMPARISON OF NUMERICAL AND PHYSICAL MODELS

The numerical and physical models were compared by comparing the force series of the physical model with the force series of the numerical model. The maximum forces and the shape of the force-stagger graphs are very important since ship motions are a function of the magnitude and duration of forces. The shape of the force stagger graphs were checked by eye to spot obvious discrepancies, but apart from an occasional phase shift, the shapes agreed well. A complete set of these figures is provided in Appendix C. One example of such a comparison, for test number 10, is provided in Figure 4-5.

The maximum forces in the numerical and physical models were compared for the sensitivity runs. The maximum forces of the physical and numerical data were directly compared against each other for sensitivities to give a visual impression of the magnitude of forces and the degree to which the calculated results differ from the measured results. These plots are attached in Appendix D.

Chapter 4: Numerical Model Validation

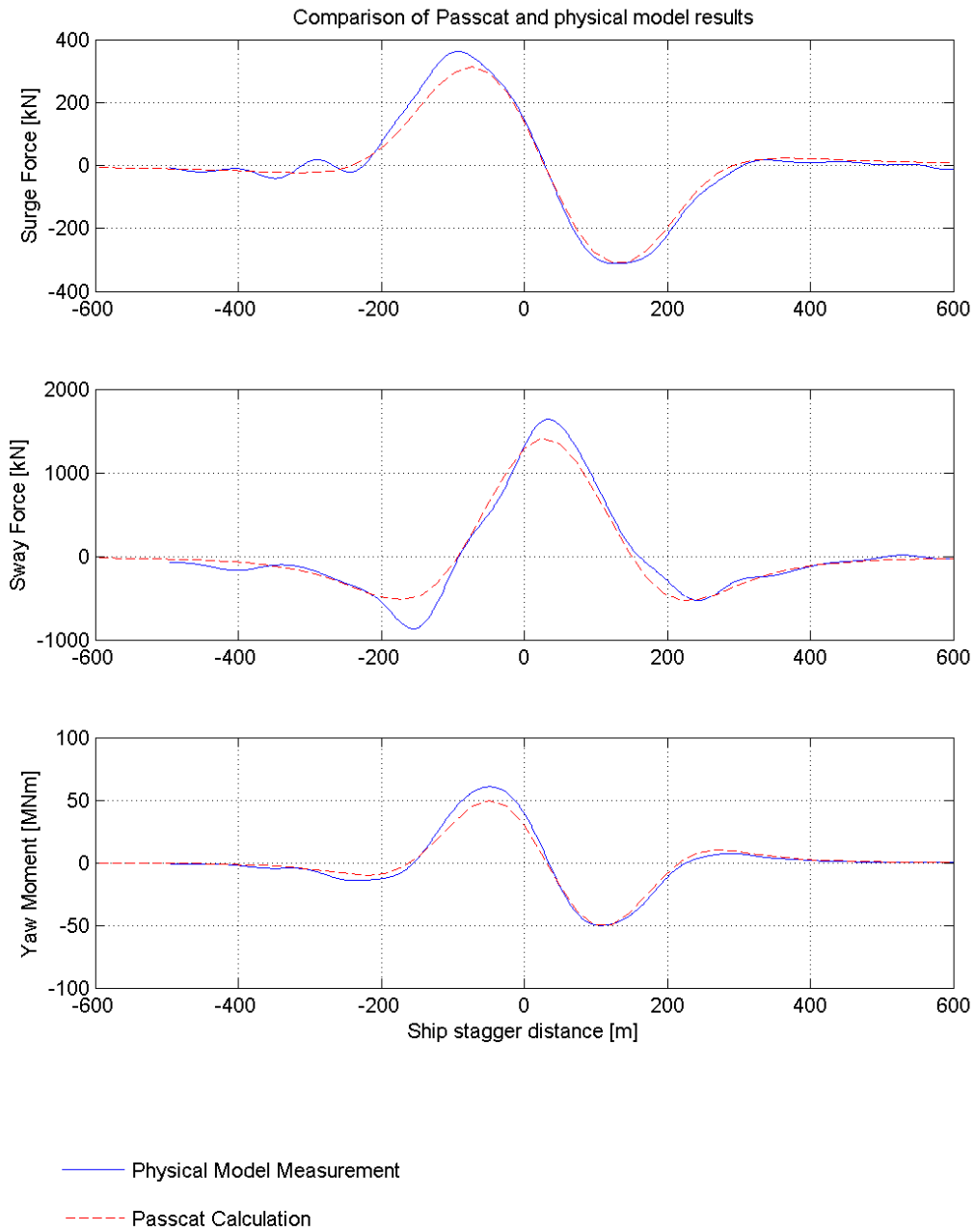


Figure 4-5: Test 10 physical and numerical model results

To assess the performance of the numerical model, a measure of agreement, called the agreement ratio, was calculated for each test by dividing the maximum calculated force by the maximum measured force (Equation 4-2). The agreement ratio's for all the tests are given in Appendix A. An agreement ratio of 1.00 means that the maximum calculated force is exactly equal to the maximum measured force. An agreement ratio smaller than 1.00 indicates that the calculated force is smaller than the measured force. If the agreement ratio is larger than 1.00, the calculated force is larger than the measured force.

Equation 4-2: Agreement ratio

$$Agreement_Ratio = \left[\frac{Calculated_Force_{MAX}}{Measured_Force_{MAX}} \right]$$

If a maximum deviation from 1.00 of 0.30 is regarded as a reasonable level agreement then agreement ratios between 0.7 and 1.3 can be regarded to indicate good agreement between the numerical and physical model. In a design situation an over prediction is more acceptable than an under prediction. If the numerical model proves to consistently under predict the forces, a correction factor can be applied to ensure that the calculated force is always an over prediction. If the numerical model is consistently overestimating the forces, the result can be left unchanged to maintain a conservative answer. The agreement ratios for the sensitivity runs were compared in Figure 4-6 to Figure 4-9. From the comparisons it was found that Passcat agrees less with the physical model measurements for larger passing speed and passing distance. Passcat agrees more with physical model measurements for larger depth draft ratios. No obvious trend regarding the agreement could be derived for the presence of quay or channel walls, there is however a large difference between the agreement ratios for different speeds when channel walls are used.

From the comparisons of the sensitivity runs in Figure 4-6 to Figure 4-9, boundaries were determined wherein the agreement of the numerical model with the physical model is regarded as acceptable. The boundaries are summarized in Table 4-1. From Figure 4-6 it was derived that the numerical model shows poor agreement at passing speeds of more than 12kt for surge and sway forces, and at passing speeds of more than 10kt for yaw moments. From Figure 4-7 it was derived that the numerical model shows poor agreement at a passing distance of more than 3Bm for yaw moments and 4Bm for surge and sway forces. From Figure 4-8 it was found that agreement ratios were lower at low depth draft ratios, but that the effect is not as strong as for passing speed. No limits were drawn for depth draft ratio from the sensitivity runs. From Figure 4-9 it can be seen that channel walls have a large positive and negative effect on the agreement ratio of sway forces at 6kt and 8kt passing speed. The conclusion is that wide channel walls (9Bm or 12Bm) cause a high level of uncertainty at speeds above 7kt for sway forces. For yaw forces a speed above 7kt together with a narrow 6Bm channel will cause poor agreement.

Chapter 4: Numerical Model Validation

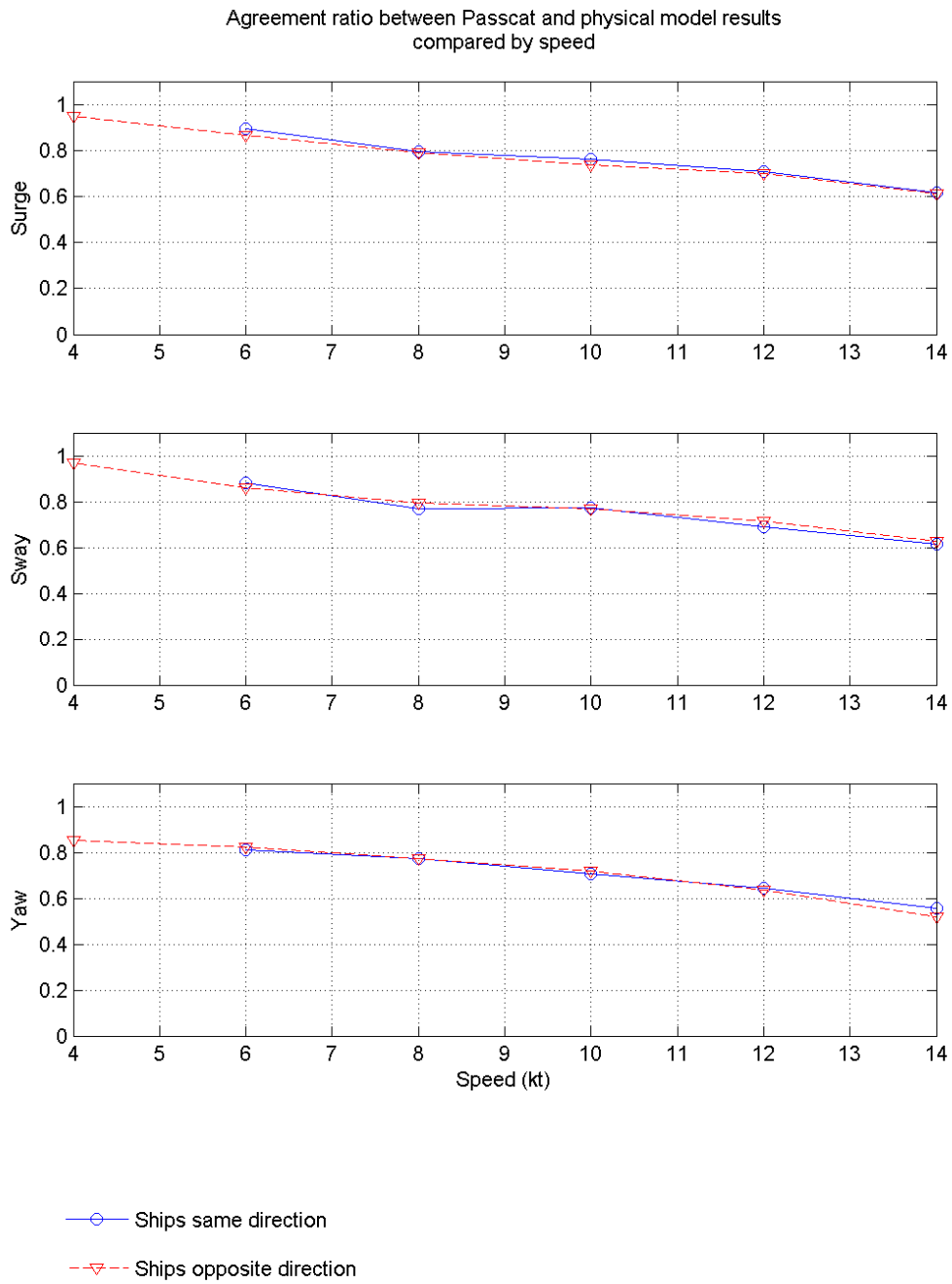


Figure 4-6: Agreement ratio for variation in speed for ships in both directions

Chapter 4: Numerical Model Validation

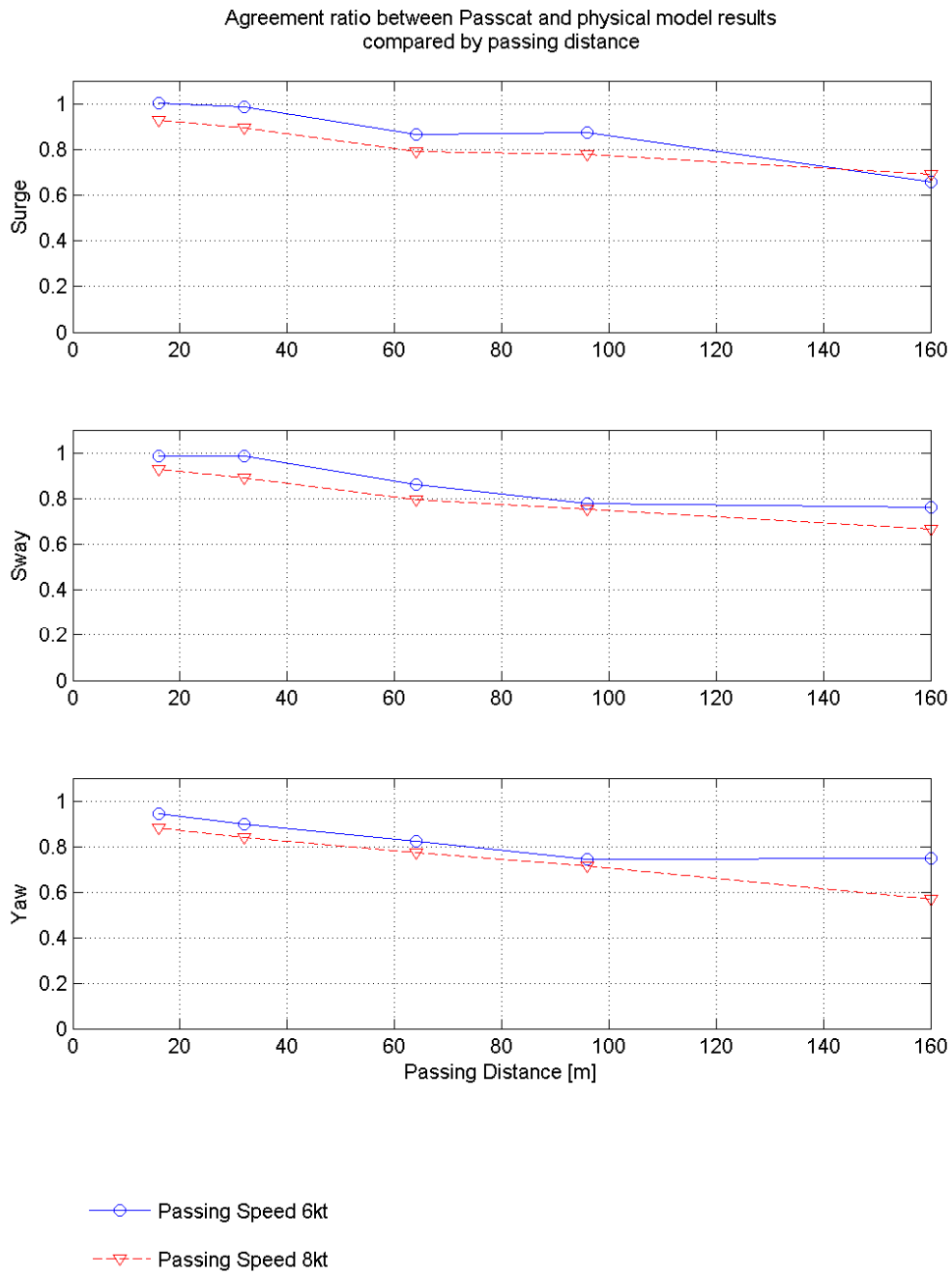


Figure 4-7: Agreement ratio for variation in passing distance for the ship passing at 6kt and 8kt

Chapter 4: Numerical Model Validation

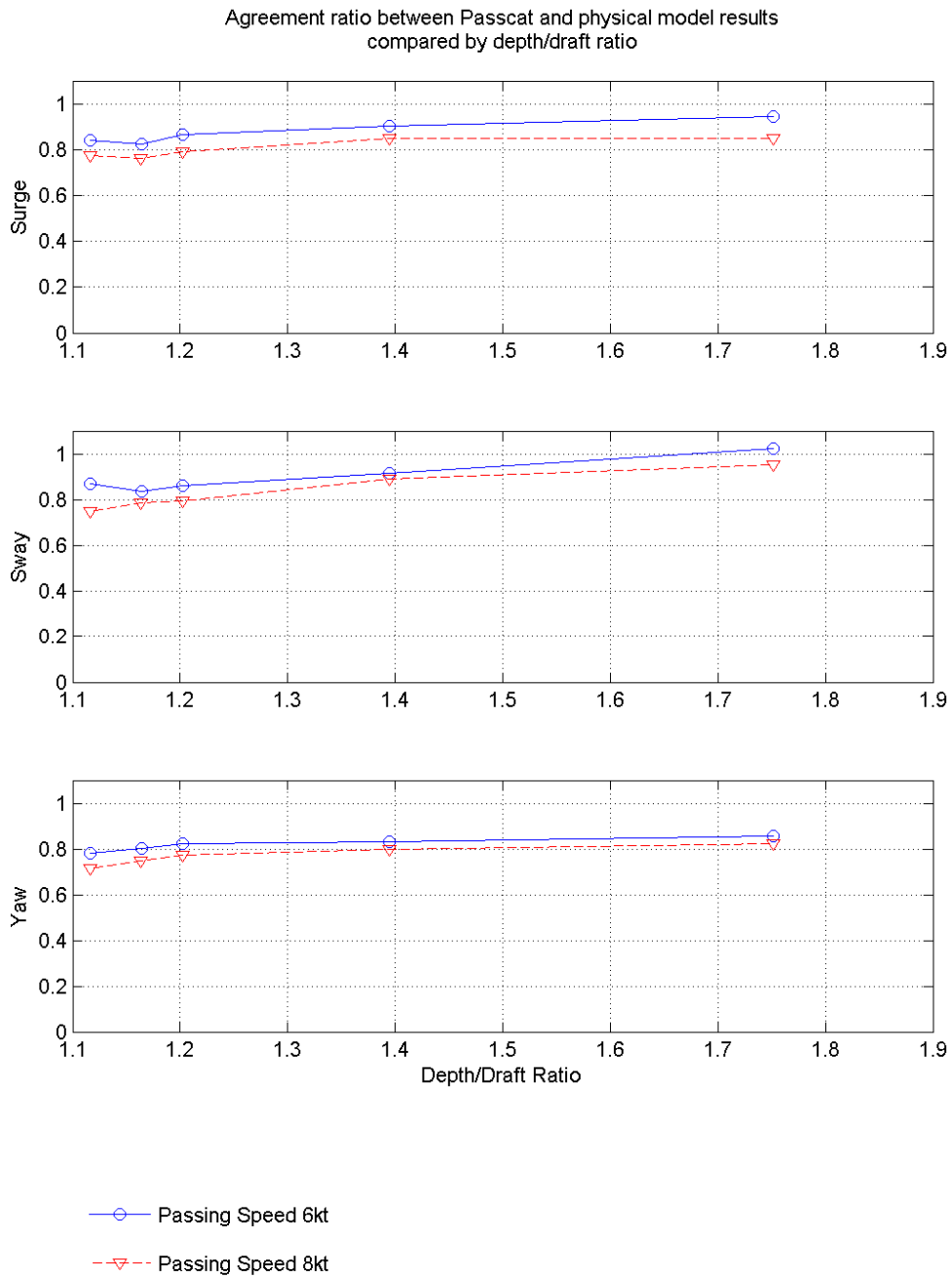


Figure 4-8: Agreement ratio for variation in depth draft ratio for the ship passing at 6kt and 8kt

Chapter 4: Numerical Model Validation

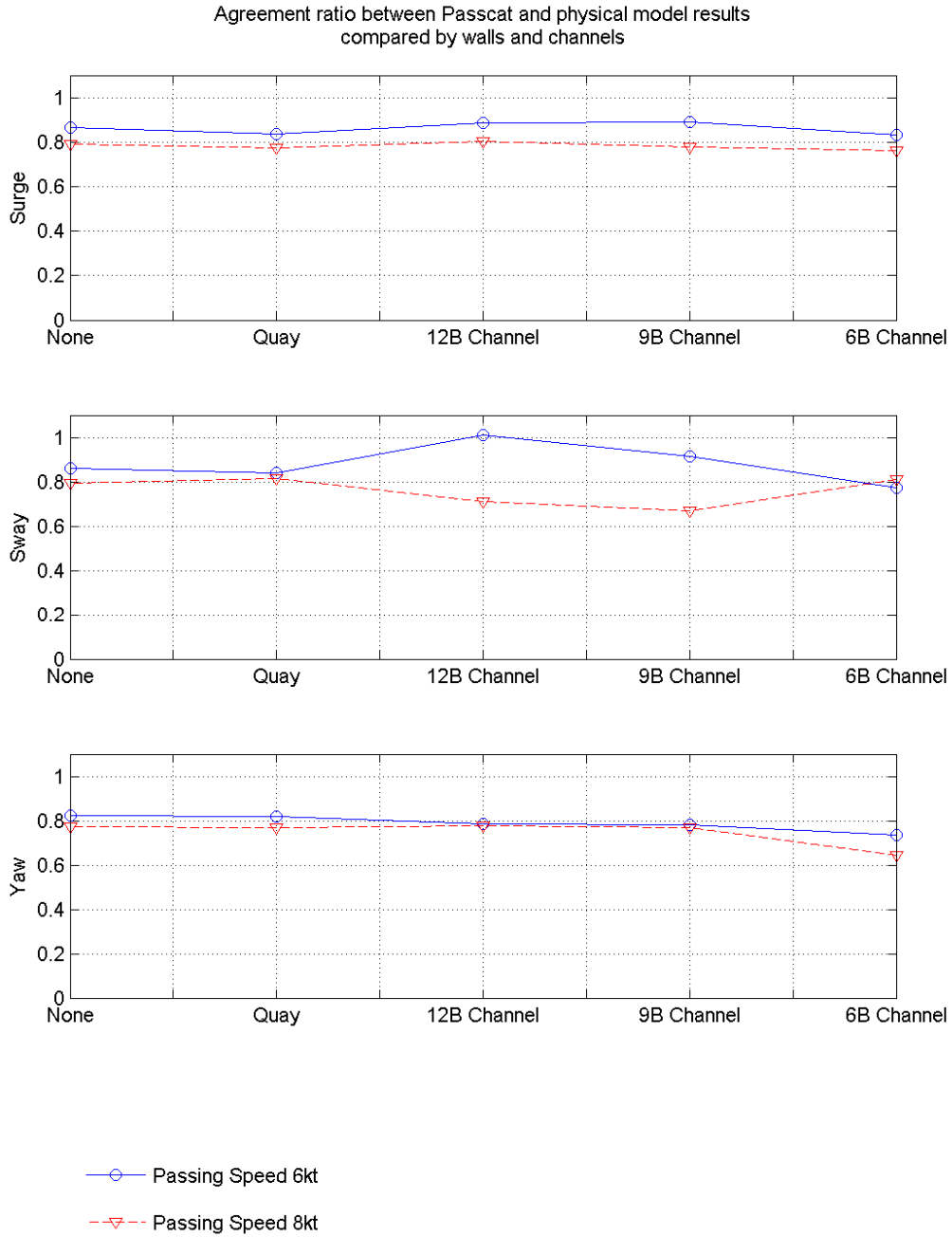


Figure 4-9: Agreement ratio for different obstructions in the water for the ship passing at 6kt and 8kt

Chapter 4: Numerical Model Validation

The sensitivity runs were done for essentially the same test, changing one variable at a time. From this the change in agreement could be derived for the change in the variable. By doing combination runs it was made clear what the combined effect of a change in more than one variable is. The combined effect of the combination runs can be assessed by observing the difference between the agreement ratio of the original sensitivity runs and the agreement ratio of the combination run. Combination runs were compared by speed, depth draft ratio and for walls and channels. The combination runs were used to assess whether conclusions drawn from sensitivity runs are still applicable when more than one variable is varied at a time.

From direct inspection of the combination runs in Figure 4-10 to Figure 4-12, the combinations that cause poor agreement or a strong trend towards poor agreement, could be found. Opposite directions of trends contribute to greater uncertainty and where it happened, limits for good agreement were selected conservatively.

Because of the combination runs, three more boundaries were added to the boundaries drawn from the sensitivity runs. For narrow 6B channels, depth draft ratio more than 1.164 and passing speed less than 6kt, yaw forces will show good agreement ratios. For quay walls and passing speed less than 9kt, surge and sway will show good agreement ratios. For open water, depth draft ratio more than 1.164 and passing speed less than 10kt, all forces will show good agreement ratios.

Table 4-1: Limits for good agreement between Passcat and the physical model

Structures	Variable	Force		
		Surge	Sway	Yaw
None	V	<10kt	<10kt	<10kt
	d/D	>1.164	>1.164	>1.164
	G	<4Bm	<4Bm	<3Bm
Quay	V	<9kt	<9kt	<10kt
	d/D	>1.164	>1.164	>1.164
	G	<4Bm	<4Bm	<3Bm
12B	V	<10kt	<7kt	<10kt
	d/D	>1.164	>1.164	>1.164
	G	<4Bm	<4Bm	<3Bm
9B	V	<10kt	<7kt	<10kt
	d/D	>1.164	>1.164	>1.164
	G	<4Bm	<4Bm	<3Bm
6B	V	<10kt	<10kt	<6kt
	d/D	>1.164	>1.164	>1.164
	G	<4Bm	<4Bm	<3Bm

Chapter 4: Numerical Model Validation

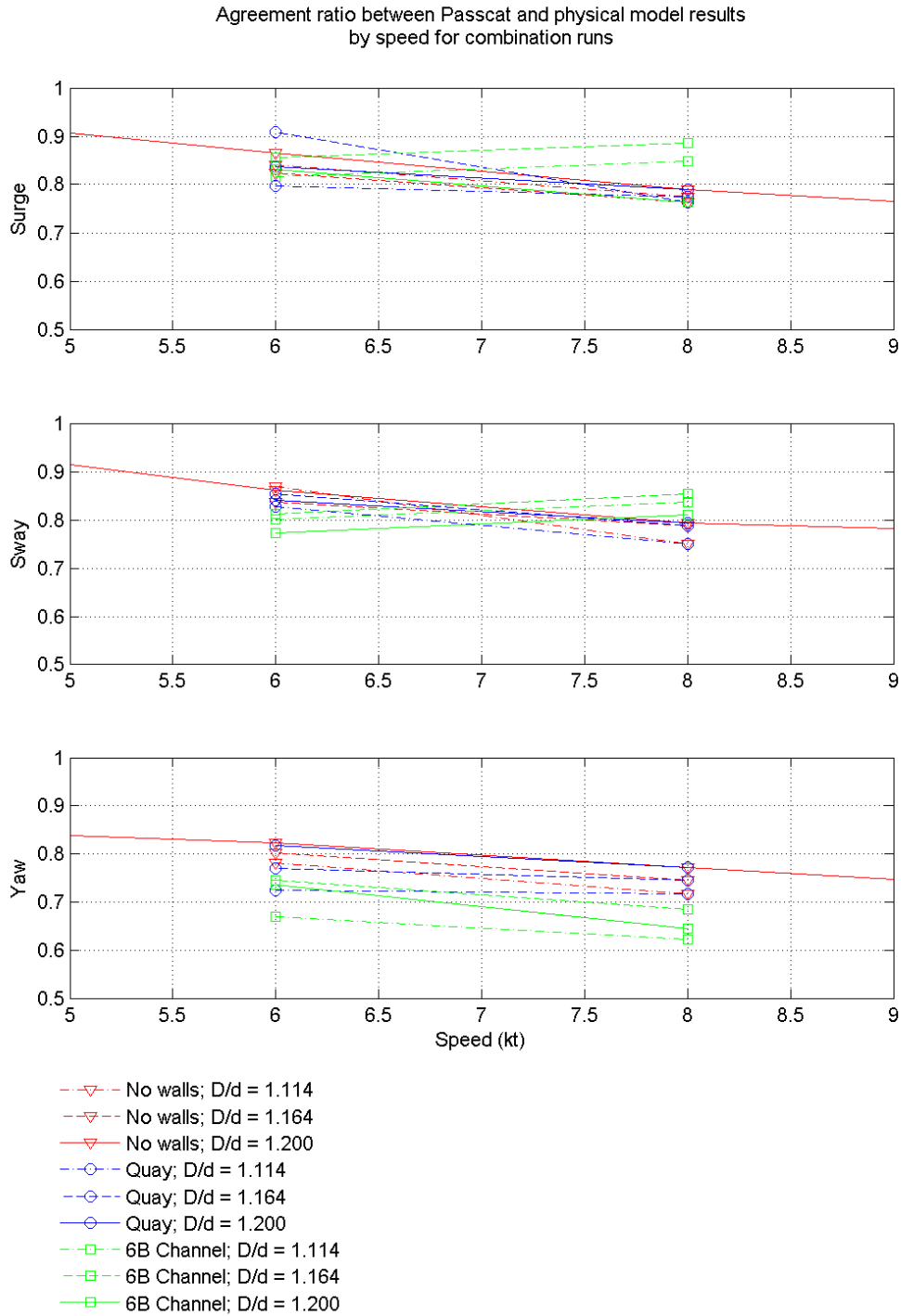


Figure 4-10: Agreement ratio percentage by speed for combination runs

Chapter 4: Numerical Model Validation

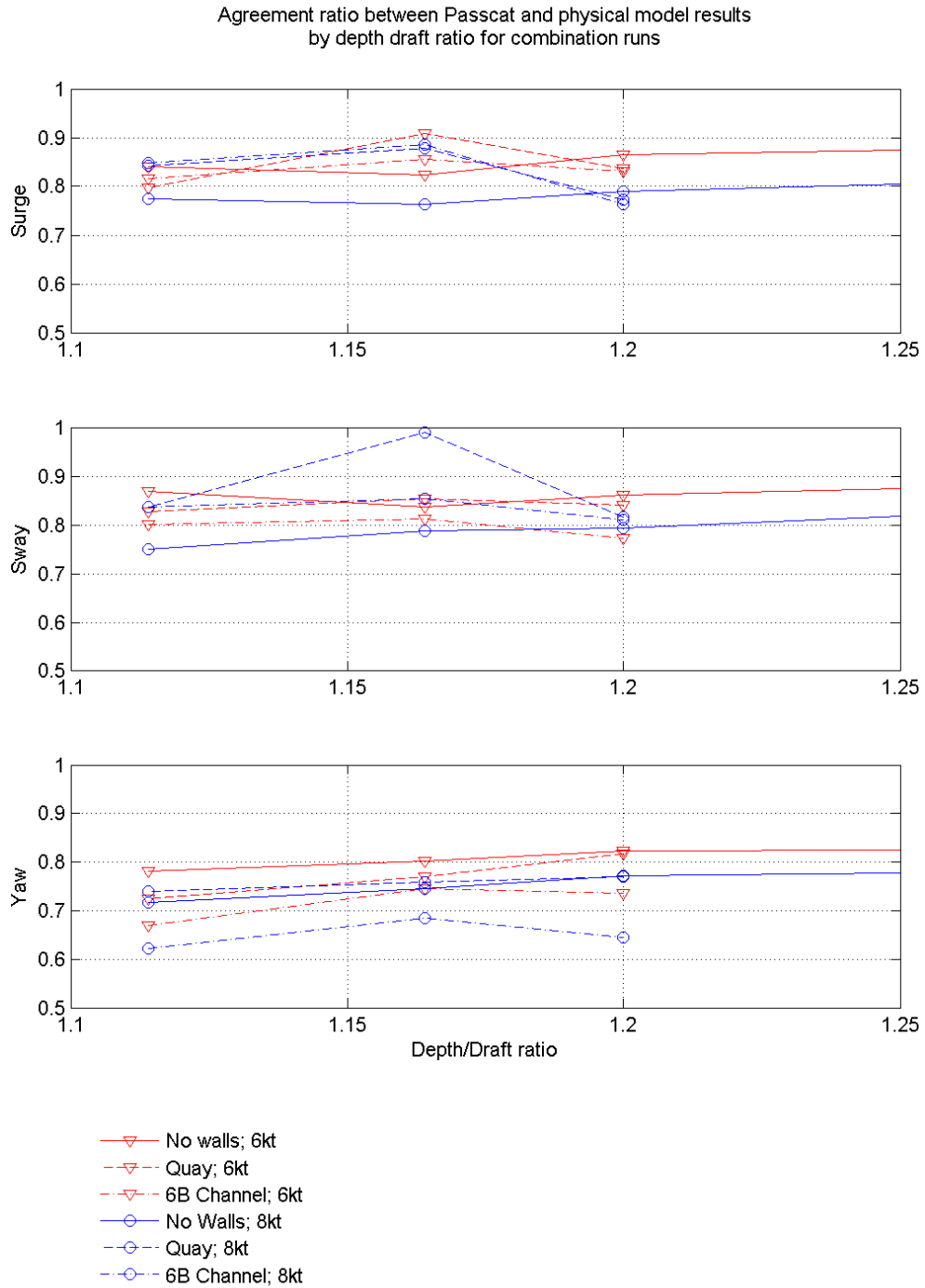


Figure 4-11: Agreement ratio by depth draft ratio for combination runs

Chapter 4: Numerical Model Validation

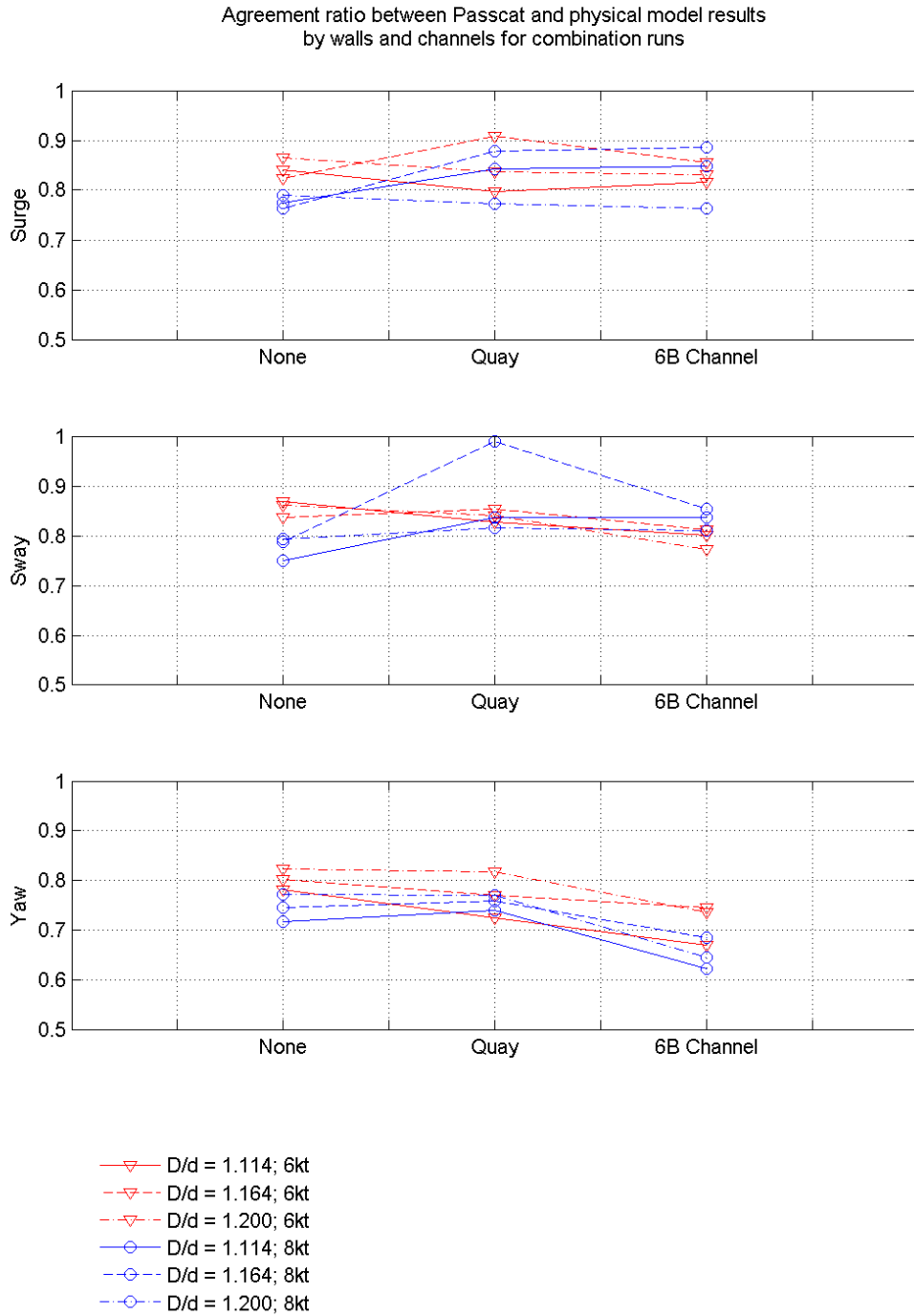


Figure 4-12: Agreement ratio by walls and channels for combination runs

From the agreement ratio graphs (Figure 4-6 to Figure 4-12) an approximate correction factor can be obtained by which the results can be multiplied. To assess whether the same correction factors could be used for ships that have significantly different shapes and sizes, data obtained from Flanders University was used. The existing runs from Flanders University are only varied for depth draft ratio. The Flanders runs were done for a bulk carrier passing a tanker. By comparing the agreement of the Flanders data with the agreement of the new data it can be seen whether the same agreement can be expected for ships of vastly different size and hull shape. From the comparison in Figure 4-13 it can be seen that the general trends are almost the same, but that there is a clear offset. The Flanders data clearly show better agreement than the new runs, but it is uncertain whether this will be the case for other ship shapes and sizes. It is therefore not recommended to use the accuracy limits or correction factors for ships that differ vastly from the dimensions of the ships used in the model study done at the CSIR.

General under prediction (agreement less than one) occurs due to the simplifying assumptions made by the potential flow theory on which Passcat is based. Since the free surface is not taken into account, wave energy will not build up between the channel walls as is the case in the physical model. The non-viscous and irrotational assumptions ignore the boundary layer effect and its drag forces due to turbulence and viscosity. The scaling effects, discussed in chapter 3.8, cause the scale model to produce slightly larger forces than the prototype condition. If a larger scale was used it might have had a small but positive influence on the agreement between the numerical and physical models.

Chapter 4: Numerical Model Validation

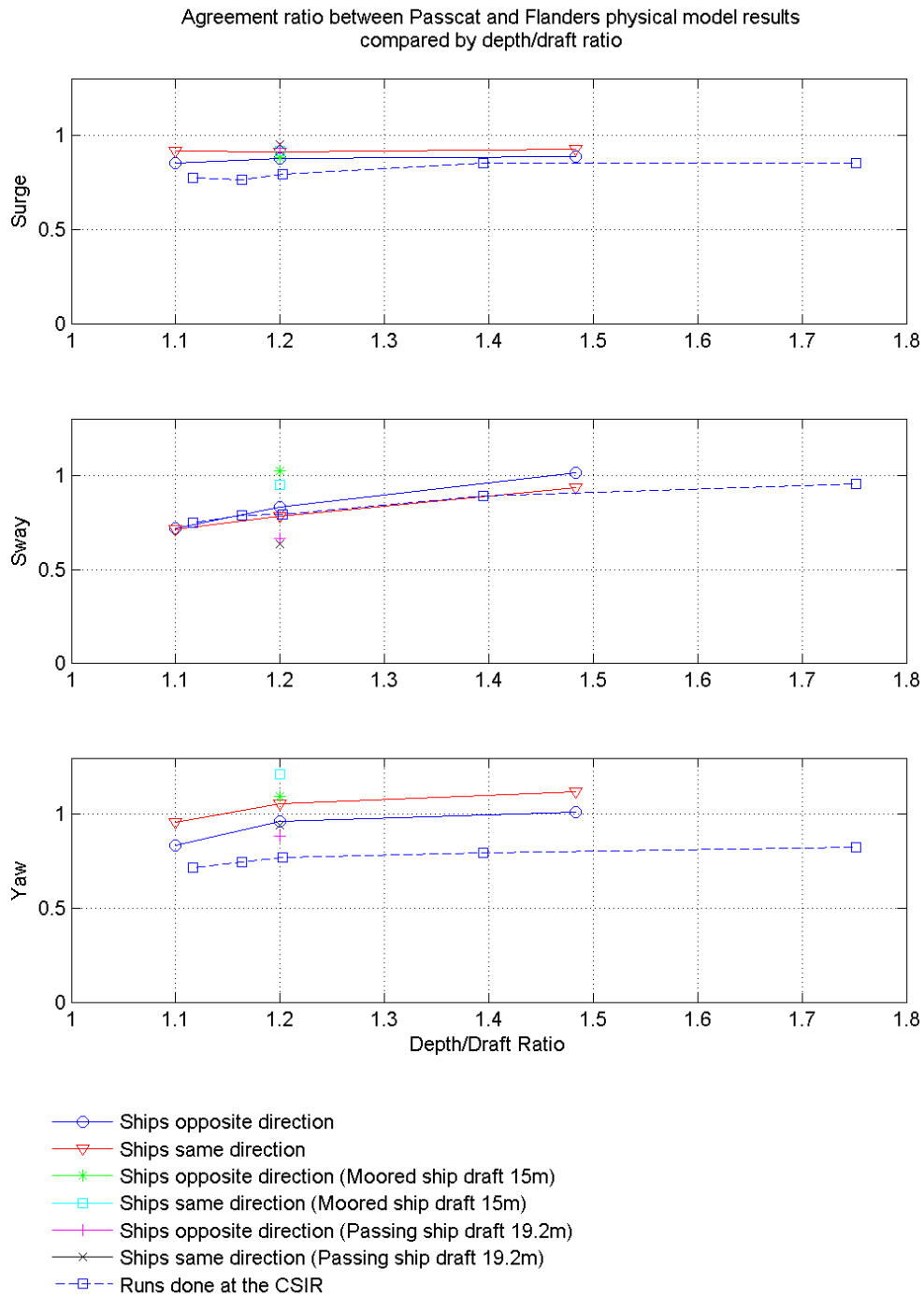


Figure 4-13: Agreement ratio for depth draft ratio of the Flanders data and CSIR data for 8kt

4.4 SUMMARY AND CONCLUSIONS

Based on the comparison with the physical model, Passcat numerical model in general under predicts the passing ship forces. Passcat shows closer agreement for low speed, small passing distance and high depth draft ratios.

Acceptable agreement ratios were defined to be between 0.7 and 1.3. Passcat provides acceptable answers if the speed is less than 10kt, depth draft ratio more than 1.164, passing distance less than 4Bm for surge and sway estimations and passing distance less than 3Bm for yaw estimations. These limits are true for no structures in the water, but are also partially true for the presence of quay walls and channels. When quay walls are present, the surge and sway forces will only provide acceptable answers at passing speeds below 9kt. When 9Bm or 12Bm channels are present the sway force will only provide acceptable answers at passing speeds below 7kt. When a 6B channel is present, the yaw moments will only provide acceptable answers at passing speeds below 6kt. Beyond these boundaries poor agreement ratios have to be accepted or alternative methods need to be used.

A correction factor, obtained from the agreement ratio graphs, could be applied to eliminate poor agreement of the numerical model. However, care should be taken to not blindly apply the correction factors when using ships of significantly different dimensions.

5 MATHEMATICAL FORMULAE EVALUATION

5.1 INTRODUCTION

This chapter compares mathematical methods, including Passcat, to the physical model measurements to evaluate their relative performance. Apart from the numerical model Passcat, the other mathematical formulae are either empirical or semi-empirical and require less computational effort. This chapter evaluates whether the empirical and semi-empirical formulae are sufficient to be used for design and whether Passcat should rather be used.

5.2 MATHEMATICAL METHODS

A brief description of the background of the mathematical models is given in the literature review Chapter 2.5. The Kriebel and Flory empirical methods as well as the Wang Seelig, Wang Kriebel and Varyani and Vantorre semi-empirical methods were evaluated against each other and against the numerical model, Passcat (Figure 5-1).

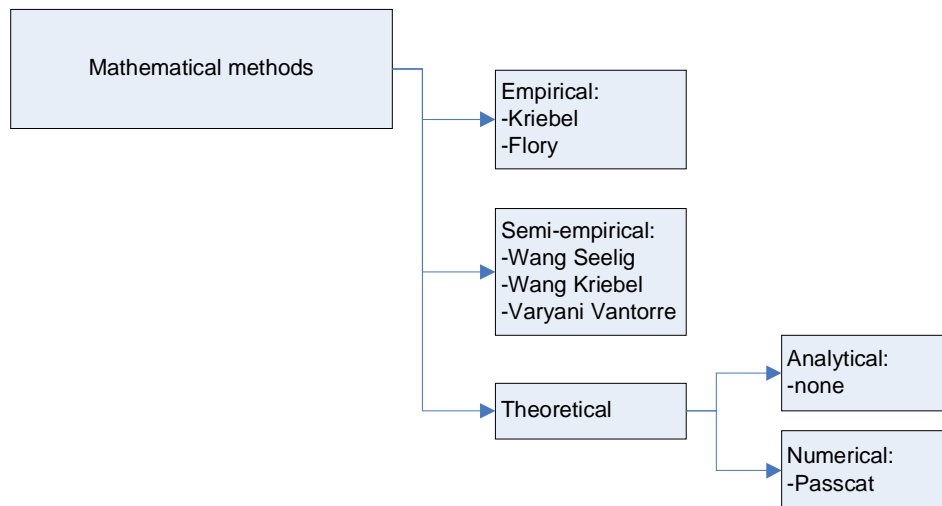


Figure 5-1: Mathematical methods evaluated

Chapter 5: Mathematical Formulae Evaluation

The Kriebel formulae only returned a maximum and minimum value based on basic formulae. The Flory method also returned maxima and minima, but these values could be used to scale a non-dimensional graph to return a force series.

The method by Varyani and Vantorre is somewhat more extensive by explicitly returning each value on the force series graph.

The two methods applying shallow water correction factors, the Wang Seelig and the Wang Kriebel methods, were the most extensive calculation methods of all. The shallow water correction factors for both methods were easy to calculate, but the deep water force series' of Wang required a significant amount of calculations. The Wang deepwater force series was found by solving a double integral for every point in the force series. The double integral was solved by programming Simpson's rule to solve each time step automatically. After the deep water force series was calculated the corresponding shallow water correction factors could be applied.

Empirical models were derived for open water, but by using multiplication factors for quay walls (Pinkster, 2004) their agreement ratios could be assessed in comparison with Passcat. There are no such multiplication factors for channels, so the same multiplication factors are assumed to be the same for channels as for quay walls. For surge, the forces would be 80% larger and for sway and yaw the forces would be 60% lower when walls or channels are present.

Passcat has been described in Chapter 4 and has been included in the graphs for comparison

5.3 COMPARISON OF MATHEMATICAL AND PHYSICAL MODELS

The mathematical models were compared by comparing their force series' with the force series of the physical model. In the comparison the maximum forces and the shape of the force series graphs are very important since ship motions are a function of forces and the time the force is applied. A complete set of these figures is provided in Appendix E. One example of such a comparison, for test number 10, is provided in Figure 5-2.

Chapter 5: Mathematical Formulae Evaluation

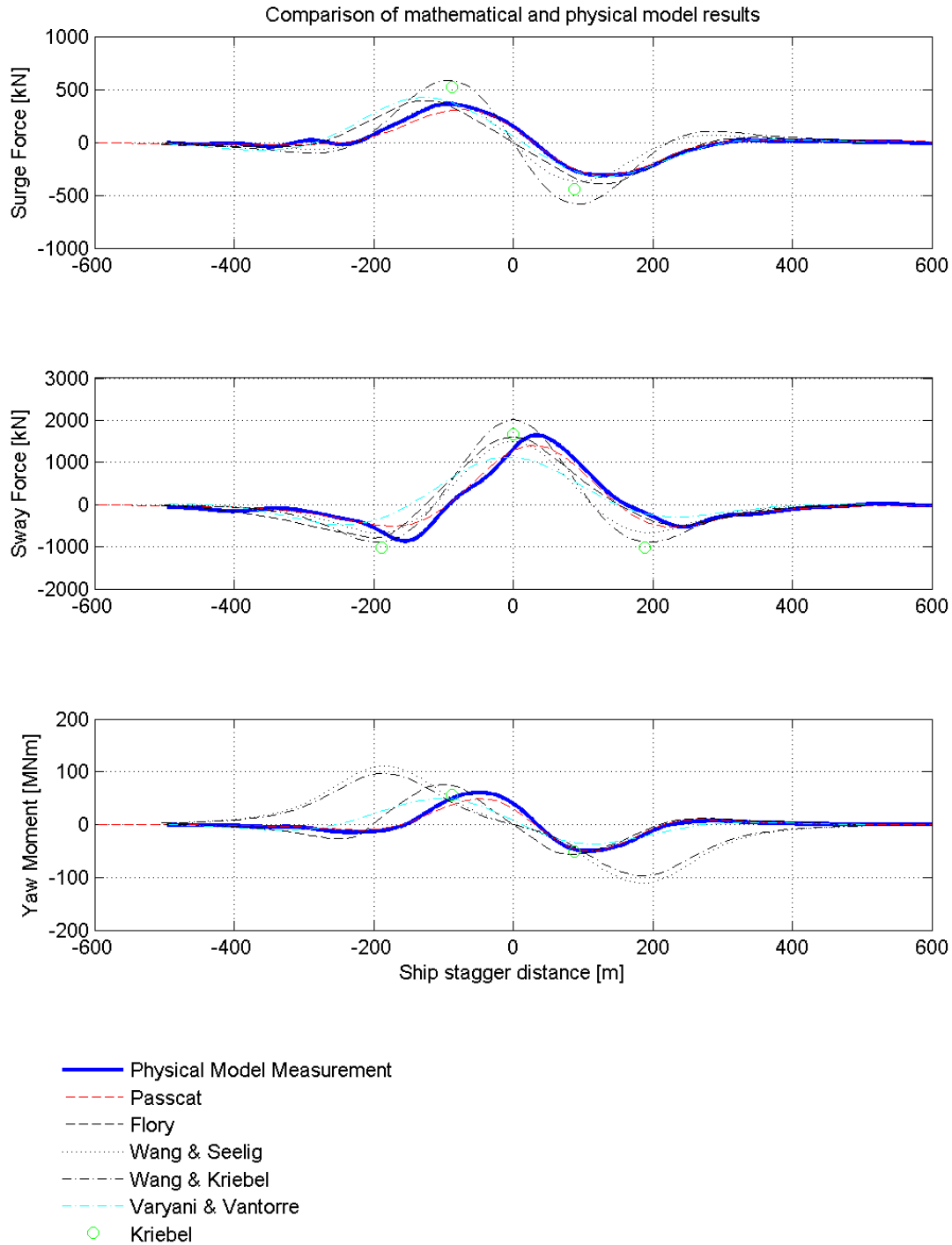


Figure 5-2: Comparison of empirical and semi-empirical calculations with numerical and physical model results for test 10

To assess the performance of the empirical and semi-empirical models, agreement ratios were calculated by dividing the maximum force of each model by the corresponding maximum force of the physical model (Equation 4-2). The agreement ratios for all the tests are given in Appendix A. From the inspection of Figure 5-3 to Figure 5-6, boundaries were drawn wherein the mathematical models would agree well to the physical model. Good agreement was regarded as agreement ratios between 0.7 and 1.3.

Chapter 5: Mathematical Formulae Evaluation

The boundaries were summarized in Table 5-1. In Table 5-1 the mathematical models were listed each with three rows for surge, sway and yaw forces. In the columns the variables were listed. When a force agreed well with the physical model for the corresponding variable, the cell was tagged as good. If it only agreed well to the physical model for a certain range of the variable, the range was given in the cell. If the calculated force did not agree at all to the physical model, the corresponding cell was tagged as bad. For a specific model to give a good prediction, all the conditions in a row should be satisfied. If one of the cells in the row is tagged as bad, then the empirical or semi-empirical model can not provide a good answer for the specific force.

Table 5-1: Boundaries wherein the empirical or semi-empirical models give good agreement with physical model measurements

Model	Force	Variable			
		Speed	Pass dist	d/D	Walls and Channels
Kriebel	Surge	>8kt	bad	>1.4	good excl 6B channel
	Sway	good	1Bm-4Bm	good	bad
	Yaw	<13kt	>1Bm	good	good excl 6B channel
Flory	Surge	good	>1Bm	<1.7	good excl 6B channel
	Sway	good	good	good	bad
	Yaw	>4kt; <14kt	1Bm-2Bm	good	good excl 6B channel
Wang Seelig	Surge	good	<4Bm	<1.9	good excl 6B channel
	Sway	<14kt	<3Bm	<1.8	bad
	Yaw	bad	bad	good	good excl 6B channel
Wang Kriebel	Surge	bad	bad	bad	good excl 6B channel
	Sway	>6kt	bad	good	bad
	Yaw	bad	bad	bad	good excl 6B channel
Varyani Vantorre	Surge	>4kt	>2Bm	<1.5	good excl 6B channel
	Sway	<6kt	<3Bm	>1.2; <1.7	good excl 6B channel
	Yaw	<10kt	>1Bm	>1.15; <1.8	good excl 6B channel
Good agreement was regarded as agreement ratios between 0.7 and 1.3					

Of the empirical and semi-empirical methods the methods that are not recommended to be used at all for passing container ships are the Kriebel method for surge forces, the Wang Seelig method for yaw, and the Wang Kriebel method for surge, sway and yaw.

To compare the empirical or semi-empirical models to the numerical model Passcat, models were ranked for the different variables by the inspection of Figure 5-3 to Figure 5-6. The ranking is given in the rows of Table 5-2, with the best agreement tagged one (1) and the worst agreement tagged six (6). Ranking was done for surge, sway and yaw for the variables speed, passing distance, depth draft ratio and for walls and channels. At the bottom of the table the ranks were added for surge, sway and yaw. The ranks for surge, sway and yaw were also added to find a total rank for each model. The model with the lowest value would be performing the best.

Table 5-2: Ranking of mathematical models

Variable	Force	Model					
		Kriebel	Flory	Wang Seelig	Wang Kriebel	Varyani Vantorre	Passcat
Speed	Surge	5	2	1	6	3	4
	Sway	1	2	4	3	6	5
	Yaw	2	1	6	5	4	3
Passing distance	Surge	6	3	1	5	4	2
	Sway	2	1	4	6	5	3
	Yaw	1	4	6	5	3	2
Depth draft ratio	Surge	5	3	2	6	4	1
	Sway	2	6	4	3	5	1
	Yaw	1	4	6	5	3	2
Walls and channels	Surge	5	1	2	6	3	4
	Sway	5	4	3	6	2	1
	Yaw	1	3	6	5	4	2
Note:	1 = Best agreement 6 = Worst agreement						

Combined ranks	Surge	21	9	6	23	14	11
	Sway	10	13	15	18	18	10
	Yaw	5	12	24	20	14	9
Total ranks		36	34	45	61	46	30

From Table 5-2 it can be seen, for surge forces, that Passcat (11) is outperformed by the Wang Seelig (6) and the Flory (9) methods for surge force estimations. For sway forces, Passcat (10) and the Kriebel (10) formulae are tied as best performers. For yaw moments Passcat (9) is outperformed by the Kriebel (5) method. From the "total ranks" row it can be seen that Passcat provides the best agreement in general by a close margin (30 vs. 34). The only time when Passcat was outperformed by a single empirical or semi-empirical model for surge, sway and yaw was with the Flory method for speed. At all other times Passcat was outperformed by a combination of three different empirical or semi-empirical methods for surge, sway and yaw.

Even though the empirical methods were derived for bulk carriers and tankers, they can be applied to passing container ships within certain limits. At first only the open water case is considered. If a designer wants to use a single mathematical method, then only the Flory method should be used. In Table 5-3, criteria are given for the selection of either the Flory method or Passcat. The criteria for the selection of Passcat or Flory overlap, but Passcat can be used over a slightly wider range. Outside the stated acceptable boundaries of empirical methods and Passcat, alternative methods, like physical modelling, need to be performed.

The addition of quay or channel walls has a very large effect on the results of the Flory method, especially for sway. It is therefore not recommended that the Flory method be used when there are any quay or channel walls in the water.

Table 5-3: Criteria for the selection of a calculation method for the open water case

	Passcat only	Passcat and Flory	Flory only
PASSING SPEED [kt]	$0 < V < 4$	$4 < V < 10$	$10 < V < 14$
DEPTH DRAFT RATIO [-]	$d/D > 1.7$	$1.7 > d/D > 1.164$	$1.164 > d/D > 1$
PASSING DISTANCE [Bm]	$0 < G < 1$ $2 < G < 3$	$1 < G < 2$	N/A
Note: The use of empirical or semi empirical methods are not recommended when there are quay or channel walls in the water. For quay or channel walls refer to section 4.4 for recommendations when using Passcat.			

Symbols used in Table 5-3

V	Passing speed	[m/s]
d	Depth	[m]
D	Draft	[m]
G	Board to board lateral distance between the ships	[m]

Chapter 5: Mathematical Formulae Evaluation

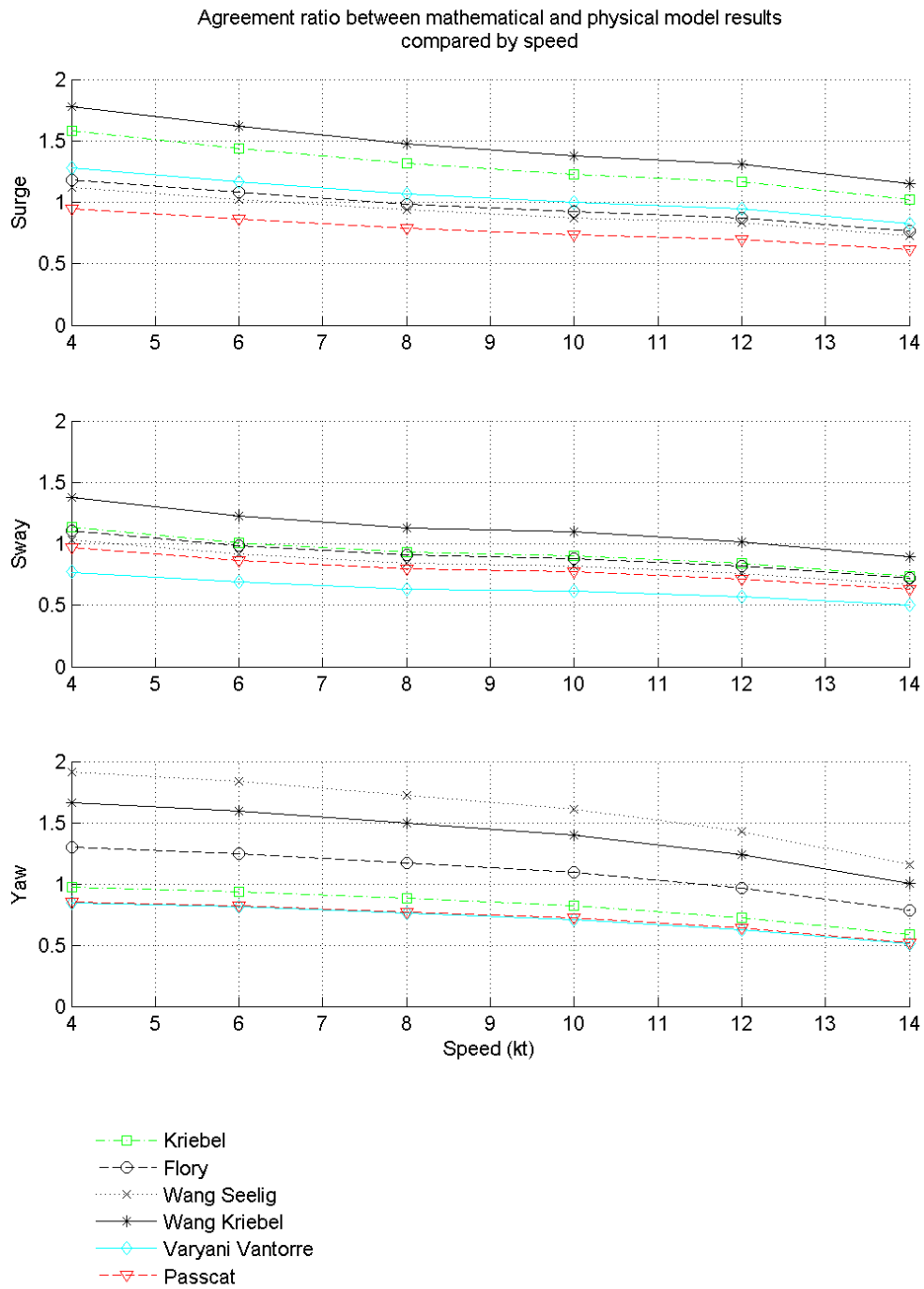


Figure 5-3: Agreement ratio by speed for mathematical and physical model results

Chapter 5: Mathematical Formulae Evaluation

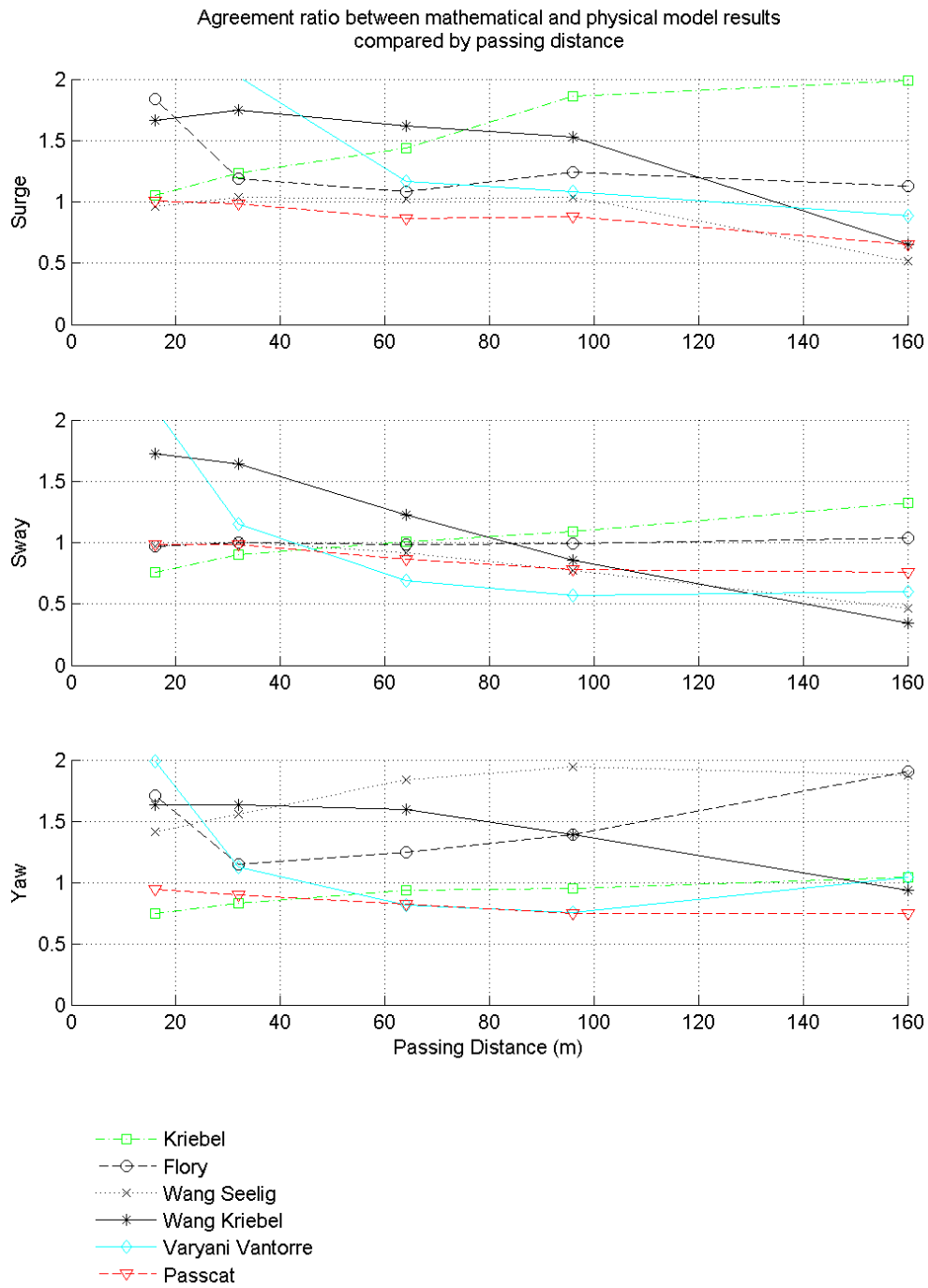


Figure 5-4: Agreement ratio by passing distance for mathematical and physical model results

Chapter 5: Mathematical Formulae Evaluation

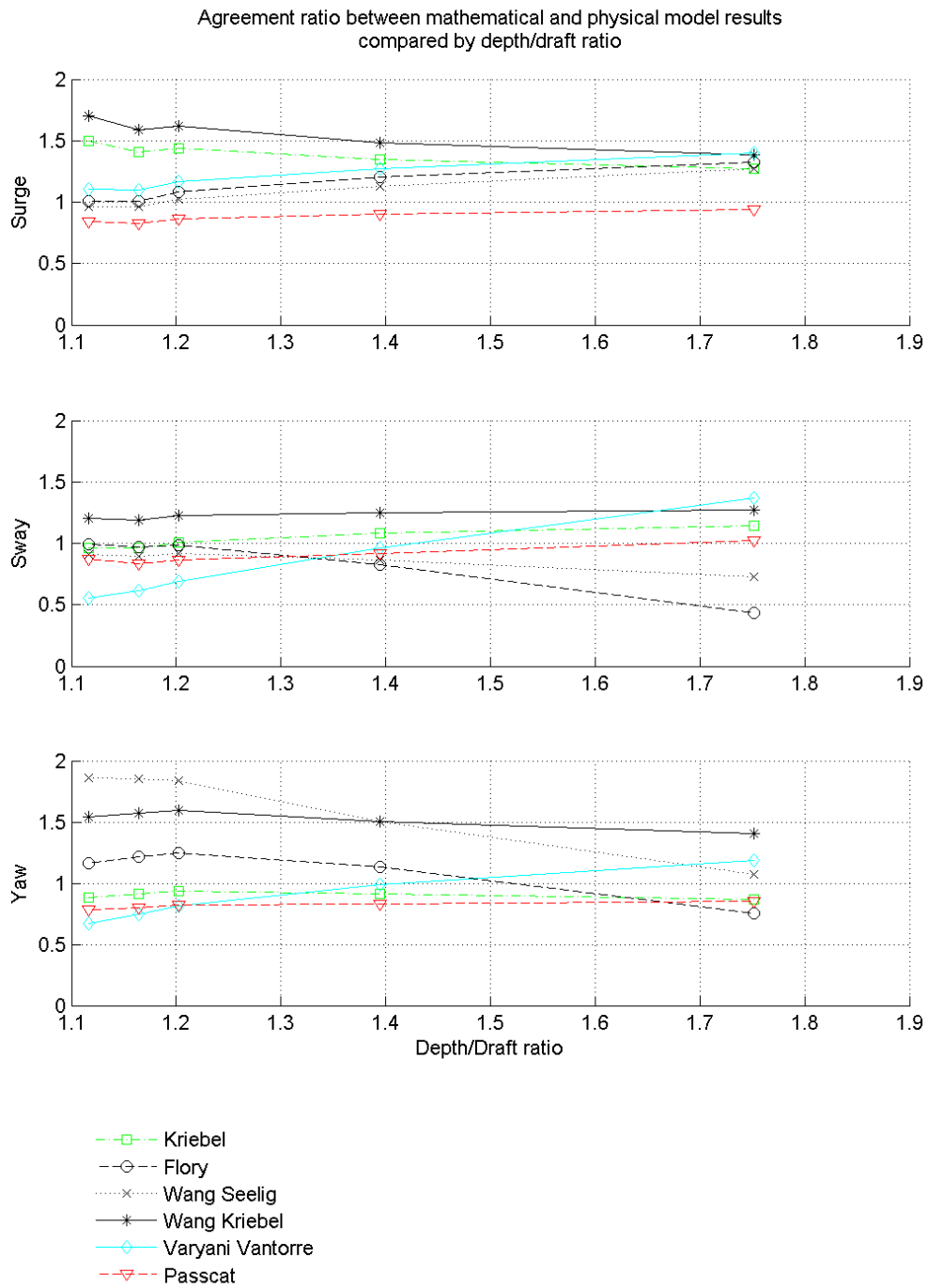


Figure 5-5: Agreement ratio by depth draft ratio for mathematical and physical model results

Chapter 5: Mathematical Formulae Evaluation

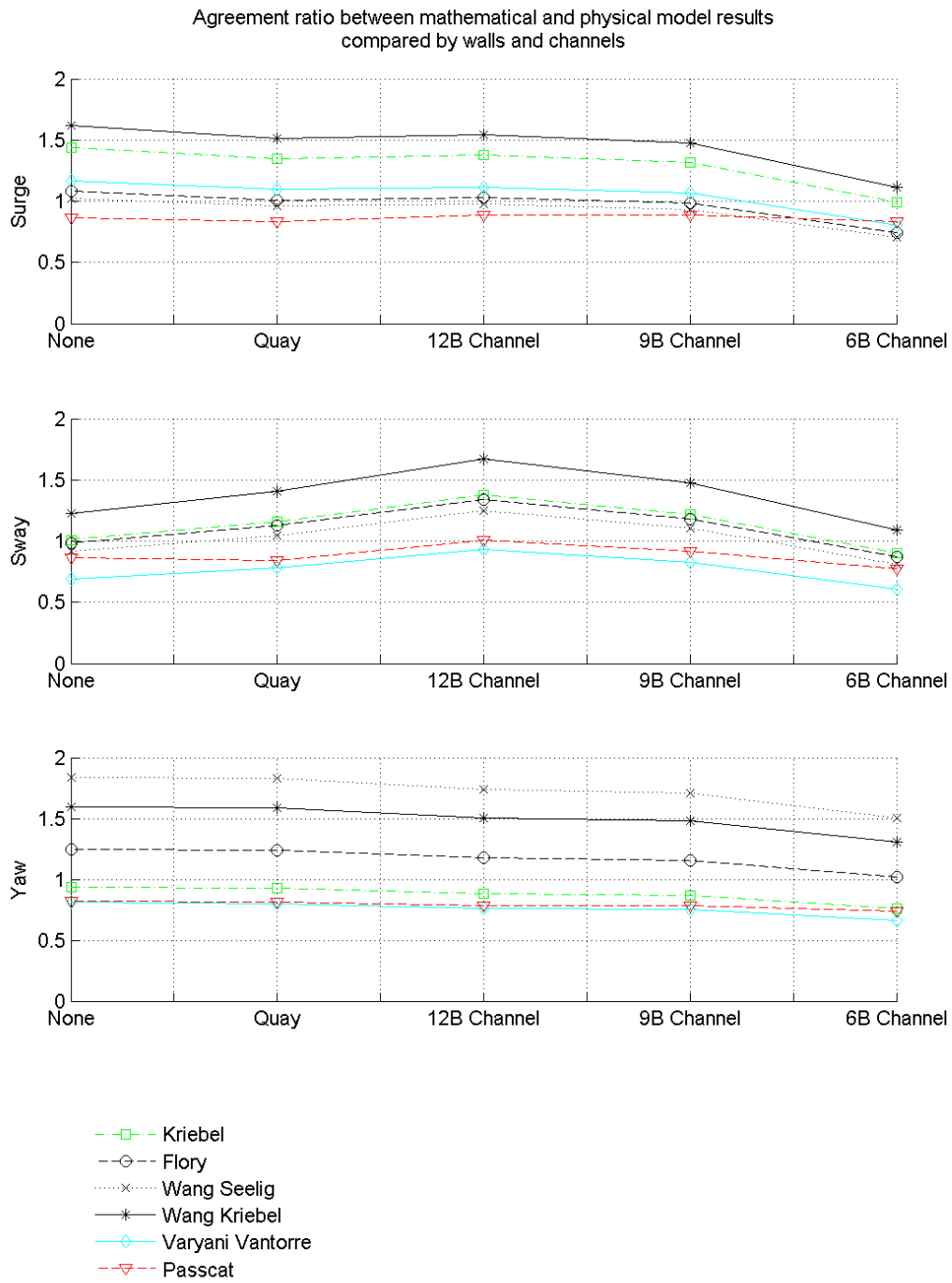


Figure 5-6: Agreement ratio by walls and channels for mathematical and physical model results

5.4 CONCLUSIONS

The conclusions have been made with the use of a physical model of a container ship passing a bulk carrier. Conclusions can not be regarded as being generic for any container ship passing any bulk carrier. The conclusions can cautiously be applied to ships with similar dimensions.

Unlike Passcat, empirical and semi empirical methods can not provide good agreement when there are quay or channel walls in the water.

For the open water case, it is only the Flory method that can provide answers with good agreement to the physical model for surge, sway and yaw forces. The Flory method can provide answers with acceptable agreement within narrow boundaries of passing distance (1 to 2 times the beam of the moored ship), passing speed (4 kt to 14 kt) and depth draft ratio (less than 1.7).

When comparing the boundaries of the Flory method to the boundaries of Passcat, Passcat proves to give results with good agreement to the physical model over a larger range of variables. Criteria for the selection of a suitable mathematical method (Flory or Passcat) for the open water case are summarized in Table 5-3. For confined water Passcat should be used within certain boundaries (boundaries summarized in section 4.4)

The boundaries are very strict. Beyond the boundaries of the Flory method and Passcat, an alternative method, like physical modelling, should be used.

6 CONCLUSIONS

The conclusions were drawn with the use of a physical model with one set of ships. The conclusions are therefore relevant for ship dimensions similar to the ships used in this study.

From the physical model, the knowledge about passing ships has been extended by some valuable relationships that were found between variables and passing ship forces. For passing speed, it was found that the passing ship forces are proportional to the passing speed to the power of 2.32. This is slightly higher than the well-known quadratic relationship for general fluid drag forces which is also generally accepted for passing ship induced forces. Due to ship squat, secondary wash waves, increased boundary layer effects at higher speed and model scale effects it is expected that the proportionality should be slightly more than two, but it is unknown what the relative effect of each influence is. For passing distance it was found that the passing ship forces are proportional to an exponential function of the passing distance multiplied by a different constants for surge (-0.0110), sway (-0.0115) and yaw (-0.0154). For depth draft ratio it was found that the passing ship forces are proportional to the depth draft ratio to the power of -1.5 for surge, -3.1 for sway and -2.3 for yaw. The effect of channels is the same as the effect of quay walls for channels wider than 9 times the beam of the moored ship. When quay walls or wide channels (more than 9 times the beam of the moored ship) are present the surge forces increased by 1.92 times, sway forces by 0.34 times and yaw forces by 0.43 times. This is close to the multiplication factors proposed by Pinkster (2004) of 1.8, 0.4 and 0.4 for surge, sway and yaw forces. When there is a narrow channel then the surge forces increased by 2.63 times, sway forces by 0.31 times and yaw forces by 0.53 times. By using the above trends, empirical relationships were derived for the prediction of relative surge, sway and yaw passing ship forces for different passing ship conditions.

From the numerical model study the numerical model, Passcat, was found to under predict the passing ship forces. Passcat shows closer agreement for low speed, small passing distance and high depth draft ratios. It was found that the numerical model, Passcat, is valid for a wide range of sensitivities and remains within the agreement ratio limits between 0.7 and 1.3 as long as passing speed is limited to 10kt, depth draft ratio to more than 1.164, passing distance to 4Bm for surge and sway estimation and passing distance to 3Bm for yaw estimations. These limits are true for no structures in the water. The same limits apply when there are structures in the water, only the passing speed has new limits under specific conditions. When quay walls are present, the surge and sway forces will only provide acceptable answers at passing speeds below 9kt. When 9Bm or 12Bm channels are present the sway force will only provide acceptable answers at passing speeds below 7kt. When a 6B channel is present, the yaw moments will only provide acceptable answers at passing speeds below 6kt. Beyond these boundaries poor agreement ratios have to be accepted or alternative methods need to be used. A correction factor, obtained from the agreement ratio graphs, could be applied to eliminate poor agreement of the numerical model. However care should be taken to not blindly apply the correction factors when using ships of significantly different dimensions.

Empirical and semi empirical methods can not provide results with good agreement to the physical model when there are quay or channel walls in the water. For the open water case, it is only the Flory method that can provide answers with good agreement to the physical model for surge, sway and yaw forces. The Flory method can provide answers with acceptable agreement within narrow boundaries of passing distance (1 to 2 times the beam of the moored ship), passing speed (4kt to 14kt) and depth draft ratio (less than 1.7). When comparing the boundaries of the Flory method to the boundaries of Passcat, Passcat proves to give results with good agreement to the physical model over a larger range of variables. Criteria for the selection of a suitable mathematical method (Flory or Passcat) for the open water case are summarized in Table 5-3. The boundaries are very strict. Beyond the boundaries of the Flory method and Passcat, an alternative method, like physical modelling, should be used.

7 RECOMMENDATIONS

When comparing the agreement ratios for the tests done for this study with the agreement ratios of the tests obtained from Flanders University, it was found that the agreement ratios are different even if similar Froude numbers, speed and depth draft ratios are used. This suggests that the block coefficients and passing ship size to moored ship size ratios have an effect on the agreement ratios. It will be useful to study other ships to find the relationship between block coefficient and the passing ship forces and the relationship between the relative sizes of the passing and moored ships to the passing ship forces. The new information, in addition to the model test information done for this study, can serve as a basis for empirical formulae for passing container ships.

It will be useful for a future study to do the same model tests on different scales and if possible to compare it with prototype measurements to see what the effect of boundary layers is within models scaled by the Froude scaling law.

In this study the passing and moored ships had the same draft. It will be useful to verify the relative effect on numerical model agreement ratio if the draft of the passing and the moored ships is different.

REFERENCES

- Balmer D. 2007. Separation of boundary layers. School of Engineering and Electronics. University of Edinburgh.
- Bertram V. 2000. Practical Ship Hydrodynamics. Elsevier. Oxford, UK
- Cohen, S.B. Beck, R.F. 1983. Experimental and theoretical Hydrodynamic Forces on a Mathematical Model in Confined Waters. Journal of Ship Research, Vol. 27, No 2.
- Colledge, J.J. Warlow, B. 2006. Ships of the Royal Navy: The Complete Record of all Ships of the Royal Navy. London, UK
- Chadwick A. Morfett J. Borthwick M. 2006. Hydraulics in Civil and Environmental Engineering. Spon Press. New York, USA.
- Fenical S. Kolomiets P. Kivva S. Zheleznyak M. 2006. Numerical modelling of passing vessel impacts on berthed vessels and shoreline. Coast & Harbor Engineering and Ukrainian Center of Environmental and Water Projects. San Francisco, USA and Kiev, Ukraine.
- Fielding S. 2005. Laminar Boundary Layer Separation. The University of Manchester. Manchester, UK.
- Flory J. 2001. A Method for Estimating Passing Ship Forces. Tension Technology International. Morristown, USA
- Flory J. 2002. The Effect of Passing Ships on Moored Ships. Tension Technology International. Morristown, USA
- Huang, E.T. Chen H. 2003. Passing Ship Effects on Moored Vessels at Piers. Naval Facilities Engineering Service Center Port Hueneme. California, USA
- Huang, E.T. Chen H. 2010. Passing Ship Effects at typical Waterfronts. Ports Conference 2010. California, USA.
- Journée J.M.J. and Massie W.W. 2001. Offshore Hydromechanics First Edition. Delft University of Technology. Delft, The Netherlands
- Korsmeyer, F.T., Lee, C.H. Newman, J.N. 1993. Computation of Ship Interaction Forces in Restricted Waters, J. Ship Res., 37(4), 298–306.
- Kriebel D. 2005. Mooring Loads due to Parallel Passing Ships TR-6065-OCN. Naval Facilities Engineering Service Center. Annapolis, USA
- Lean, G.H. Price, W.A. 1977. The effect of passing vessels on a moored ship. Dock and Harbour Authority. London, UK
- Marin, 2010. Ropes JIP. [online]. Available at: <<http://www.marin.nl/web/web/JIPs-Networks/Public/ROPES.htm>>. [Accessed 10 March 2011]
- Muga, B.J. Duke, U. and Fang, S. 1975. Passing Ship Effects – From Theory and Experiment OTC 2368. Exxon Research and Engineering Co. Texas, USA

O'Brien P. O'Brien T. Hens C. 2007. Vessel Interaction - A Case Study. OMC International PTY Ltd. Melbourne, Australia.

Permanent International Association of Navigational Congresses (PIANC). 1995. Criteria for movements of moored ships in harbours: a practical guide (Supplement to Bulletin no. 88. Report of working group PTC II-24.

Pinkster, J.A. 2009. Suction, Seiche and Wash Effects of Passing Ships in Ports. PMH B.V. Rotterdam, The Netherlands

Pinkster, J.A. 2004. The Influence of a Free Surface on Passing Ship Effects. Int. Shipbuilding Progr. 51(4). 313–338.

Pinkster, J.A. Ruijter, M.N. 2004. The Influence of Passing Ships on Ships moored in Restricted Waters.

Remery, G.F.M. 1974. Mooring Forces Induced by Passing Ships OTC 2066. Offshore Technology Conference. Texas, USA

Savioli J. Johnson C. Rolph G. Kirkegaard J. Dwyer K. Sloth P. 2005. Vessel Interaction Investigations at the Port of Brisbane. DHI water and Environment. Australia.

Seelig, W.N. 2001. Passing Ship Effects on Moored Ships TR-6027-OCN. Naval Facilities Engineering Service Center. USA

Spencer J. McBride M. Shennan D. 2008. Simulating moored and passing ship interaction for harbour and navigation channel design. Proceedings of the International Conference of Coastal Engineering 2008 (ICCE 2008). Hamburg, Germany.

USA Department of Defence. 2005. Design: Moorings (UFC 4-159-03). Unified Facilities Criteria. USA.

USA Department of the Interior. 1980. Hydraulic Laboratory Techniques. Bureau of Reclamation. Colorado, USA

van der Molen W. 2006. Behaviour of Moored Ships in Harbours. Delft University of Technology. Enchede, The Netherlands.

van der Molen W. Moes J. Swiegers, P.B. Vantorre M. 2011. Calculation of Forces on Moored Ships due to Passing Ships. 2nd International Conference on Ship Manoeuvring in Shallow and Confined Water: Ship to Ship Interaction. Trondheim, Norway.

van der Molen W. Rossouw M. Phelp D. Tulsi K. Terblanche L. 2010. Innovative technologies to accurately model waves and moored ship motions. Science real and relevant conference 2010. Stellenbosch, South Africa.

van der Molen, W. Wenneker, I. Borsboom, M. 2005. Moored Ship Motions due to Passing Ships. Proc. Port-Maritime Innovation and R&D Conf. Rotterdam, The Netherlands.

Van Wijhe, H.J. and Pinkster, J.A. 2008. The effects of ships passing moored container vessels in the Yangtzehaven, Port of Rotterdam. The International Conference on Safety and Operations in Canals and Waterways 2008.

Vantorre M. Laforce E. Verzhbitskaya E. 2001. Model test based formulations of ship-ship interaction forces for simulation purposes. International Maritime Statistics Forum 2001.

Varyani, K.S. and Vantorre M. 2006. New Generic Equation for Interaction Effects on a Moored Containership Due to a Passing Tanker. *Journal of Ship Research*, Vol 50, No 3. Glasgow, UK.

Wang S. 1975. *Dynamic Effects of Ship Passage on Moored Vessels*. ASCE Ports Proceedings 1975. California, USA

Webber, N.B. 1974. *Fluid Mechanics for Civil Engineers*. William Clowes and Sons, Limited. London, UK

Woodman R. 1998. *The History of the Ship: The Comprehensive Story of Seafaring from the Earliest Times to the Present Day*. Lyons Press. New York, USA

APPENDIX A: GENERAL

LIST OF FIGURES:

Table 01: Test matrix

Table 02: Agreement ratios of numerical model runs

Table 03: Agreement ratios of empirical calculations

Appendix A: General

Table 01: Test matrix

Run No.	Depth (m)	Passing Ship					Moored Ship			UKC	Walls	Comment
		Ship	Direction of Travel	Draft [m]	U [kn]	Dist. [m]	Ship	Draft [m]	Depth /Draft			
Repeatability												
1	16.8	4500 TEU	same	14	6	64	66 kdwt	14	1.200	2.8	none	
2	16.8	4500 TEU	same	14	6	64	66 kdwt	14	1.200	2.8	none	
3	16.8	4500 TEU	same	14	6	64	66 kdwt	14	1.200	2.8	none	
4	16.8	4500 TEU	same	14	6	64	66 kdwt	14	1.200	2.8	none	
5	16.8	4500 TEU	same	14	6	64	66 kdwt	14	1.200	2.8	none	
Sensitivity: Direction												
1	16.8	4500 TEU	same	14	6	64	66 kdwt	14	1.200	2.8	none	Already done
6	16.8	4500 TEU	same	14	8	64	66 kdwt	14	1.200	2.8	none	
7	16.8	4500 TEU	same	14	10	64	66 kdwt	14	1.200	2.8	none	
8	16.8	4500 TEU	same	14	12	64	66 kdwt	14	1.200	2.8	none	
9	16.8	4500 TEU	same	14	14	64	66 kdwt	14	1.200	2.8	none	
10	16.8	4500 TEU	opposite	14	6	64	65 kdwt	14	1.200	2.8	none	
11	16.8	4500 TEU	opposite	14	8	64	65 kdwt	14	1.200	2.8	none	
12	16.8	4500 TEU	opposite	14	10	64	65 kdwt	14	1.200	2.8	none	
13	16.8	4500 TEU	opposite	14	12	64	65 kdwt	14	1.200	2.8	none	
14	16.8	4500 TEU	opposite	14	14	64	65 kdwt	14	1.200	2.8	none	
Sensitivity: Walls and channels												
10	16.8	4500 TEU	opposite	14	6	64	65 kdwt	14	1.200	2.8	none	Already done
11	16.8	4500 TEU	opposite	14	8	64	65 kdwt	14	1.200	2.8	none	Already done
15	16.8	4500 TEU	opposite	14	6	64	65 kdwt	14	1.200	2.8	quay	
16	16.8	4500 TEU	opposite	14	8	64	65 kdwt	14	1.200	2.8	quay	
17	16.8	4500 TEU	opposite	14	6	64	65 kdwt	14	1.200	2.8	6B Channel	
18	16.8	4500 TEU	opposite	14	8	64	65 kdwt	14	1.200	2.8	6B Channel	
19	16.8	4500 TEU	opposite	14	6	64	65 kdwt	14	1.200	2.8	9B Channel	
20	16.8	4500 TEU	opposite	14	8	64	65 kdwt	14	1.200	2.8	9B Channel	
21	16.8	4500 TEU	opposite	14	6	64	65 kdwt	14	1.200	2.8	12B Channel	
22	16.8	4500 TEU	opposite	14	8	64	65 kdwt	14	1.200	2.8	12B Channel	
Sensitivity: Passing distance												
23	16.8	4500 TEU	opposite	14	6	16	65 kdwt	14	1.200	2.8	none	
24	16.8	4500 TEU	opposite	14	8	16	65 kdwt	14	1.200	2.8	none	
25	16.8	4500 TEU	opposite	14	6	32	65 kdwt	14	1.200	2.8	none	
26	16.8	4500 TEU	opposite	14	8	32	65 kdwt	14	1.200	2.8	none	
10	16.8	4500 TEU	opposite	14	6	64	65 kdwt	14	1.200	2.8	none	Already done
11	16.8	4500 TEU	opposite	14	8	64	65 kdwt	14	1.200	2.8	none	Already done
27	16.8	4500 TEU	opposite	14	6	96	65 kdwt	14	1.200	2.8	none	
28	16.8	4500 TEU	opposite	14	8	96	65 kdwt	14	1.200	2.8	none	
29	16.8	4500 TEU	opposite	14	6	160	65 kdwt	14	1.200	2.8	none	
30	16.8	4500 TEU	opposite	14	8	160	65 kdwt	14	1.200	2.8	none	

Appendix A: General

...Table 01 continued

Sensitivity: Depth / Draft												
33	15.6002	4500 TEU	opposite	14	6	64	65 kdwt	14	1.114	1.6	none	
34	15.6002	4500 TEU	opposite	14	8	64	65 kdwt	14	1.114	1.6	none	
31	16.3002	4500 TEU	opposite	14	6	64	65 kdwt	14	1.164	2.3	none	
32	16.3002	4500 TEU	opposite	14	8	64	65 kdwt	14	1.164	2.3	none	
10	16.8	4500 TEU	opposite	14	6	64	65 kdwt	14	1.200	2.8	none	Already done
11	16.8	4500 TEU	opposite	14	8	64	65 kdwt	14	1.200	2.8	none	Already done
35	19.6	4500 TEU	opposite	14	6	64	65 kdwt	14	1.400	5.6	none	
36	19.6	4500 TEU	opposite	14	8	64	65 kdwt	14	1.400	5.6	none	
37	24.5	4500 TEU	opposite	14	6	64	65 kdwt	14	1.750	10.5	none	
38	24.5	4500 TEU	opposite	14	8	64	65 kdwt	14	1.750	10.5	none	
Sensitivity: Passing speed												
39	16.8	4500 TEU	opposite	14	4	64	65 kdwt	14	1.200	2.8	none	
10	16.8	4500 TEU	opposite	14	6	64	65 kdwt	14	1.200	2.8	none	Already done
11	16.8	4500 TEU	opposite	14	8	64	65 kdwt	14	1.200	2.8	none	Already done
12	16.8	4500 TEU	opposite	14	10	64	65 kdwt	14	1.200	2.8	none	Already done
13	16.8	4500 TEU	opposite	14	12	64	65 kdwt	14	1.200	2.8	none	Already done
14	16.8	4500 TEU	opposite	14	14	64	65 kdwt	14	1.200	2.8	none	Already done
Combination: Depth/Draft, Walls and channels, Speed												
33	15.6002	4500 TEU	opposite	14	6	64	65 kdwt	14	1.114	1.6	none	Already done
31	16.3002	4500 TEU	opposite	14	6	64	65 kdwt	14	1.164	2.3	none	Already done
10	16.8	4500 TEU	opposite	14	6	64	65 kdwt	14	1.200	2.8	none	Already done
41	15.6002	4500 TEU	opposite	14	6	64	65 kdwt	14	1.114	1.6	quay	
40	16.3002	4500 TEU	opposite	14	6	64	65 kdwt	14	1.164	2.3	quay	
15	16.8	4500 TEU	opposite	14	6	64	65 kdwt	14	1.200	2.8	quay	Already done
43	15.6002	4500 TEU	opposite	14	6	64	65 kdwt	14	1.114	1.6	6B channel	
42	16.3002	4500 TEU	opposite	14	6	64	65 kdwt	14	1.164	2.3	6B channel	
17	16.8	4500 TEU	opposite	14	6	64	65 kdwt	14	1.200	2.8	6B channel	Already done
34	15.6002	4500 TEU	opposite	14	8	64	65 kdwt	14	1.114	1.6	none	Already done
32	16.3002	4500 TEU	opposite	14	8	64	65 kdwt	14	1.164	2.3	none	Already done
11	16.8	4500 TEU	opposite	14	8	64	65 kdwt	14	1.200	2.8	none	Already done
45	15.6002	4500 TEU	opposite	14	8	64	65 kdwt	14	1.114	1.6	quay	
44	16.3002	4500 TEU	opposite	14	8	64	65 kdwt	14	1.164	2.3	quay	
16	16.8	4500 TEU	opposite	14	8	64	65 kdwt	14	1.200	2.8	quay	Already done
47	15.6002	4500 TEU	opposite	14	8	64	65 kdwt	14	1.114	1.6	6B channel	
46	16.3002	4500 TEU	opposite	14	8	64	65 kdwt	14	1.164	2.3	6B channel	
18	16.8	4500 TEU	opposite	14	8	64	65 kdwt	14	1.200	2.8	6B channel	Already done

Appendix A: General

Table 02: Agreement ratios of numerical model runs

Agreement ratios of numerical runs			
Test No	Surge	Sway	Yaw
	%	%	%
1	0.90	0.88	0.81
2	0.92	0.90	0.80
3	0.90	0.90	0.81
4	0.91	0.89	0.80
5	0.89	0.88	0.80
6	0.80	0.77	0.77
7	0.76	0.78	0.71
8	0.71	0.69	0.64
9	0.62	0.61	0.56
10	0.86	0.86	0.82
11	0.79	0.79	0.77
12	0.74	0.77	0.72
13	0.70	0.71	0.64
14	0.61	0.63	0.52
15	0.84	0.84	0.82
16	0.77	0.82	0.77
17	0.83	0.77	0.74
18	0.76	0.81	0.64
19	0.89	0.92	0.78
20	0.78	0.67	0.77
21	0.88	1.01	0.79
22	0.80	0.71	0.78
23	1.00	0.99	0.94
24	0.93	0.93	0.88
25	0.98	0.98	0.90
26	0.90	0.89	0.84
27	0.88	0.78	0.74
28	0.78	0.75	0.71
29	0.66	0.76	0.75
30	0.69	0.67	0.57
31	0.82	0.84	0.80
32	0.76	0.79	0.75
33	0.84	0.87	0.78
34	0.77	0.75	0.72
35	0.90	0.91	0.83
36	0.85	0.89	0.80
37	0.94	1.02	0.85
38	0.85	0.95	0.82
39	0.95	0.97	0.85

Appendix A: General

... Table 02 continued

40	0.91	0.85	0.77
41	0.80	0.83	0.72
42	0.85	0.81	0.75
43	0.82	0.80	0.67
44	0.88	0.99	0.76
45	0.84	0.84	0.74
46	0.89	0.85	0.69
47	0.85	0.84	0.62

Appendix A: General

Table 03: Agreement ratios of empirical calculations

Test No	Agreement ratios of empirical calculations														
	Kriebel			Flory			Wang Seelig			Wang Kriebel			Varyani Vantorre		
	Fx	Fy	Mz	Fx	Fy	Mz	Fx	Fy	Mz	Fx	Fy	Mz	Fx	Fy	Mz
1	1.49	1.05	0.89	1.12	1.02	1.19	1.06	0.95	1.76	1.68	1.27	1.52	1.21	0.71	0.77
6	1.49	1.05	0.89	1.12	1.02	1.19	1.06	0.95	1.76	1.68	1.27	1.52	1.21	0.71	0.77
7	1.49	1.05	0.89	1.12	1.02	1.19	1.06	0.95	1.76	1.68	1.27	1.53	1.21	0.71	0.77
8	1.49	1.05	0.89	1.12	1.02	1.19	1.06	0.95	1.76	1.68	1.27	1.52	1.21	0.71	0.77
9	1.49	1.05	0.89	1.12	1.02	1.19	1.06	0.95	1.76	1.68	1.27	1.53	1.21	0.71	0.77
10	1.32	0.91	0.85	0.99	0.89	1.14	0.94	0.83	1.68	1.49	1.11	1.46	1.07	0.62	0.73
11	1.27	0.92	0.78	0.95	0.90	1.04	0.90	0.83	1.54	1.42	1.12	1.33	1.03	0.62	0.67
12	1.18	0.82	0.71	0.88	0.80	0.94	0.83	0.74	1.40	1.32	1.00	1.21	0.95	0.56	0.61
13	1.03	0.73	0.61	0.77	0.71	0.82	0.73	0.66	1.21	1.16	0.89	1.05	0.83	0.49	0.53
14	1.44	1.01	0.94	1.08	0.98	1.25	1.02	0.91	1.84	1.62	1.23	1.60	1.17	0.69	0.81
15	1.31	0.93	0.88	0.99	0.91	1.17	0.94	0.84	1.73	1.48	1.13	1.50	1.07	0.63	0.76
16	1.23	0.91	0.82	0.92	0.88	1.09	0.88	0.82	1.61	1.38	1.10	1.40	1.00	0.61	0.71
17	1.17	0.84	0.73	0.88	0.82	0.97	0.83	0.76	1.42	1.31	1.02	1.24	0.95	0.57	0.63
18	1.02	0.74	0.59	0.77	0.72	0.78	0.73	0.67	1.16	1.15	0.90	1.00	0.83	0.50	0.51
19	1.35	1.16	0.93	1.01	1.13	1.24	0.96	1.05	1.83	1.52	1.41	1.59	1.10	0.78	0.80
20	1.25	1.12	0.88	0.93	1.09	1.17	0.89	1.02	1.72	1.40	1.36	1.49	1.01	0.76	0.76
21	0.99	0.90	0.76	0.74	0.88	1.02	0.70	0.81	1.50	1.11	1.09	1.30	0.80	0.61	0.66
22	0.91	0.94	0.67	0.68	0.92	0.89	0.65	0.85	1.32	1.02	1.14	1.14	0.74	0.64	0.58
23	1.32	1.22	0.87	0.99	1.18	1.16	0.94	1.10	1.71	1.48	1.48	1.48	1.07	0.82	0.75
24	1.15	0.89	0.86	0.86	0.87	1.14	0.82	0.81	1.68	1.29	1.08	1.46	0.93	0.60	0.74
25	1.38	1.37	0.88	1.03	1.34	1.18	0.98	1.25	1.74	1.55	1.67	1.51	1.12	0.93	0.76
26	1.25	0.97	0.87	0.93	0.94	1.16	0.89	0.88	1.72	1.40	1.17	1.49	1.01	0.66	0.76
27	1.05	0.76	0.74	1.84	0.97	1.70	0.96	0.97	1.41	1.67	1.73	1.63	3.86	2.09	1.99
28	0.97	0.71	0.69	1.70	0.91	1.59	0.89	0.91	1.32	1.54	1.62	1.52	3.56	1.96	1.86
29	1.23	0.90	0.83	1.19	1.00	1.15	1.04	1.01	1.55	1.75	1.64	1.63	2.02	1.15	1.13
30	1.12	0.81	0.77	1.08	0.90	1.07	0.94	0.91	1.45	1.59	1.48	1.52	1.84	1.04	1.05
31	1.86	1.09	0.95	1.24	0.99	1.39	1.04	0.78	1.95	1.53	0.86	1.39	1.08	0.57	0.76
32	1.65	1.05	0.91	1.10	0.96	1.33	0.92	0.75	1.87	1.36	0.83	1.33	0.96	0.55	0.73
33	1.99	1.33	1.04	1.13	1.04	1.90	0.52	0.46	1.87	0.65	0.35	0.93	0.88	0.60	1.04
34	2.10	1.16	0.79	1.19	0.91	1.45	0.55	0.40	1.43	0.69	0.30	0.71	0.93	0.52	0.80
35	1.41	0.96	0.91	1.01	0.97	1.22	0.96	0.89	1.85	1.59	1.19	1.57	1.10	0.61	0.75
36	1.30	0.91	0.85	0.93	0.91	1.13	0.89	0.84	1.73	1.47	1.11	1.46	1.02	0.58	0.70
37	1.50	0.96	0.88	1.00	0.99	1.16	0.97	0.91	1.86	1.70	1.20	1.54	1.11	0.56	0.67
38	1.38	0.83	0.81	0.92	0.86	1.07	0.89	0.78	1.71	1.57	1.04	1.41	1.02	0.48	0.61
39	1.35	1.09	0.91	1.21	0.82	1.13	1.13	0.86	1.51	1.48	1.25	1.50	1.27	0.96	0.99
40	1.27	1.06	0.87	1.14	0.80	1.08	1.06	0.84	1.44	1.40	1.22	1.44	1.20	0.94	0.94
41	1.27	1.15	0.87	1.33	0.43	0.76	1.27	0.73	1.07	1.38	1.27	1.41	1.40	1.37	1.19
42	1.15	1.07	0.83	1.20	0.40	0.73	1.15	0.68	1.03	1.25	1.18	1.35	1.26	1.27	1.14
43	1.58	1.14	0.97	1.18	1.11	1.30	1.12	1.03	1.91	1.78	1.38	1.66	1.28	0.77	0.84
44	1.50	1.14	0.86	1.08	1.14	1.15	1.03	1.05	1.75	1.69	1.40	1.49	1.17	0.73	0.71
45	1.36	1.02	0.78	0.91	1.06	1.04	0.88	0.97	1.66	1.55	1.28	1.37	1.01	0.59	0.60
46	1.04	0.92	0.77	0.74	0.93	1.03	0.71	0.86	1.56	1.17	1.14	1.33	0.81	0.59	0.63
47	1.02	0.85	0.67	0.68	0.88	0.88	0.66	0.81	1.42	1.16	1.06	1.17	0.75	0.49	0.51

APPENDIX B: IMAGES

LIST OF FIGURES:

- Figure 1: The moored bulk carrier in the force frame
Figure 2: The container ship in the passing ship rail
Figure 3: The AC induction motor drive and 20:1 reduction gearbox
Figure 4: The passing container ship alongside the moored bulk carrier
Figure 5: One of the two sliding pinned connections between the rail trolley and the container ship that allows heave roll and pitch of the passing ship
Figure 6: A universal joint between one of the three force rods and the bulk carrier
Figure 7: A universal joint between one of the three force rods and the force transducer
Figure 8: A data acquisition unit recording the measurements from the three force transducers
Figure 9: The quay wall next to the bulk carrier consisting of blue marine ply sheets and a lower red steel section to allow space for the force rods.
Figure 10: Aligning of the force rod
Figure 11: Connection between a force frame and a fixed structure
Figure 12: The passing ship basin
Figure 13: Close view of the passing and moored ship setup

Appendix B: Images



Figure 1: The moored bulk carrier in the force frame



Figure 2: The container ship in the passing ship rail

Appendix B: Images



Figure 3: The AC induction motor drive and 20:1 reduction gearbox

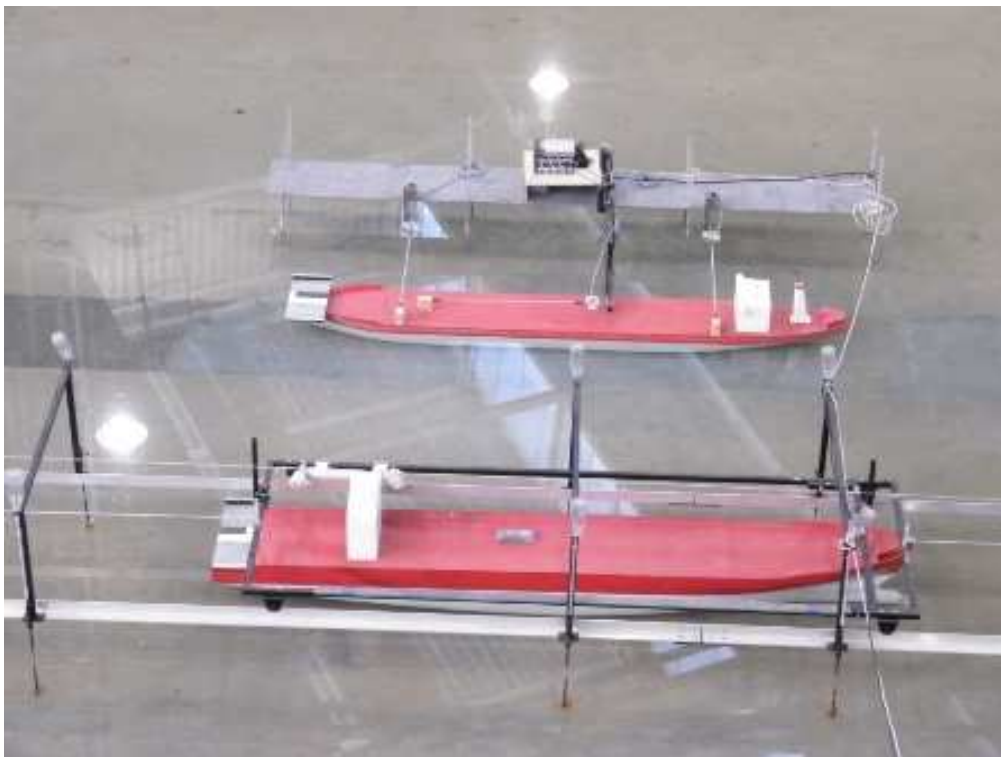


Figure 4: The passing container ship alongside the moored bulk carrier

Appendix B: Images

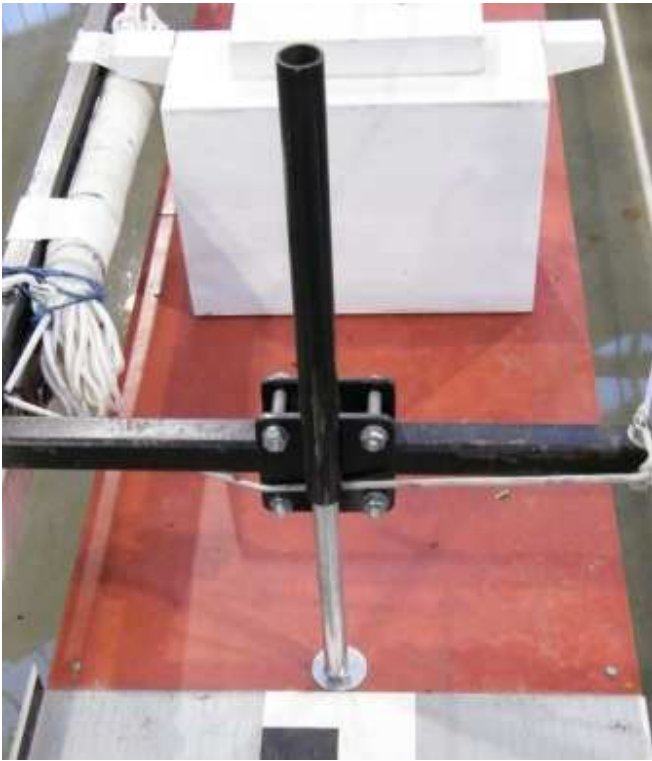


Figure 5: One of the two sliding pinned connections between the rail trolley and the container ship that allows heave roll and pitch of the passing ship

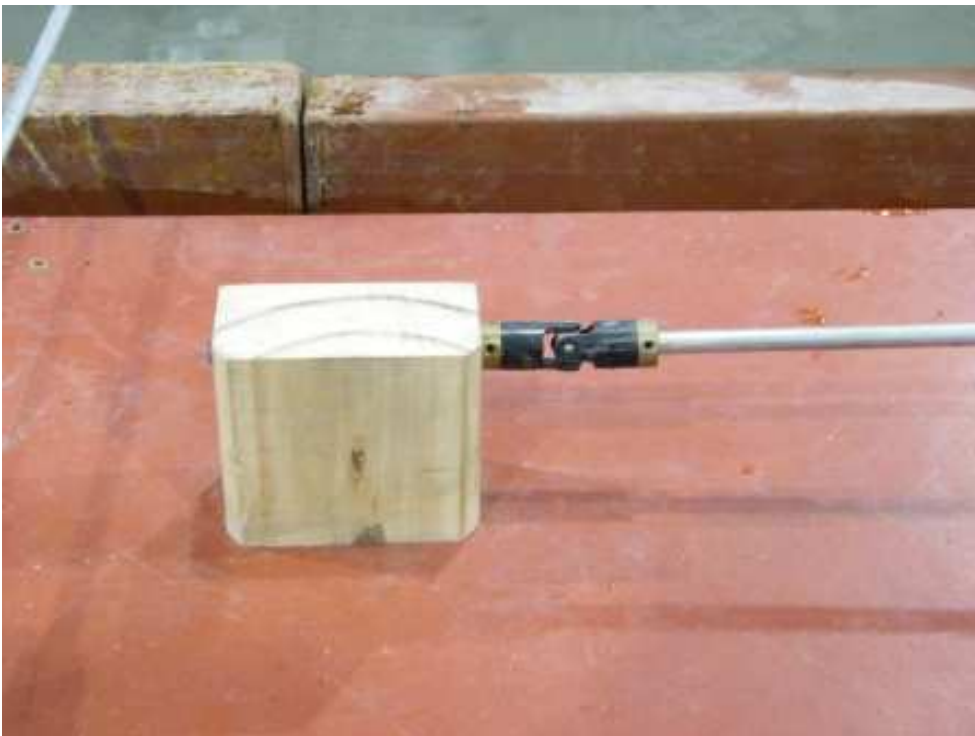


Figure 6: A universal joint between one of the three force rods and the bulk carrier

Appendix B: Images

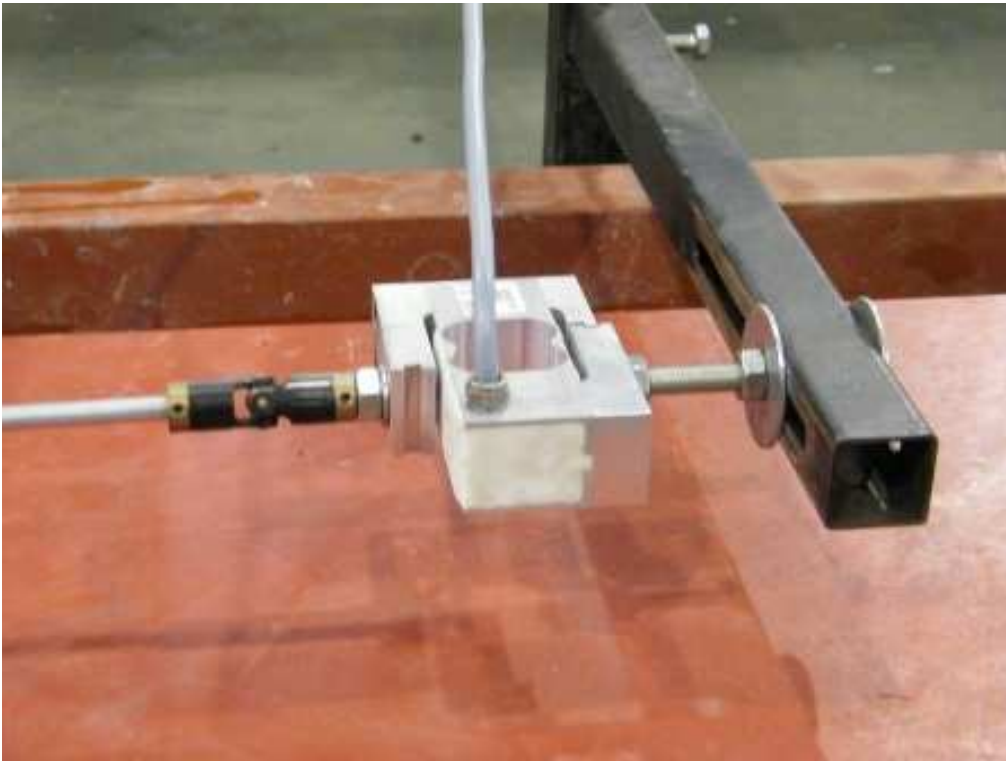


Figure 7: A universal joint between one of the three force rods and the force transducer



Figure 8: A data acquisition unit recording the measurements from the three force transducers

Appendix B: Images



Figure 9: The quay wall next to the bulk carrier consisting of blue marine ply sheets and a lower red steel section to allow space for the force rods.



Figure 10: Aligning of the force rod

Appendix B: Images

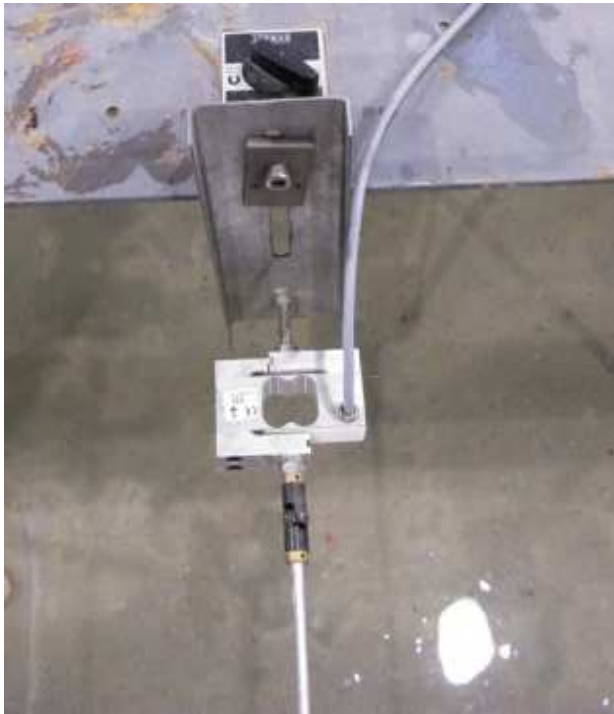


Figure 11: Connection between a force frame and a fixed structure



Figure 12: The passing ship basin

Appendix B: Images



Figure 13: Close view of the passing and moored ship setup

APPENDIX C: COMPARISON OF NUMERICAL AND PHYSICAL MODELS

LIST OF FIGURES:

- Figure 1: Comparison of test 01 (left) and test 06 (right) physical model measurements and numerical model calculations
- Figure 2: Comparison of test 07 (left) and test 08 (right) physical model measurements and numerical model calculations
- Figure 3: Comparison of test 09 (left) and test 10 (right) physical model measurements and numerical model calculations
- Figure 4: Comparison of test 11 (left) and test 12 (right) physical model measurements and numerical model calculations
- Figure 5: Comparison of test 13 (left) and test 14 (right) physical model measurements and numerical model calculations
- Figure 6: Comparison of test 15 (left) and test 16 (right) physical model measurements and numerical model calculations
- Figure 7: Comparison of test 17 (left) and test 18 (right) physical model measurements and numerical model calculations
- Figure 8: Comparison of test 19 (left) and test 20 (right) physical model measurements and numerical model calculations
- Figure 9: Comparison of test 21 (left) and test 22 (right) physical model measurements and numerical model calculations
- Figure 10: Comparison of test 23 (left) and test 24 (right) physical model measurements and numerical model calculations
- Figure 11: Comparison of test 25 (left) and test 26 (right) physical model measurements and numerical model calculations
- Figure 12: Comparison of test 27 (left) and test 28 (right) physical model measurements and numerical model calculations
- Figure 13: Comparison of test 29 (left) and test 30 (right) physical model measurements and numerical model calculations
- Figure 14: Comparison of test 31 (left) and test 32 (right) physical model measurements and numerical model calculations
- Figure 15: Comparison of test 33 (left) and test 34 (right) physical model measurements and numerical model calculations
- Figure 16: Comparison of test 35 (left) and test 36 (right) physical model measurements and numerical model calculations

Appendix C: Comparison of numerical and physical models

Figure 17: Comparison of test 37 (left) and test 38 (right) physical model measurements and numerical model calculations

Figure 18: Comparison of test 39 (left) and test 40 (right) physical model measurements and numerical model calculations

Figure 19: Comparison of test 41 (left) and test 42 (right) physical model measurements and numerical model calculations

Figure 20: Comparison of test 43 (left) and test 44 (right) physical model measurements and numerical model calculations

Figure 21: Comparison of test 45 (left) and test 46 (right) physical model measurements and numerical model calculations

Figure 22: Comparison of test 47 (left) physical model measurements and numerical model calculations

Appendix C: Comparison of numerical and physical models

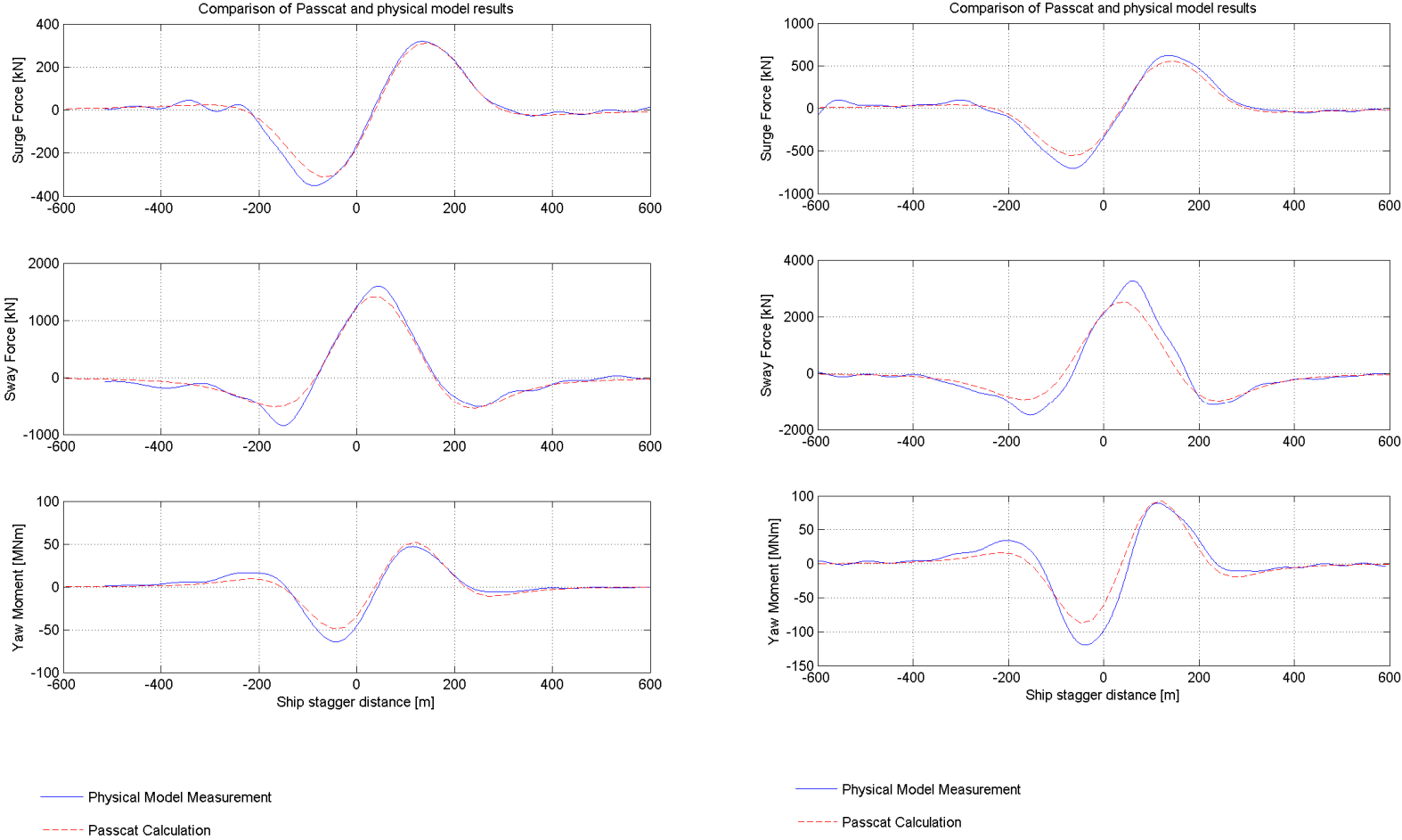


Figure 1: Comparison of test 01 (left) and test 06 (right) physical model measurements and numerical model calculations

Appendix C: Comparison of numerical and physical models

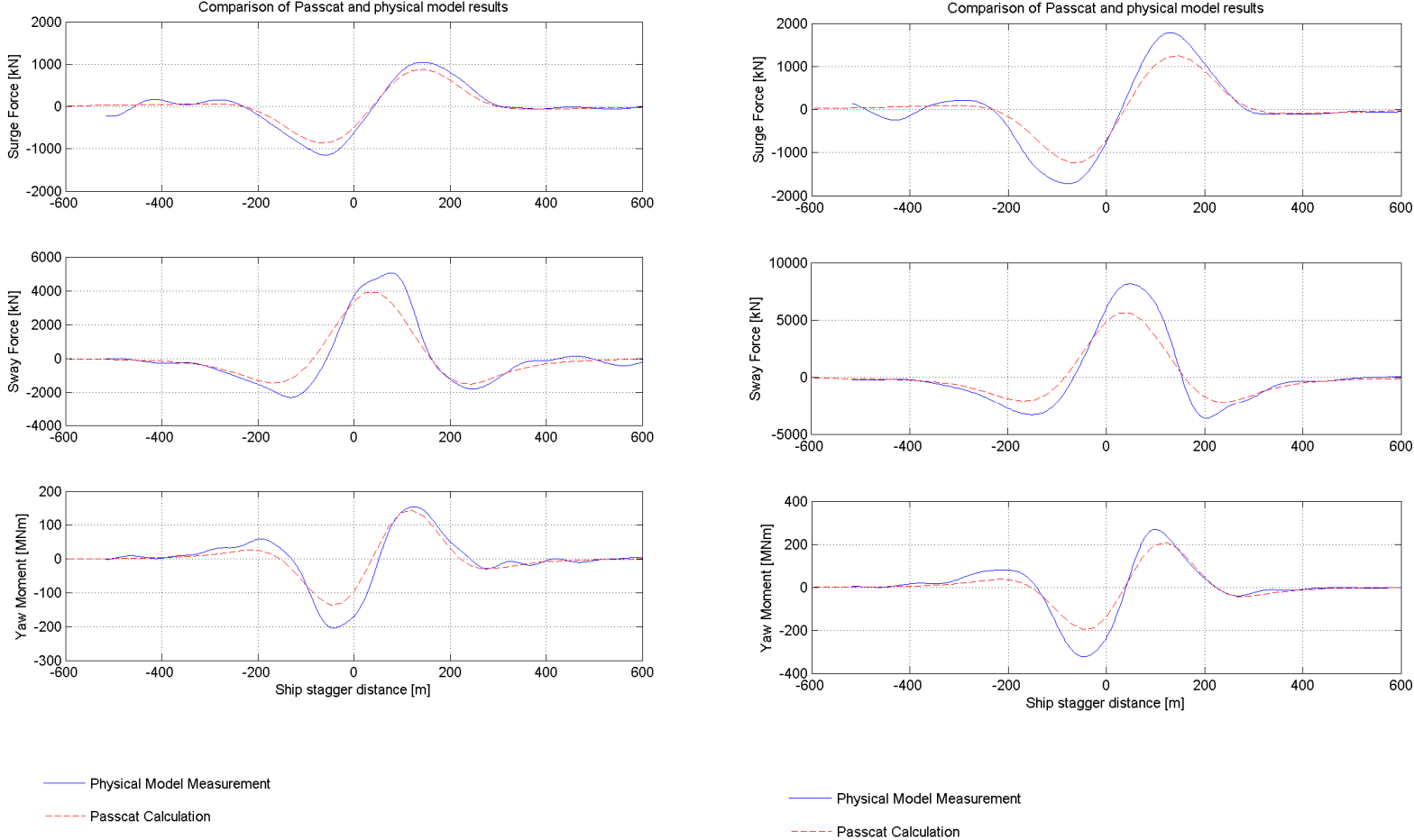


Figure 2: Comparison of test 07 (left) and test 08 (right) physical model measurements and numerical model calculations

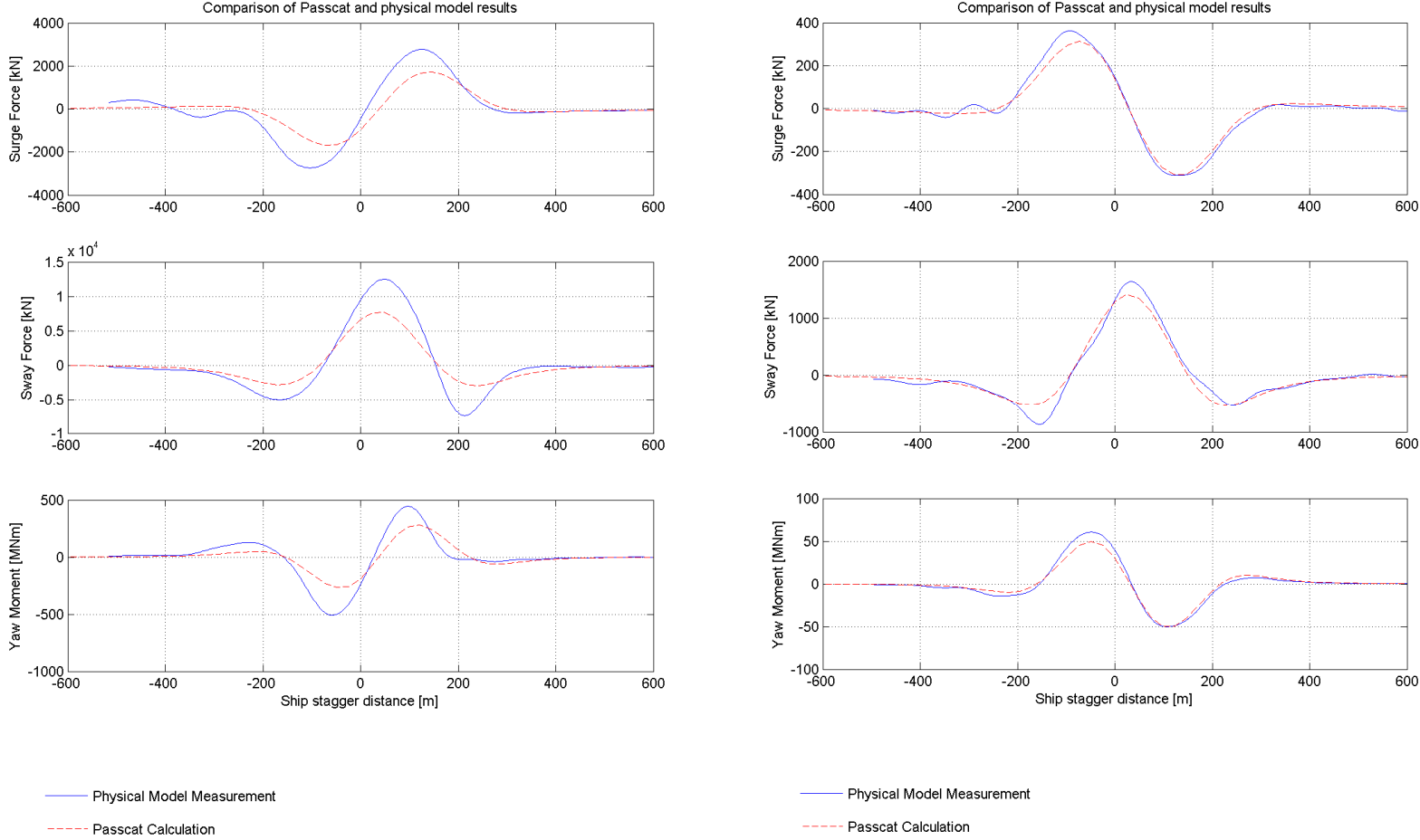


Figure 3: Comparison of test 09 (left) and test 10 (right) physical model measurements and numerical model calculations

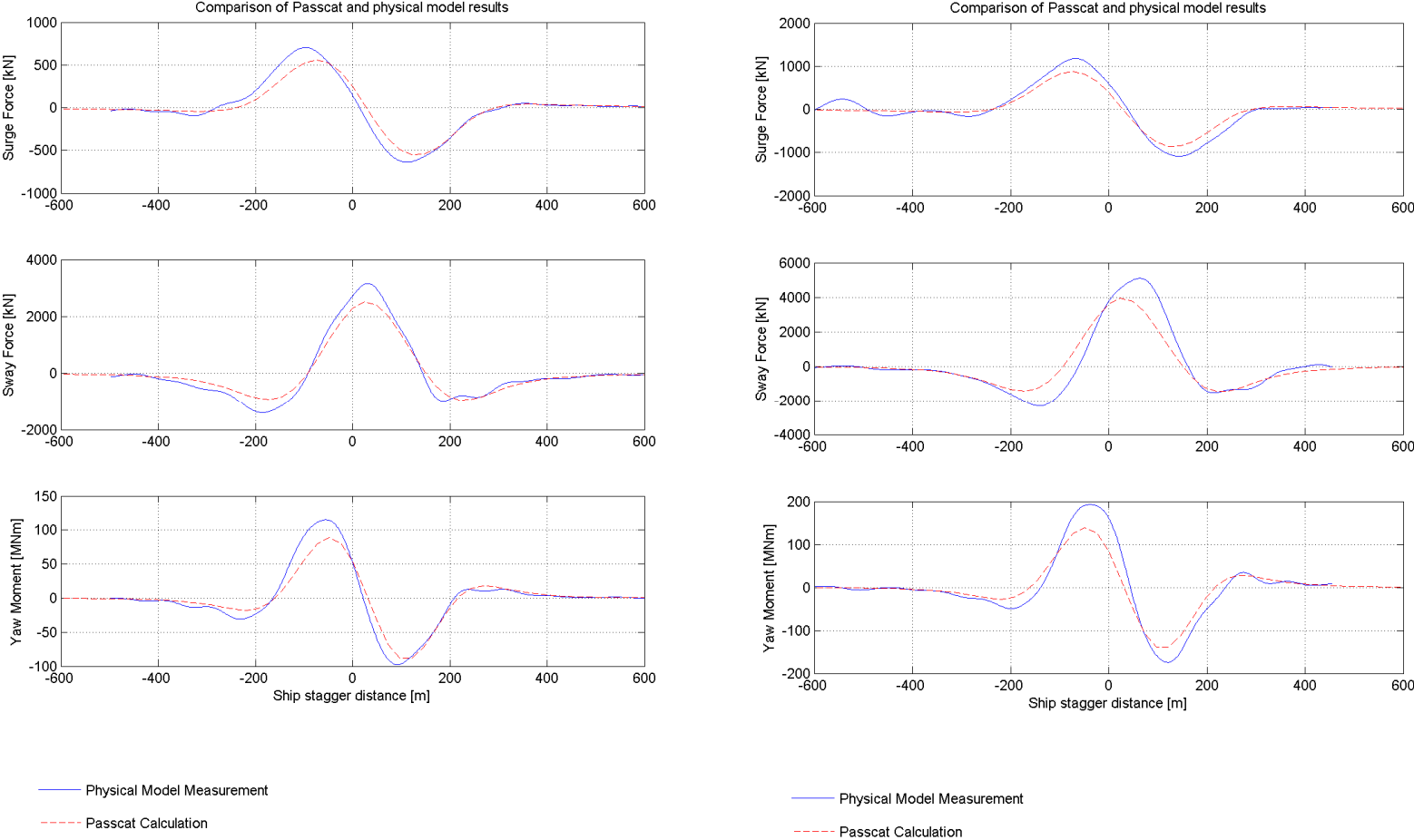


Figure 4: Comparison of test 11 (left) and test 12 (right) physical model measurements and numerical model calculations

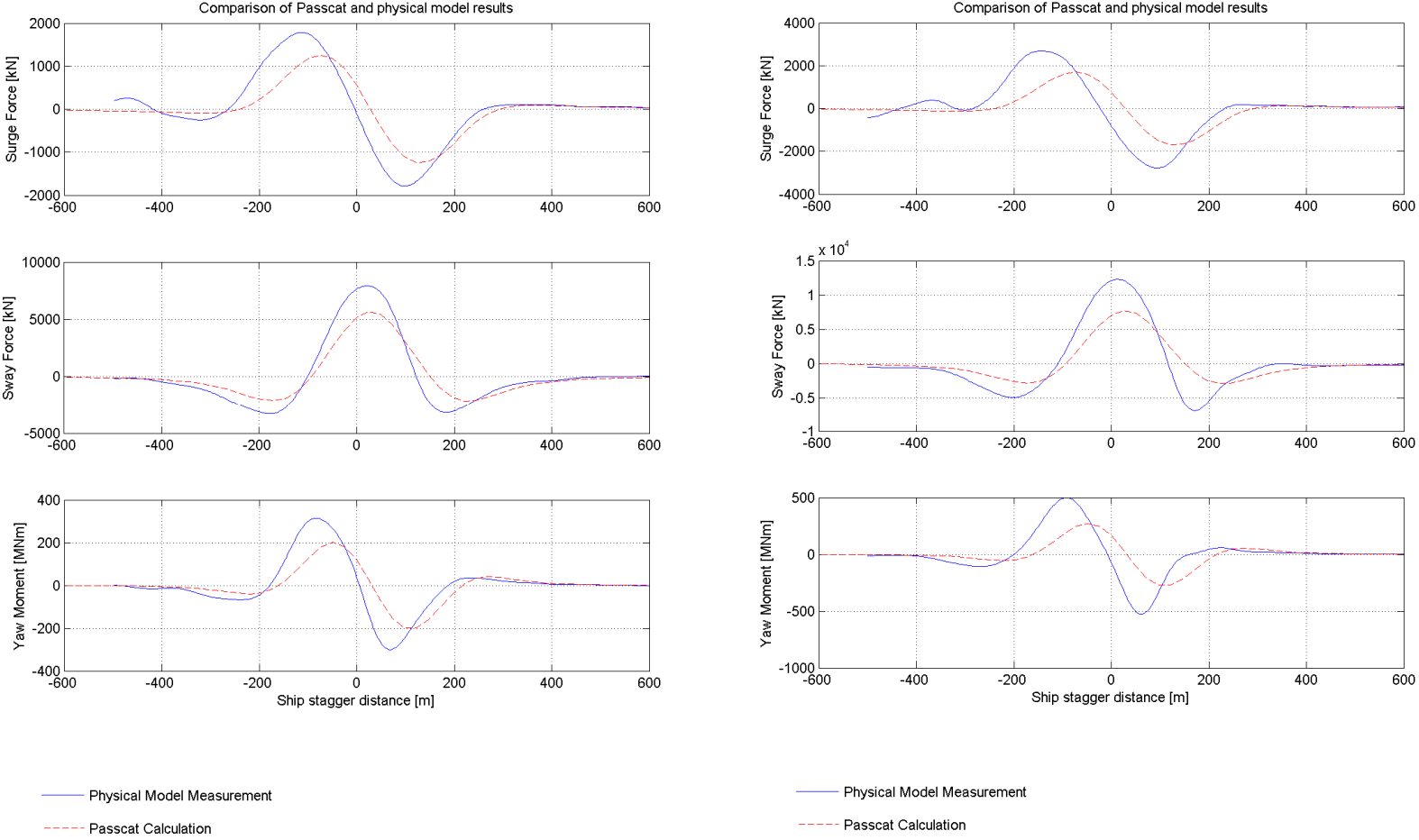


Figure 5: Comparison of test 13 (left) and test 14 (right) physical model measurements and numerical model calculations

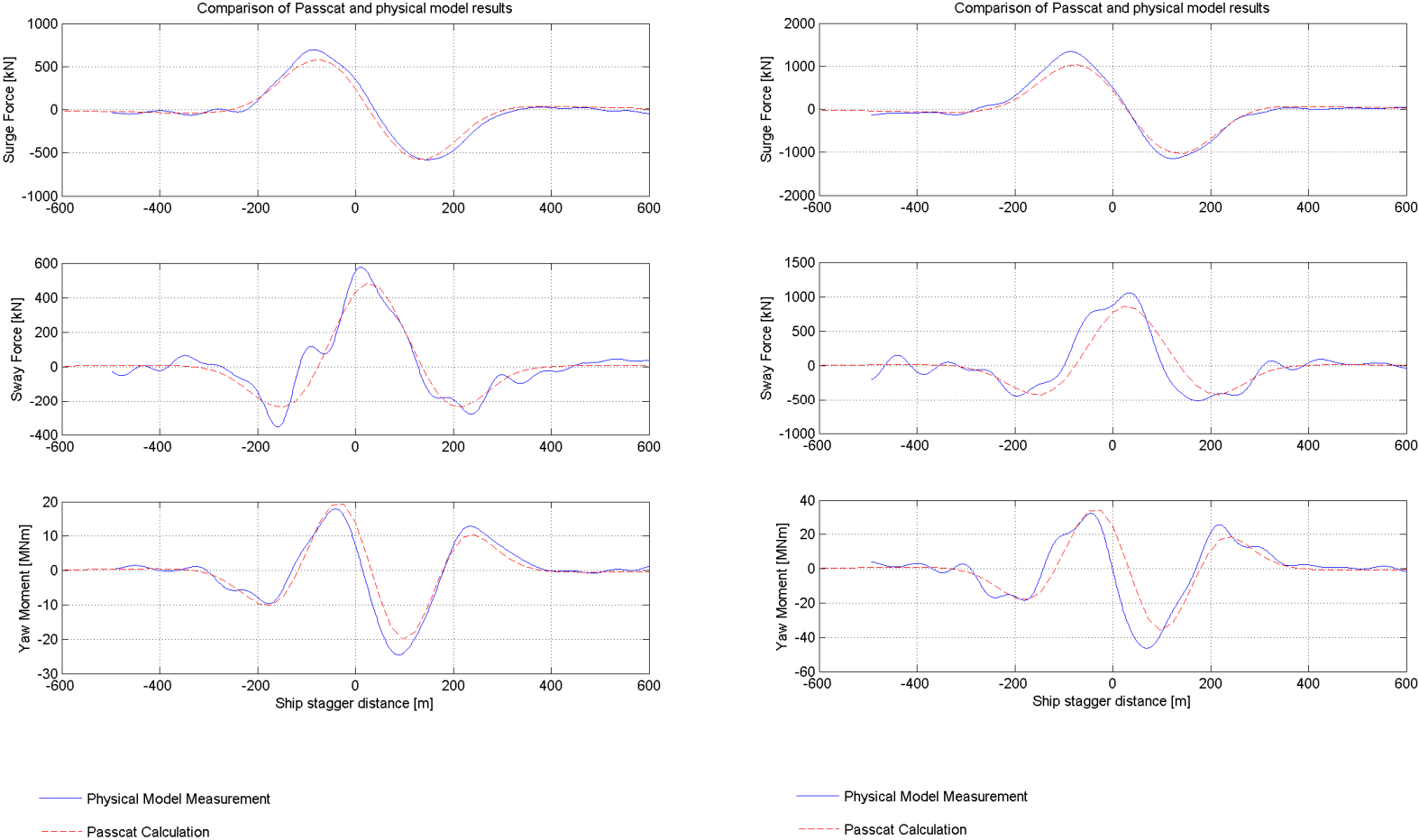


Figure 6: Comparison of test 15 (left) and test 16 (right) physical model measurements and numerical model calculations

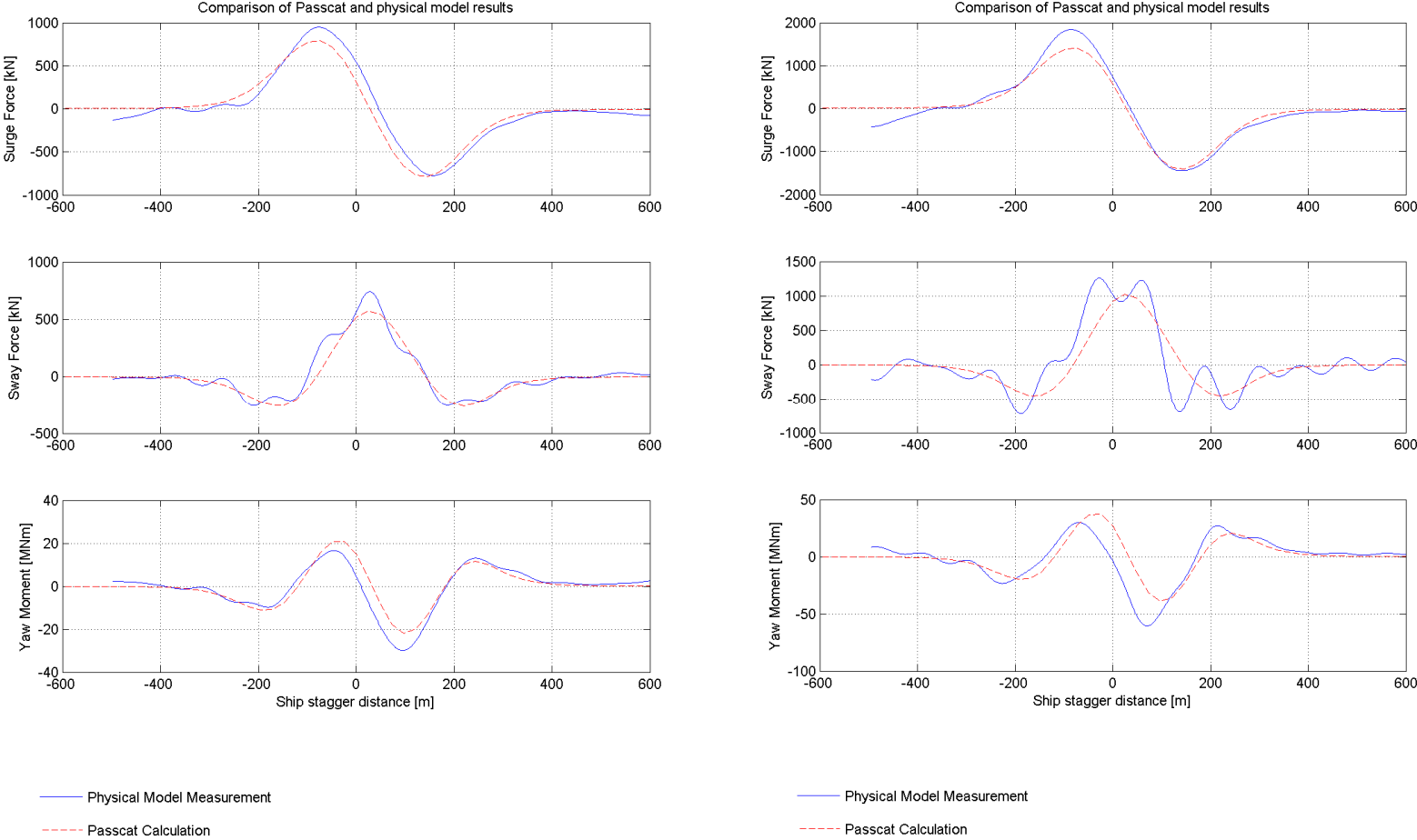


Figure 7: Comparison of test 17 (left) and test 18 (right) physical model measurements and numerical model calculations

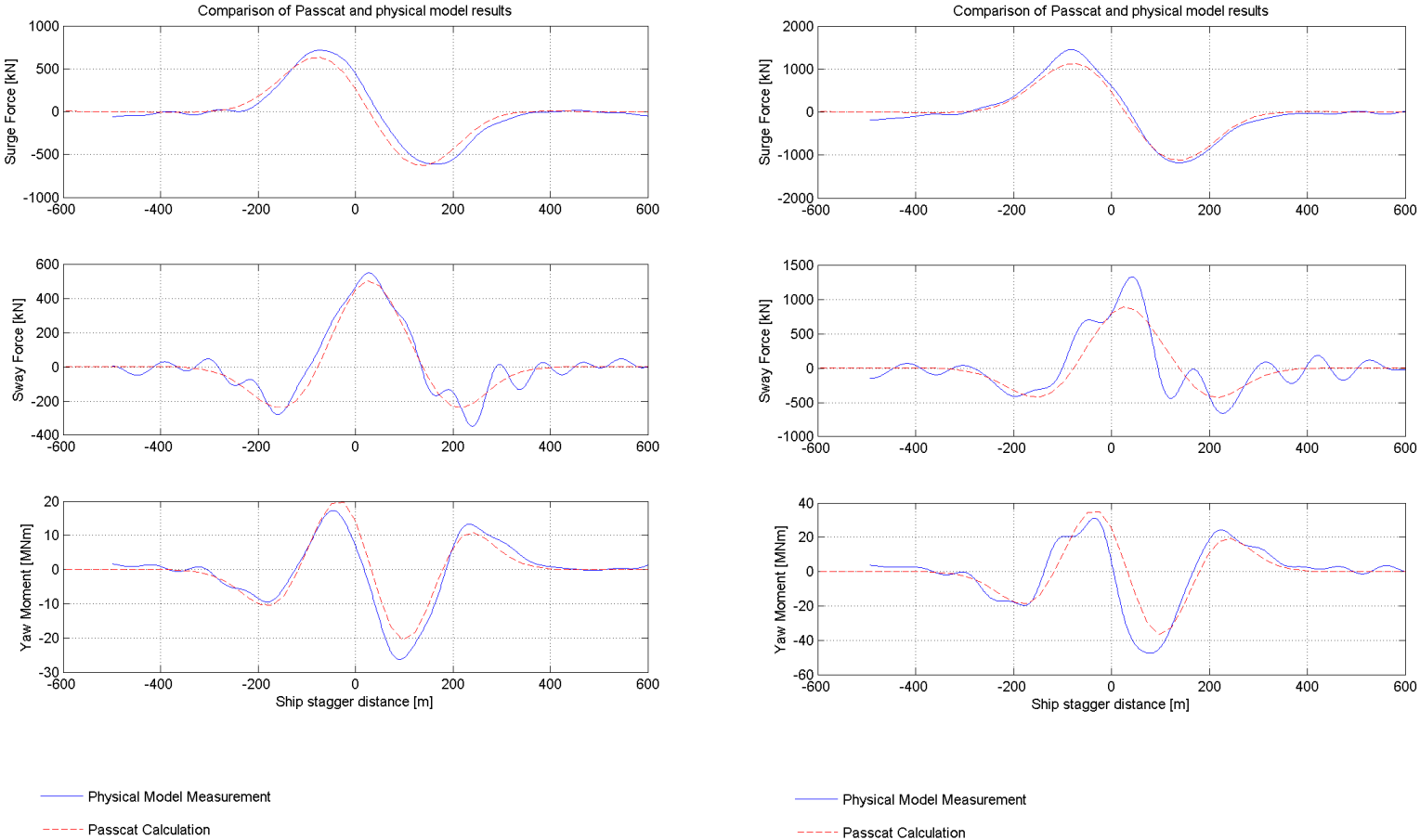


Figure 8: Comparison of test 19 (left) and test 20 (right) physical model measurements and numerical model calculations

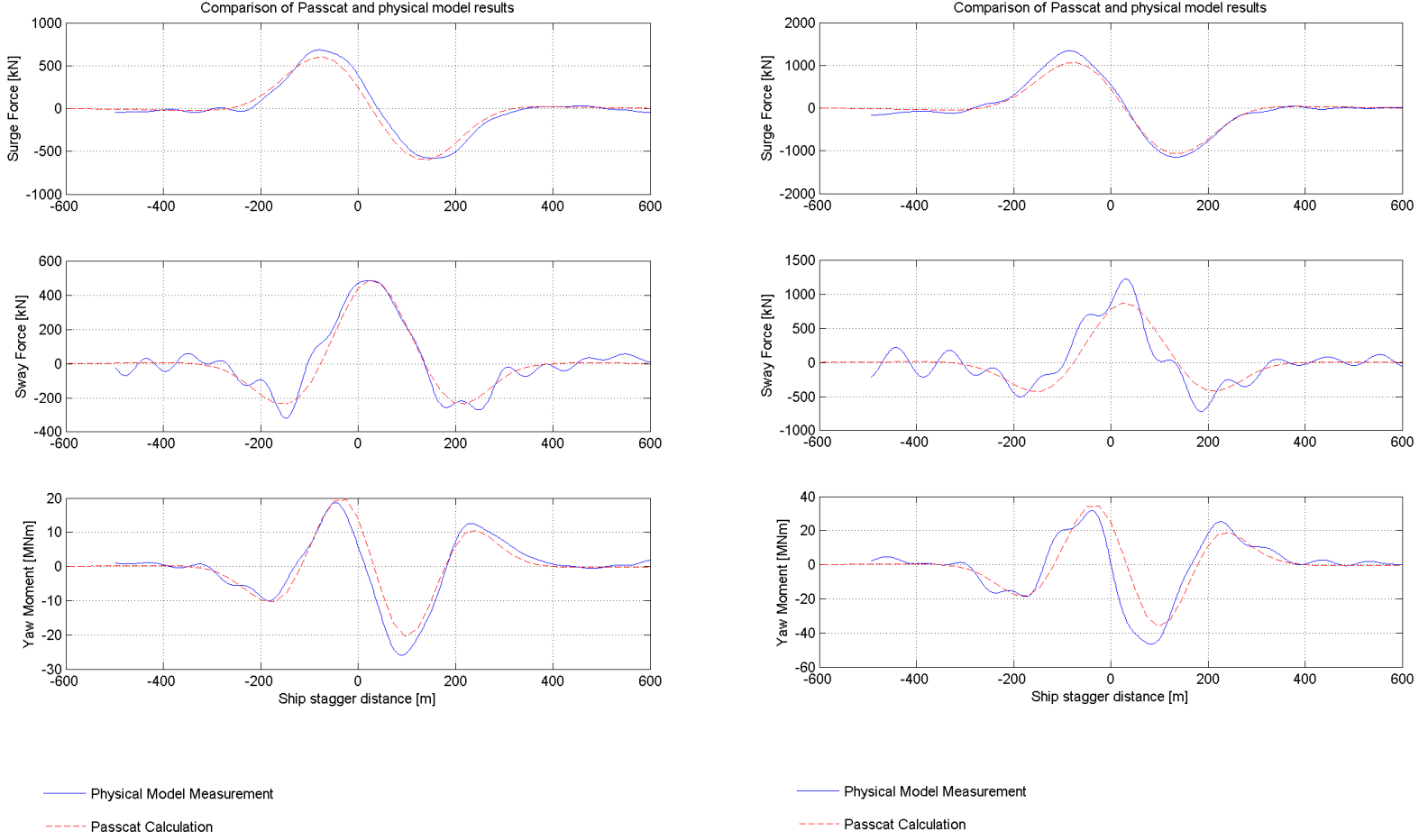


Figure 9: Comparison of test 21 (left) and test 22 (right) physical model measurements and numerical model calculations

Appendix C: Comparison of numerical and physical models

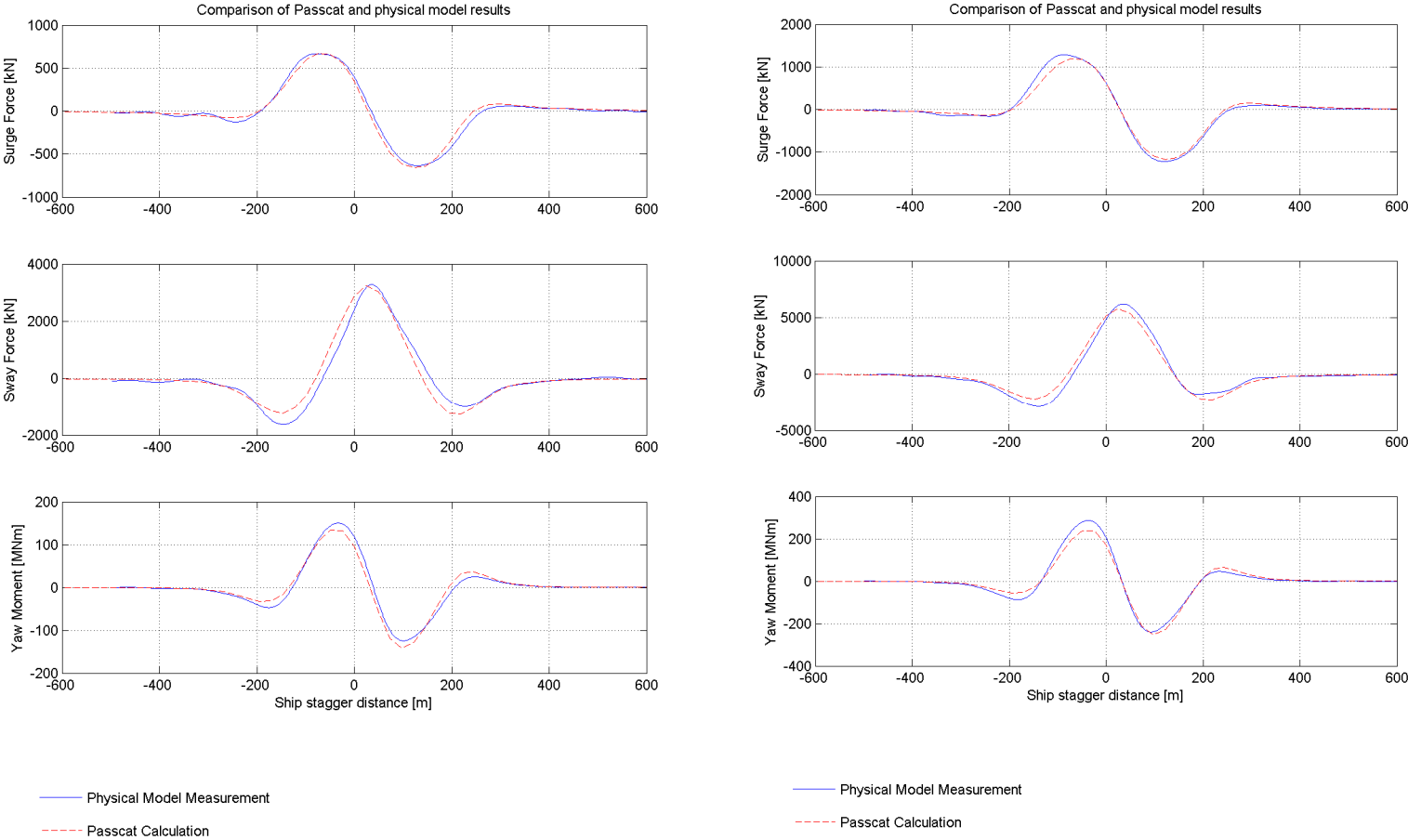


Figure 10: Comparison of test 23 (left) and test 24 (right) physical model measurements and numerical model calculations

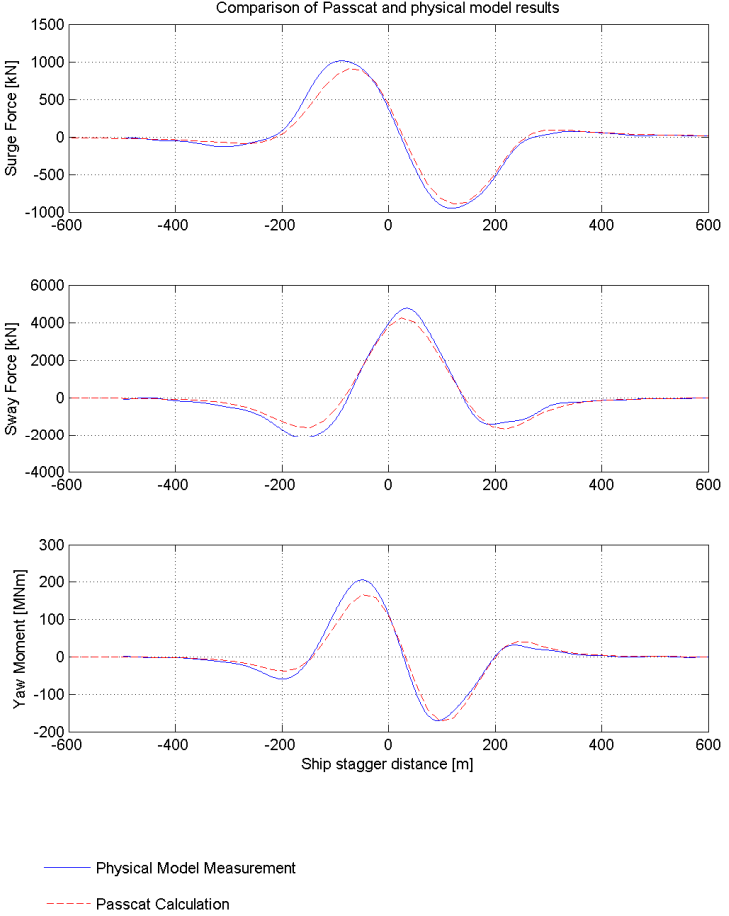
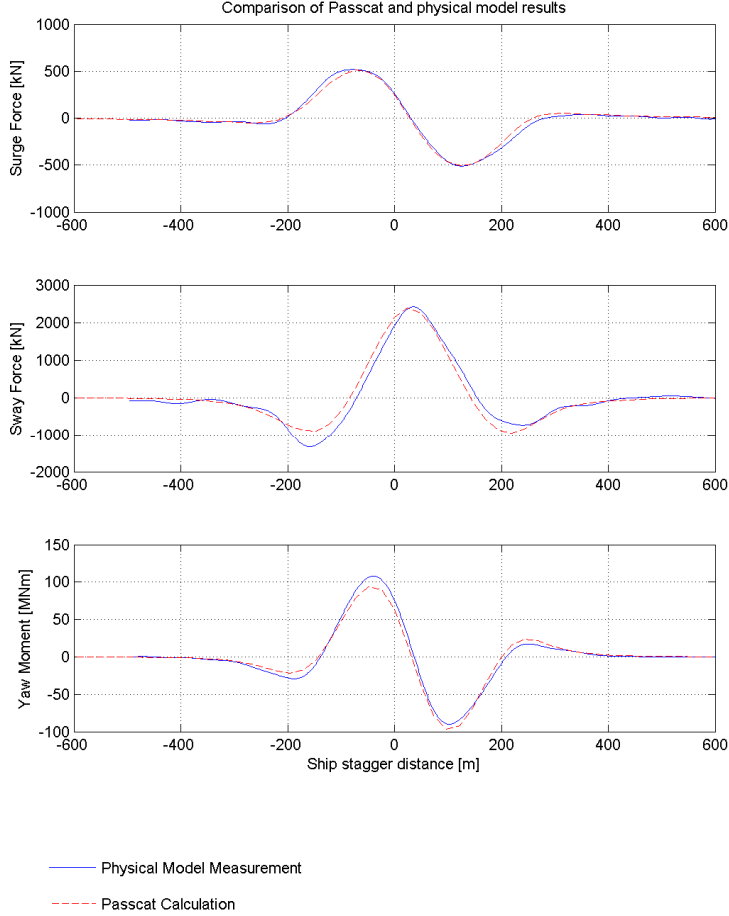


Figure 11: Comparison of test 25 (left) and test 26 (right) physical model measurements and numerical model calculations

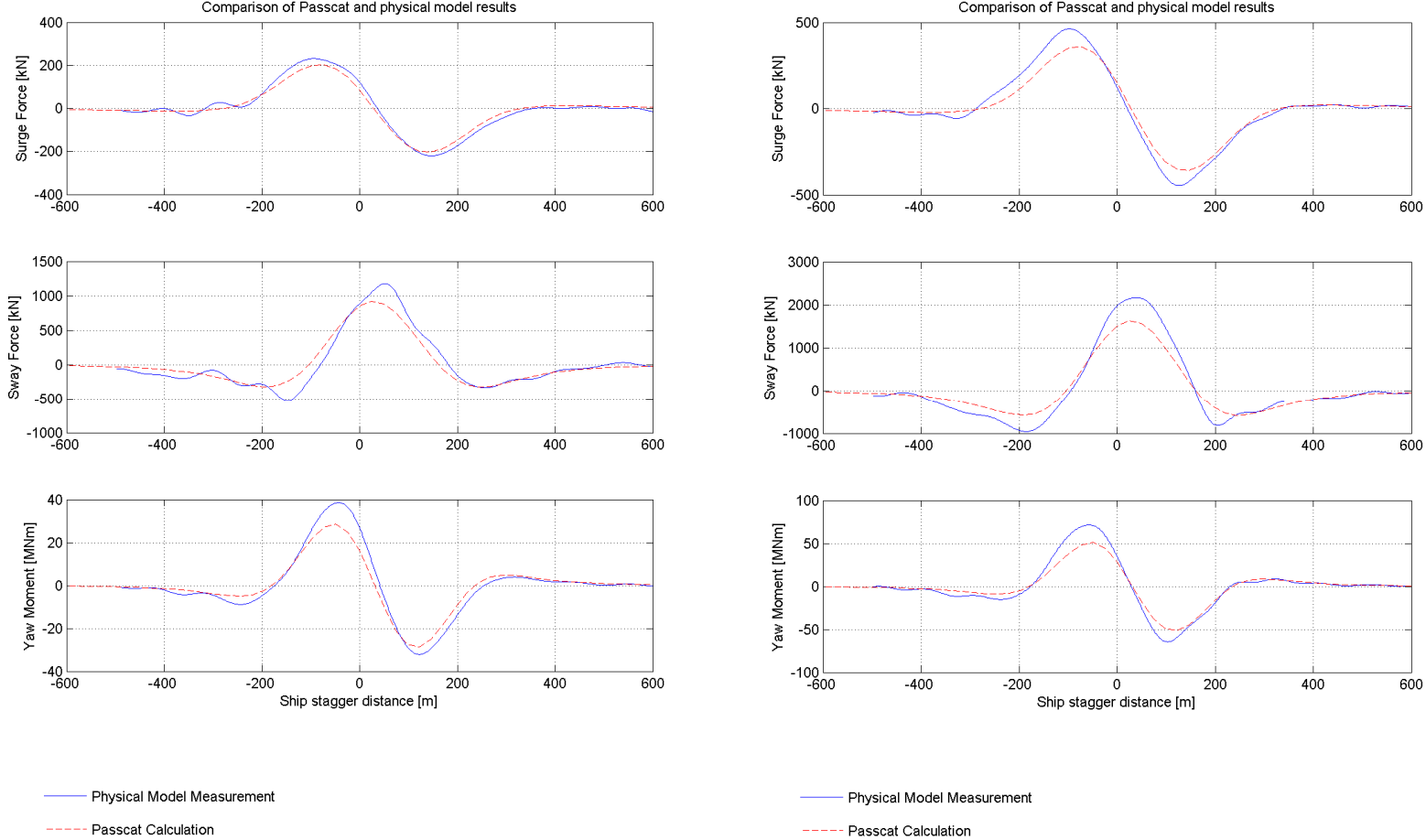


Figure 12: Comparison of test 27 (left) and test 28 (right) physical model measurements and numerical model calculations

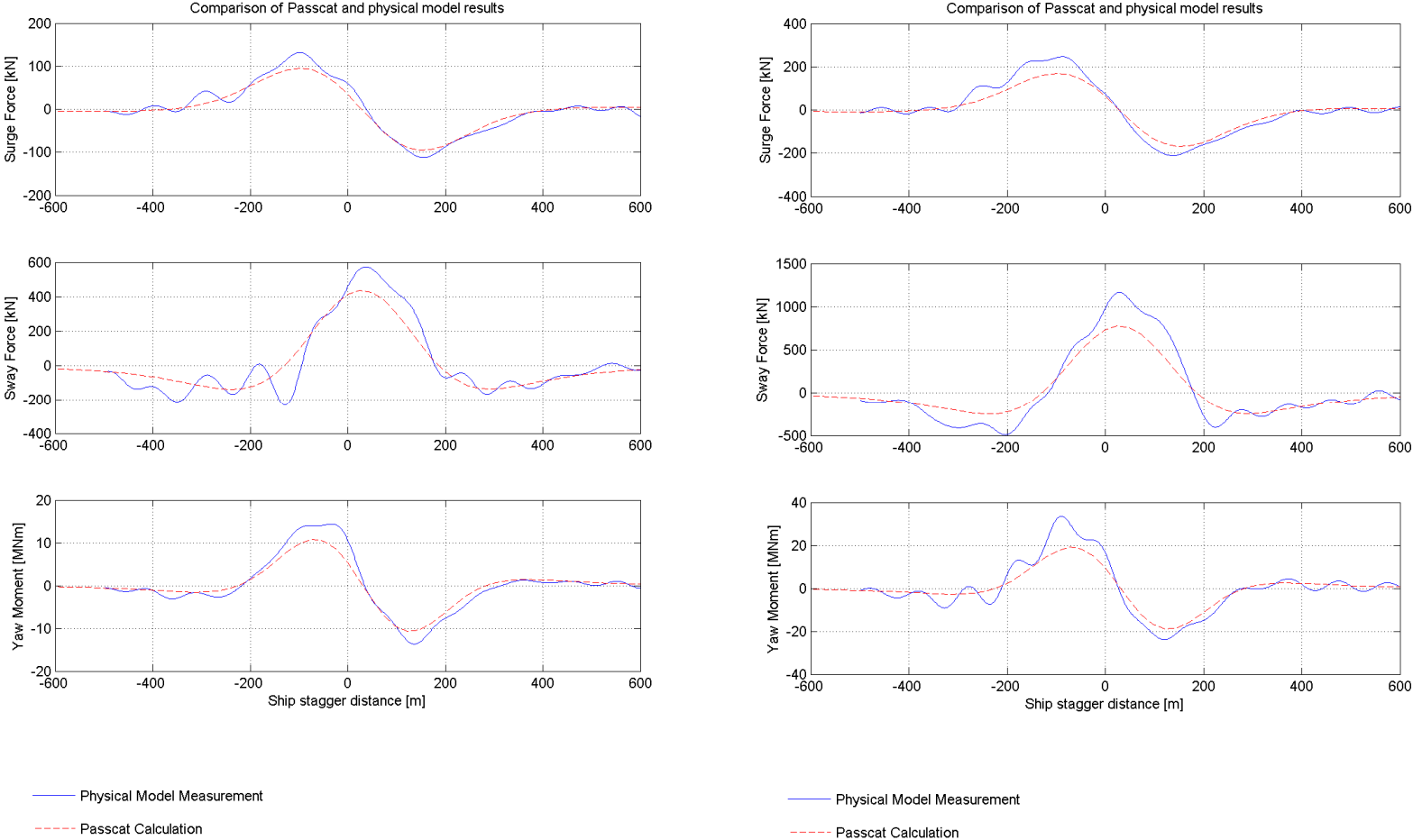


Figure 13: Comparison of test 29 (left) and test 30 (right) physical model measurements and numerical model calculations

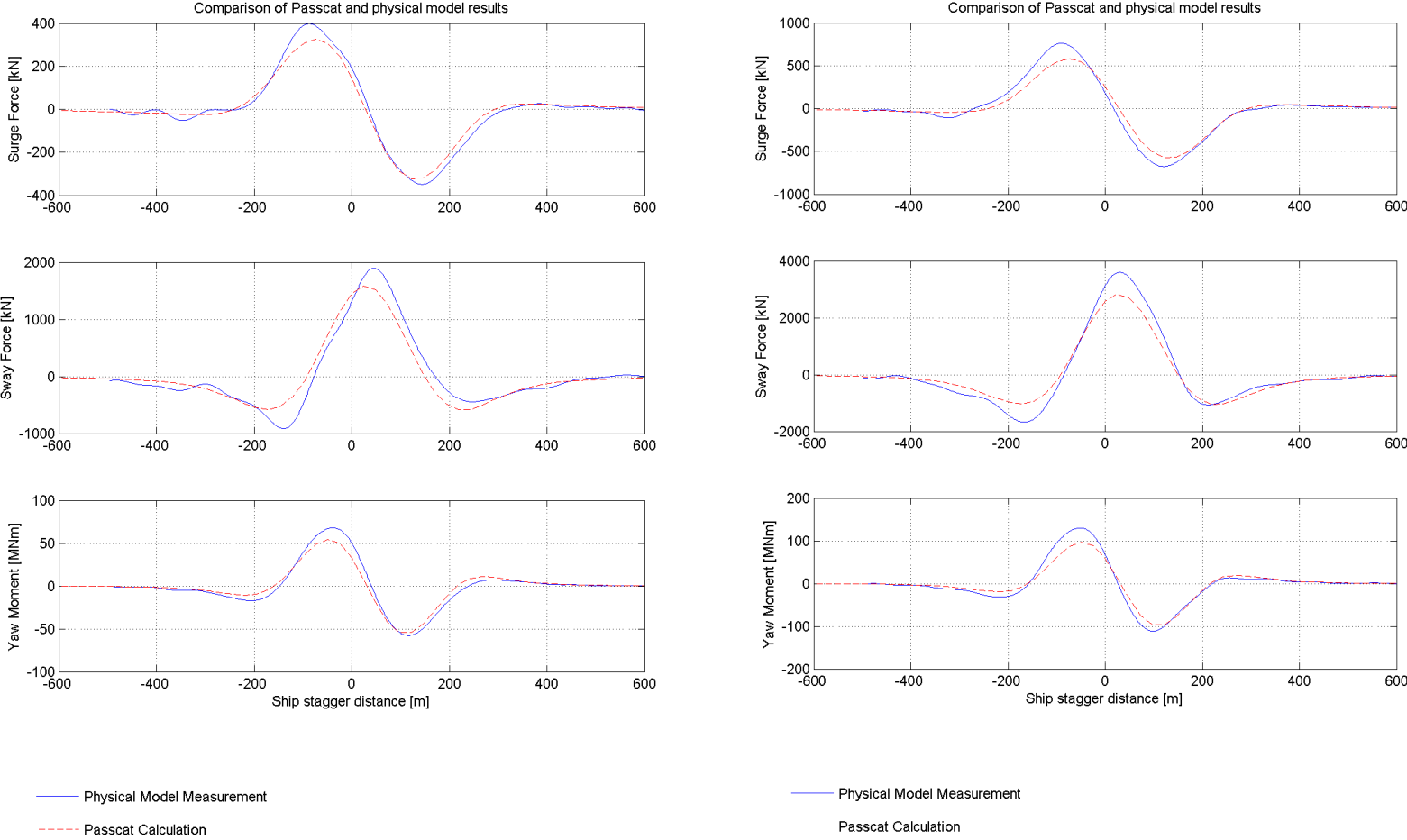


Figure 14: Comparison of test 31 (left) and test 32 (right) physical model measurements and numerical model calculations

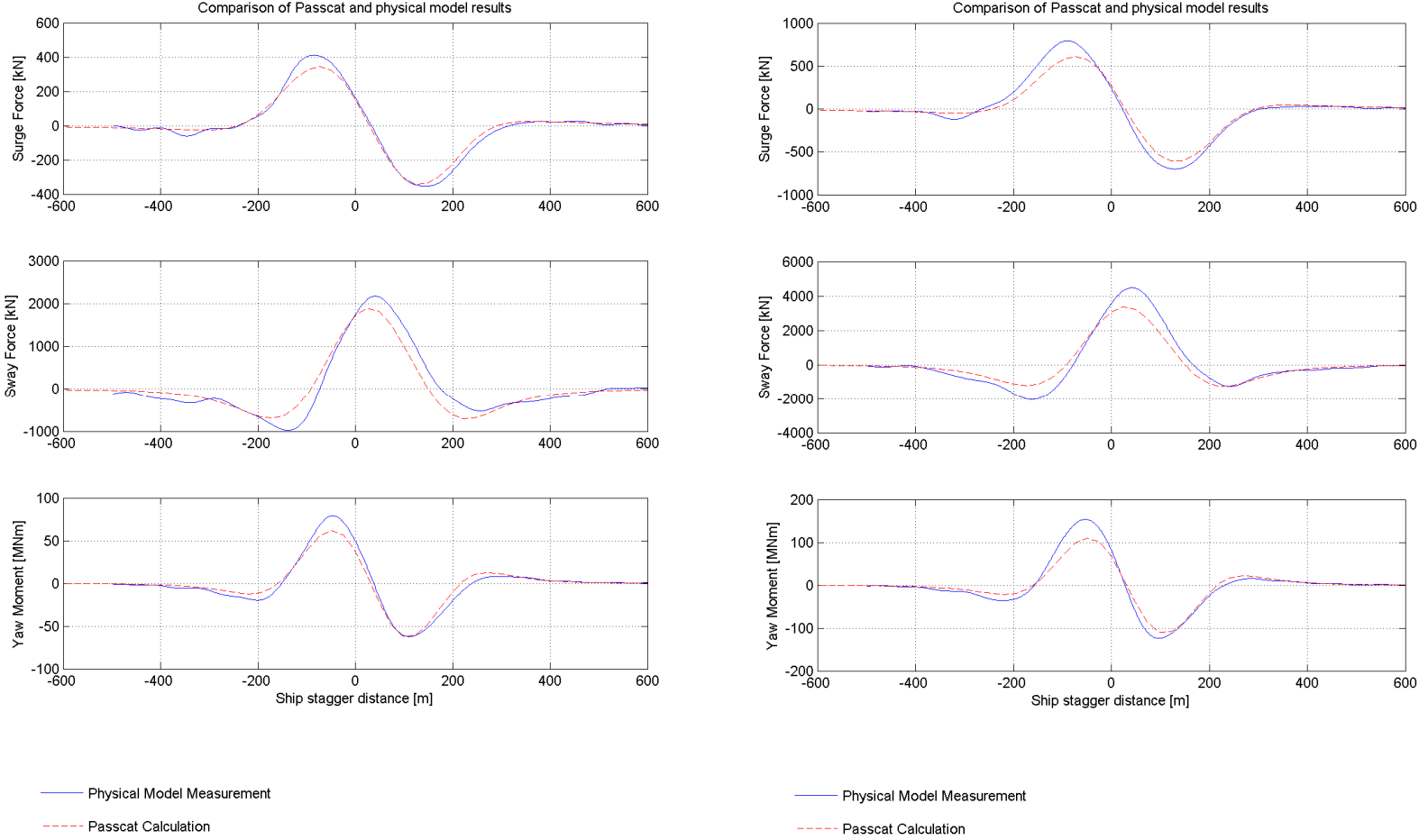


Figure 15: Comparison of test 33 (left) and test 34 (right) physical model measurements and numerical model calculations

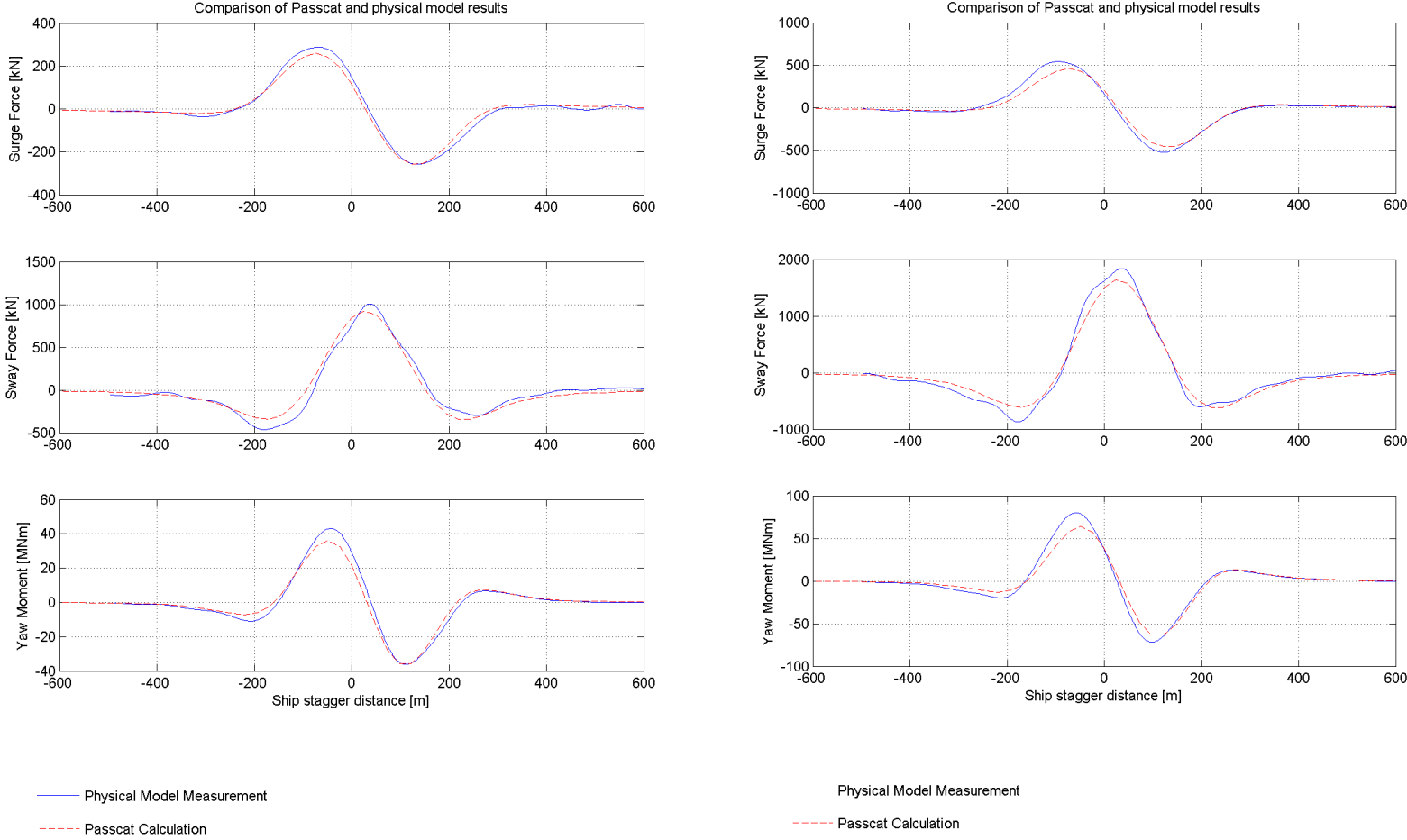


Figure 16: Comparison of test 35 (left) and test 36 (right) physical model measurements and numerical model calculations

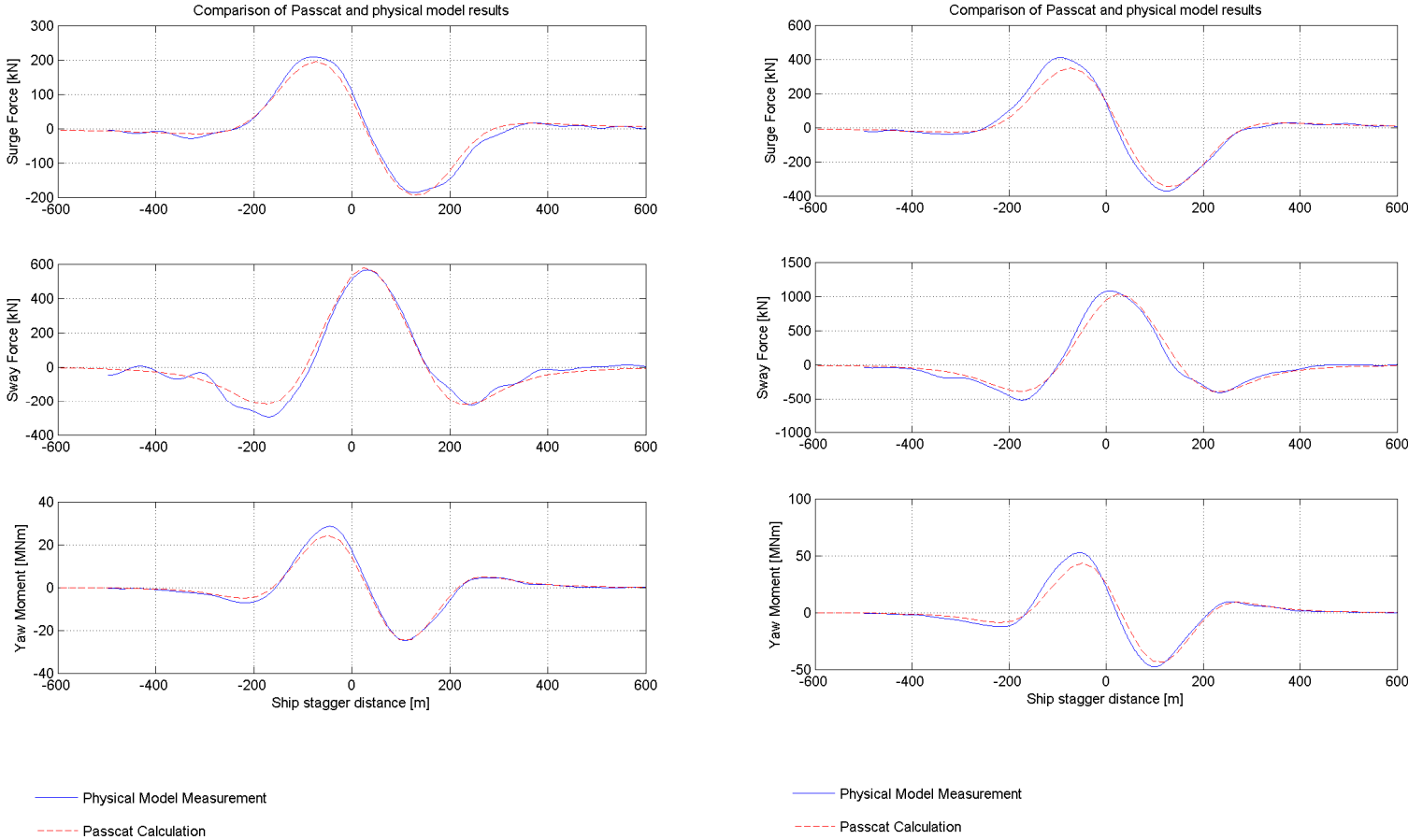


Figure 17: Comparison of test 37 (left) and test 38 (right) physical model measurements and numerical model calculations

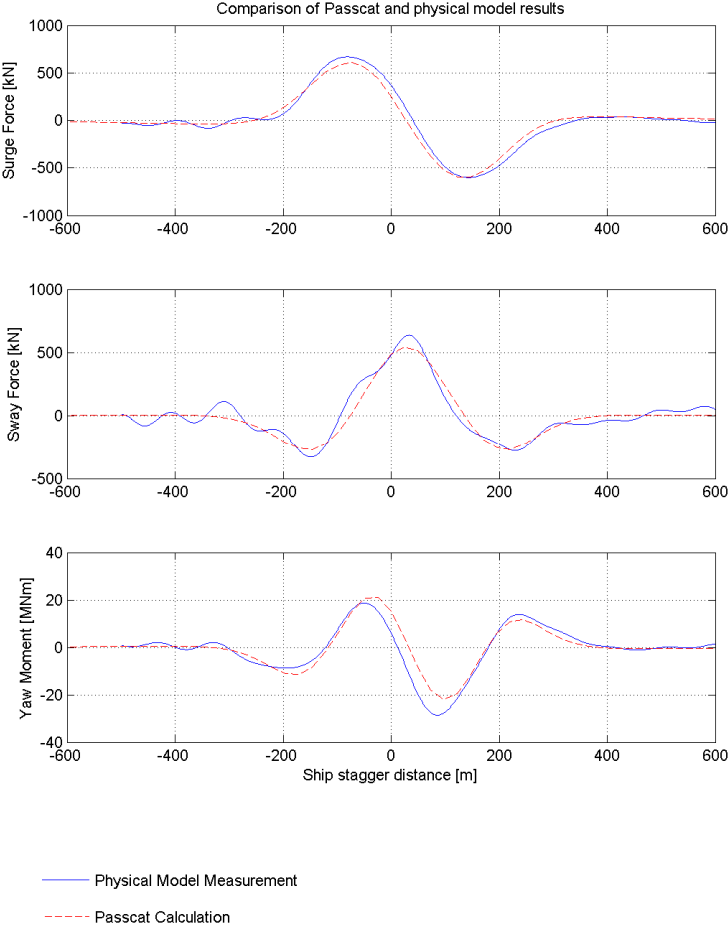
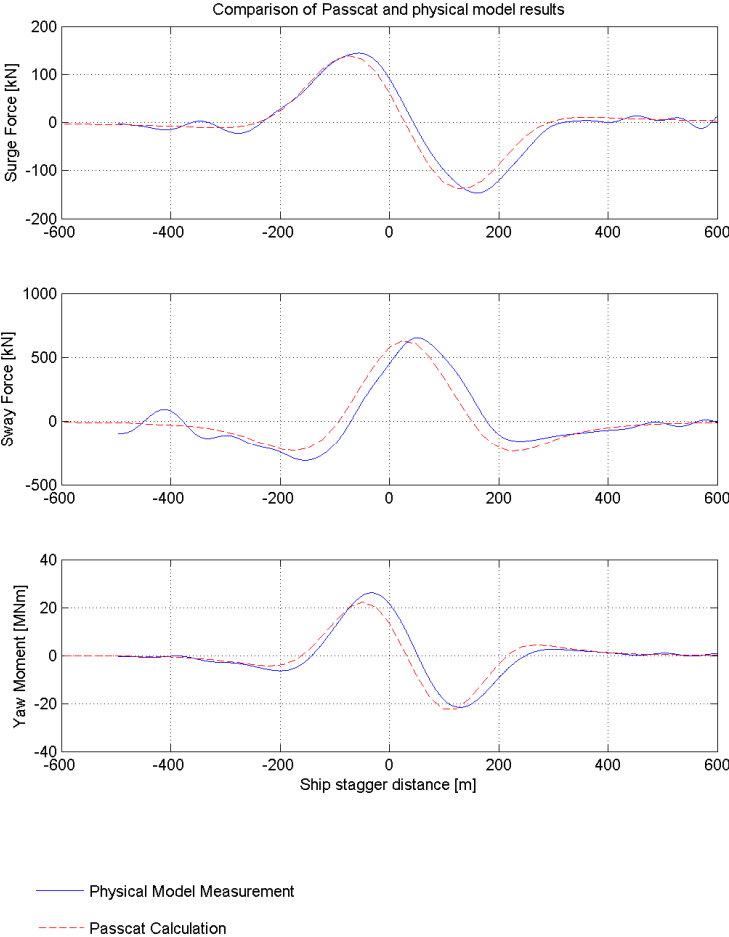


Figure 18: Comparison of test 39 (left) and test 40 (right) physical model measurements and numerical model calculations

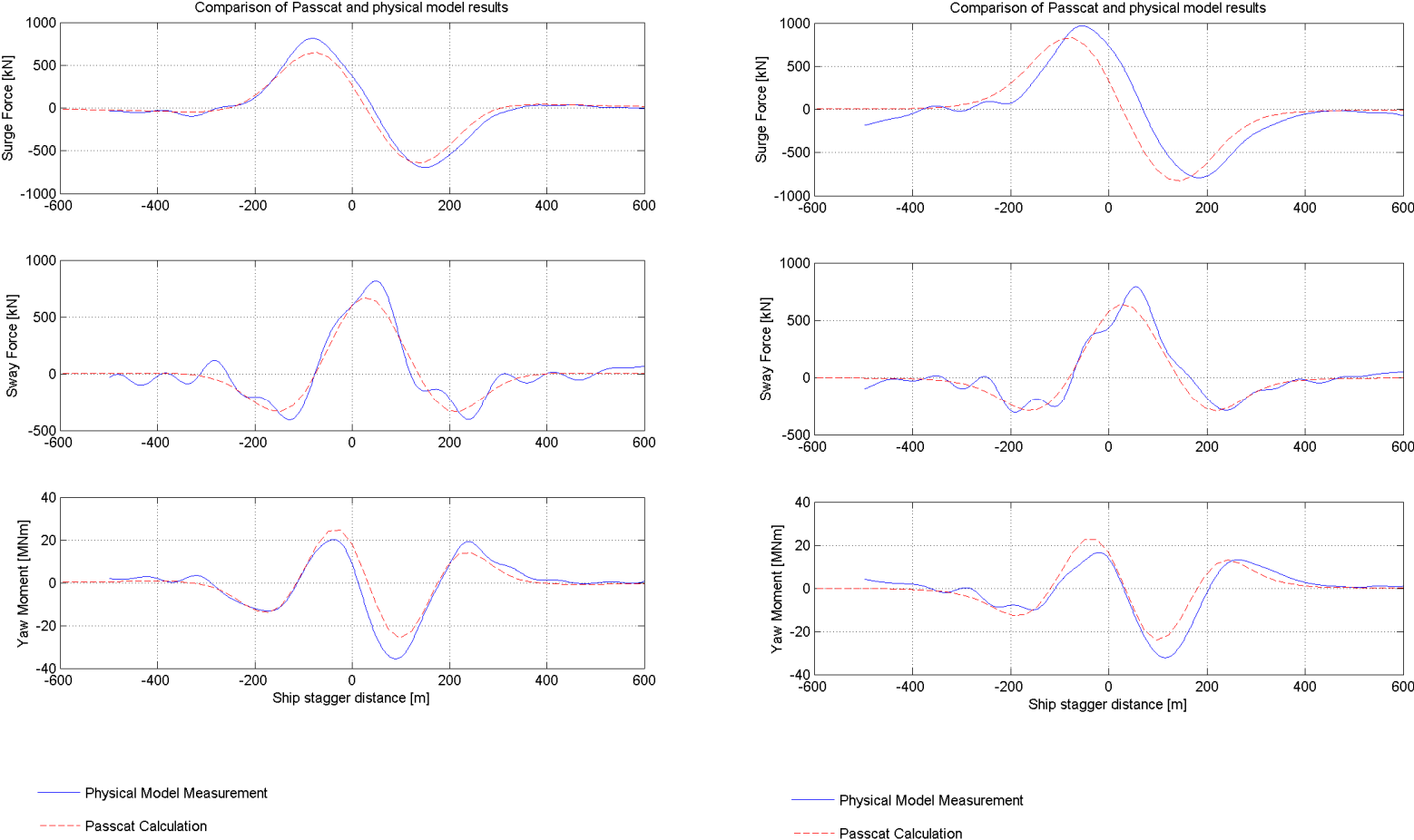


Figure 19: Comparison of test 41 (left) and test 42 (right) physical model measurements and numerical model calculations

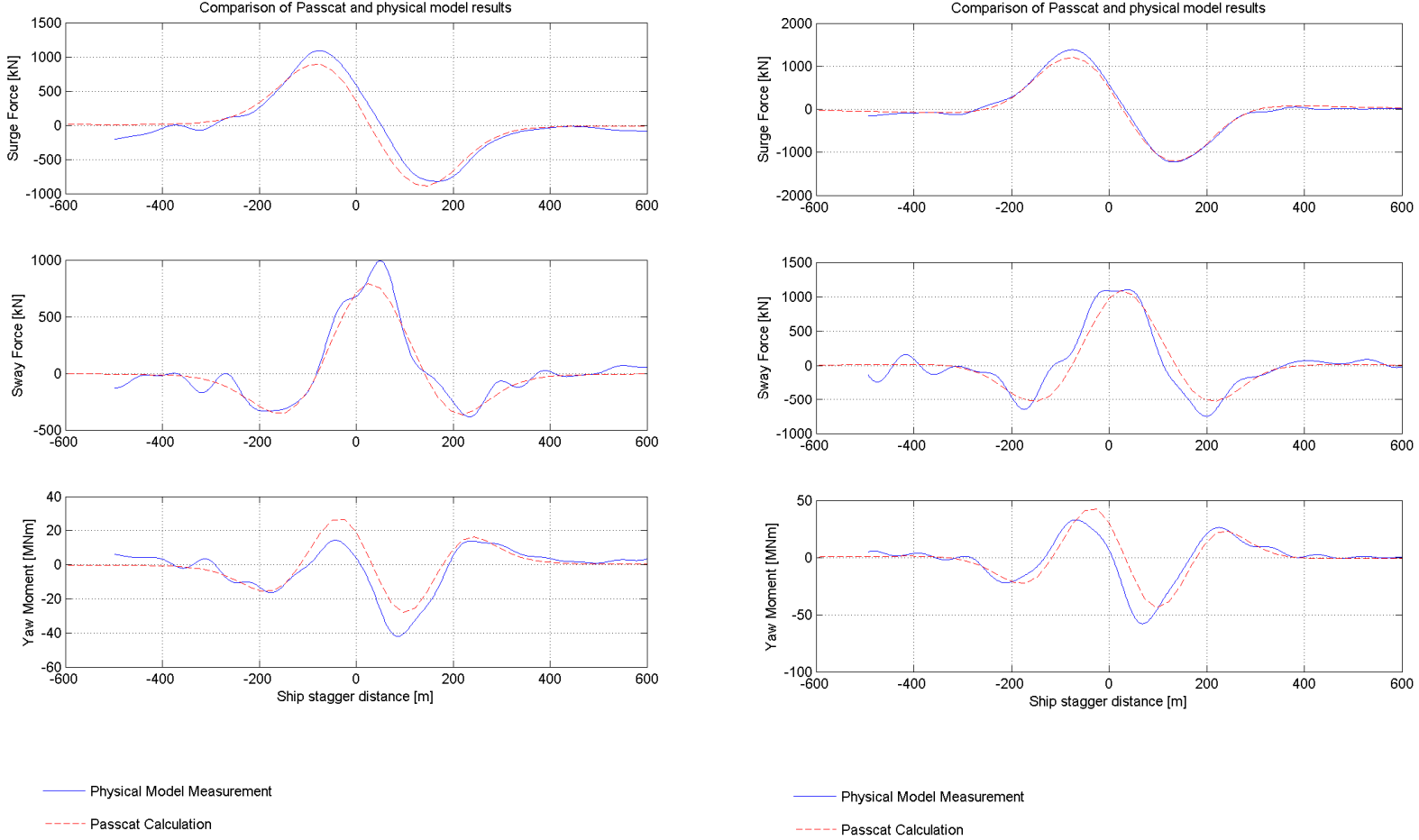


Figure 20: Comparison of test 43 (left) and test 44 (right) physical model measurements and numerical model calculations

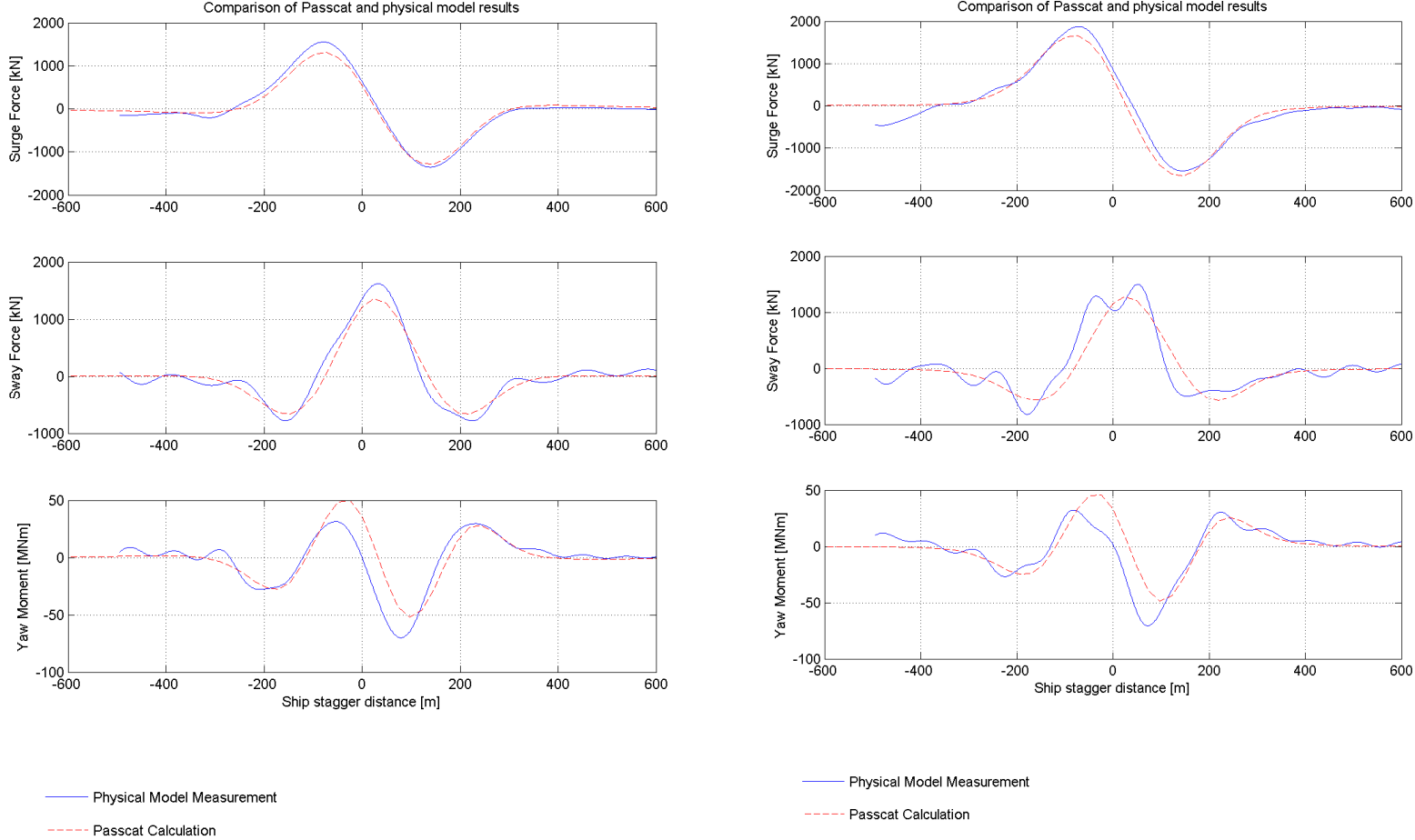


Figure 21: Comparison of test 45 (left) and test 46 (right) physical model measurements and numerical model calculations

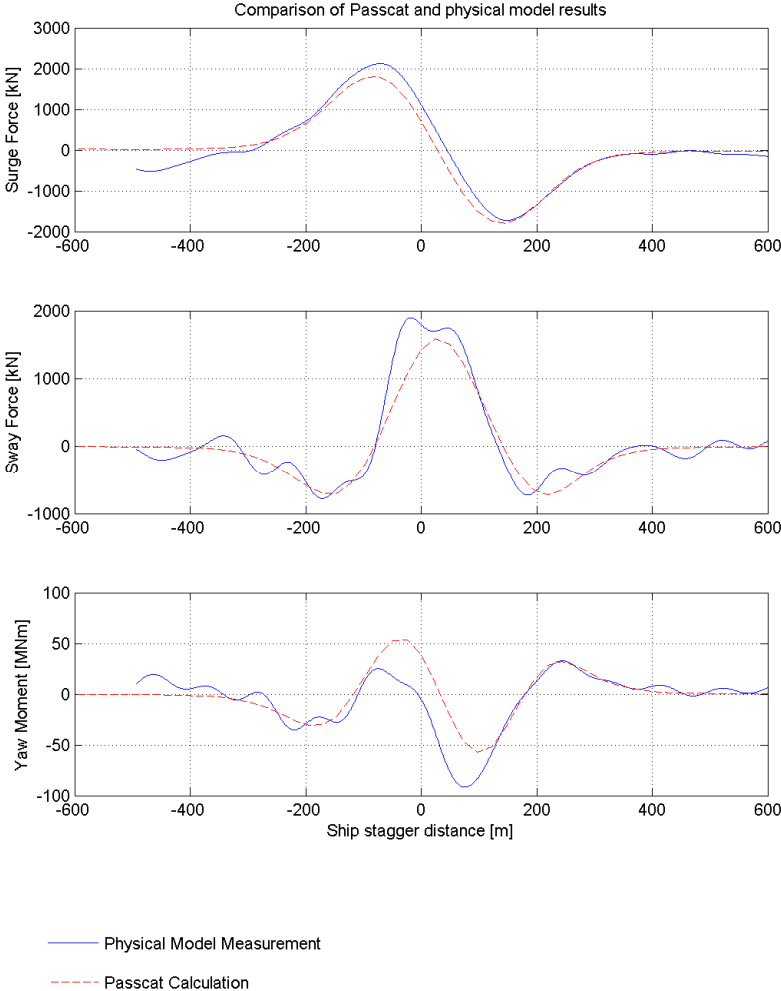


Figure 22: Comparison of test 47 (left) physical model measurements and numerical model calculations

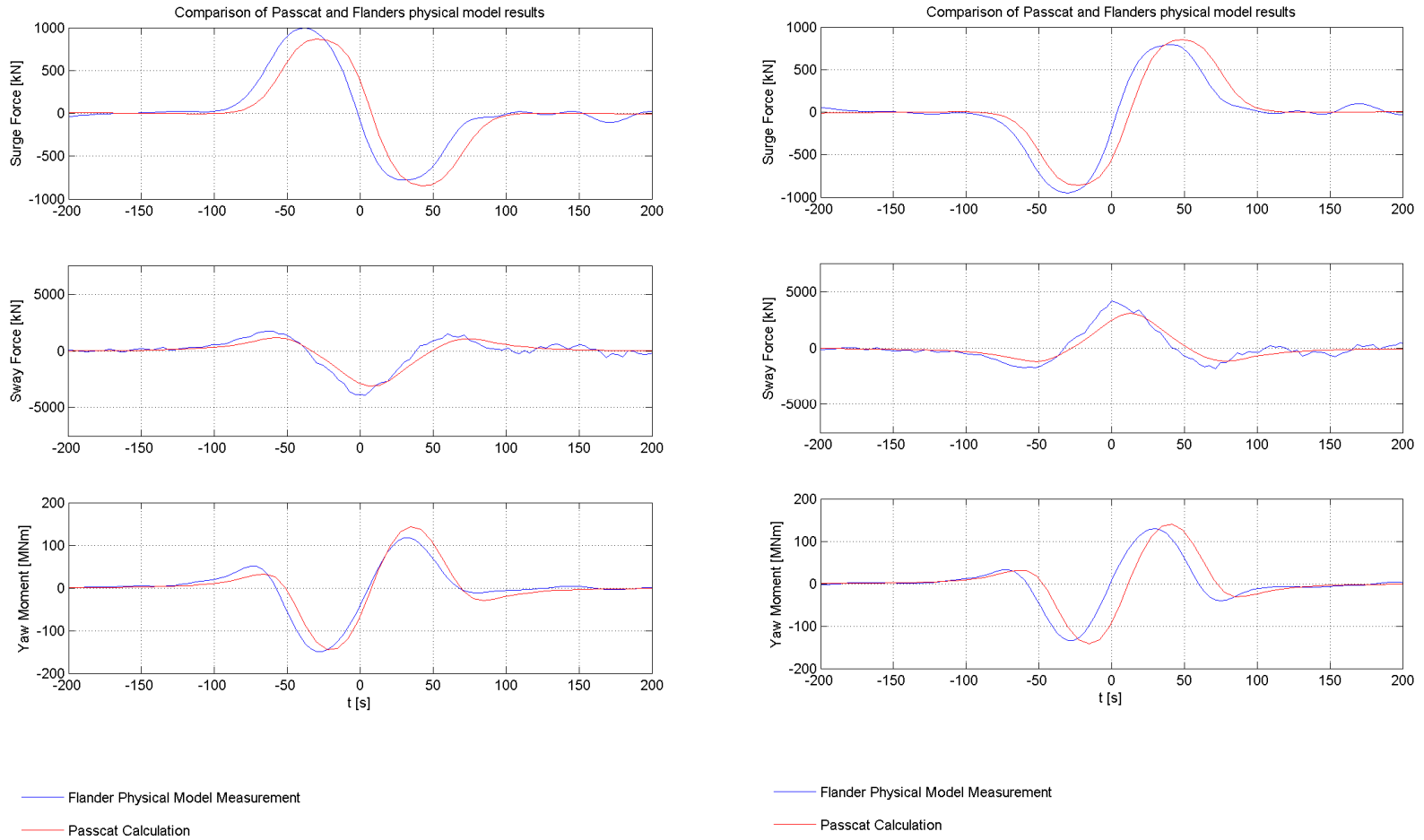


Figure 23: Comparison of Flanders test 01 (left) and Flanders test 02 (right) physical model measurements and numerical model calculations

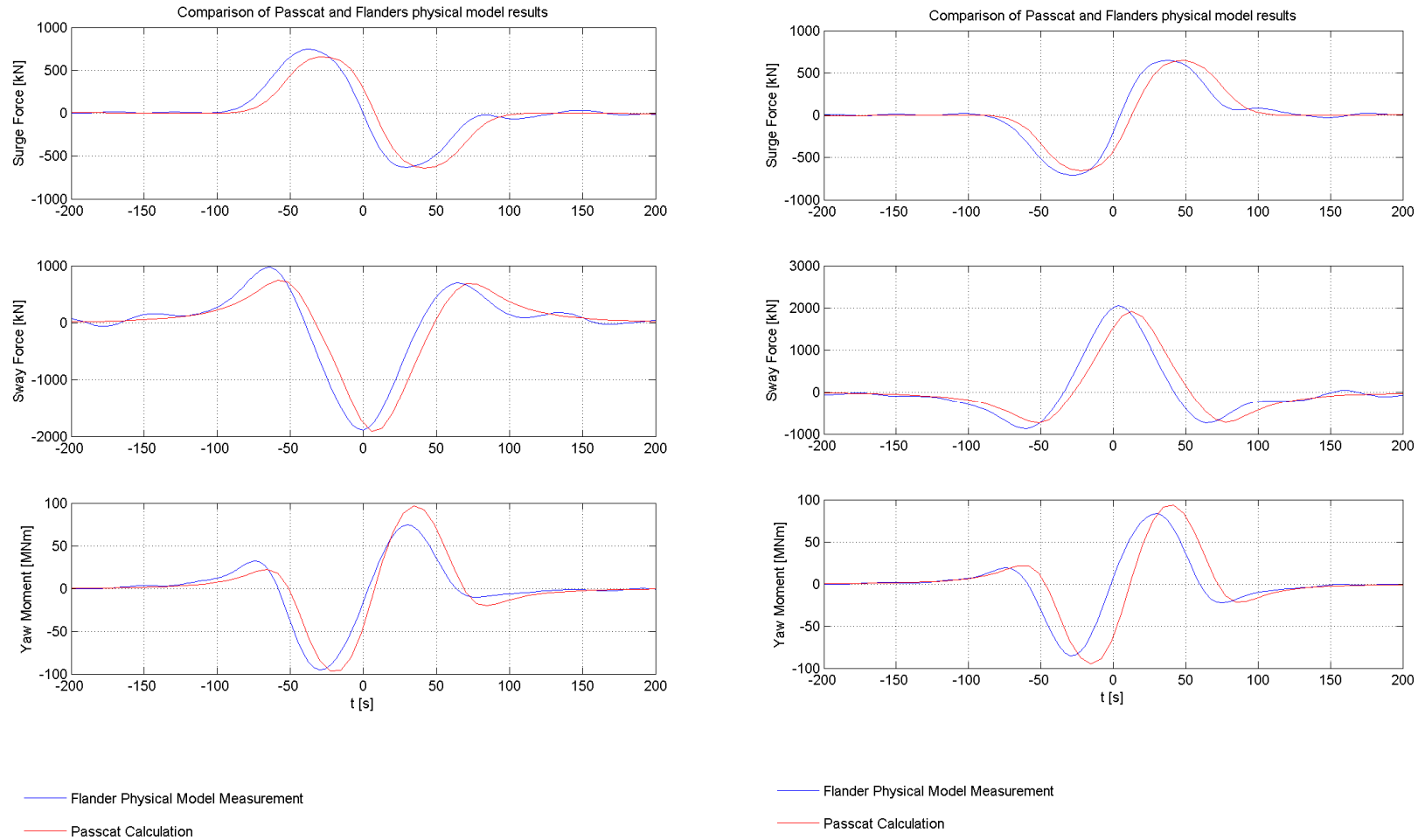


Figure 24: Comparison of Flanders test 03 (left) and Flanders test 04 (right) physical model measurements and numerical model calculations

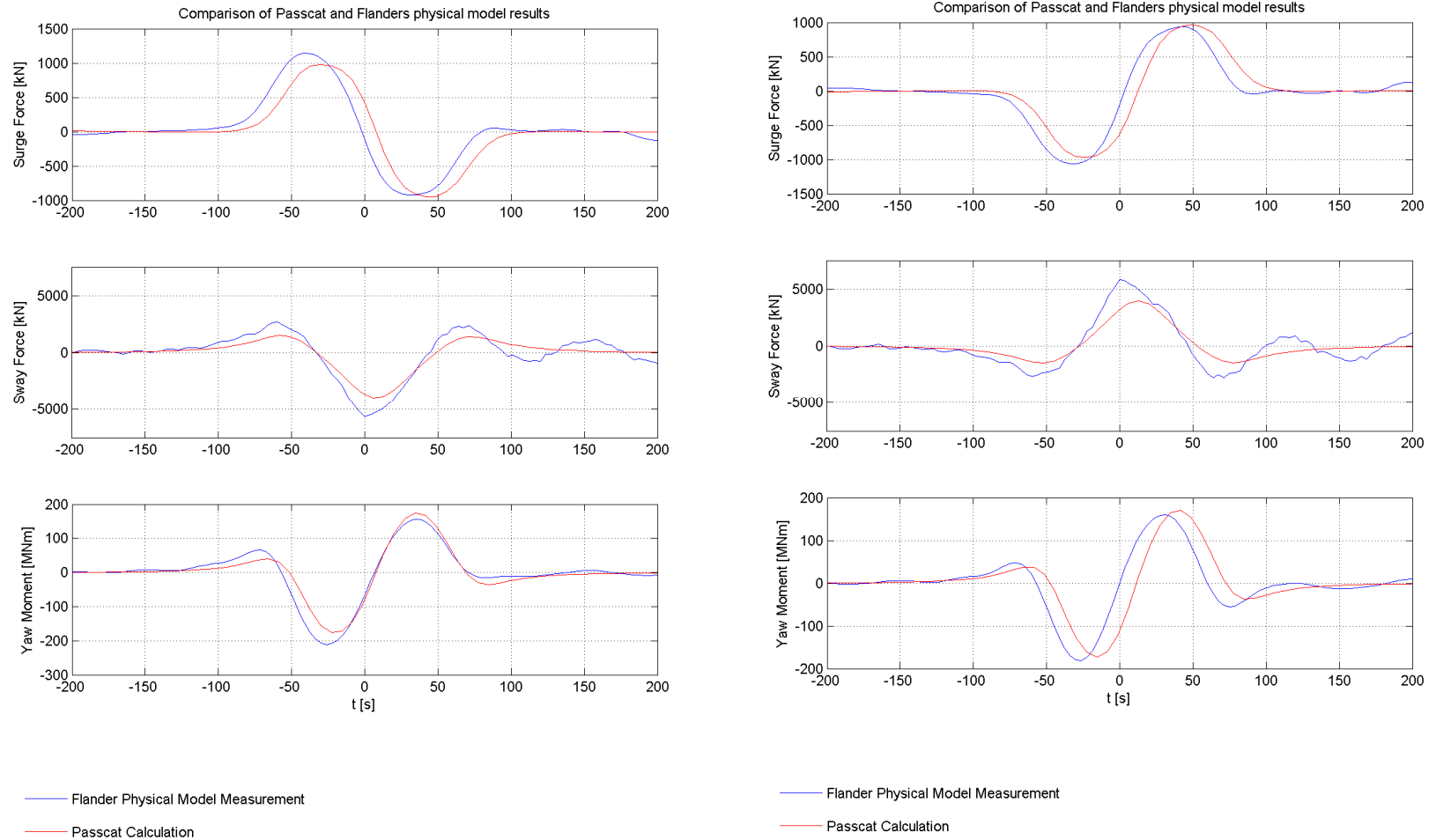


Figure 25: Comparison of Flanders test 05 (left) and Flanders test 06 (right) physical model measurements and numerical model calculations

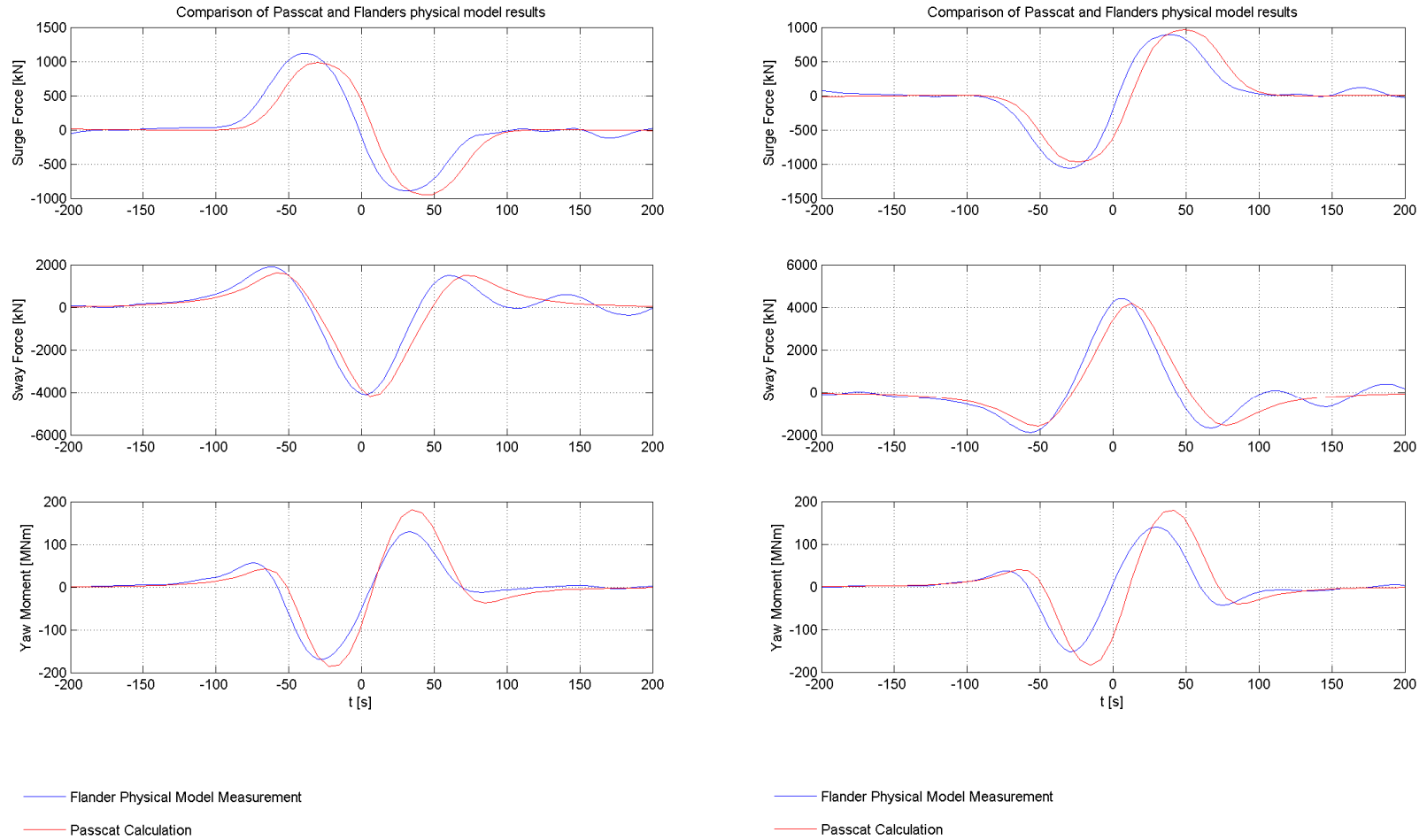


Figure 26: Comparison of Flanders test 07 (left) and Flanders test 08 (right) physical model measurements and numerical model calculations

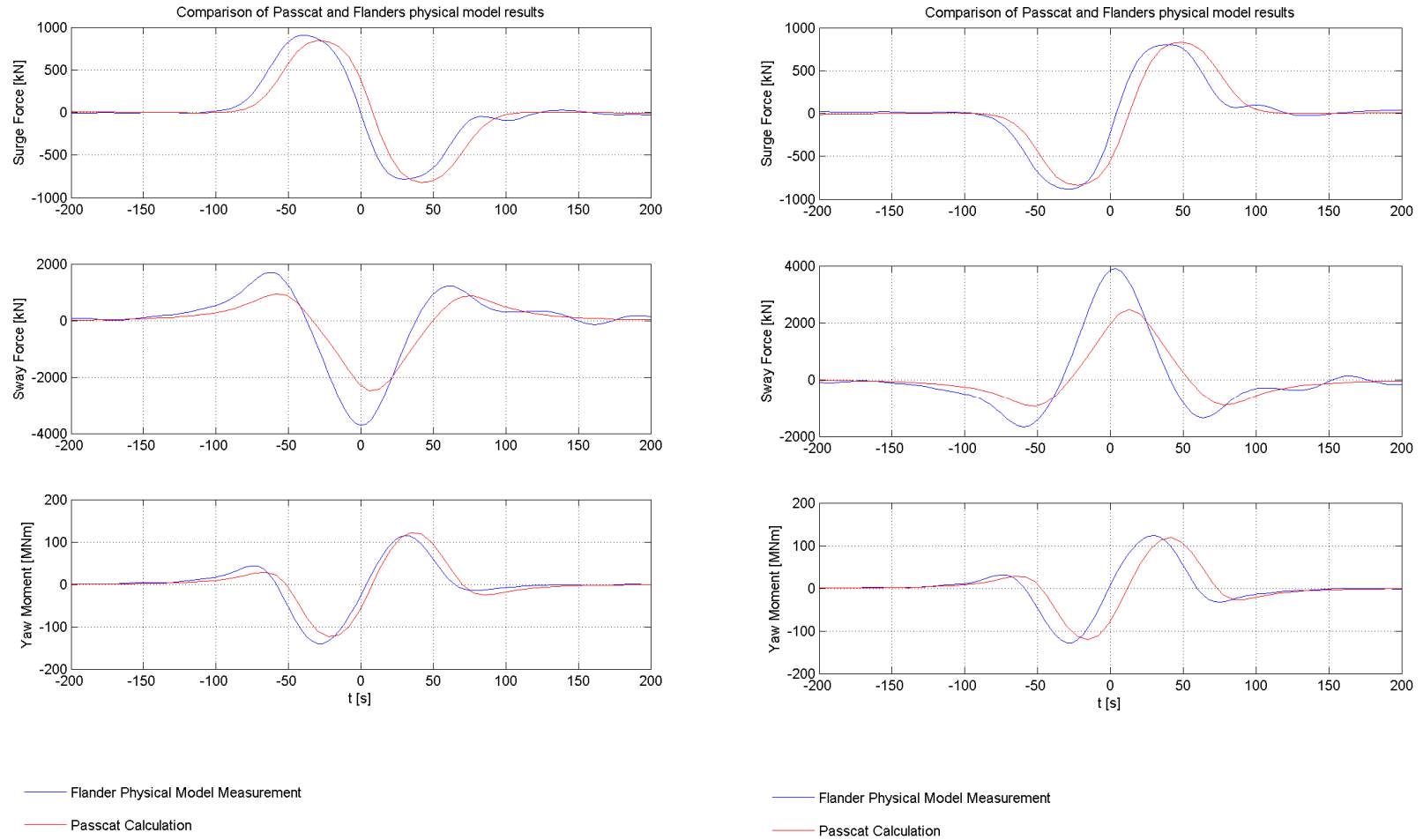


Figure 27: Comparison of Flanders test 09 (left) and Flanders test 10 (right) physical model measurements and numerical model calculations

APPENDIX D: TRENDS IN PHYSICAL AND NUMERICAL MODEL RESULTS

LIST OF FIGURES:

- Figure 1: Measured and calculated results compared by passing distance at 6kn (left) and by passing distance at 8kn (right).
- Figure 2: Measured and calculated results compared by depth draft ratio at 6kn (left) and by depth draft ratio at 8kn (right).
- Figure 3: Measured and calculated results compared by walls or channels at 6kn (left) and by walls or channels at 8kn (right).
- Figure 4: Measured and calculated results compared by speed.

Appendix D: Trends in Physical and Numerical Model Results

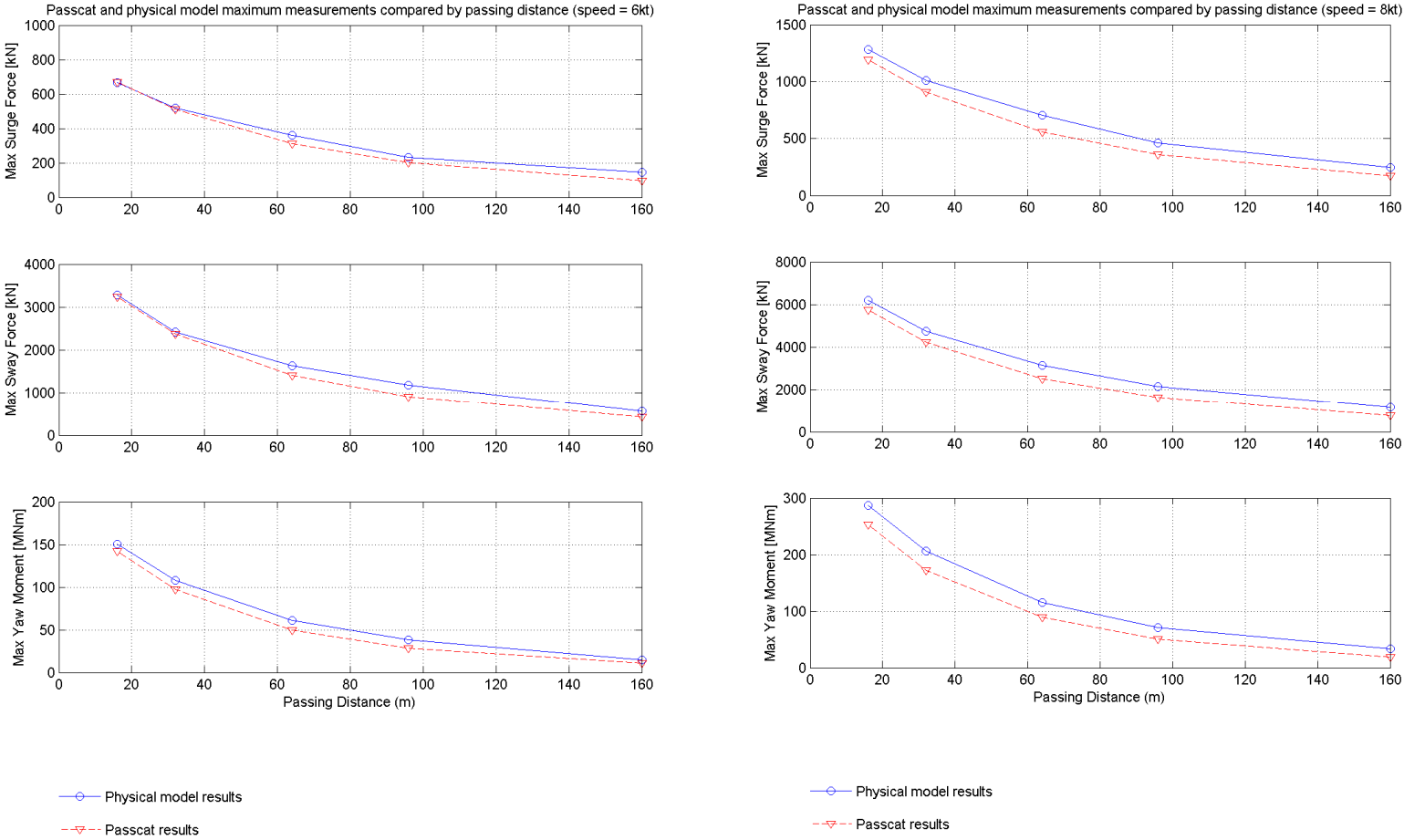


Figure 1: Measured and calculated results compared by passing distance at 6kn (left) and by passing distance at 8kn (right).

Appendix D: Trends in Physical and Numerical Model Results

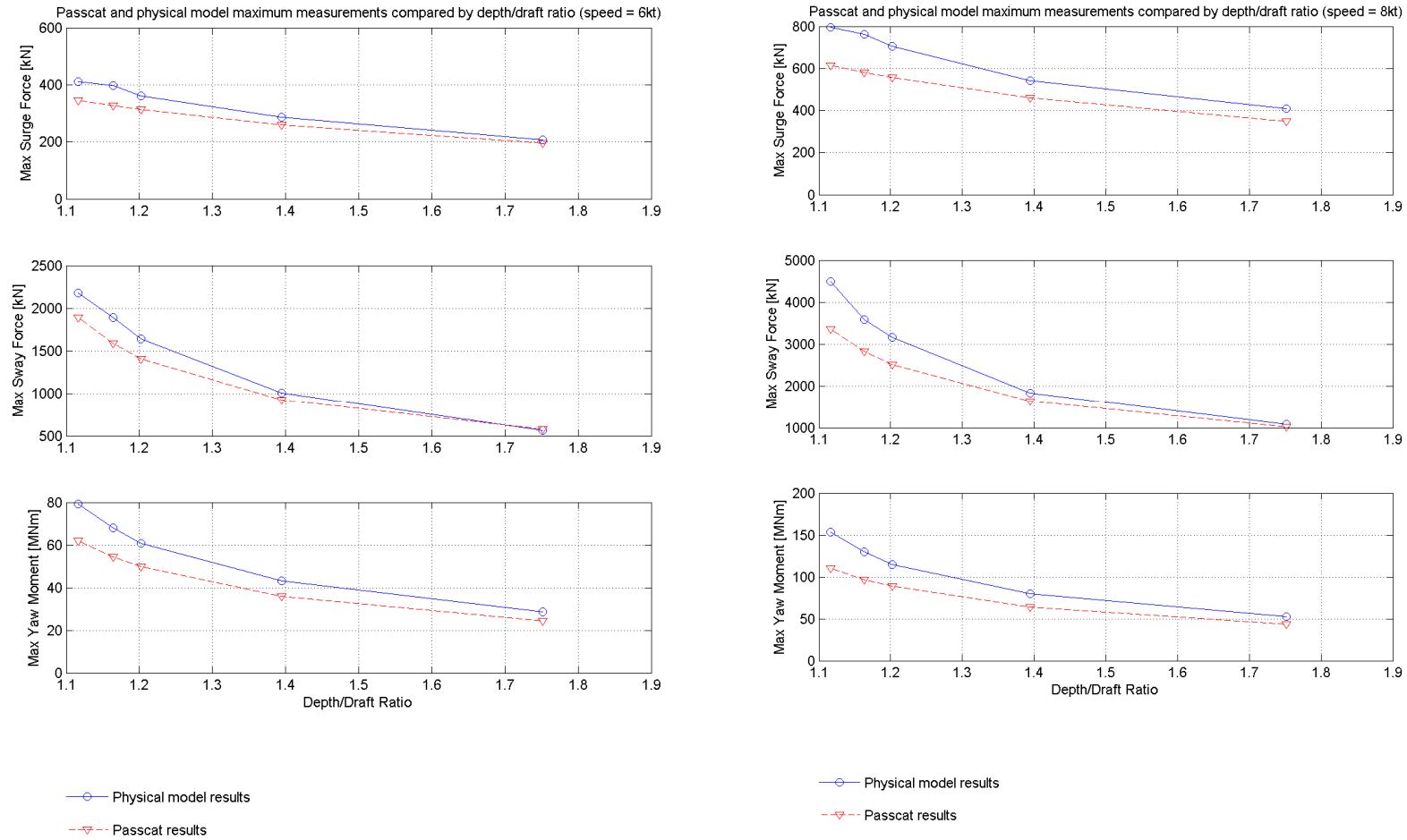


Figure 2: Measured and calculated results compared by depth draft ratio at 6kn (left) and by depth draft ratio at 8kn (right).

Appendix D: Trends in Physical and Numerical Model Results

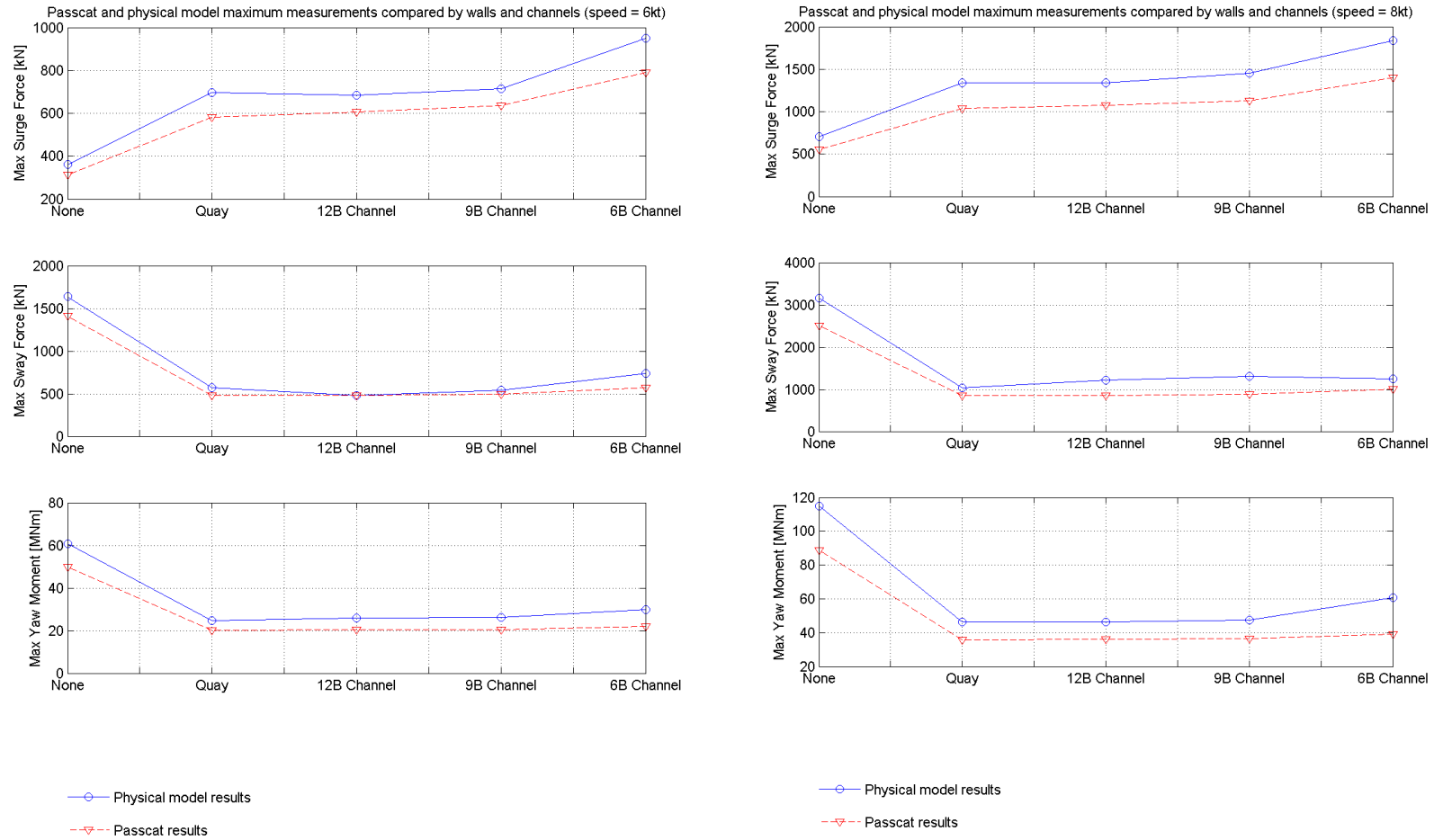


Figure 3: Measured and calculated results compared by walls or channels at 6kn (left) and by walls or channels at 8kn (right).

Appendix D: Trends in Physical and Numerical Model Results

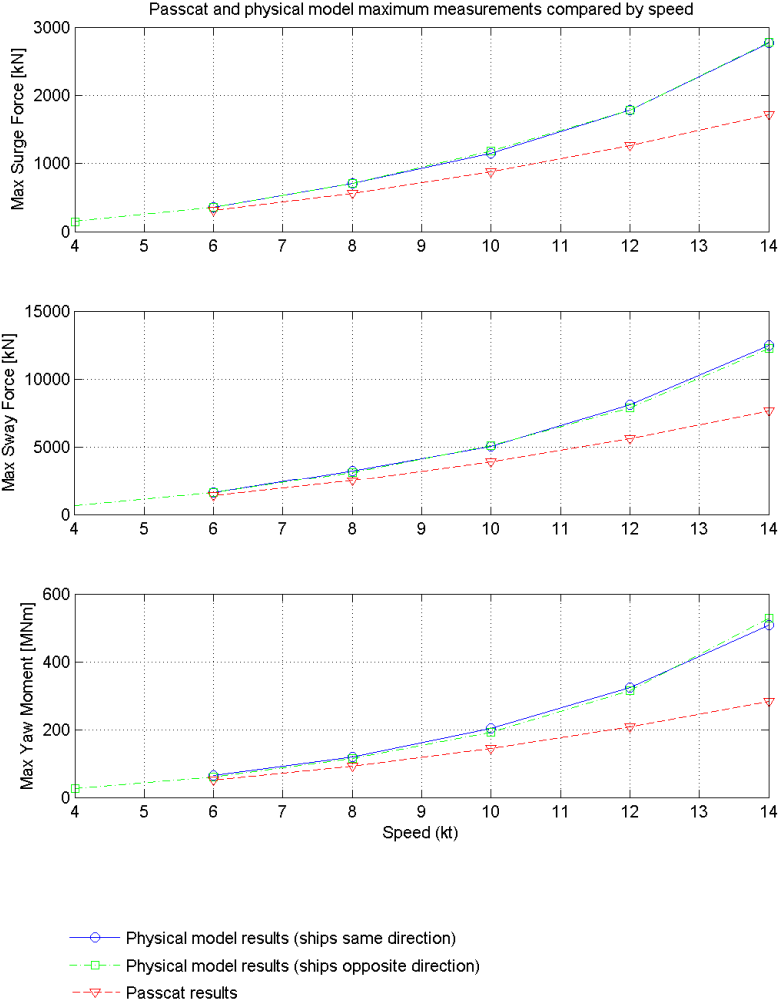


Figure 4: Measured and calculated results compared by speed.

APPENDIX E: COMPARISON OF MATHEMATICAL AND PHYSICAL MODELS

LIST OF FIGURES:

Figure 1: Comparison of test 01 (left) and test 06 (right) physical model measurements and mathematical model calculations

Figure 2: Comparison of test 07 (left) and test 08 (right) physical model measurements and mathematical model calculations

Figure 3: Comparison of test 09 (left) and test 10 (right) physical model measurements and mathematical model calculations

Figure 4: Comparison of test 11 (left) and test 12 (right) physical model measurements and mathematical model calculations

Figure 5: Comparison of test 13 (left) and test 14 (right) physical model measurements and mathematical model calculations

Figure 6: Comparison of test 15 (left) and test 16 (right) physical model measurements and mathematical model calculations

Figure 7: Comparison of test 17 (left) and test 18 (right) physical model measurements and mathematical model calculations

Figure 8: Comparison of test 19 (left) and test 20 (right) physical model measurements and mathematical model calculations

Figure 9: Comparison of test 21 (left) and test 22 (right) physical model measurements and mathematical model calculations

Figure 10: Comparison of test 23 (left) and test 24 (right) physical model measurements and mathematical model calculations

Figure 11: Comparison of test 25 (left) and test 26 (right) physical model measurements and mathematical model calculations

Appendix E: Comparison of mathematical and physical models

Figure 12: Comparison of test 27 (left) and test 28 (right) physical model measurements and mathematical model calculations

Figure 13: Comparison of test 29 (left) and test 30 (right) physical model measurements and mathematical model calculations

Figure 14: Comparison of test 31 (left) and test 32 (right) physical model measurements and mathematical model calculations

Figure 15: Comparison of test 33 (left) and test 34 (right) physical model measurements and mathematical model calculations

Figure 16: Comparison of test 35 (left) and test 36 (right) physical model measurements and mathematical model calculations

Figure 17: Comparison of test 37 (left) and test 38 (right) physical model measurements and mathematical model calculations

Figure 18: Comparison of test 39 (left) and test 40 (right) physical model measurements and mathematical model calculations

Figure 19: Comparison of test 41 (left) and test 42 (right) physical model measurements and mathematical model calculations

Figure 20: Comparison of test 43 (left) and test 44 (right) physical model measurements and mathematical model calculations

Figure 21: Comparison of test 45 (left) and test 46 (right) physical model measurements and mathematical model calculations

Figure 22: Comparison of test 47 (left) physical model measurements and mathematical model calculations

Appendix E: Comparison of mathematical and physical models

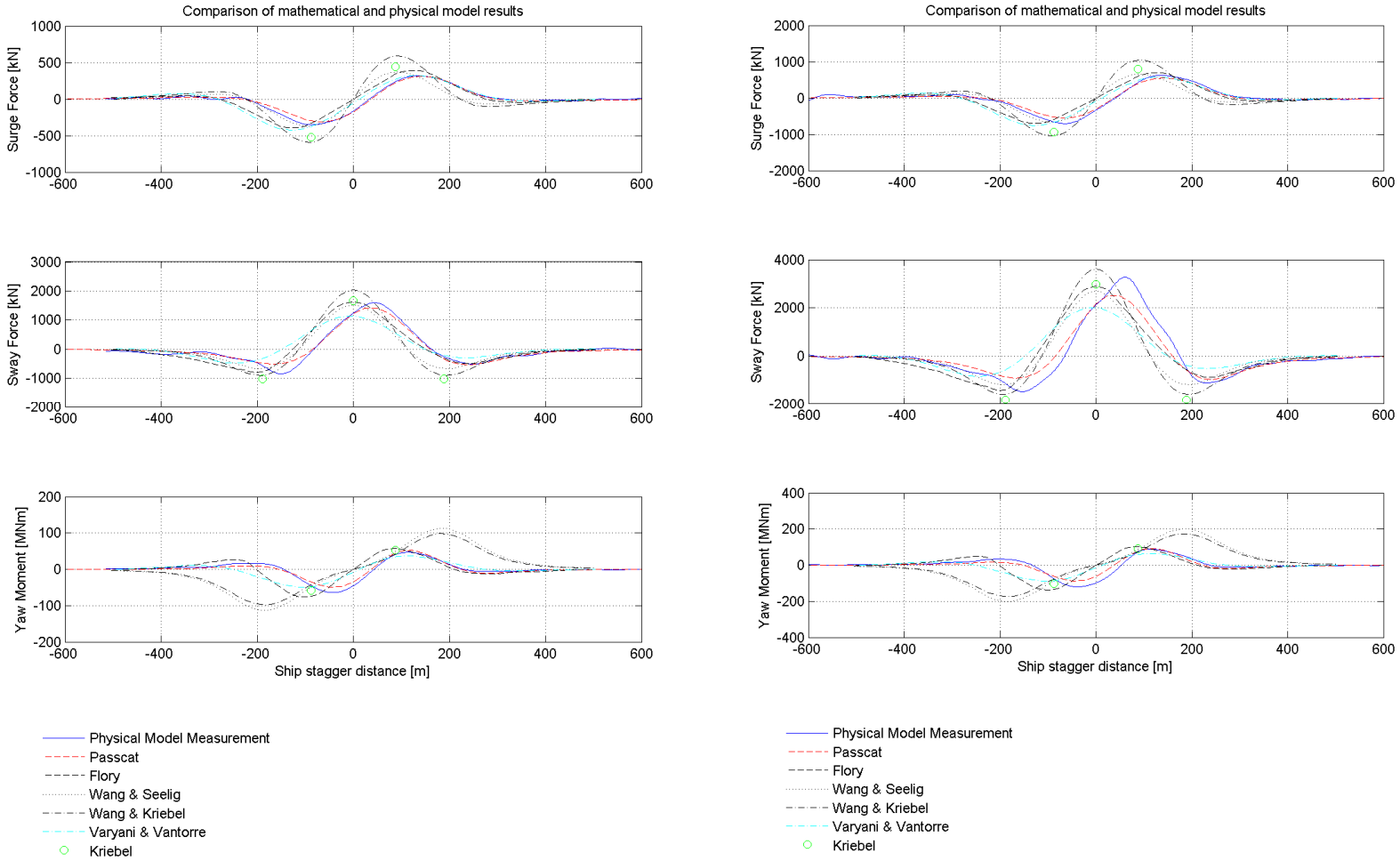


Figure 1: Comparison of test 01 (left) and test 06 (right) physical model measurements and mathematical model calculations.

Appendix E: Comparison of mathematical and physical models

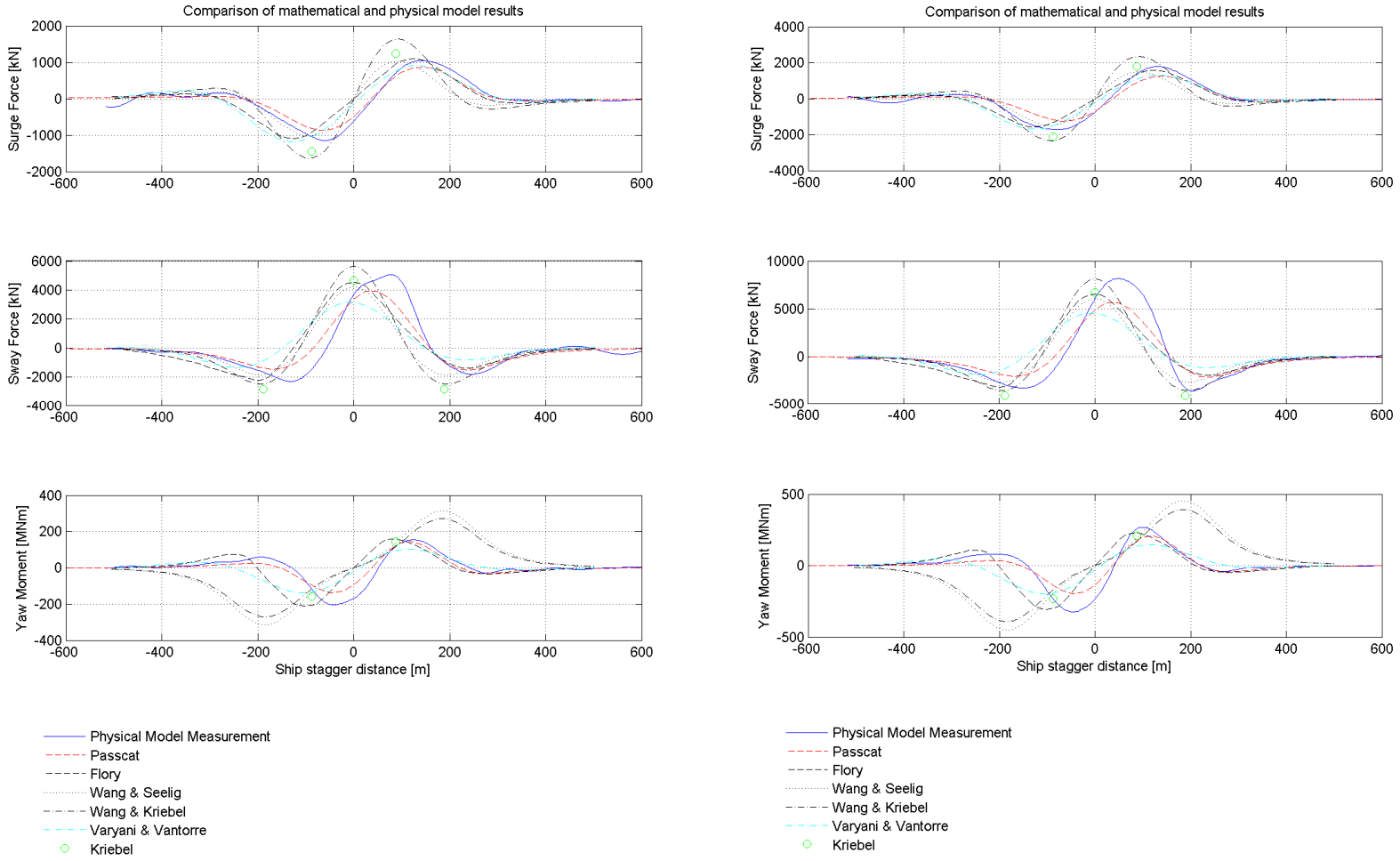


Figure 2: Comparison of test 07 (left) and test 08 (right) physical model measurements and mathematical model calculations

Appendix E: Comparison of mathematical and physical models

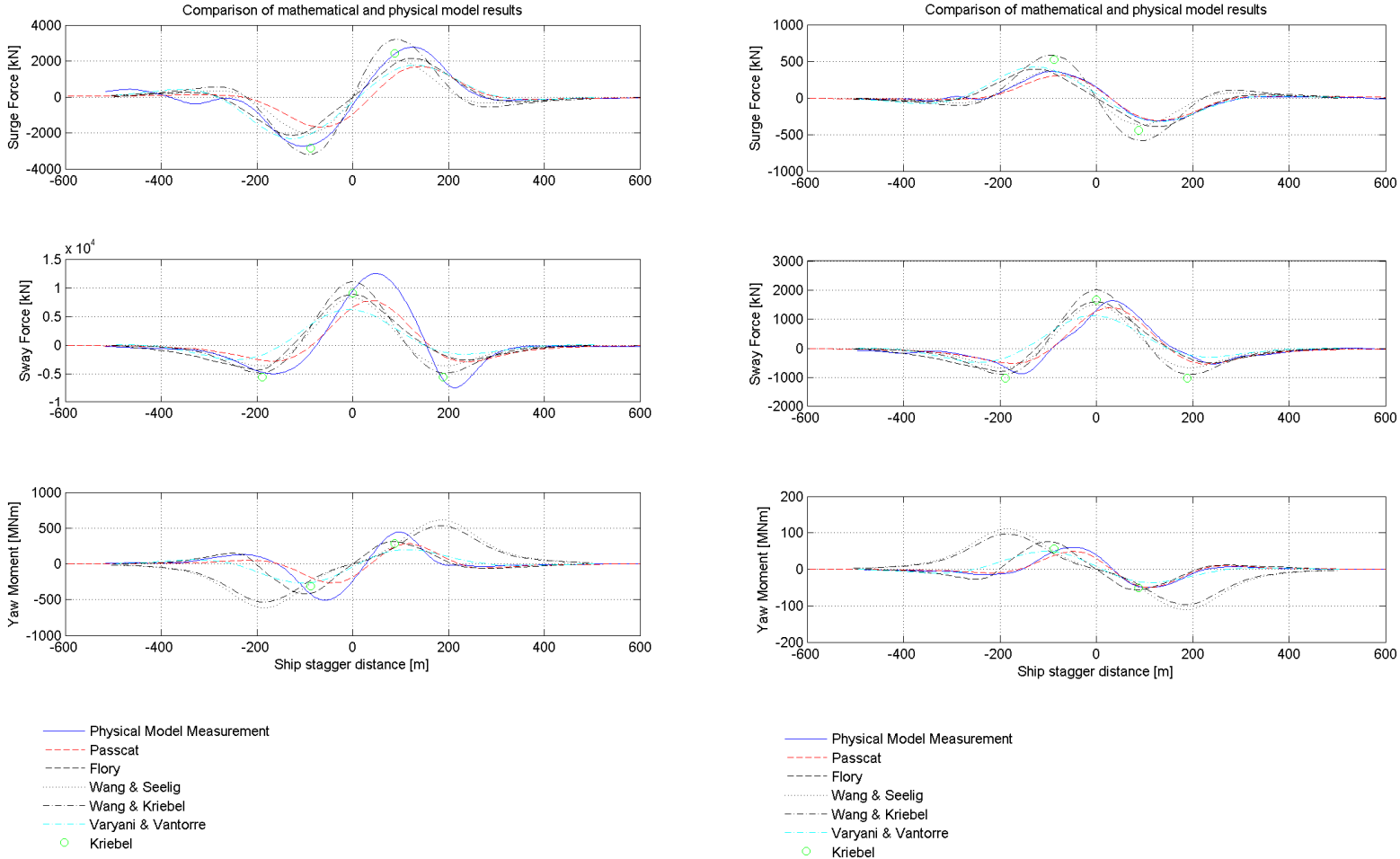


Figure 3: Comparison of test 09 (left) and test 10 (right) physical model measurements and mathematical model calculations

Appendix E: Comparison of mathematical and physical models

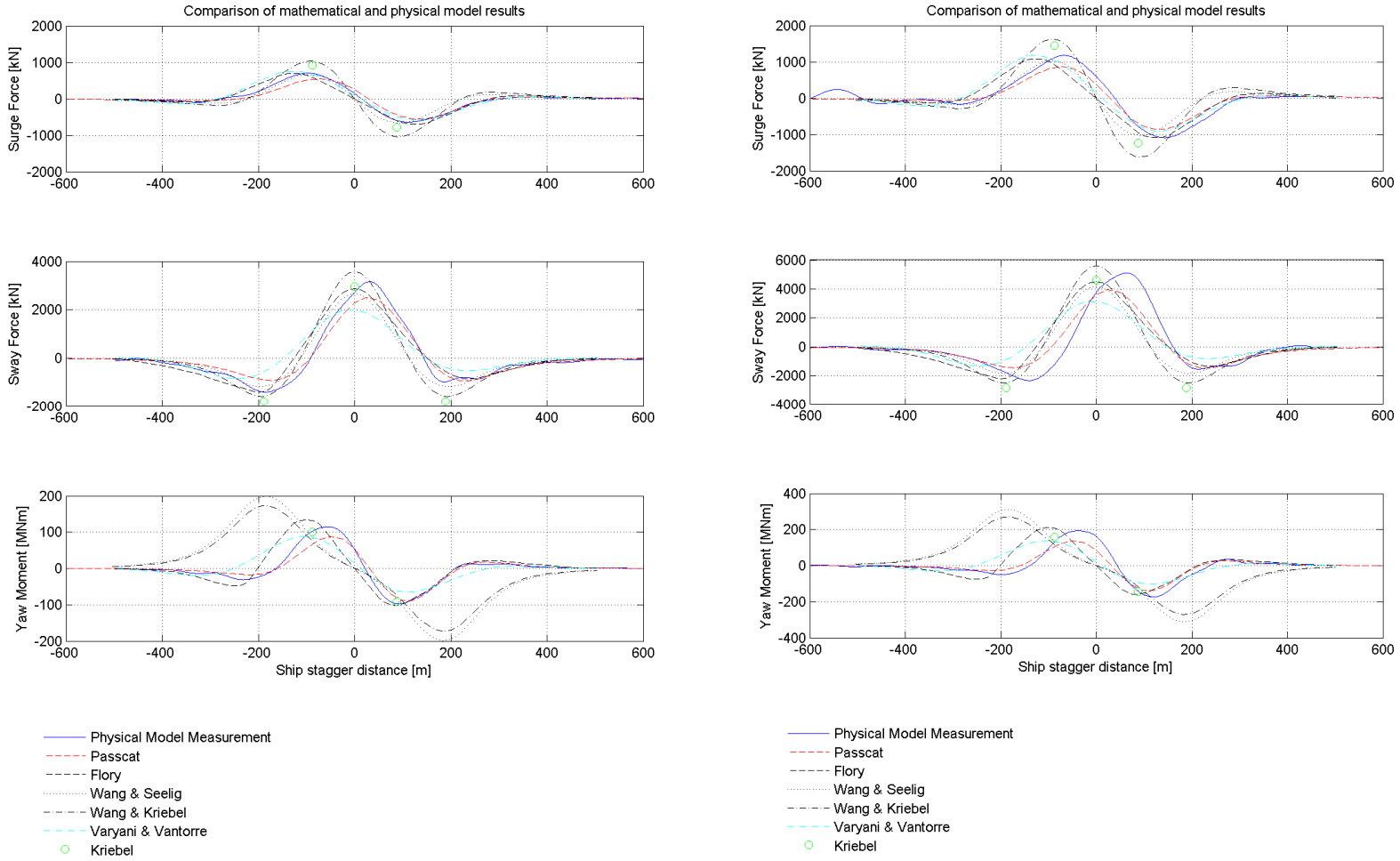


Figure 4: Comparison of test 11 (left) and test 12 (right) physical model measurements and mathematical model calculations

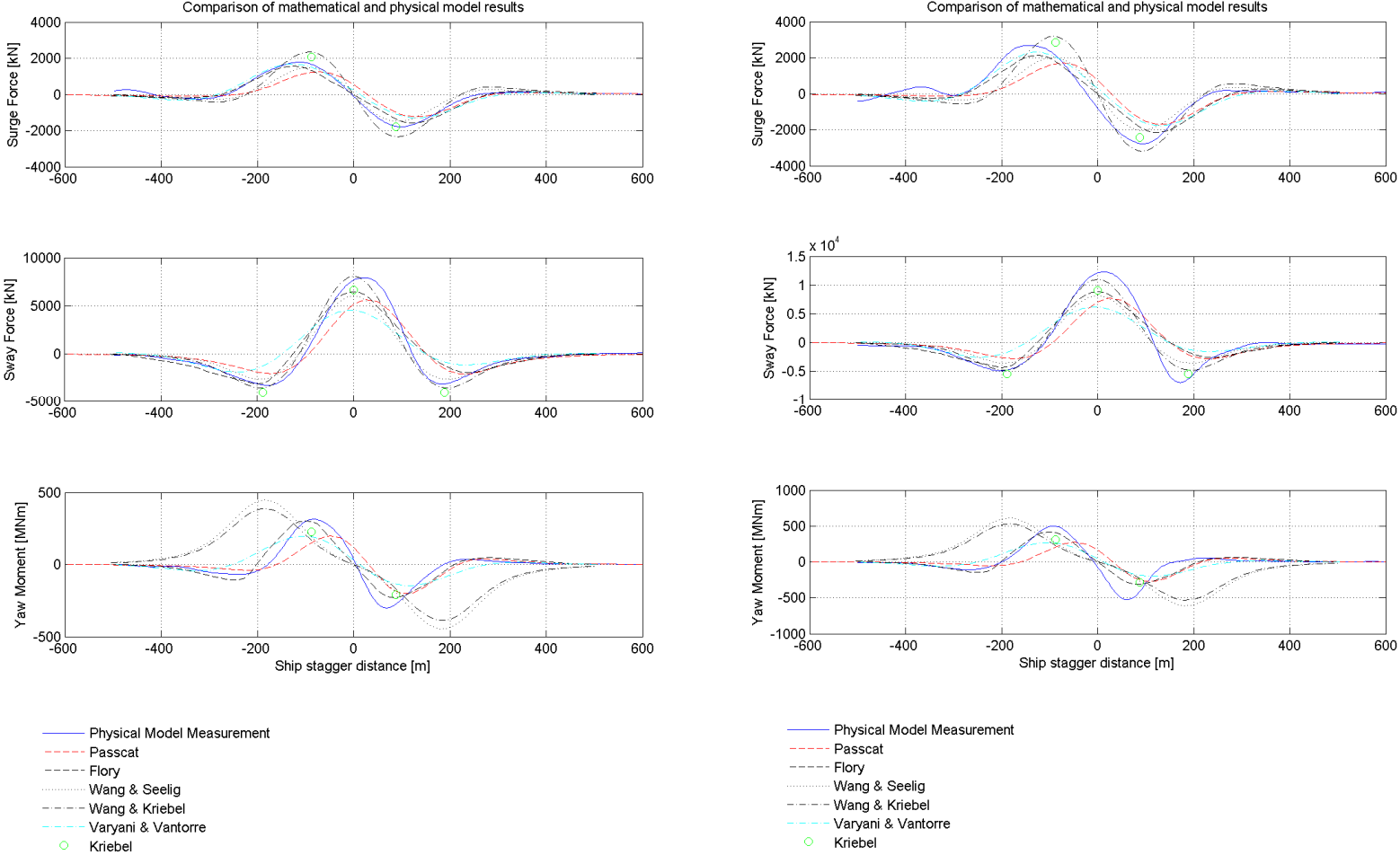


Figure 5: Comparison of test 13 (left) and test 14 (right) physical model measurements and mathematical model calculations

Appendix E: Comparison of mathematical and physical models

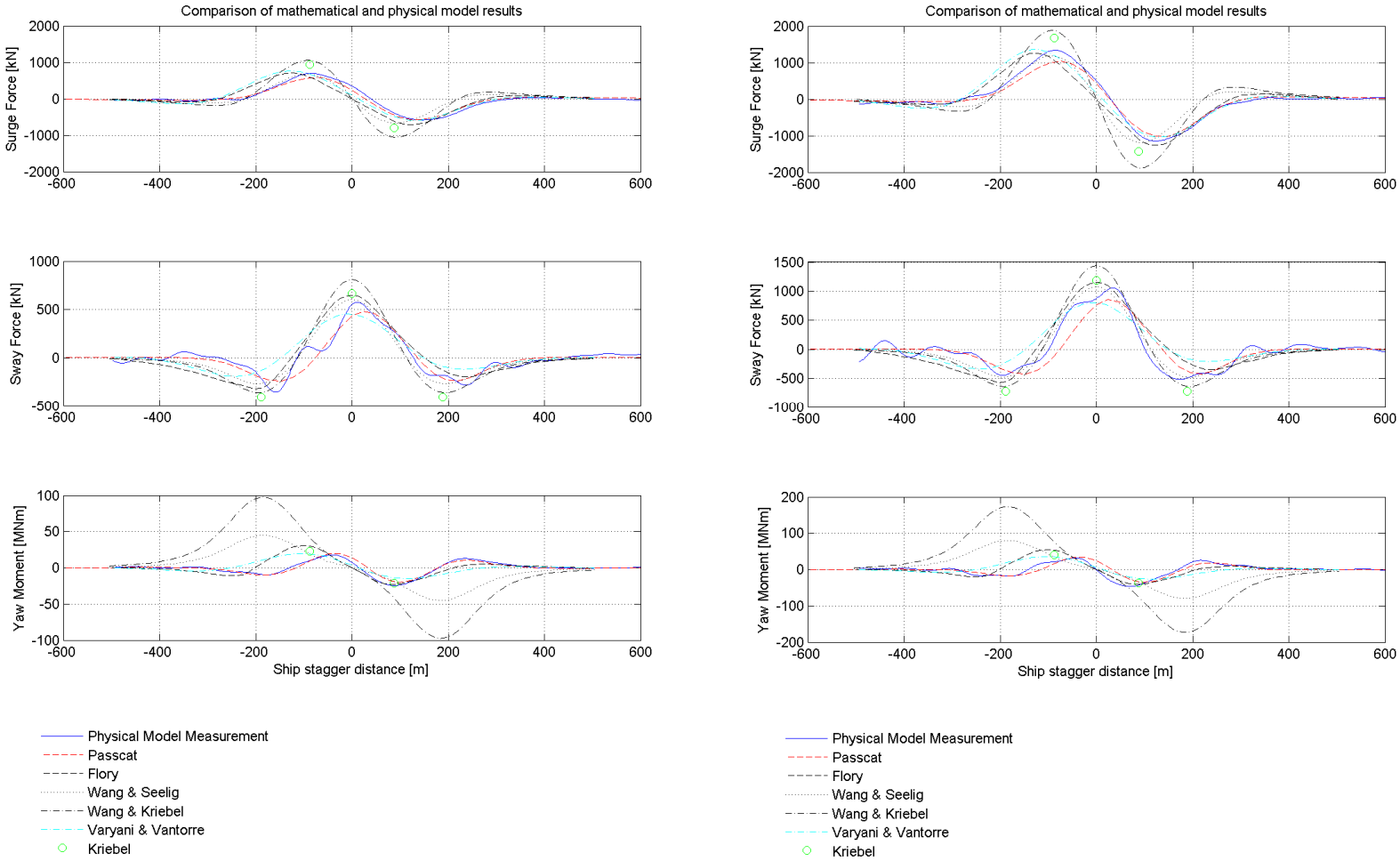


Figure 6: Comparison of test 15 (left) and test 16 (right) physical model measurements and mathematical model calculations

Appendix E: Comparison of mathematical and physical models

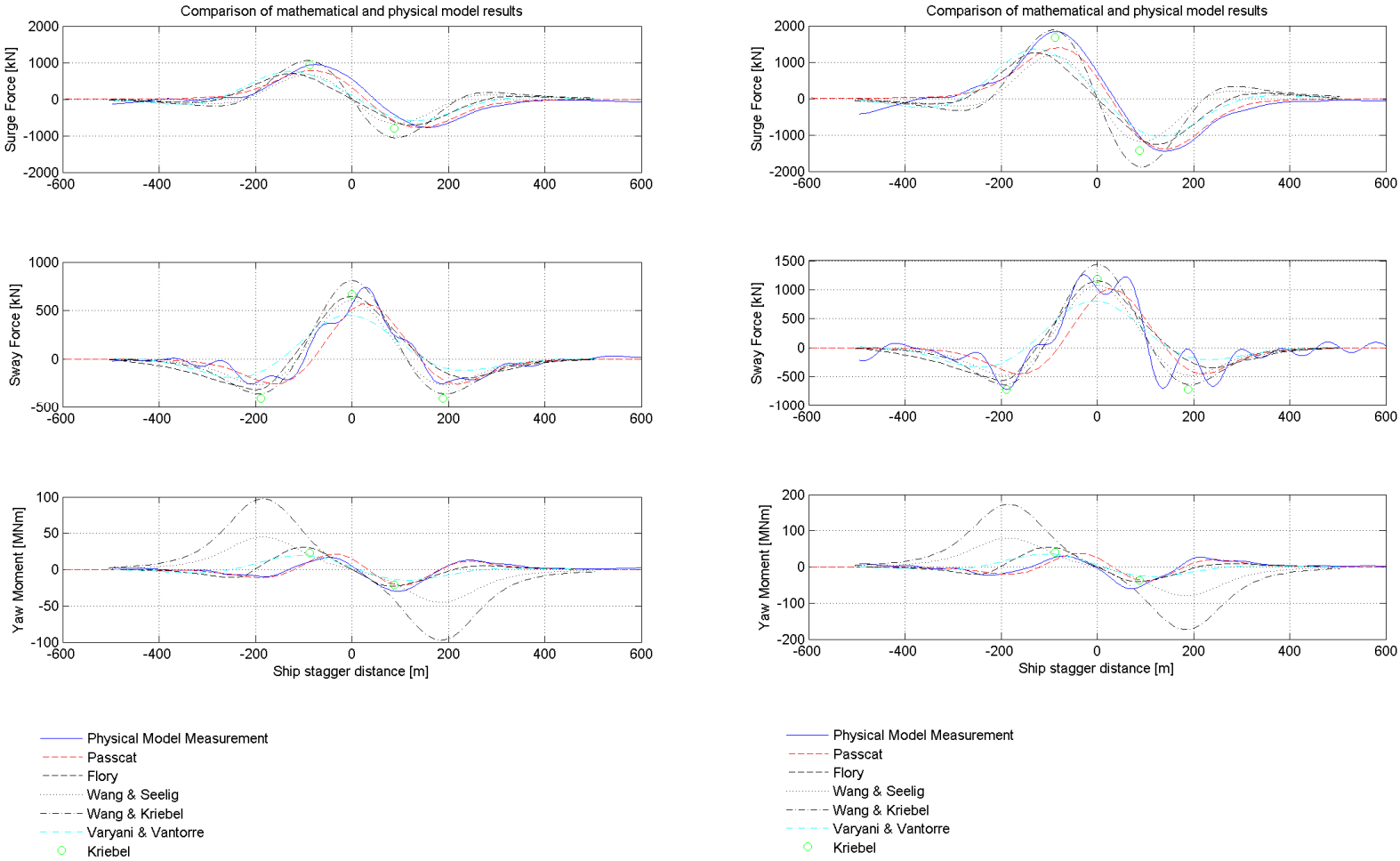


Figure 7: Comparison of test 17 (left) and test 18 (right) physical model measurements and mathematical model calculations

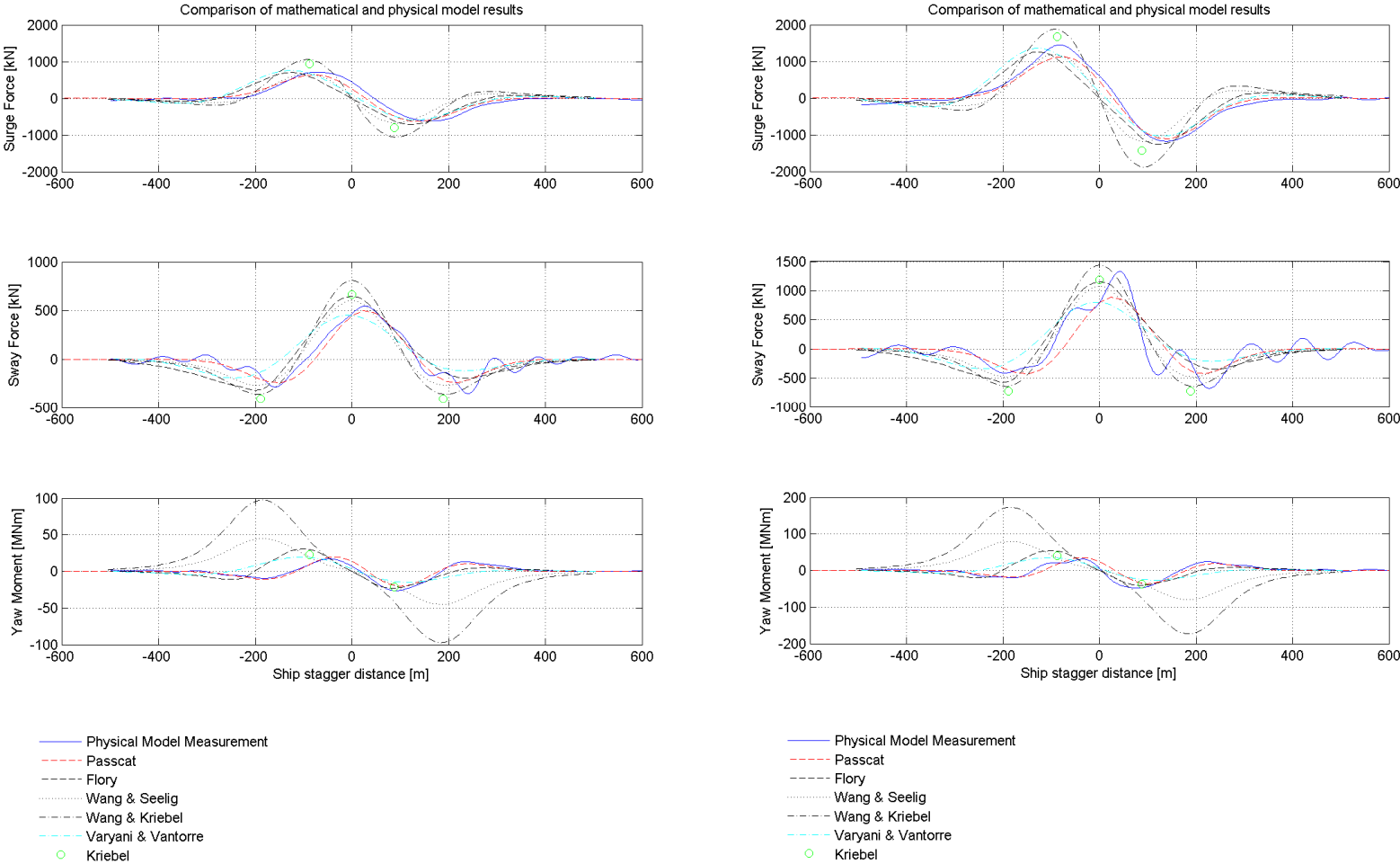


Figure 8: Comparison of test 19 (left) and test 20 (right) physical model measurements and mathematical model calculations

Appendix E: Comparison of mathematical and physical models

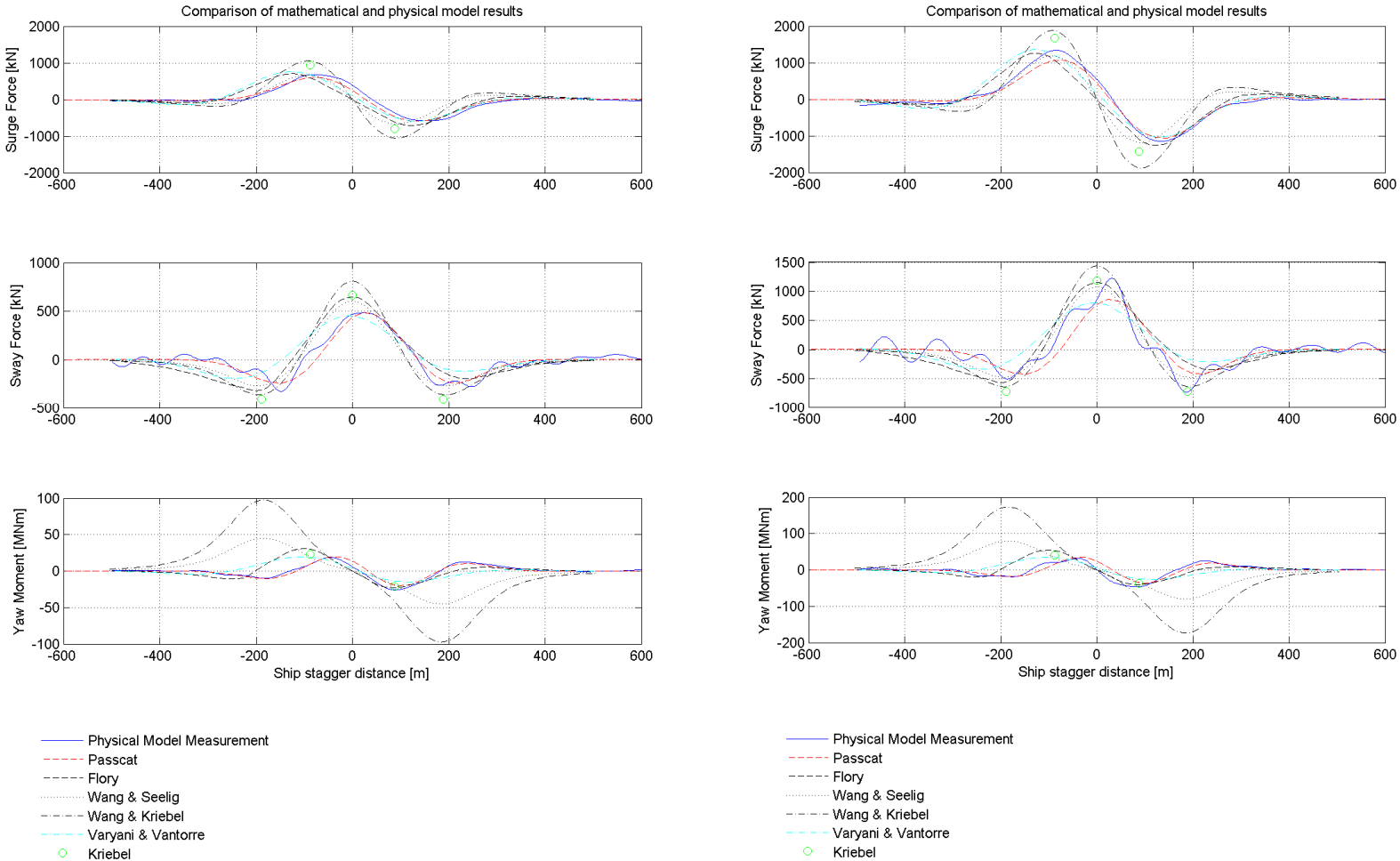


Figure 9: Comparison of test 21 (left) and test 22 (right) physical model measurements and mathematical model calculations

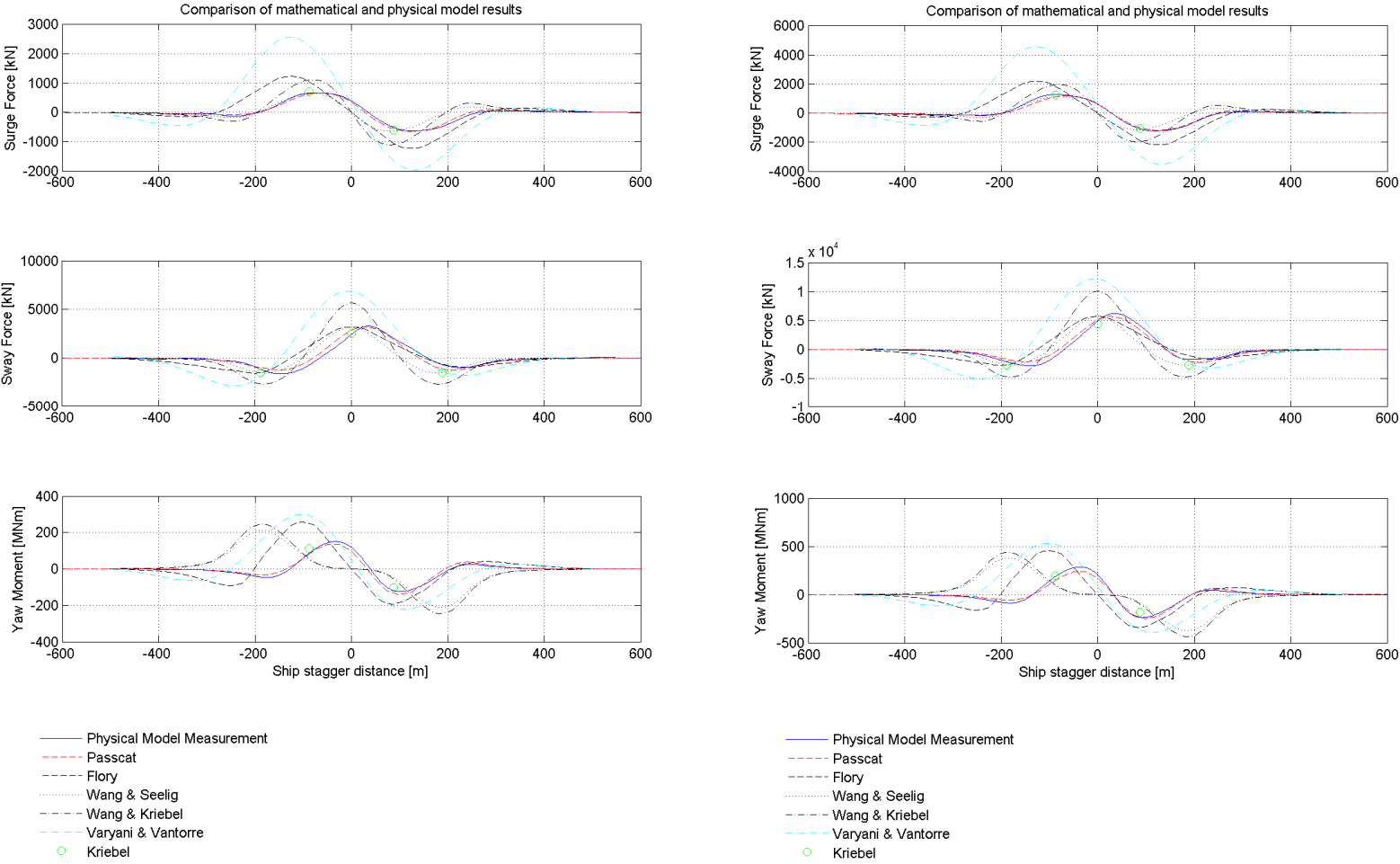


Figure 10: Comparison of test 23 (left) and test 24 (right) physical model measurements and mathematical model calculations

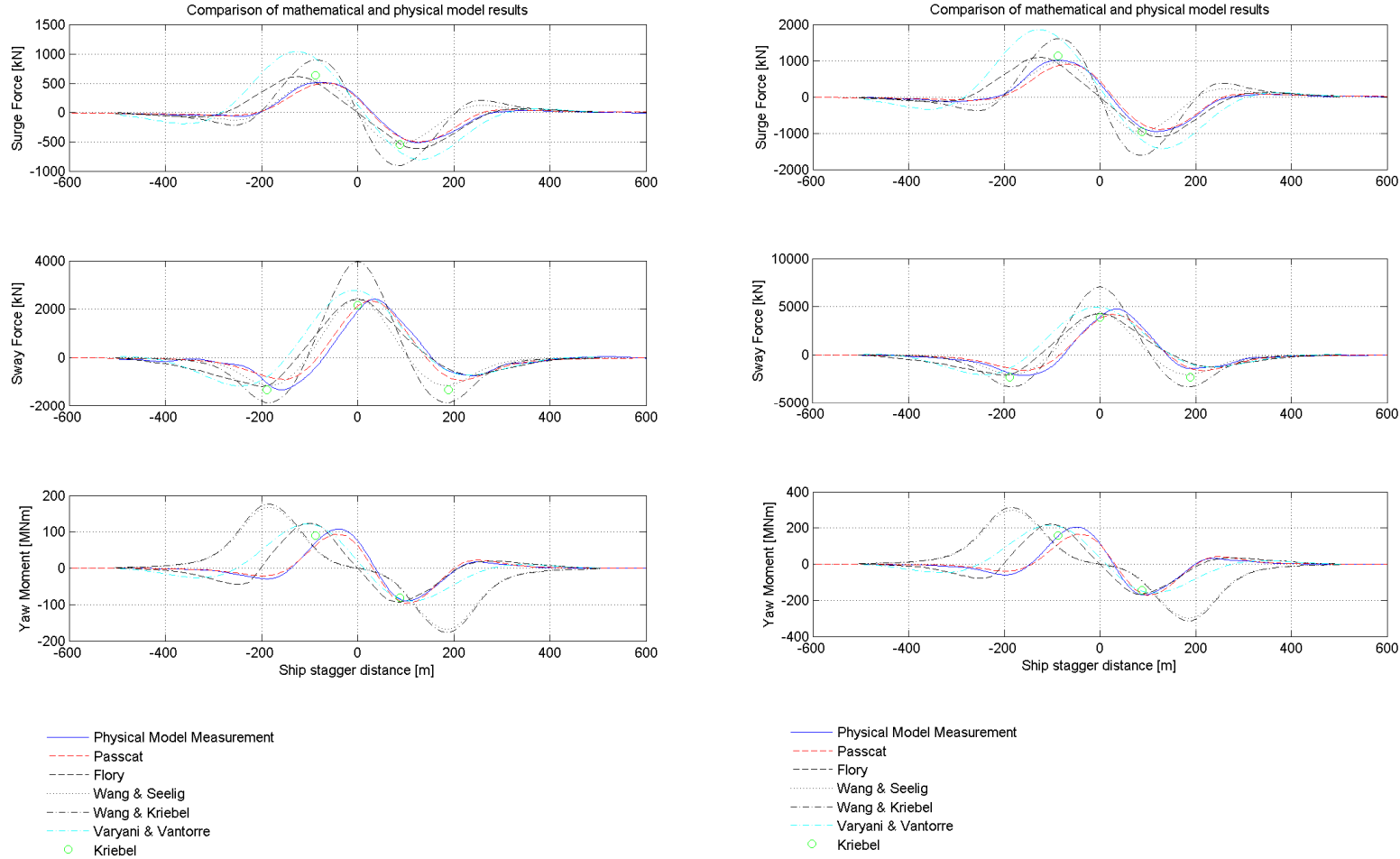


Figure 11: Comparison of test 25 (left) and test 26 (right) physical model measurements and mathematical model calculations

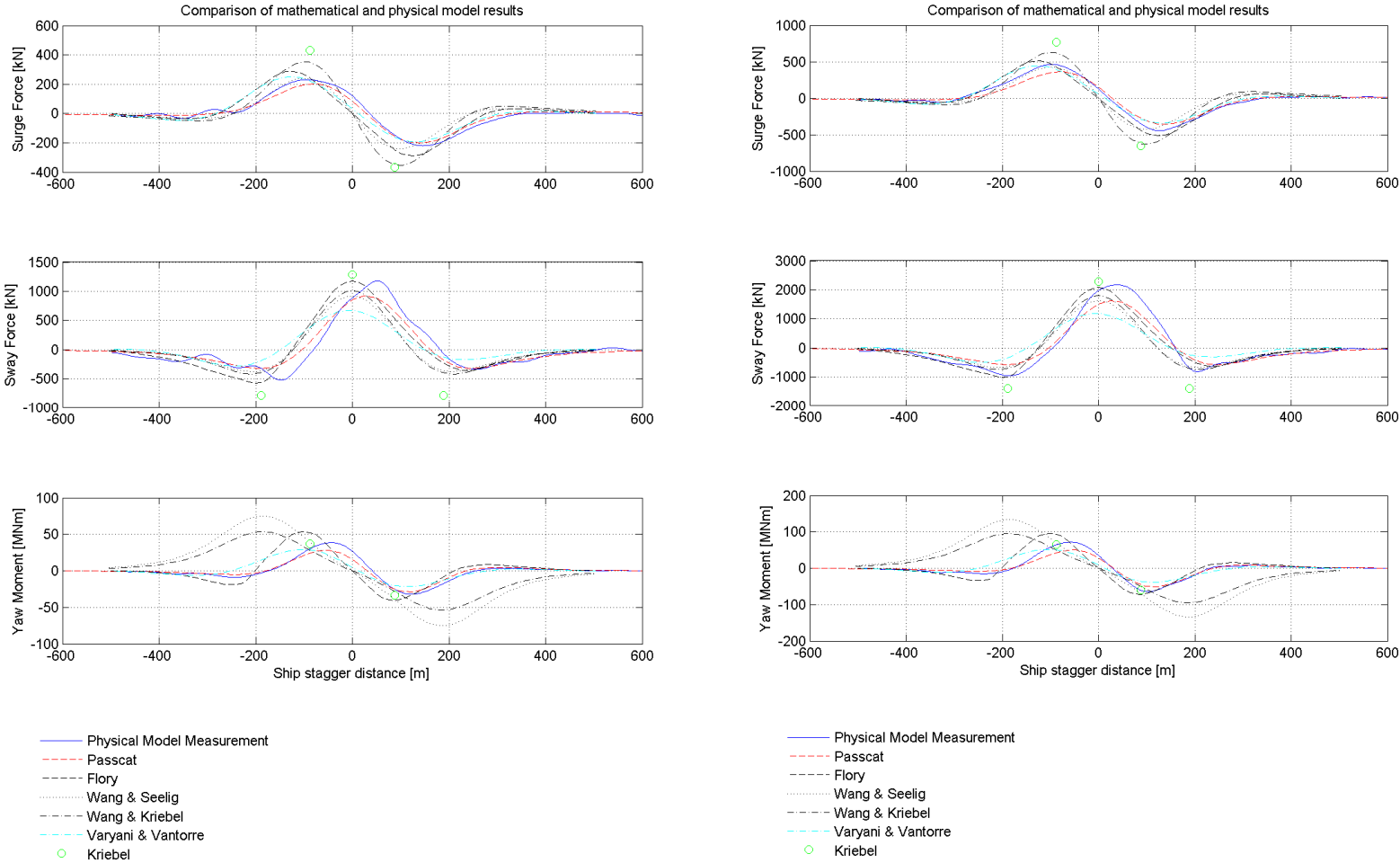


Figure 12: Comparison of test 27 (left) and test 28 (right) physical model measurements and mathematical model calculations

Appendix E: Comparison of mathematical and physical models

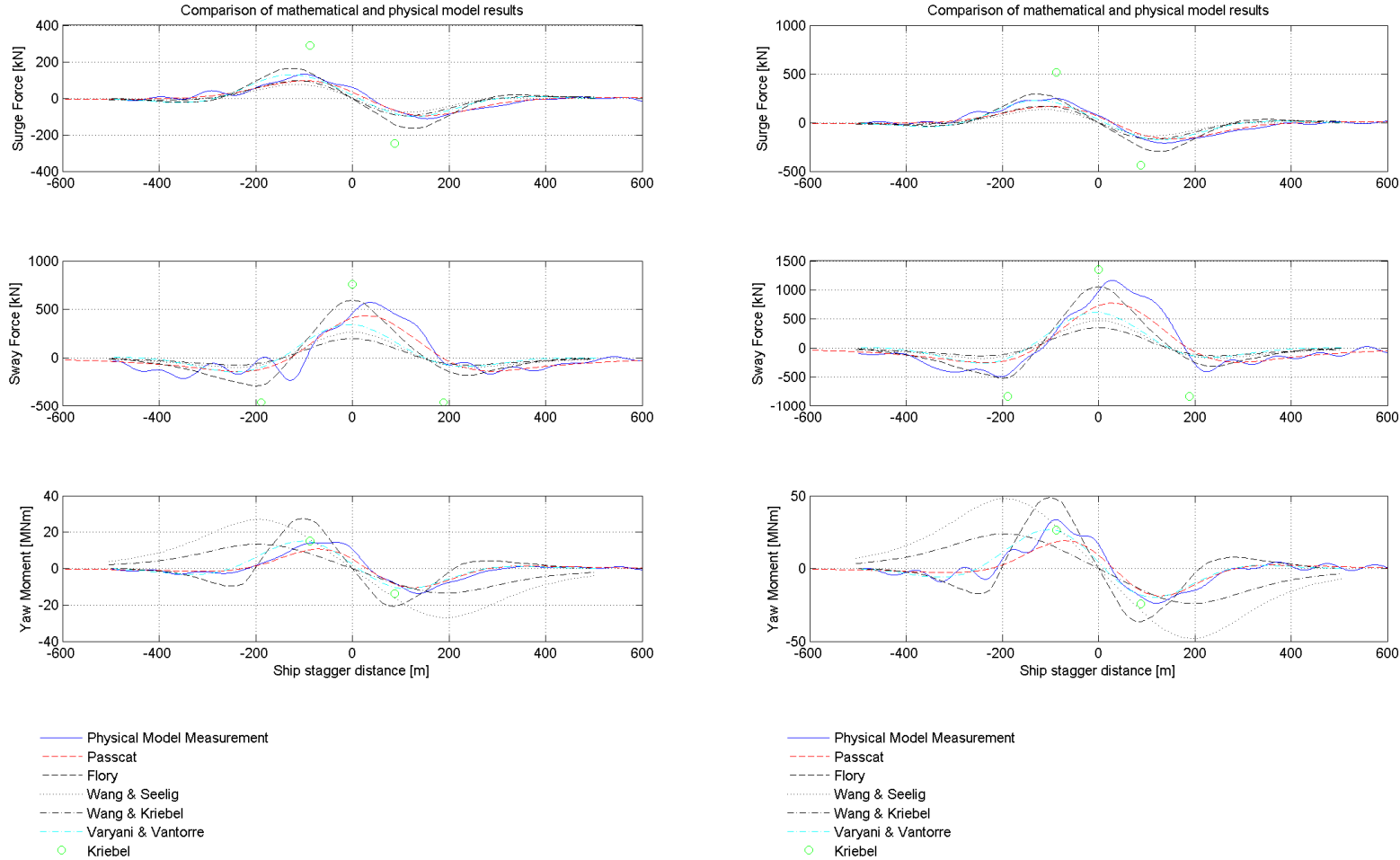


Figure 13: Comparison of test 29 (left) and test 30 (right) physical model measurements and mathematical model calculations

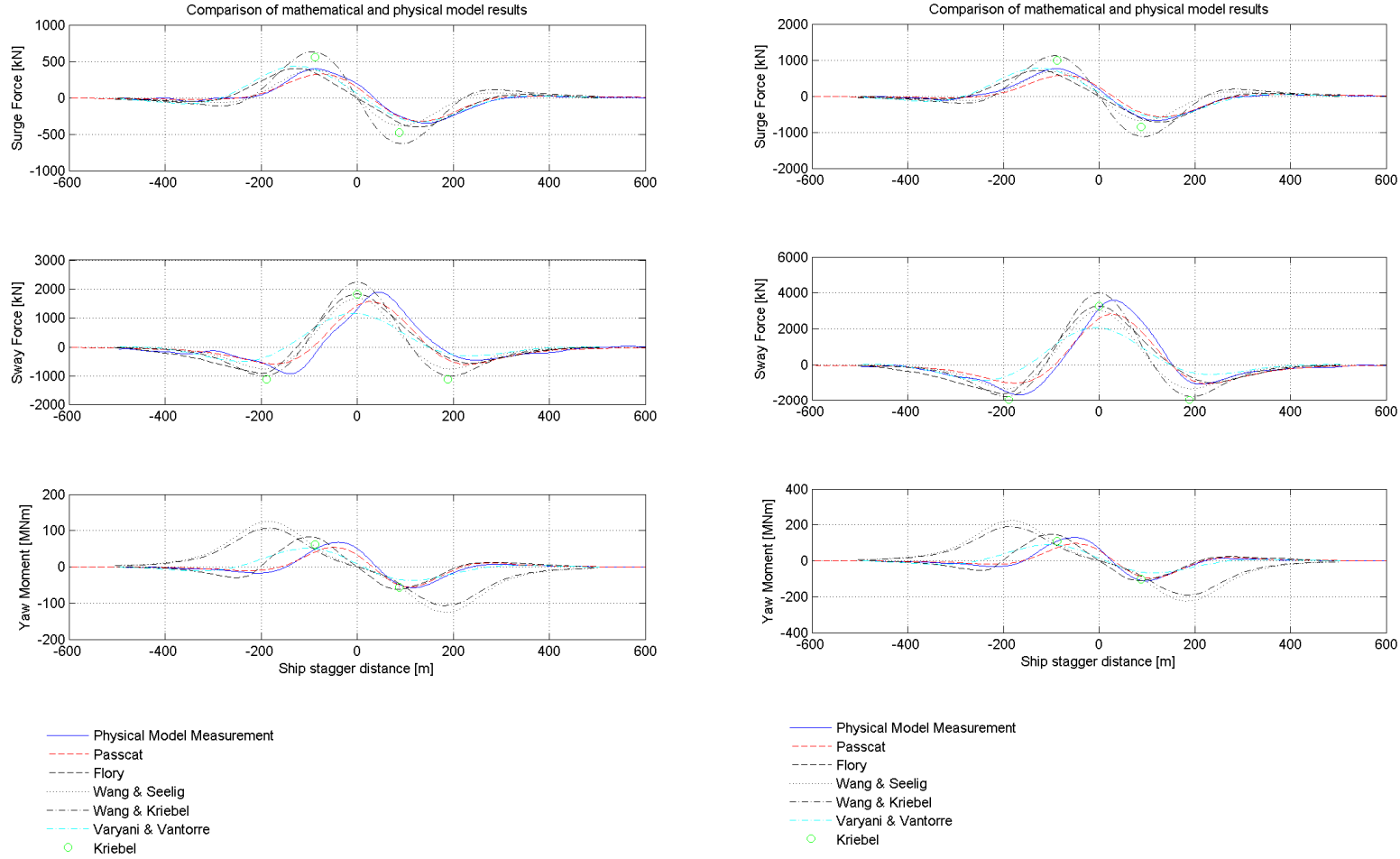


Figure 14: Comparison of test 31 (left) and test 32 (right) physical model measurements and mathematical model calculations

Appendix E: Comparison of mathematical and physical models

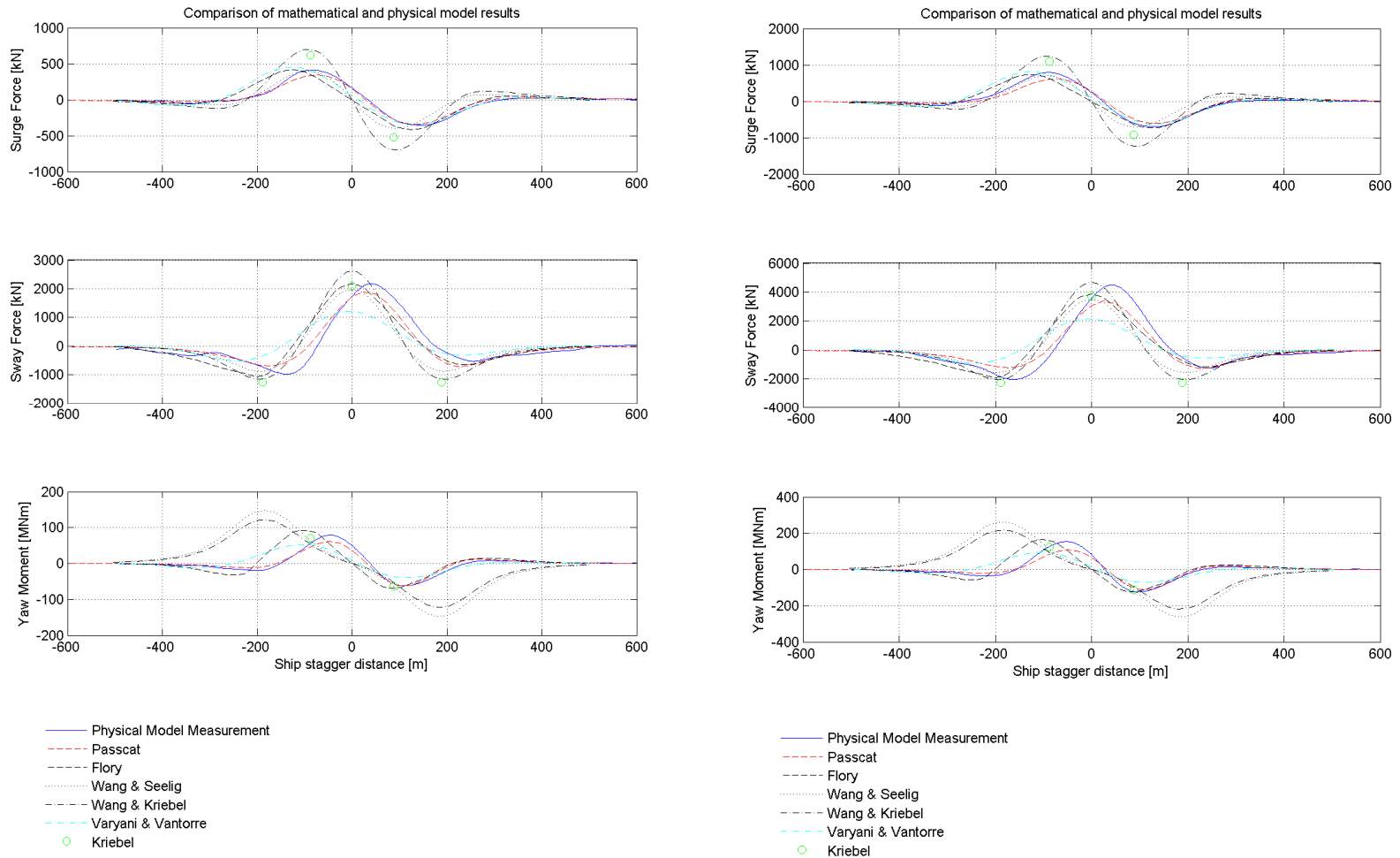


Figure 15: Comparison of test 33 (left) and test 34 (right) physical model measurements and mathematical model calculations

Appendix E: Comparison of mathematical and physical models

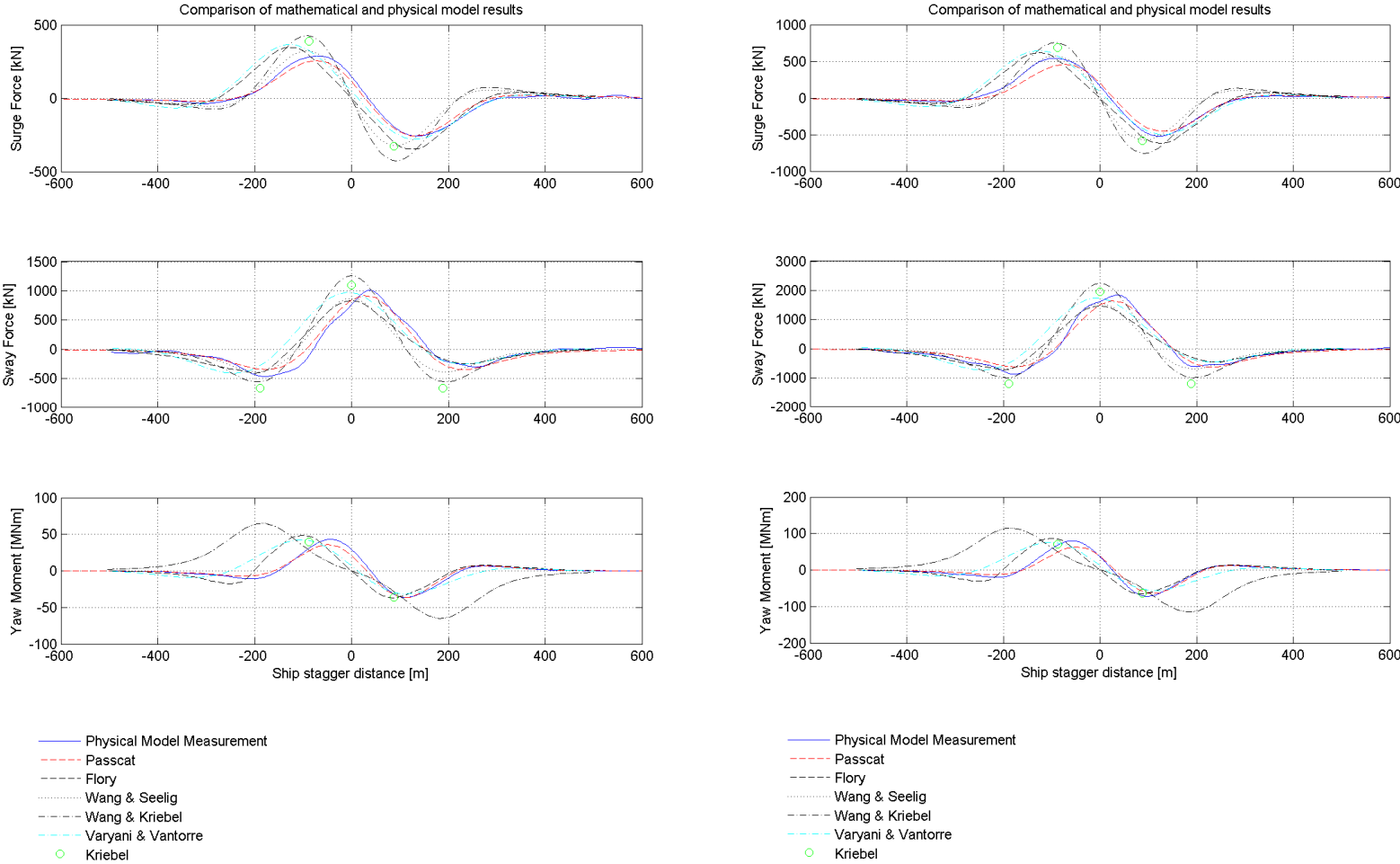


Figure 16: Comparison of test 35 (left) and test 36 (right) physical model measurements and mathematical model calculations

Appendix E: Comparison of mathematical and physical models

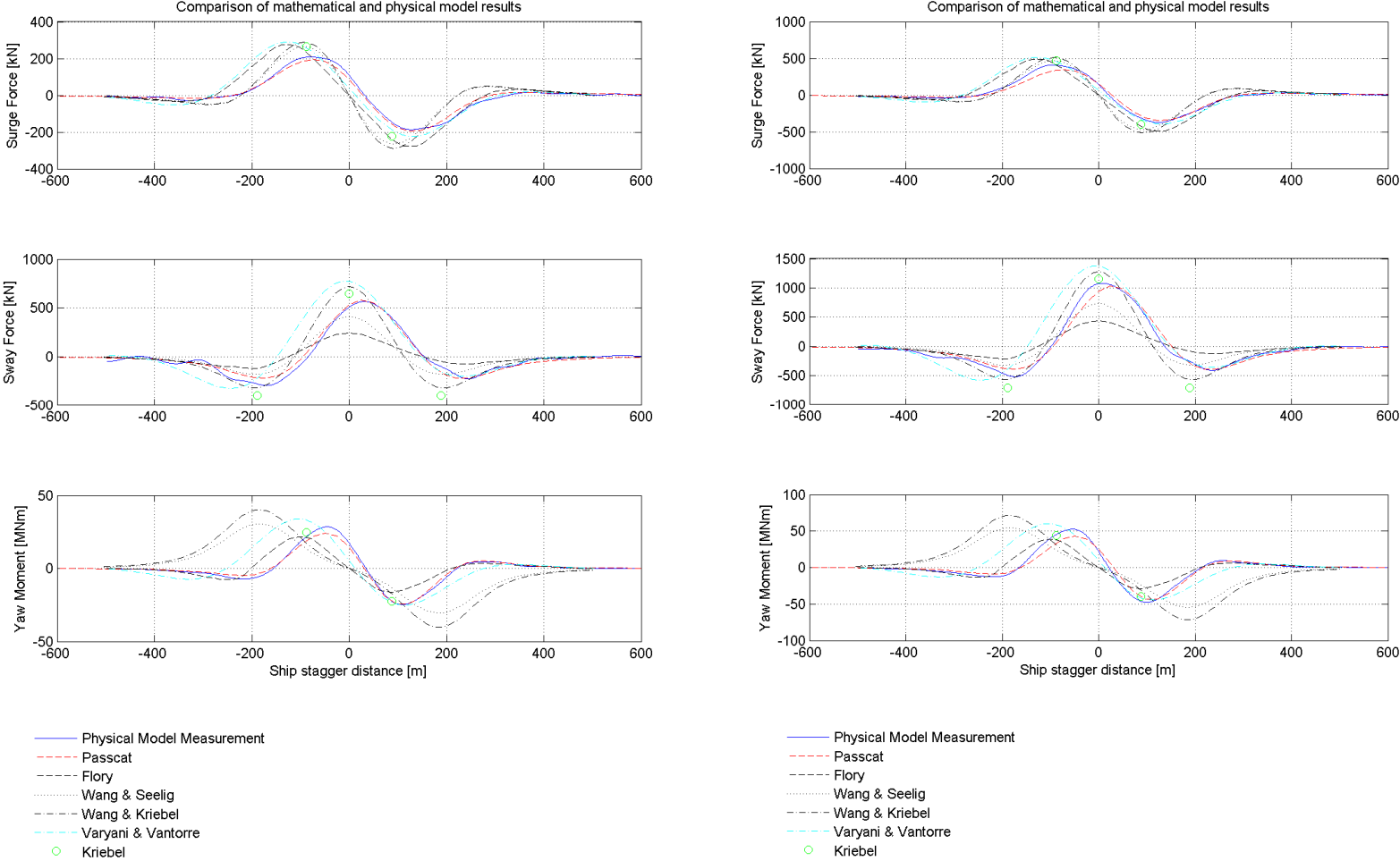


Figure 17: Comparison of test 37 (left) and test 38 (right) physical model measurements and mathematical model calculations

Appendix E: Comparison of mathematical and physical models

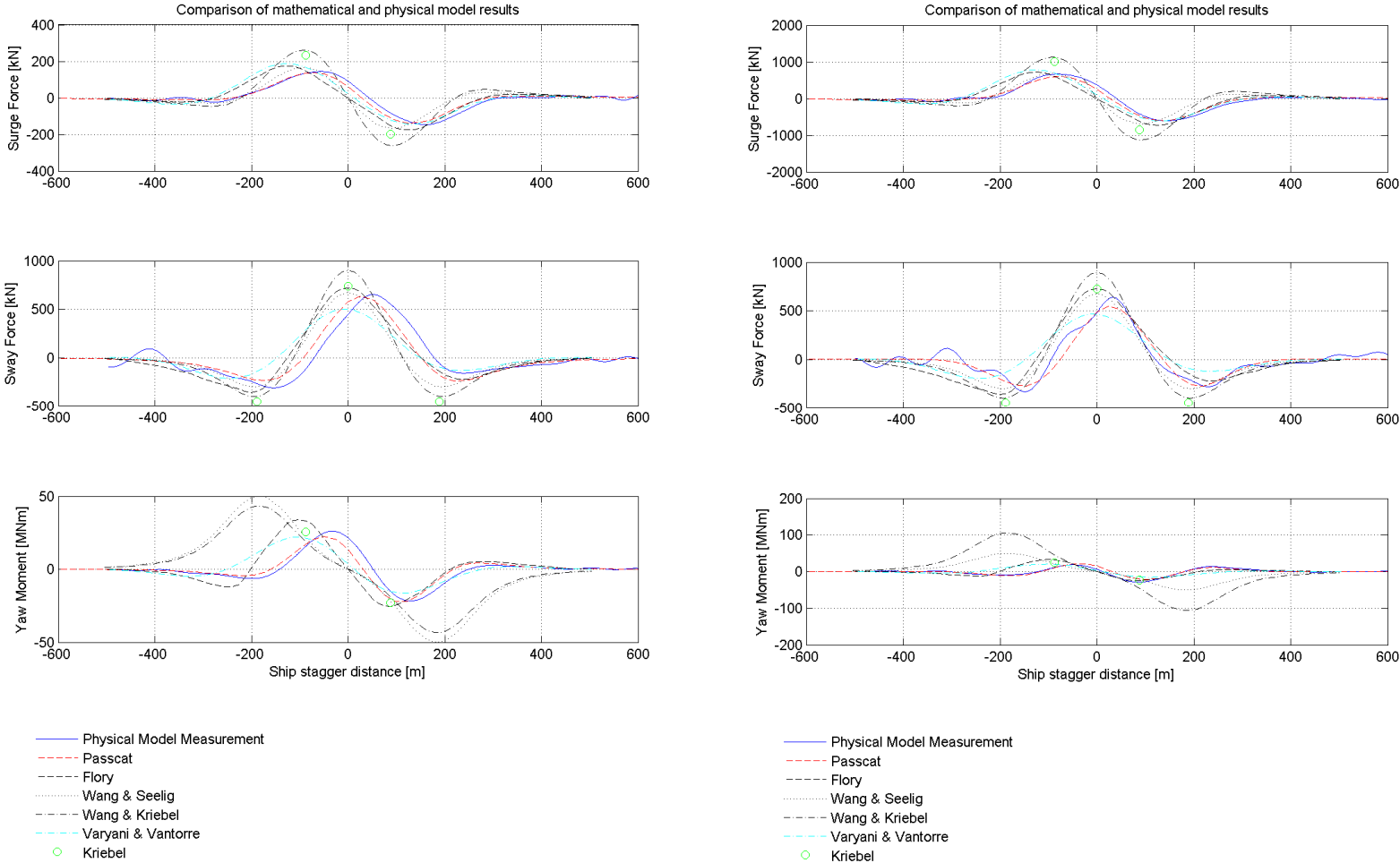


Figure 18: Comparison of test 39 (left) and test 40 (right) physical model measurements and mathematical model calculations

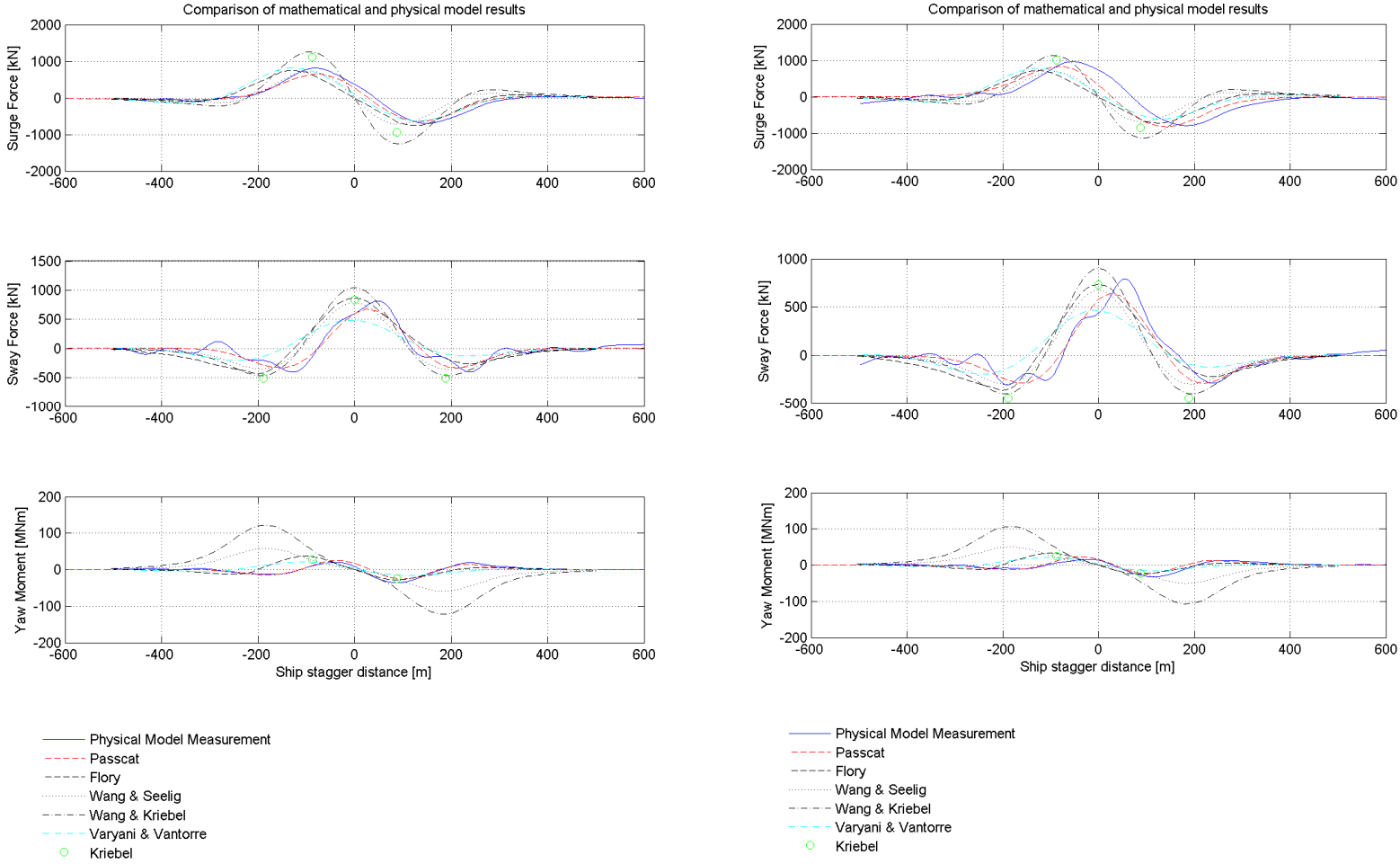


Figure 19: Comparison of test 41 (left) and test 42 (right) physical model measurements and mathematical model calculations

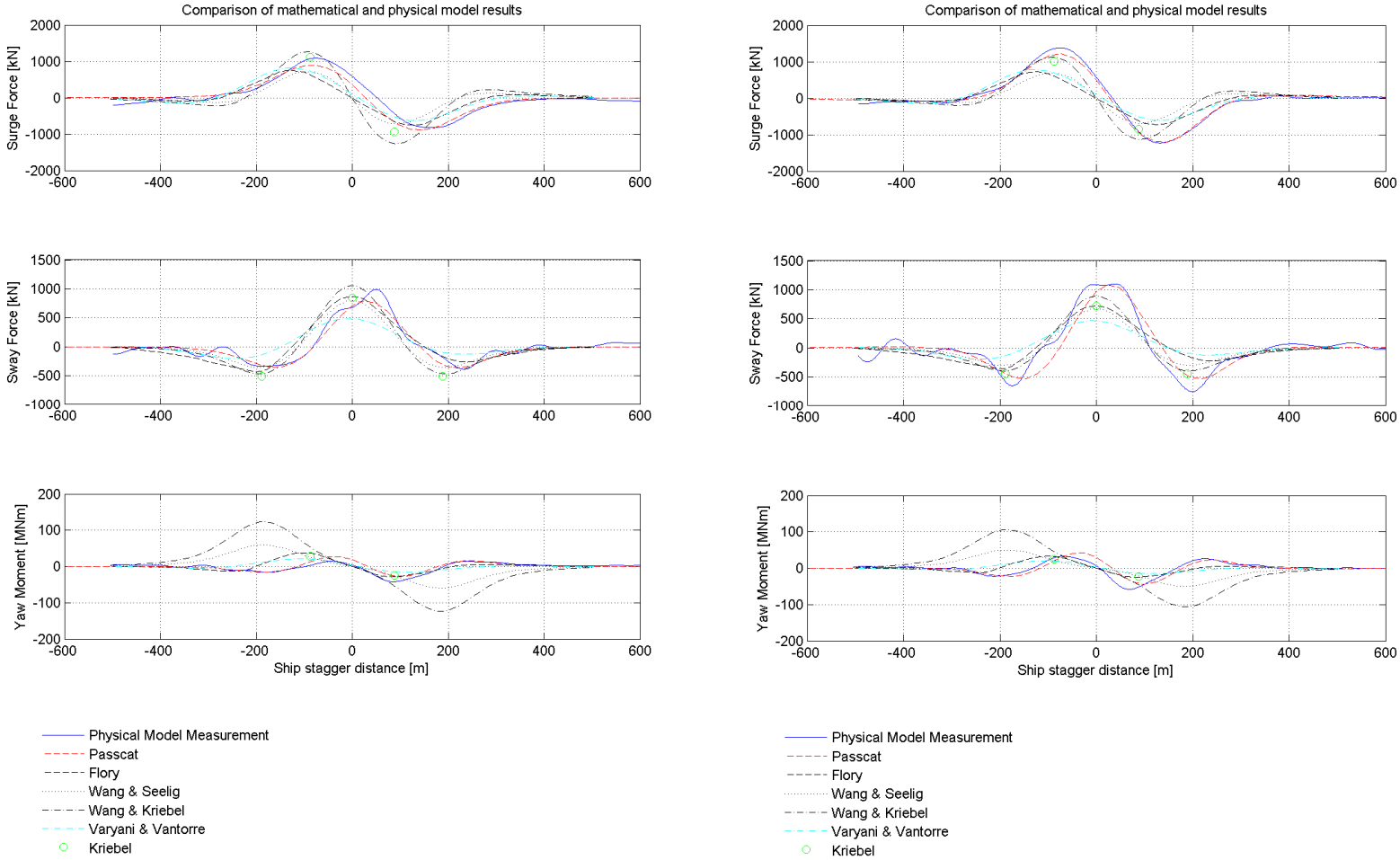


Figure 20: Comparison of test 43 (left) and test 44 (right) physical model measurements and mathematical model calculations

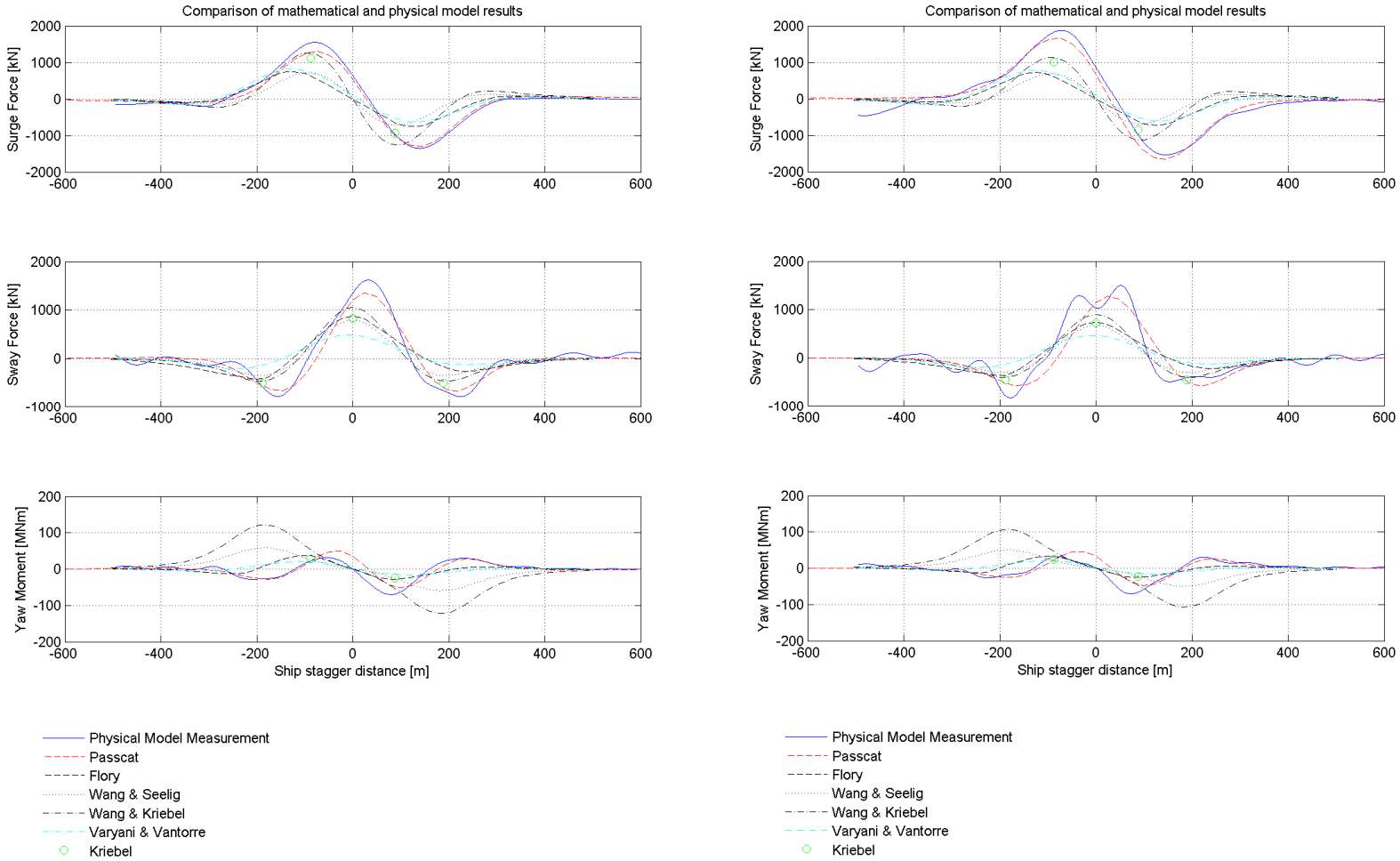


Figure 21: Comparison of test 45 (left) and test 46 (right) physical model measurements and mathematical model calculations

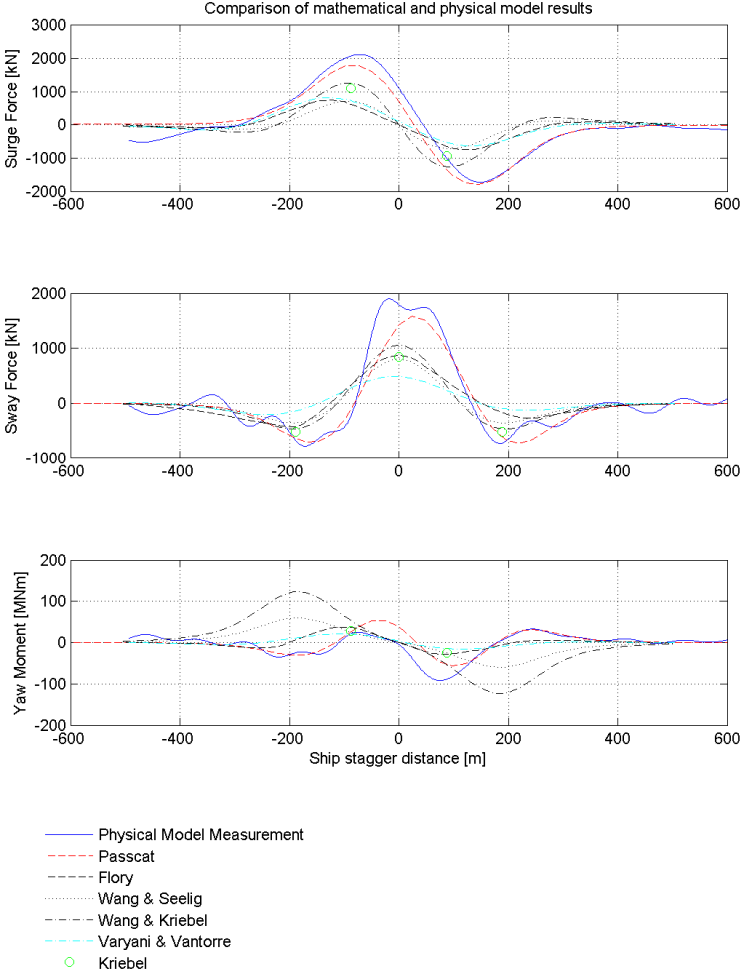


Figure 22: Comparison of test 47 (left)

Appendix F: Conference Paper

APPENDIX F: CONFERENCE PAPER

2nd International Conference on Ship Manoeuvring in Shallow and Confined Water: Ship to Ship Interaction

May 18 - 20, 2011,
Trondheim, Norway

Conference
Proceedings

CALCULATION OF FORCES ON MOORED SHIPS DUE TO PASSING SHIPS

W van der Molen and J Moes, CSIR, South Africa

P B Swiegers, WSP Africa, South Africa

M Vantorre, Ghent University, Belgium

SUMMARY

Ships moored along channels in ports experience forces due to ships passing in the channel, which can lead to breaking of mooring lines or excessive ship motions. A numerical model to predict these passing ship effects is described in this paper. The model, which is based on boundary-integral equations, is validated against model tests for a container ship passing a bulk carrier. The results focus on the effect of quay and channel walls on the forces on the moored ship, and on the non-linear effects of the forces at high (but subcritical) passing speeds.

1. INTRODUCTION

Ships sailing in a fairway or a confined channel generate a disturbance that interacts with ships moored alongside the waterway. This can lead to breaking of mooring lines or delays in the loading process due to ship motions. A good understanding of the phenomenon is essential to provide sufficient passing distance in the design of new terminals and waterways, and to provide operational regulations with respect to speed limits and minimum passing distances.

Physical model tests were carried by Remery [1] and Muga & Fang (1975) [2] on VLCC tankers in open water. These results were used by Seelig [3] and Flory [4] to provide empirical relationships for the maximum forces due to a passing ship. Vantorre et al. [5] used data from an extensive model test program on a bulk carrier, a container ship and two tankers to derive similar empirical relationships. More model test data on two tankers are available from Lataire et al. [6]. These empirical relations can be used to obtain quick estimates in early design phases. However, the formulae are very generic with respect to hull shapes and the effect of other structures and a bottom topography are not included.

Besides the growing number of physical model data, advances were also made in the numerical modelling of passing ship effects. These models can be used in further design stages. Pinkster [7] has developed a panel model to calculate the disturbance due to a passing ship including free surface effects, such as the generation of oscillations in partly enclosed basins alongside the channel. Huang & Chen [8] have developed a RANS model to calculate the flow in arbitrarily shaped channels and basins, which provides accurate results but is difficult to set up and requires long computation times.

The panel model presented in this paper is relatively straightforward to set up and run, and can be applied for open jetties, quay walls and confined channels. The model is validated against physical model tests for these three situations and for different passing speeds.

2. MODEL DESCRIPTION

The model to determine the flow around a passing ship and the forces on a moored ship is a 3D potential flow model. The model is based on the double-body flow assumption with restricted water depth, similar to Korsmeyer et al. [9] and the double-body model of Pinkster [7]. However, a few terms relative to the depth-related Froude number have been added to make the results more accurate at higher passing speeds. The double-body flow assumption implies that water level fluctuations can be computed, but the flow pattern is not affected by these fluctuations. Hence, inertia effects of the changing flow pattern are neglected and the flow is calculated for a horizontal free surface. This assumption also implies that the computation focuses on the disturbance due to the primary return flow due to the passing ship. Shorter so-called wash waves are neglected. Wash waves become important at near-critical or supercritical speeds, such as for high-speed ferries (Van der Molen et al. [10]). For simplicity, the case, as shown in Figure 1, is considered here where the passing ship travels parallel to the moored ship at a constant speed and without the effect of an ambient current.

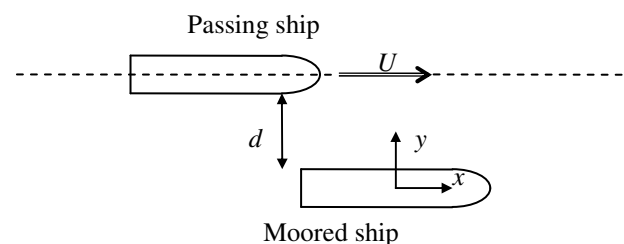


Figure 1: Definition sketch for a ship passing the moored ship in the same direction with speed U at distance d .

The fluid is considered incompressible, irrotational and homogeneous with a density ρ . The model domain \mathcal{D} is bounded by the body surfaces \mathcal{H}_P and \mathcal{H}_M of the passing ship and the moored ship respectively, the surface of any nearby structures \mathcal{W} , the fluid surface \mathcal{F} and the sea bed \mathcal{B} . The sea bed may have an arbitrary bathymetry above an ambient horizontal sea bed with a water depth h . The wetted surface of all bodies (\mathcal{H}_P , \mathcal{H}_M , \mathcal{W} and \mathcal{B}) is denoted as \mathcal{S} . The coordinate system $Oxyz$ is a right-

handed system with the origin at the still water level, the x -axis in the passing direction and the z -axis positive upwards.

The fluid flow around the bodies due to the steady forward speed U of the passing ship is described by means of a velocity potential ϕ , which is defined such that the gradient of ϕ is equal to the flow velocity. The velocity potential has to meet the following conditions:

$$\nabla^2 \phi = F_h^2 \phi_{xx}, \quad (1)$$

$$\phi_n = Un_x \text{ on } \mathcal{H}_p, \quad (2)$$

$$\phi_n = 0 \text{ on } \mathcal{H}_M, \mathcal{B} \text{ and } \mathcal{W}, \quad (3)$$

$$\phi_z = 0 \text{ on } z = 0 \text{ and } z = -h, \quad (4)$$

$$\phi = 0 \text{ for } R \rightarrow \infty, \quad (5)$$

where $F_h = U/\sqrt{gh}$ is the depth-related Froude number (g is the acceleration of gravity), \vec{n} is the unit normal vector directed out of the fluid domain and R is a horizontal distance. The subscripts denote partial derivatives. The Laplace equation (Eq. 1) has been modified to account for deformations of the free surface due to the flow around the passing ship in a similar manner as in slender body, shallow water theory (see e.g. Tuck [11] and Gourlay [12]).

The velocity potentials are solved using a boundary-integral equation method based on the source potential formulation:

$$\phi(\vec{x}) = \iint_S G(\vec{x}, \vec{\xi}) \sigma(\vec{\xi}) dS_{\xi}. \quad (6)$$

The source strengths σ follow from the integral equation:

$$2\pi A \sigma(\vec{x}) + \int_S G_{n_x}(\vec{x}, \vec{\xi}) \sigma(\vec{\xi}) dS_{\xi} = \begin{cases} Un_x \text{ on } \mathcal{H}_p \\ 0 \text{ elsewhere.} \end{cases} \quad (7)$$

The right-hand side of this equation denotes the boundary condition on the body surface. A is a parameter (close to 1) which accounts for the modification of the Laplace equation (Eq. 1) and the subsequent modification of the Green function $G(\vec{x}, \vec{\xi})$, which is the potential in \vec{x} due to a unit source in $\vec{\xi}$ with a constant source strength:

$$G = \frac{1}{r'} + \frac{1}{r_2'} + 2 \int_0^{\infty} \frac{e^{-kh}}{\sinh kh} \cosh k(z+h) \cosh k(\zeta+h) J_0(kR') dk \quad (8)$$

where $r' = \sqrt{[(x-\xi)^2/(1-F_h^2)] + (y-\eta)^2 + (z-\zeta)^2}$ is the modified radial distance between (x,y,z) and (ξ,η,ζ) , r_2' is the modified radial distance to the image source below the bottom and R' is the modified horizontal distance. This Green function is the zero-frequency limit of the free surface Green function. The Green function and its

derivatives are computed using algorithms described in Newman [13]. For $R/h < 1/2$ the integral is expressed by the contribution of an array of Rankine image sources above the free surface and below the sea floor. For larger R/h the Green function is approximated by a Fourier series in terms of modified Bessel functions. The determination of A is given in the Appendix.

The source strengths are solved numerically by discretising the mean wetted body surfaces with a large number of quadrilateral or triangular panels with the collocation points of the source strengths at the panel centroids. The velocity potentials are computed for subsequent positions of the passing ship as it passes the moored ship. In this process, it is assumed that the changes of the flow pattern are slow, so that for each time step the flow can be considered as a steady-state solution.

The fluid pressure p due to the passing ship can be determined based on Bernoulli's equation:

$$p = -\rho U \frac{\partial \phi}{\partial X_p} - \frac{1}{2} \rho |\nabla \phi|^2, \quad (9)$$

which is given here in terms of the potentials ϕ and the position of the passing ship X_p . The first term refers to the (almost hydrostatic) pressures in the primary wave generated by the passing ship. The second term refers to the pressure reduction due the flow velocity squared. The derivatives with respect to X_p in the first term are evaluated after the potentials have been determined for all passing ship positions using a polynomial approximation of the potentials with respect to the passing ship position. The fluid velocities $\nabla \phi$ are easily evaluated using the gradients of the Green function in Eq. 6. The force \vec{F} and moment \vec{M} on the moored ship is obtained by integration of the pressures over the submerged hull:

$$\vec{F} = \iint_{\mathcal{H}_M} p \vec{n} dS, \quad (10)$$

$$\vec{M} = \iint_{\mathcal{H}_M} p(\vec{x} - \vec{x}_G) \times \vec{n} dS, \quad (11)$$

where x_G is the position of the centre of gravity. These forces can be input in a moored ship response model to determine the motions of the moored ship and the forces in mooring lines.

3. PHYSICAL MODEL TESTS

3.1 TEST SET-UP

Model tests were conducted in a large basin of 55 m by 36 m at the Hydraulics Laboratory of the CSIR in Stellenbosch, South Africa. The passing ship was towed along a straight track parallel to the moored ship. The passing ship was connected to a trolley rolling over a long rail. The wheels on one side of the rail are

transversely fixed. Two hollow vertical pipes are mounted on the trolley. These pipes guide two vertical rods that are able to slide inside the pipes and are connected to the deck of the passing ship. With this set-up the ship is firmly fixed to the trolley in the horizontal directions, while it is able to move freely in heave and pitch. A rope is connected to the trolley. The speed is regulated by an electromotor and set at a specified constant speed for each test.

The moored ship is firmly connected to the wharf with a fixed force frame. The forces in the force frame are measured with three force transducers aligned such to measure the horizontal forces and moment on the ship in surge, sway and yaw. The force transducers are connected to the ship with thin rods. This allows the force transducers to measure both compression and tension forces, while the ship is free to move in heave, roll and pitch.

3.2 SHIPS

The tests were conducted for a Post-Panamax container ship as the passing ship and a Panamax bulk carrier as the moored ship at a scale of 1:100. Both ships were fully laden to the same draught. The main ship dimensions are given in Table 1.

Table 1: Ship dimensions

Ship type			Container	Bulk
Position			Passing	Moored
Length betw. perps.	L	m	260.0	243.4
Breadth	B	m	40.0	32.0
Draught	T	m	14.0	14.0
Displacement	Δ	m ³	85 989	90 412
CoB forw. midship	LCB	m	-6.7	5.5



Figure 2: Model test set-up with the passing container ship in the rail and the moored bulk carrier in the force frame along a straight quay wall.

3.3 TEST CONDITIONS

The tests were carried out for the container ship passing the bulk carrier in parallel but opposite directions along

port side of both ships, as shown in Figure 2. The tests were done (among others) for different passing speeds between 4 kn and 14 kn in open water, for a ship moored at a quay wall and for a ship passing in a confined channel. The quay wall was inserted as a long straight wall leaving a gap of 4 m between the wall and the moored ship. Another wall was added to create a 192 m wide channel. The tests were conducted on a horizontal floor with a water depth of 16.8 m, for a depth-to-draught ratio of 1.2. The passing distance is 64 m, defined as the board-to-board distance between the two ships.

4. VALIDATION RESULTS

The numerical model was validated against the results of the physical model tests. The hulls of the ships were discretised in the model by 1464 panels for the container ship and 1430 panels for the bulk carrier, as shown in Figure 3. The basin was sufficiently large to neglect the effects of the basin boundaries. The quay wall and the channel walls were modelled as long arrays of panels, measuring 8.3 m by 8.4 m away from the moored ship and 8.3 m by 5.6 m in the gap between the moored ship and the quay. The flat bottom is represented in the formulation of the Green function (Eq. 8).

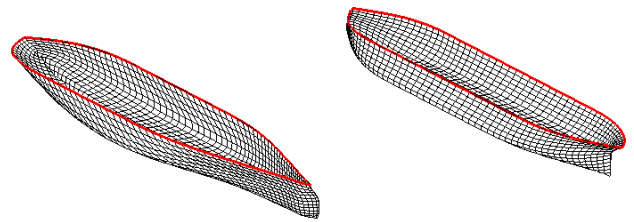


Figure 3: Panel descriptions of the container ship (left) and the bulk carrier (right).

The time series of the forces on the moored ship, for the ship passing with a speed of 6 kn in open water, along a quay wall and in a channel, are given in Figure 4. The position of the passing ship X_P is given with respect to the position where the ships are side by side. The forces and moment are made non-dimensional with respect to the displacement of the moored ship Δ_M and the depth-related Froude number F_h .

The open water case yields the smallest surge forces, but the largest sway forces and yaw moments. The surge forces are significantly larger in the channel, but they are comparable to the case with only a quay wall for sway and yaw. The correspondence between the measured and calculated results is very good for the open water case. For the case with a channel, the surge forces are slightly underestimated and there is a phase shift in the yaw moment.

The amplitudes of the forces on the moored ship for passing speeds of 4 kn to 14 kn ($F_h = 0.16$ to 0.56) are given in Figure 5. The surge force and yaw moment

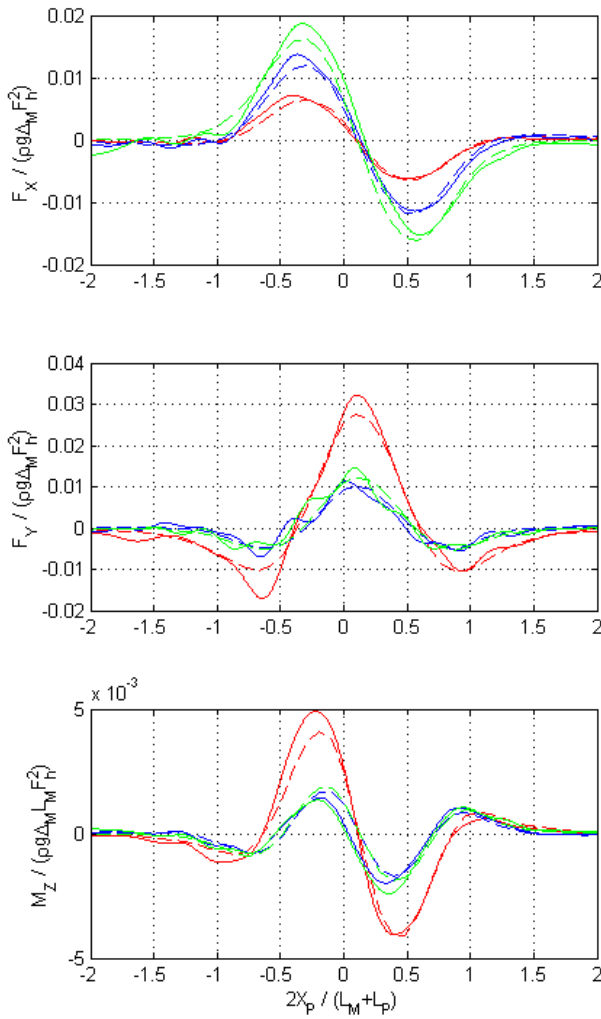


Figure 4: Measured (solid) and calculated (dashed) forces on the moored ship for surge (top), sway (middle) and yaw (bottom) in open water (red), along a quay wall (blue) and in a channel (green) for a ship passing at 6 kn.

amplitudes are defined as the average of the positive and negative extremes, and the sway force amplitude is the maximum positive sway force. Because the plotted forces are divided by the Froude number squared, it is easy to observe that the forces are more than proportional to the passing speed squared. The further increase of the forces is about 50% for a Froude number $F_h = 0.5$. This effect is stronger for larger passing distances (not shown here). However, for low speeds the assumption that the forces are proportional to the passing speed squared is valid.

The nonlinear effect of the forces for high speeds is also observed in the calculated results, albeit not as strongly as for the measured forces and only significantly for surge. Some nonlinear effects were not considered, such as more confined flows underneath the passing ship due to squat. Another possible explanation for the differences at higher speeds is the neglect of turbulence and viscous effects in the numerical model, which is based on

potential flow theory. E.g. the flow underneath the

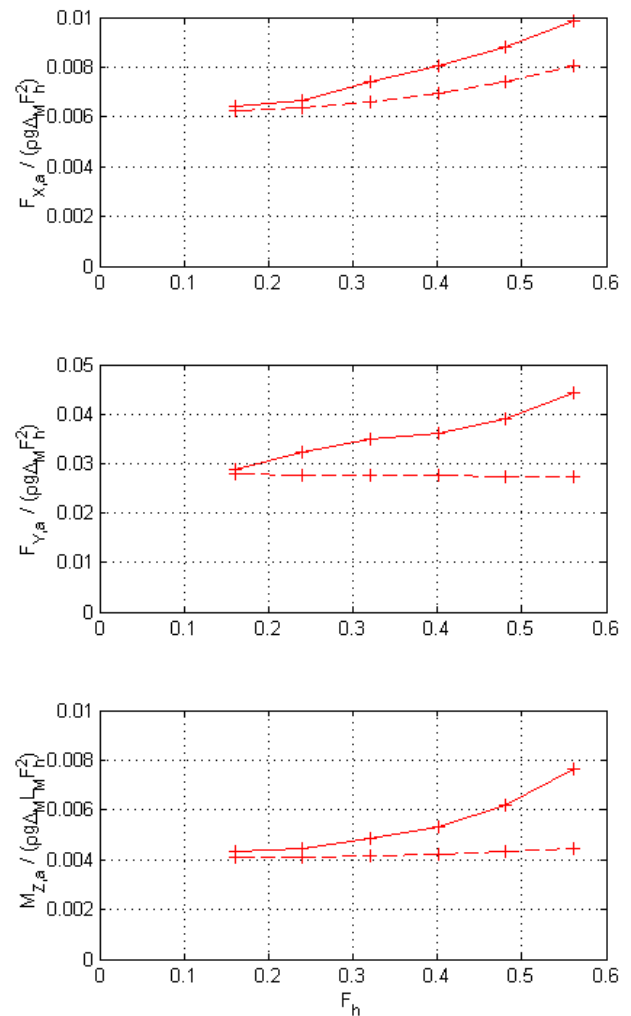


Figure 5: Amplitudes of measured (solid) and calculated (dashed) forces on the moored ship for surge (top), sway (middle) and yaw (bottom) as function of the Froude number.

passing ship will be affected by shear stresses, so that more water is pushed to the sides leading to stronger flows adjacent to the passing ship and around the moored ship. These effects are relatively stronger at higher speeds. This could also partly clarify the differences observed for the ship moored at a quay wall, where the flow in between the ship and the quay experiences friction effects. A different approach of the numerical model, e.g. using a direct diffraction potential formulation instead of the indirect source potential formulation, may lead to improved nonlinear behaviour of the sway forces and yaw moments. This is a subject for further research.

5. CONCLUSIONS

A numerical model has been developed to calculate the forces on a moored ship induced by a passing ship. The model is based on boundary-integral equations which

makes it relatively easy to set up for different types of ships and to include nearby structures and bottom topographies, such as quay walls and channel slopes. The model has been validated against physical model tests. The model provides good results in open water as well as including a quay wall and channel walls. The calculated results show the same nonlinear pattern of the forces on the moored ship at higher speeds as observed in the model test measurements, albeit less strongly and mainly for the surge forces.

The assumption that the forces on a moored ship due to a passing ship are proportional to the passing speed squared is valid for low speeds. However, the forces can be significantly larger for larger Froude numbers. The forces significantly divert from this assumption roughly for a depth related Froude number $F_h > 0.25$.

REFERENCES

1. REMERY, G.F.M., 'Mooring Forces Induced by Passing Ships', OTC Paper 2066, *Offshore Technology Conf.*, Richardson, TX, 1974.
2. MUGA, B.J. and FANG, S.T., 'Passing Ship Effects from Theory and Experiment', OTC Paper 2368, *Offshore Technology Conf.*, Richardson, TX, 1975.
3. SEELIG, W.N., 'Passing Ship Effects on Moored Ships', Technical Report TR-6027-OCN, *Naval Facilities Engineering Command, East Coast Detachment*, Washington, DC, 2001.
4. FLORY, J.F., 'The Effect of Passing Ships on Moored Ships', *Prevention First Symp.*, Long Beach, CA, 2002.
5. VANTORRE, M., VERZHBITSKAYA, E. and LAFORCE, E., 'Model Test Based Formulations of Ship-Ship Interaction Forces', *Ship Techn. Res.*, 49, 124–141, 2002.
6. LATAIRE, E., VANTORRE, M. and DELEFORTRIE, G., 'Captive Model Testing for Ship-to-Ship Operations', *Proc. MARSIM '09 Conf.*, Panama City, Panama, 2009.
7. PINKSTER, J.A., 'The Influence of a Free Surface on Passing Ship Effects', *Int. Shipbuilding Progr.*, 51(4), 313–338, 2004.
8. HUANG, E.T. and CHEN, H.C., 'Influences of Site Specifics on Passing Ship Effects', *Proc. 17th ISOPE Conf.* (Vol. IV, pp. 2356–2363), Lisbon, Portugal, 2007.
9. KORSMEYER, F.T., LEE, C.H. and NEWMAN, J.N., 'Computation of Ship Interaction Forces in Restricted Waters', *J. Ship Res.*, 37(4), 298–306, 1993.
10. VAN DER MOLEN, W., WENNEKER, I. and BORSBOOM, M., 'Moored Ship Motions due to Passing

Ships', *Proc. Port-Maritime Innovation and R&D Conf.*, Rotterdam, the Netherlands, 2005.

11. TUCK, E.O., 'Shallow Water Flows past Slender Bodies', *J. Fluid Mech.*, 26, 81–95.
12. GOURLAY, T., 'Sinkage and Trim of Two Ships Passing Each Other on Parallel Courses', *Ocean Eng.*, 36(14), 1119–1127, 2009.
13. NEWMAN, J.N., 'The Approximation of Free Surface Green Functions', *Wave Asymptotics* (pp. 107–135), 1992.

APPENDIX. DETERMINATION OF THE SOURCE STRENGTH MODIFICATION PARAMETER

The parameter A is introduced in Eq. 7 to account for the effect of reduced source strengths for a non-zero Froude number. The value of A can be determined from the integral of the radial derivative of the principal singularity of the Green function, $1/r'$ (not considering the mirror sources above the free surface and below the bottom), over the surface of a sphere:

$$A = \frac{1}{4\pi} \int_0^{2\pi} \int_{-\frac{\pi}{2}}^{\frac{\pi}{2}} \frac{\partial}{\partial r} \frac{r^2}{r'} \cos \varphi d\varphi d\theta \quad (12)$$

using a spherical coordinate system $Or\varphi\theta$ with the origin at the source point. A nonlinearity parameter, $\varepsilon = 1/(1 - F_h^2) - 1$, is defined such that the modified radial distance can be written as $r' = \sqrt{(r^2 + \varepsilon x^2)}$. Substituting this in Eq. 12, leads to

$$A = \frac{1}{4\pi} \int_0^{2\pi} \int_{-\frac{\pi}{2}}^{\frac{\pi}{2}} \frac{1}{\sqrt{1 + \tan^2 \varphi + \varepsilon \cos^2 \theta}} d\varphi d\theta. \quad (13)$$

The integral is equal to 4π for $\varepsilon = 0$, so that Eqs. 6 and 7 reduce to a set of equations for the flow between two horizontal plates (one at $z = 0$ and one at $z = -h$). The integral can be easily evaluated numerically for non-zero ε .

AUTHORS BIOGRAPHIES

Wim van der Molen is a research engineer at the Hydraulics Laboratory of the CSIR in Stellenbosch, South Africa. Recent research activities at the CSIR include the development of numerical models for wave-ship interaction, passing ship effects and moored ship response, and the development of video monitoring techniques for waves and moored ship motions in a laboratory. He holds a PhD at the University of Delft, the Netherlands, with the subject to couple wave propagation models and ship motion models for the calculation of moored ship response in harbours.

2nd International Conference on Ship Manoeuvring in Shallow and Confined Water: Ship to Ship Interaction

Pierre Swiegers is a coastal engineer at WSP in Stellenbosch, South Africa. He has a BSc degree in Civil Engineering at the University of Stellenbosch. He has conducted the physical model tests and numerical model calculations for passing ship effects as part of his coastal engineering MSc graduation project at the same university.

Hans Moes is a (now retired) port and coastal engineer at the CSIR. Research activities over the past 35 years among others include physical and numerical modelling of waves and moored ship response as well as ship

navigation in port entrance channels. He is an active member of PIANC with participation in several working groups.

Marc Vantorre holds the position of senior full professor of marine hydrodynamics at Ghent University, where he is head of the Maritime Technology Division. His research, in close co-operation with Flanders Hydraulics Research, Antwerp, mainly focuses on ship hydrodynamics in shallow and restricted waters, including captive model testing, simulation and access channel policy.

